

**The *in vitro* Characterisation of
Drug-Drug Interactions
Arising from Inhibition of
Drug Metabolising Enzymes**

by

Attarat Pattanawongsa

Thesis

Submitted to Flinders University

for the degree of

Doctor of Philosophy

College of Medicine and Public Health

Flinders University

4th October, 2018

TABLE OF CONTENTS

TABLE OF CONTENTS	ii
LIST OF FIGURES	viii
LIST OF TABLES	xi
DECLARATION	xiv
ACKNOWLEDGEMENTS	xv
PEER-REVIEWED WORK	xvii
ABSTRACT	xix
ABBREVIATIONS AND SYMBOLS	xxi

CHAPTER 1: BACKGROUND

1.1 DRUG METABOLISM	1
1.2 CYTOCHROME P450 (CYP)	5
1.2.1 Catalytic cycle	6
1.2.2 Cytochrome P450 heterogeneity and nomenclature	9
1.2.3 Cytochrome P450: membrane topology and structure	12
1.2.4 Substrate selectivities of human cytochrome P450 enzymes	16
1.3 CYTOCHROME P450 2C8 (CYP2C8).....	21
1.3.1 General background.....	21
1.3.2 Substrate selectivity	22
1.4 UDP-GLUCURONOSYLTRANSFERASES (UGTs)	26
1.4.1 The glucuronidation reaction.....	26
1.4.2 UDP-Glucuronosyltransferase heterogeneity and nomenclature	29
1.4.3 UDP-Glucuronosyltransferase tissue expression and membrane topology	32

1.4.4	UDP-Glucuronosyltransferase structure-function	36
1.4.5	UDP-Glucuronosyltransferase enzyme substrate selectivity.....	40
1.5	INTER-INDIVIDUAL VARIABILITY IN DRUG METABOLISM	44
1.6	DRUG-DRUG INTERACTIONS	44
1.6.1	Inhibitory drug-drug interactions	45
1.6.2	Drug-drug interactions arising from inhibition of cytochrome P450 enzymes	46
1.6.3	Drug-drug interactions arising from inhibition of UDP- glucuronosyltransferase enzymes	49
1.7	ENZYME KINETICS AND MECHANISMS OF INHIBITION OF DRUG METABOLISING ENZYMES	51
1.7.1	Enzyme kinetics.....	51
1.7.2	The kinetics of drug metabolising enzyme inhibition <i>in vitro</i>	57
1.7.3	Mechanism-based inhibition	60
1.8	<i>IN VITRO</i> – <i>IN VIVO</i> EXTRAPOLATION (IV-IVE)	68
1.8.1	Reaction phenotyping	69
1.8.2	Quantitative prediction of hepatic metabolic clearance and inhibitory drug-drug interaction potential	73
1.8.3	Experimental factors affecting the prediction accuracy of <i>in vitro</i> – <i>in vivo</i> extrapolation.....	77
1.8.4	Physiologically-based pharmacokinetic modelling	83
1.9	RESEARCH AIMS	85
 CHAPTER 2: MATERIALS AND GENERAL METHODS		
2.1	MATERIALS AND EQUIPMENT	86
2.2	METHODS.....	92
2.2.1	Recombinant human UGTs and human liver microsomes (HLM)	92
2.2.2	1-Naphthol (1NP) glucuronidation by recombinant UGT2B10.....	92
2.2.3	Measurement of recombinant UGT enzyme activities, with and without inhibitors.....	93

2.2.3.1	4-Methylumbelliferone (4MU) glucuronidation	96
2.2.3.2	Lamotrigine (LTG) glucuronidation	96
2.2.3.3	Codeine (COD) glucuronidation	97
2.2.3.4	β -Estradiol (EST) glucuronidation	98
2.2.3.5	Propofol (PRO) glucuronidation	99
2.2.3.6	Cotinine glucuronidation by recombinant UGTs and human liver microsomes	100
2.2.3.7	Linearity of cotinine N-glucuronidation by recombinant UGT2B10 with respect to protein concentration and incubation time	103
2.2.3.8	Paclitaxel 6 α -hydroxylation by recombinant CYP2C8	105
2.2.4	Measurement of the non-specific binding of drugs to recombinant UGT enzyme sources, HLM and BSA using equilibrium dialysis	106
2.2.5	Bacterial culture, DNA manipulation and cytochrome P450 (CYP) expression	108
2.2.5.1	Preparation of competent cells for bacterial transformation ...	108
2.2.5.2	Wild type human CYP2C8 and rat oxidoreductase (rCPR) cDNA construct	109
2.2.5.3	Polymerase chain reaction (PCR) conditions for wild-type CYP2C8 and CYP2C8 mutants.....	111
2.2.5.4	Gel purification	115
2.2.5.5	Ligation of DNA fragments	119
2.2.5.6	Identification of plasmid DNA.....	121
2.2.5.7	Agarose gel electrophoresis	121
2.2.5.8	Bacterial transformation	121
2.2.5.9	Enzyme expression.....	122
2.2.5.10	Cytochrome P450 (CYP) and cytochrome P450 oxidoreductase (CPR) quantification	125
2.2.5.11	Assessment of recombinant CYP2C8 protein expression by western immunoblotting.....	126
2.3	DATA ANALYSIS	129

CHAPTER 3: HUMAN UDP-GLUCURONOSYLTRANSFERASE (UGT) 2B10: VALIDATION OF COTININE AS A SELECTIVE PROBE SUBSTRATE, INHIBITION BY UGT ENZYME SELECTIVE INHIBITORS AND ANTIDEPRESSANT AND ANTIPSYCHOTIC DRUGS, AND STRUCTURAL DETERMINANTS OF ENZYME INHIBITION

3.1 INTRODUCTION.....	134
3.2 MATERIALS AND METHODS	140
3.2.1 Enzyme sources	140
3.2.2 4-Methylumbelliferone (4MU) and 1-naphthol (1NP) glucuronidation by recombinant UGT2B10 (Supersomes)	140
3.2.3 Cotinine N-glucuronidation by recombinant human UGTs and HLM..	140
3.2.4 Inhibition of recombinant human UGT2B10 activity by antidepressants, antipsychotics and other compounds	141
3.2.5 Inhibition of recombinant human UGT enzyme activities by desloratadine and nicotine	141
3.2.6 Inhibition of human liver microsomal cotinine N-glucuronidation by hecogenin and desloratadine.....	142
3.2.7 Kinetic characterisation of amitriptyline, doxepin and mianserin inhibition of human liver microsomal cotinine N-glucuronidation.....	143
3.2.8 Measurement of the non-specific binding of cotinine to Supersomes, HLM and BSA, and amitriptyline, doxepin and mianserin to HLM and BSA.....	143
3.2.9 Molecular modelling	145
3.2.10 Data analysis.....	146
3.3 RESULTS.....	148
3.3.1 The glucuronidation of 4MU, 1NP and cotinine by Supersome UGT2B10	148
3.3.2 Kinetics of cotinine N-glucuronidation	148
3.3.3 Confirmation of the UGT2B10 substrate selectivity of cotinine and the inhibitor selectivity of desloratadine and nicotine.....	151
3.3.4 Inhibition of recombinant UGT2B10 by UGT enzyme-selective inhibitors.....	154

3.3.5	The contribution of UGT2B10 to human liver microsomal cotinine N-glucuronidation.....	155
3.3.6	Inhibition of recombinant UGT2B10 by antidepressant and antipsychotic drugs: modelling and structure-activity relationships	156
3.3.7	The kinetics of amitriptyline, doxepin and mianserin inhibition of human liver microsomal UGT2B10 and <i>in vitro</i> – <i>in vivo</i> extrapolation	164
3.4	DISCUSSION	167

CHAPTER 4: INHIBITION OF HUMAN UDP- GLUCURONOSYLTRANSFERASE (UGT) ENZYMES BY SGLT2 INHIBITORS

4.1	INTRODUCTION.....	173
4.2	METHODS.....	182
4.2.1	Inhibition of recombinant and human liver microsomal UGT activities	182
4.2.2	Kinetic characterisation of canagliflozin, dapagliflozin and empagliflozin inhibition of recombinant and human liver microsomal UGT 1A1 and 1A9 activities	182
4.2.3	Binding of canagliflozin, dapagliflozin, empagliflozin, β -estradiol, and propofol to HEK293 cell lysates, HLM and BSA	183
4.2.4	Quantification of fraction unbound in dialysate media	185
4.2.5	Data analysis.....	185
4.3	RESULTS.....	187
4.3.1	Canagliflozin, dapagliflozin and empagliflozin inhibition of recombinant human UGT enzymes	187
4.3.2	Binding of canagliflozin, dapagliflozin and empagliflozin to HEK293 cell lysate and HLM, with and without BSA	190
4.3.3	Kinetics of canagliflozin, dapagliflozin and empagliflozin inhibition of recombinant and human liver microsomal UGT1A1 and UGT1A9	197
4.4	DISCUSSION	202

CHAPTER 5: MOLECULAR BASIS OF THE INHIBITION OF CYTOCHROME P450 2C8 (CYP2C8) BY GLUCURONIDE CONJUGATES	
5.1 INTRODUCTION.....	210
5.2 MATERIALS AND METHODS	217
5.2.1 Enzyme expression	217
5.2.2 Kinetics of paclitaxel (PAC) 6 α -hydroxylation and time-dependent inhibition of CYP2C8 by glucuronides and aglycones	217
5.2.3 Molecular docking.....	219
5.2.4 Data analysis.....	219
5.3 RESULTS.....	221
5.3.1 <i>In silico</i> docking experiments: rationale for CYP2C8 mutant design ...	221
5.3.2 Expression of cytochrome P450 (CYP) 2C8 and cytochrome P450 oxidoreductase (CPR) in <i>E. coli</i> DH5 α cells.	229
5.3.3 Kinetics of paclitaxel 6 α -hydroxylation.....	234
5.3.4 Inhibition of wild-type and mutant CYP2C8 enzyme activities by gemfibrozil, gemfibrozil acyl glucuronide, diclofenac, diclofenac acyl glucuronide and estradiol 17- β -D-glucuronide.....	239
5.4 DISCUSSION	255
CHAPTER 6: GENERAL DISCUSSION AND CONCLUSION.....	263
APPENDIX.....	284
REFERENCES.....	292

LIST OF FIGURES

Figure 1.1 CYP catalytic cycle.....	8
Figure 1.2 Attachment of CYP2C5 to the microsomal membrane.	13
Figure 1.3 X-ray crystal structure of CYP2C8 (PDB - 1PQ2).....	14
Figure 1.4 Proportion of clinically used drugs metabolised by the individual CYP enzymes.	17
Figure 1.5 The glucuronidation reaction.	27
Figure 1.6 Dendrogram showing relationships between human UGT families based on the similarity of amino acid sequence.	30
Figure 1.7 UGT1A exon arrangement.....	31
Figure 1.8 UDP-Glucuronosyltransferase topology model.	36
Figure 1.9 Signature sequence of human UDP-glucuronosyltransferase enzymes....	38
Figure 1.10 Graphical representations of hyperbolic kinetics.....	53
Figure 1.11 Simulations of direct and Eadie-Hofstee plots for atypical kinetics.....	56
Figure 1.12 Dixon plots for competitive (panel A), non-competitive (panel B), uncompetitive (panel C) and mixed (panel D) inhibition.....	59
Figure 1.13 Reaction scheme for MBI.	60
Figure 1.14 Mechanisms of mechanism-based inactivation.	63
Figure 1.15 Plots of a CYP TDI experiment to generate k_{inact} and K_I values.	65
Figure 1.16 Plots of time-dependent inactivation from IC_{50} shift experiments.....	67
Figure 1.17 Qualitative IV-IVE.....	69
Figure 1.18 Scheme for the extrapolation of <i>in vitro</i> intrinsic clearance to hepatic metabolic clearance.	74
Figure 2.1 Representative chromatograms of cotinine and cotinine N-glucuronide.	102
Figure 2.2 Linearity of protein concentration and incubation time for cotinine N-glucuronide formation by human liver microsomal UGT2B10.	104

Figure 2.3 Plasmids used in molecular biology experiments.....	112
Figure 2.4 pBS II SK(+) – 17 α -CYP2C8 plasmid preparation.....	119
Figure 2.5 pCW – mutant 17 α -CYP2C8 plasmid preparation.....	120
Figure 3.1 N-terminal sequence identity of UGT1A and 2B proteins.	135
Figure 3.2 Cotinine metabolic pathway.	137
Figure 3.3 Rate vs. substrate concentration and Eadie-Hofstee (inset) plots for cotinine N-glucuronidation by recombinant UGT2B10 (Panel A), HLM (Panel B), and HLM plus BSA (Panel C).	150
Figure 3.4 Formation of cotinine N-glucuronidation by recombinant human UGTs.....	151
Figure 3.5 Inhibition of recombinant human UGT enzymes by nicotine (Panel A) and desloratadine (Panel B).	153
Figure 3.6 Inhibition of human liver microsomal cotinine N-glucuronidation at four substrate concentrations (0.25, 1, 3 and 6 mM) by hecogenin (10 μ M), desloratadine (10 μ M), and hecogenin plus desloratadine.....	156
Figure 3.7 Overlay of tri- and tetra-cyclic dataset molecules on the structure of amitriptyline.....	160
Figure 3.8 Structural overlay of dataset molecules lacking a tri- or tetra-cyclic scaffold or a scaffold without a central 6- or 7-membered ring.	161
Figure 3.9 Overlay of representative molecules with a tricyclic scaffold on the structure of amitriptyline.	163
Figure 4.1 Mechanism of action of SGLT2 inhibitors.....	175
Figure 4.2 Chemical structures of SGLT inhibitors.....	177
Figure 4.3 Sites (shown by arrows) of glucuronidation of canagliflozin (A), dapagliflozin (B) and empagliflozin (C).....	180
Figure 4.4 Inhibition of recombinant human UGT enzymes by canagliflozin (Panel A), dapagliflozin (Panel B) and empagliflozin (Panel C).	188
Figure 4.5 Dixon plots for canagliflozin inhibition of UGT activities.....	198
Figure 4.6 Dixon plots for dapagliflozin inhibition of UGT activities.	199
Figure 4.7 Dixon plots for empagliflozin inhibition of UGT activities.	200

Figure 5.1 Proposed mechanism for the irreversible inhibition of CYP2C8 by gemfibrozil glucuronide.....	212
Figure 5.2 Chemical structures of paclitaxel (PAC), 6 α -hydroxy PAC, gemfibrozil, diclofenac, β -estradiol, gemfibrozil acyl glucuronide, diclofenac acyl glucuronide and estradiol 17- β -D-glucuronide.	216
Figure 5.3 Diclofenac acyl glucuronide docked in the active site of CYP2C8.....	225
Figure 5.4 Gemfibrozil acyl glucuronide docked in the active site of CYP2C8.....	226
Figure 5.5 Estradiol 17- β -D-glucuronide docked in the active site of CYP2C8.....	226
Figure 5.6 Paclitaxel docked in the active site of CYP2C8.	227
Figure 5.7 Chemical structures of amino acids relevant to site-directed mutagenesis.....	228
Figure 5.8 Western blots for wild-type and mutant CYP2C8 proteins.	232
Figure 5.9 Rate vs. substrate concentration plots and Eadie-Hofstee (inset) plots for paclitaxel 6 α -hydroxylation formation by recombinant wild-type and mutant CYP2C8 enzymes.	236
Figure 5.10 Mean relative Cl_{int} values of the CYP2C8 mutants (normalised to wild-type CYP2C8).	239
Figure 5.11 Inhibition of CYP2C8 activity by gemfibrozil acyl glucuronide following a 30 min pre-incubation in the absence (blue line) and presence (red line) of NADPH.	246
Figure 5.12 Inhibition of CYP2C8 activity by gemfibrozil following a 30 min pre-incubation in the absence (blue line) and presence (red line) of NADPH.	248
Figure 5.13 Inhibition of CYP2C8 activity by diclofenac acyl glucuronide following a 30 min pre-incubation in the presence (red line) and absence (blue line) of NADPH.....	250
Figure 5.14 Inhibition plots of CYP2C8 activity by diclofenac (30 min pre-incubation in the absence (blue line) and presence (red line) of NADPH).	252
Figure 5.15 Inhibition of CYP2C8 activity by estradiol 17- β -D-glucuronide following a 30 min pre-incubation in the absence (blue line) and presence (red line) of NADPH.	254
Appendix figure 1. Chemical structures of compounds screened as inhibitors of UGT2B10.	284

LIST OF TABLES

Table 1.1 Major human xenobiotic metabolising enzymes.....	4
Table 1.2 Classification of human CYP enzymes based on major substrate class. ...	11
Table 1.3 Representative substrates of cytochrome P450 enzymes.....	20
Table 1.4 Drugs that are metabolised by CYP2C8 to a major (> 70%) or intermediate (20 – 70%) extent.....	23
Table 1.5 Representative substrates of human UGT enzymes.....	42
Table 1.6 Representative strong and moderate perpetrators of DDIs arising from inhibition of cytochrome P450 enzymes in humans.....	48
Table 1.7 Representative selective substrates and inhibitors of hepatically-expressed human UDP-glucuronosyltransferase enzymes for reaction phenotyping.	72
Table 2.1 Drugs and metabolites used in enzyme activity assays and for protein expression.	86
Table 2.2 Chemicals and reagents used in experimental procedures.....	88
Table 2.3 Enzymes, buffers and kits used in incubations and molecular biology procedures.....	89
Table 2.4 Equipment used in experimental procedures.	90
Table 2.5 Software used for data analysis, molecular modeling and oligonucleotide design.	91
Table 2.6 Protein concentrations, incubation times, probe substrate (4-methylumbelliferone, 4MU; lamotrigine; LTG; codeine, COD; cotinine, COT) concentrations and positive control inhibitors used for the measurement of recombinant UGT enzyme activities.....	95
Table 2.7 NZY ⁺ broth and Lauria Bertani medium for bacterial culture.....	109
Table 2.8 RF1 and RF2 preparation.....	109
Table 2.9 Forward and reverse primers for the cloning of wild-type CYP2C8 and site-directed mutagenesis.....	116
Table 2.10 Modified Terrific Broth, TES buffer and Spheroplast Resuspension Buffer preparation for enzyme expression.	124

Table 2.11 Preparation of Lowry-Folin reagents for protein quantification.	124
Table 3.1 HPLC conditions for the quantification of amitriptyline, doxepin and mianserin in dialysates from equilibrium dialysis experiments.....	145
Table 3.2 Derived kinetic constants for cotinine N-glucuronidation by recombinant UGT2B10 and human liver microsomes (\pm BSA, 1% w/v).	149
Table 3.3 IC ₅₀ values for nicotine and desloratadine inhibition of recombinant UGT enzymes.	154
Table 3.4 IC ₅₀ values for the inhibition of recombinant UGT2B10 by UGT enzyme-selective inhibitors, azoles, and antidepressant and antipsychotic drugs.	157
Table 3.5 Binding of cotinine to protein sources (Supersomes and HLM) in the absence and presence of BSA (1% w/v).	164
Table 3.6 Binding of amitriptyline, doxepin and mianserin to HLM in the presence of BSA (1% w/v).	165
Table 3.7 Published kinetic parameters for cotinine N-glucuronidation by UGT2B10 and human liver microsomes.	169
Table 4.1 Selectivity of SGLT2 inhibitors.	176
Table 4.2 HPLC conditions for the quantification of drug binding in dialysates from equilibrium dialysis experiments.	186
Table 4.3 IC ₅₀ values for CNF, DPF and EPF inhibition of recombinant UGT enzymes.	190
Table 4.4 Binding of CNF to protein sources (HEK cell lysate and HLM) in the absence and presence of BSA (0.5% w/v).	193
Table 4.5 Binding of DPF to protein sources (HEK cell lysate and HLM) in the absence and presence of BSA (1% w/v).	194
Table 4.6 Binding of EPF to protein sources (HEK cell lysate and HLM) in the absence and presence of BSA (1% w/v).	195
Table 4.7 Binding of propofol to protein sources (HEK cell lysate and HLM) in the presence of BSA (0.5 and 1% w/v).	196
Table 4.8 Binding of β -estradiol to HEK cell lysate and HLM.	196
Table 4.9 Derived K _{i,u} values for CNF, DPF and EPF inhibition of recombinant and human liver microsomal UGT1A1 and UGT1A9.....	201

Table 5.1 CYP2C8 residues within 4Å of the glucuronic acid and aglycone moieties of docked diclofenac acyl glucuronide, gemfibrozil acyl glucuronide, and estradiol 17-β-D-glucuronide.....	222
Table 5.2 Cytochrome P450 and NADPH cytochrome P450 oxidoreductase (CPR) contents of CYP2C8 proteins co-expressed with CPR in <i>E. coli</i>	231
Table 5.3 Expression levels of wild-type cytochrome P450 2C8 and mutants from western blotting.....	233
Table 5.4 Derived kinetic constants for PAC 6α-hydroxylation by recombinant wild-type CYP2C8 and CYP2C8 mutants.....	235
Table 5.5 IC ₅₀ and k _{inact} /K _I values for gemfibrozil acyl glucuronide inhibition of recombinant wild type CYP2C8 and CYP2C8 mutants.	245
Table 5.6 IC ₅₀ and k _{inact} /K _I values for gemfibrozil inhibition of recombinant wild type CYP2C8 and CYP2C8 mutants.	247
Table 5.7 IC ₅₀ and k _{inact} /K _I values for diclofenac acyl glucuronide inhibition of recombinant wild type CYP2C8 and CYP2C8 mutants.	249
Table 5.8 IC ₅₀ and k _{inact} /K _I values for diclofenac inhibition of recombinant wild type CYP2C8 and CYP2C8 mutants.	251
Table 5.9 IC ₅₀ and k _{inact} /K _I values for estradiol 17-β-D-glucuronide inhibition of recombinant wild type CYP2C8 and CYP2C8 mutants.	253

DECLARATION

I certify that this thesis does not incorporate without acknowledgement any material previously submitted for a degree or diploma in any University and that to the best of my knowledge and belief, it does not contain any material previously published or written by another person except where due reference is made in the text.

Attarat Pattanawongsa

September 2018

ACKNOWLEDGEMENTS

I would like to express my sincere appreciation to the following people who have been foremost in assisting and supporting me throughout my PhD studies.

I owe sincerest gratitude to my principal supervisor, Matthew Flinders Distinguished Professor John O. Miners, for his invaluable scientific knowledge, guidance, and ability to motivate. He encouraged me and believed in my ability to complete a PhD. Together we shared some challenging struggles, but were successful in overcoming these. Above all, I will be forever indebted to him for being a man of character who was an inspiring role model. Professor Miners went to great lengths to support me and my studies. I am very lucky indeed to know him and have him as my mentor.

I am deeply grateful to my co-supervisors, Dr. Andrew Rowland and Dr. Benjamin C. Lewis. They shared their scientific expertise and time in ways that made my work much easier, and taught me so much.

I also wish to thank Ms Kushari Burns, Ms Nuy Chau and Dr. Pornnipa Korprasertthaworn for providing invaluable suggestions relating to my laboratory work, and Dr. Pramod C. Nair for his invaluable input into the molecular modelling studies that form part of Chapter 3. I additionally thank the staff and students of the Department of Clinical Pharmacology of Flinders University for their support and friendship during the period of my PhD studies, in particular Ms Heather Bailey and Ms Karli Goodwin for their advice and assistance with thesis format and preparation.

On a personal level, many others played a major role 'behind the scenes'. I sincerely thank my wife Phanita and her parents in Thailand, who stood loyally beside me during

my lengthy time abroad and cheered me up at the times when I needed it most. Dr. Pritsana Raungrut and her family also motivated and supported me, as did Kannika and her family, offering a warm welcome and friendliness. My lovely landlords, Ms Ingrid Krumins and Mr Stephen Balaban, often gave me lessons in English, and my Thai friends in Australia protected me from loneliness I felt being away from home.

I am sincerely grateful to Professor Amnuay Thithapandha, Professor Thirayudh Glinsukon, Professor Sunibhond Pummangura, Professor Taweeporn Sittiracha and Professor Witthaya Anarmnart for supporting me and advising me to study at Flinders University, and I wish to thank all of my teachers for sharing their remarkable knowledge over many years.

I dedicate this thesis to my dearly loved grandfather and grandmother, Jang and Saree Ratchaneewong, who have raised me since birth. To them I say, “I would like to let you know that this part of my success is yours.” Finally, I would like to express vast gratitude to all of my family for their love and support. To those others who helped me in many ways, please forgive me for not mentioning you all by name, but I will remember you with deepest gratitude and I thank you most sincerely.

PEER-REVIEWED WORK

Journal Articles

Pattanawongsa, A, Chau, N, Rowland, A and Miners, JO (2015), 'Inhibition of human UDP-glucuronosyltransferase enzymes by canagliflozin and dapagliflozin: Implications for drug-drug interactions', *Drug Metabolism and Disposition*, 43 (10): 1468-1476.

Pattanawongsa, A, Nair, PC, Rowland, A and Miners, JO (2016), 'Human UDP-glucuronosyltransferase (UGT) 2B10: Validation of cotinine as a selective probe substrate, inhibition by UGT enzyme-selective inhibitors and antidepressant and antipsychotic drugs, and structural determinants of enzyme inhibition', *Drug Metabolism and Disposition*, 44 (3): 378-388.

Miners, JO, Pattanawongsa, A and Rowland, A (2018), 'Response to *in vitro* and physiologically-based pharmacokinetic assessment of the drug–drug interaction potential of canagliflozin', *British Journal of Clinical Pharmacology*, 84 (2): 392-393.

Published Abstracts

Pattanawongsa A, Rowland A, and Miners JO (2014), Characterisation of the UDP-glucuronosyltransferase enzyme inhibition selectivity of dapagliflozin: Implications for drug-drug interactions. *Proceedings: Australasian Society of Clinical and Experimental Pharmacologists and Toxicologists (ASCEPT)*, Abstract 594.

Pattanawongsa A, Pramod CN, Rowland A, and Miners JO (2015), The inhibition of human UDP-glucuronosyltransferase 2B10 (UGT2B10) by antidepressant and

antipsychotic drugs: Implications for drug-drug interactions. *Proceedings: Australasian Pharmaceutical Science Association - Australasian Society of Clinical and Experimental Pharmacologists and Toxicologists (ASPA – ASCEPT)*, Abstract 506.

ABSTRACT

The overarching theme of the studies described in this thesis is the *in vitro* characterisation of drug-drug interactions (DDIs) arising from drug metabolising enzymes. Two studies characterised potential DDIs arising from the inhibition of UDP-glucuronosyltransferase (UGT) enzymes while the third investigated the molecular basis of the inhibition of cytochrome P450 (CYP), namely CYP2C8, by glucuronide conjugates.

The first major study (Chapter 3) primarily aimed to characterise the inhibition of UGT2B10 by 34 amine-containing antidepressant and antipsychotic drugs and identify potential perpetrators of DDIs. Initial experiments confirmed that cotinine is selective substrate of UGT2B10 while desloratadine is a selective inhibitor, and these compounds may be used as 'probes' for reaction phenotyping. Amitriptyline, doxepin and mianserin were the most potent inhibitors of human liver microsomal UGT2B10, with K_i values $< 1 \mu\text{M}$. *In vitro* – *in vivo* extrapolation (IV-IVE) suggested that all three drugs may act as perpetrators of DDIs arising from inhibition of UGT2B10-catalysed drug glucuronidation. Molecular modelling demonstrated that moderate to potent inhibitors all contained a hydrophobic domain (comprising a tetra-, tri- or bi-cyclic ring structure or a single aromatic ring as the central 'scaffold') and an amine functional group that was located 3 C-C or C-N bond lengths from the central scaffold.

Studies described in Chapter 4 continued the theme of the *in vitro* characterisation of human UGT inhibition. Canagliflozin (CNF), dapagliflozin (DPF) and empagliflozin (EPF) are the first SGLT2 inhibitors introduced into clinical practice

for the treatment of type 2 diabetes. While all three ‘flozins’ inhibited UGT enzyme activity to some extent, CNF inhibited recombinant UGT1A1, UGT1A9 and the extrahepatic UGT1A10 with IC₅₀ values ranging from 6.9 to 9.5 μM. IV-IVE using mean K_i values for CNF inhibition of human liver microsomal UGT1A1 (7.2 μM) and UGT1A9 (3.0 μM) predicted that CNF may perpetrate DDIs with drugs glucuronidated by these enzymes. The results indicate that characterisation of the DDI potential of new SGLT2 inhibitors currently in clinical development is warranted.

In Chapter 5, the focus changed from inhibition of glucuronide formation to inhibition of CYP2C8 by glucuronide conjugates. Docking of the mechanism-based inhibitor gemfibrozil glucuronide and the diclofenac and estradiol glucuronides, both known to be hydroxylated by CYP2C8, in the CYP2C8 X-ray crystal structure confirmed that the side-chains of Asn99, Ser100, Ser103, Thr107, Ser114 and Gln214 were within hydrogen bonding distance to the polar groups of the glucuronide moiety. Based on these observations, 14 mutants (8 single, 2 double, 1 triple, 1 quadruple, and 2 quintuple) were generated by site-directed mutagenesis, and each was characterised for time-dependent inhibition (TDI) and non-TDI by the three glucuronides.

Although TDI studies with the multiple mutants was not possible due to their instability when pre-incubated with NADPH, the non-TDI (co-incubation) experiments with all mutants and the TDI experiments with the single mutants demonstrated that neither Asn99, Ser100, Ser103, Thr107, Ser114 nor Gln214 alone are ‘critical’ for glucuronide conjugate binding in the CYP2C8 active site. Rather, all six residues appear to contribute to the binding of the glucuronic acid moiety to a similar extent.

ABBREVIATIONS AND SYMBOLS

1NP	1-naphthol	DMSO	dimethyl sulfoxide
4MU	4-methylumbelliferone	DNA	deoxyribonucleic acid
20-HETE	20-hydroxyeicosatetraenoic acid	dNTP	deoxyribonucleotide triphosphate
Abs	absorbance	DPF	dapagliflozin
ALA	5-aminolevulinic acid	DTT	dithiothreitol
Ala	alanine	dTTP	deoxythymidine triphosphate
ANOVA	analysis of variance	E	Enzyme
AO	aldehyde oxidase	<i>E. coli</i>	<i>Escherichia coli</i>
Asn	asparagine	EDTA	ethylenediamine tetraacetic acid
AU	absorbance unit	E_H	hepatic extraction ratio
AUC	area under the plasma concentration-time curve	EH	epoxide hydrolase
AUC_i	AUC of a victim drug co-administered with an inhibitor	EI	enzyme-inhibitor complex
BSA	bovine serum albumin	EI*	enzyme-reactive metabolite complex
°C	degrees Celsius	EMA	European Medicines Agency
μCi	microCurie	EPF	empagliflozin
ca / ~	approximately	ES	enzyme-substrate complex
cDNA	complementary deoxyribonucleic acid	EIS	enzyme-inhibitor-substrate complex
C_{max}	maximal drug concentration in plasma	EST	estradiol
Cl	clearance	EX	inactivated enzyme
Cl_s	systemic clearance	F_a	fraction of the dose absorbed from the gastrointestinal tract
Cl_H	hepatic clearance	FAD	flavin adenine dinucleotide
Cl_{int}	intrinsic clearance	FDA	Food and Drug Administration
Cl_{max}	maximal clearance	Fe²⁺	ferrous ion
CNF	canagliflozin	Fe³⁺	ferric ion
CO	carbon monoxide	F_g	fraction of the absorbed dose escaping metabolism in the intestine
COD	codeine	f_m	fraction of hepatic metabolic clearance mediated by a specific enzyme
COT	cotinine	FMN	flavin mononucleotide
CPR	cytochrome P450 oxidoreductase	FMO	flavin-containing monooxygenase
C_{ss}	drug concentration in plasma at steady state	fs	femto second
CYP/P450	cytochrome(s) P450	f_umic	unbound fraction of drug in incubation medium
dATP	deoxyadenosine triphosphate	g	gram
dCTP	deoxycytidine triphosphate	Gln	glutamine
D	dose	GLUT	glucose transporter
DES	diethylstilbestrol	GST	glutathione-S-transferase
DDI	drug-drug interaction	HbA1C	haemoglobin A1C
dGTP	deoxyguanosine triphosphate		
DMEM	Dulbecco's modified eagle medium		

hr	hour(s)	K_{si}	inhibition constant for substrate inhibition
HCl	hydrochloric acid	l	litre
HClO₄	perchloric acid	μl	microlitre
HEK293	human embryonic kidney cell line	LB	Lauria-Bertani
HF	high fidelity	LC-MS	liquid chromatography-mass spectrometry
His	histidine	Leu	leucine
HIV	human immunodeficiency virus	LTG	lamotrigine
HLM	human liver microsomes	M	molar
HMG-CoA	3-hydroxyl-3-methylglutaryl-coenzyme A	μm	micrometer (micron)
H₂O₂	hydrogen peroxide	μM	micromolar
HPLC	high-performance liquid chromatography	mA	milliampere(s)
H₃PO₄	phosphoric acid	MAOI	monoamine oxidase inhibitor
I	inhibitor	MBI	mechanism-based inactivation or mechanism-based inactivator
[I]	inhibitor concentration	MDS	molecular dynamics simulation
[I_{inlet}]	hepatic input concentration of inhibitor	MIC	metabolite-intermediate complex (complexation)
[I_{max}]	maximal unbound concentration of inhibitor	mg	milligram
IC₅₀	concentration of inhibitor producing 50% inhibition	MgCl₂	magnesium chloride
IgG	immunoglobulin G	min	minute(s)
IPTG	isopropyl β-D-1-thiogalactopyranoside	ml	millilitre
IS	internal standard	mm	millimetre
IV-IVE	<i>in vitro</i> – <i>in vivo</i> extrapolation	mM	millimolar
k_a	absorption rate constant	mmol	millimole
kb	kilobases	MT	N-methyltransferase
KCN	potassium cyanide	n	Hill coefficient
k_{deg}	rate constant for degradation of the inactivated enzyme	N/A	not appreciable or not available
kDa	kilodaltons	NaCl	sodium chloride
KH₂PO₄	potassium dihydrogen phosphate	NADP	nicotinamide adenine dinucleotide phosphate, oxidised form
K₂HPO₄	dipotassium hydrogen phosphate	NADPH	nicotinamide adenine dinucleotide phosphate, reduced form
K_i	inhibitor constant for the EI complex	NAT	N-acetyltransferase
K_i'	inhibitor constant for the EIS complex	ND	not determined
K_I	concentration of MBI producing half-maximal inactivation (inactivation constant)	NI	negligible inhibition
k_{inact}	maximal rate of inactivation	ng	nanogram
K_m	Michaelis constant	nm	nanometre
k_{obs}	observed inactivation rate constant	nmol	nanomole
KOH	potassium hydroxide	NSAID	non-steroidal anti-inflammatory drug
		O₂'	superoxide
		OATP	organic anion transporter peptide
		OD	optical density
		P	product

PAC	paclitaxel	SULT	sulfotransferase
PAGE	polyacrylamide gel electrophoresis	TAE	Tris-acetate EDTA
PBPK	physiologically-based pharmacokinetics	TB	Terrific broth
PCR	polymerase chain reaction	TBS	Tris-buffered saline
Phe	phenylalanine	TBST	Tris-buffered saline Tween-20
PMSF	phenylmethylsulfonyl fluoride	TCA	tricyclic antidepressant
pmol	picomole	TDI	time-dependent inhibition or time-dependent inhibitor
PRO	propofol	TEMED	N,N,N',N'-tetramethylethylenediamine
Pro	proline	Thr	threonine
Q_H	liver blood flow	TLC	thin layer chromatography
RED	rapid equilibrium dialysis	UDPGA	uridine diphosphate glucuronic acid
RNA	ribonucleic acid	UDP-Glc	uridine diphosphate glucose
RNase	ribonuclease	UV-VIS	ultraviolet-visible
ROS	reactive oxygen species	UGT	uridine diphosphate glucuronosyltransferase
rpm	revolutions per minute	v	reaction rate (rate of product formation)
[S]	substrate concentration	V	volt(s)
S₅₀	substrate concentration at half V _{max} in Hill equation	v_i	reaction rate in the presence of inhibitor
SGLT	sodium-glucose co-transporter	V_{max}	maximal velocity of an enzyme reaction
SD	standard deviation	Val	valine
SDS	sodium dodecyl sulphate	v/v	volume/volume
SE	standard error	W	watt(s)
sec	second(s)	w/v	weight/volume
Ser	serine	XO	xanthine oxidase
SNRI	serotonin and noradrenaline reuptake inhibitor	Å	Angstrom unit
SRB	spheroplast resuspension buffer		
SRS	substrate recognition site		
SSRI	selective serotonin reuptake inhibitor		

CHAPTER 1

BACKGROUND

1.1 Drug metabolism

Drug metabolism (or biotransformation) is the chemical modification of a drug by the body. About 75% of all clinical drugs undergo metabolism to a significant extent. Drug metabolism is important for three reasons. Firstly, it is an elimination mechanism – by converting the drug to another chemical (the metabolite), metabolism clears the parent drug from the circulation. Additionally, it facilitates the removal of the drug from the body as polar metabolites in urine and bile. Further, metabolism generally results in drug detoxification (Correia 2012; Testa and Abraham 2003), although many metabolites are known to be pharmacologically (e.g. nortriptyline (formed from amitriptyline) and morphine 6-glucuronide) or toxicologically (paracetamol quinoneimine) active. In fact, prodrugs represent the special case where an inactive compound undergoes metabolism to produce the pharmacologically active drug. Metabolism is also an essential elimination and detoxification mechanism for non-drug xenobiotics (e.g. dietary chemicals and environmental pollutants, including numerous carcinogens) and endogenous compounds (e.g. fatty acids and steroid hormones).

Importantly, metabolic clearance determines the dose of drugs eliminated by hepatic biotransformation, as shown by the following relationship (Buxton and Benet 2011).

Equation 1.1,

$$\text{Dose rate (mg/hr)} = Cl_s \times C_{ss}$$

where Cl_s is systemic clearance (equivalent to metabolic clearance for a drug eliminated solely by metabolism) and C_{ss} is the concentration of the drug in blood at

steady-state. Thus, for any desired pharmacodynamic response (given by C_{ss}), dose is determined by clearance. It follows that factors that alter the efficiency of drug metabolism (e.g. drug-drug interactions (DDIs) resulting from enzyme induction or inhibition, genetic polymorphism, liver disease, etc) may necessitate a change in dose to avoid drug-related toxicity or a reduction in efficacy.

Most textbooks of pharmacology, for example Goodman and Gilman's: The Pharmacological Basis of Therapeutics (Gonzalez, Coughtrie and Tukey 2011), and toxicology, for example Casarett and Doull's Toxicology (Gregus 2012), classify drug metabolism reactions as either Phase I or Phase II, based on the original classification proposed by RT Williams in 1959 (Jones 2015). Phase I reactions include oxidation, reduction and hydrolysis, leading to the introduction or 'unmasking' of a functional group, typically $-OH$, $-COOH$, $-O-$ or $-NH_2$, in the lipophilic drug substrate. Phase II reactions involve the conjugation of an 'acceptor' functional group introduced by Phase I metabolism with an endogenous compound, most commonly glucuronic acid, sulfate, glutathione and the acetyl group, in most cases derived from a nucleoside-containing cofactor (e.g. UDP-glucuronic acid). Sequential metabolism is proposed to decrease biological activity and increase polarity, thereby promoting urinary excretion.

While widespread in use, the Phase I/II classification has been challenged by Josephy, Guengerich and Miners (2005) since it no longer accurately reflects current knowledge of xenobiotic metabolism. In particular, a large number of drugs, non-drug xenobiotics and endogenous compounds undergo conjugation without prior Phase I metabolism due to the pre-existence of a suitable 'acceptor' functional group. Examples include the conjugative metabolism of isoniazid, morphine, paracetamol and salbutamol, to name a few. In addition, some drugs, for example, codeine, undergo concurrent Phase I and II metabolism. The terms Phase I and II imply sequential metabolism, which is

clearly incorrect. More generally, the classification lacks any chemical or mechanistic basis. While Josephy, Guengerich and Miners (2005) proposed a classification based on oxidation, reduction, hydrolysis and conjugation, a simplified nomenclature adopted by this laboratory classifies drug metabolism reactions as ‘functionalisation’ and ‘conjugation’. The former, which combines oxidation, reduction and hydrolysis, involves the introduction or ‘unmasking’ (e.g. dealkylation reactions) of a polar functional group (e.g. -OH, -NHR) in the substrate molecule, while conjugation reactions involve the covalent linkage of an acceptor functional group on the substrate molecule with an endogenous compound.

Drug metabolism reactions are almost invariably enzymatically-mediated (Gibson and Skett 2001; Gonzalez, Coughtrie and Tukey 2011). Following on from the classification of drug metabolism reactions, drug metabolising enzymes may be classified as functionalisation (or Phase I) or conjugation (or Phase II) enzymes (Table 1.1). It should be noted that the term ‘drug metabolising enzyme’ as used in the literature is also taken to mean xenobiotic metabolising enzyme. Quantitatively, the most important drug metabolising enzymes are cytochrome P450 (CYP or P450) and UDP-glucuronosyltransferase (UGT). Together, these enzymes are responsible for the metabolism of approximately 90% of drugs eliminated by biotransformation (Guengerich 2010). Both enzymes have the capacity to metabolise a structurally diverse range of drugs and other chemicals. This versatility arises from the fact that both CYP and UGT exist as enzyme ‘superfamilies’; the individual CYP and UGT enzymes exhibit distinct, but sometimes overlapping, substrate and inhibitor selectivities and differ in terms of regulation of expression (e.g. tissue distribution, induction, ontogeny, etc) and genetic polymorphism (occurrence and frequency) (Guengerich 2005; Guillemette, Lévesque and Rouleau 2014; Johansson and

Ingelman-Sundberg 2011; Mackenzie et al. 2005; Miners et al. 2006; Miners et al. 2010b; Miners et al. 2004; Rendic and Guengerich 2015; Zanger and Schwab 2013).

Enzymes of the UGT and CYP families are the focus of the research described in this thesis, and will be discussed in greater detail in subsequent sections. Other representative enzymes that contribute to the metabolism of drugs and non-drug xenobiotics are listed in Table 1.1.

Table 1.1 Major human xenobiotic metabolising enzymes

Adapted from Gibson and Skett (2001) and Gonzalez, Coughtrie and Tukey (2011).

Enzymes	Reaction(s)
Functionalisation reactions	
Aldehyde oxidase (AO)	Aldehyde oxidation, aromatic heterocycle oxidation
Cytochromes P450 (CYP or P450)	Hydroxylation, epoxidation, O-, N- and S- dealkylation, others
Epoxide hydrolases (EH)	Hydrolysis of epoxides
Esterases (e.g. carboxyl esterases, CES)	Hydrolysis of esters
Flavin-containing monooxygenases (FMO)	N, S and P oxidation
Xanthine oxidase (XO)	Oxidation of xanthines
Conjugation reactions	
N-Acetyltransferases (NAT)	Covalent addition of the acetyl group
Glutathione-S-transferases (GST)	Covalent addition of glutathione
N-Methyltransferases (MT)	Covalent addition of the methyl group
Sulfotransferases (SULT)	Covalent addition of sulphate
UDP-Glucuronosyltransferases (UGT)	Covalent addition of glucuronic acid

The majority of drug metabolising enzymes, including CYP and UGT, are expressed primarily in the liver (Gonzalez, Coughtrie and Tukey 2011). Hence, for most drugs the liver is the main site of metabolism and hepatic metabolic clearance is the primary elimination mechanism. Within the hepatocyte, both UGT and drug metabolising CYP enzymes localise to the smooth endoplasmic reticulum and are therefore recovered in the microsomal fraction of liver homogenates (Knights et al. 2016b). Consequently, liver microsomes and isolated hepatocytes are used widely to investigate CYP- and UGT- catalysed drug and chemical metabolism and kinetics *in vitro*. In contrast to CYP and UGT, some drug metabolising enzymes, particularly sulfotransferases, are found in the cytosol of hepatocytes (Gonzalez, Coughtrie and Tukey 2011).

Although the liver is quantitatively the most important organ involved in drug metabolism, many drug metabolising enzymes additionally occur in extra-hepatic tissues (Gundert-Remy et al. 2014). Notably, several CYP and UGT enzymes are expressed at a functionally significant level in the proximal small intestine where they are involved in the pre-hepatic metabolism of orally ingested drugs and other xenobiotics (Paine et al. 2006; Rowland, Miners and Mackenzie 2013). Similarly, some CYP and UGT enzymes occur in the kidney and are believed to modulate the intra-renal exposure to drugs, nephrotoxic compounds and physiological mediators (Miners et al. 2017b).

1.2 Cytochrome P450 (CYP)

The cytochromes P450 (CYP) comprise a superfamily of heme monooxygenases that catalyse the transfer of one atom of oxygen (from atmospheric oxygen) to a typically lipophilic substrate (see below). Apart from oxygen, CYP catalysed reactions require the accessory protein NADPH cytochrome P450 oxidoreductase (CPR) for the transfer

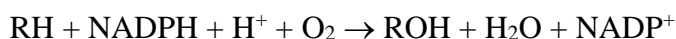
of electrons from NADPH to the substrate (Munro et al. 2013). Thus, CYP enzymes most commonly function as monooxygenases in hydroxylation, epoxidation, O-, N- and S- dealkylation, and oxidative deamination and decarboxylation reactions (Guengerich 2003 and 2015). However, given the chemical characteristics of the CYP catalytic cycle (see below), these enzymes also catalyse other reactions such as desaturation and carbon – carbon bond cleavage (Guengerich, Waterman and Egli 2016). In terms of the scope of substrates metabolised, CYP is considered the most important enzyme involved in the biotransformation of drugs and non-drug chemicals. CYP catalyses approximately 95% of all oxidation – reduction reactions involving drugs, non-drug xenobiotics, and endogenous physiological mediators (Rendic and Guengerich 2015). In particular, CYP accounts for the metabolism of approximately 75% of clinically-used drugs (Guengerich, Waterman and Egli 2016). As indicated previously, this versatility arises from the fact that CYP exists as a superfamily of proteins.

1.2.1 Catalytic cycle

The CYP catalytic cycle is complex, involving at least eight steps (Guengerich 2010). A simplified version of the cycle is shown in Figure 1.1 (Panel A), while Panel B shows the interaction of CPR (and cytochrome b₅) with the CYP protein. As shown in Panel B, CPR consists of an N-terminal domain that associates with the membrane of the endoplasmic reticulum, a flavin mononucleotide (FMN) binding domain, a flavin adenine dinucleotide (FAD) binding domain, and a NADPH binding domain. Interaction of FAD and FMN via their distinct binding domains facilitates the transfer of electrons from NADPH to microsomal CYP proteins. In the resting state, the iron of the heme prosthetic group is in the oxidised ferric state (Fe³⁺) (Panel A). It is generally believed that the catalytic cycle is initiated by the binding of substrate (RH).

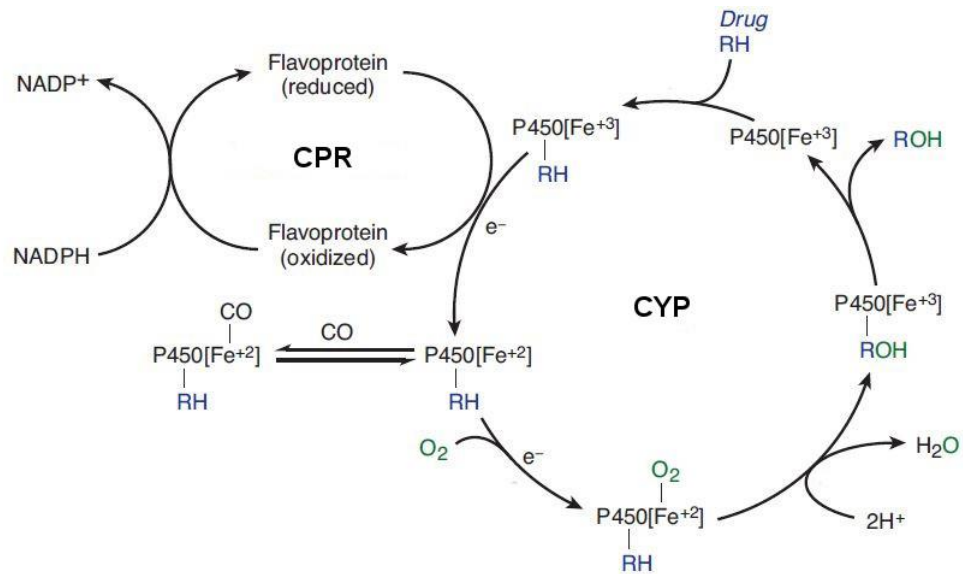
The optimal distance for substrate binding is 4 to 6 Å from the heme iron. One electron is then transferred from CPR to the substrate-bound complex, reducing the iron to the ferrous (Fe^{2+}) state. Substrate binding is followed by the binding of one molecule of atmospheric oxygen to form a $\text{Fe}^{2+} - \text{O}_2$ - drug complex (shown at the bottom of Panel A), which receives a second electron from CPR. In some instances, the second electron can be donated by cytochrome b_5 . Subsequent steps include protonation, scission of the dioxygen bond, loss of a molecule of water, and then formation of a reactive oxo-ferryl (FeO^{3+} - RH complex that is responsible for insertion of oxygen into the substrate (i.e. formation of ROH).

The overall reaction may be summarised as:



It should be noted that after formation of the $\text{Fe}^{2+} - \text{O}_2$ - drug complex, all subsequent intermediates are unstable. For example, the $\text{Fe}^{2+} - \text{O}_2 - \text{RH}$ and $(\text{FeO})^{3+} - \text{RH}$ complexes can dissociate, releasing hydrogen peroxide (H_2O_2) and O_2^- , respectively. Dissociation of these complexes results in so-called ‘uncoupling’ of the catalytic cycle, with lack of product (ROH) formation. When uncoupling occurs, the reaction deviates from the stoichiometry shown in the above equation and the cycle operates at less than optimal efficiency. Furthermore, the production of reactive oxygen species may cause heme inactivation (Guengerich 2010).

A



B

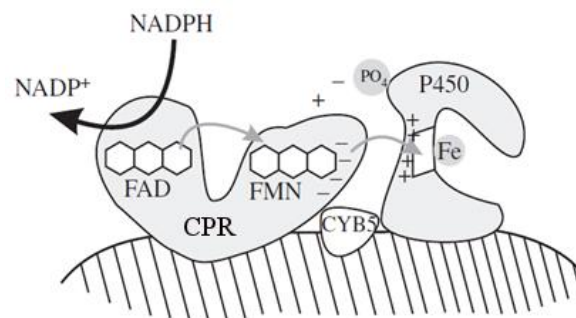


Figure 1.1 CYP catalytic cycle.

CYP oxidative and electron transport cycle (Panel A), and schematic of electron transport system, including the FAD-FMN complex and cytochrome b₅ (abbreviated CYB5) (Panel B). CPR refers to cytochrome P450 oxidoreductase, FAD to flavin adenine dinucleotide, and FMN to flavin mononucleotide.

Reproduced with permission from Correia, MA (2012), 'Drug biotransformation', In Basic and Clinical Pharmacology, 12 edition, eds BG Katzung and AJ Trevor, Chapter 4: 53-68, McGraw-Hill, New York, and Nebert, DW, Wikvall, K and Miller, WL (2013), 'Human cytochromes P450 in health and disease', Philosophical Transactions of the Royal Society B, 368 (1612): 20120431. Copyright (2012) McGraw-Hill Education, and copyright (2013) corresponding author (Nebert, DW).

Carbon hydroxylation is intuitive from the reaction scheme shown in Figure 1.1. However, as indicated above, heteroatom (N, O, S) dealkylation is a common reaction catalysed by CYP. Dealkylation reactions appear to involve initial one electron oxidation of the heteroatom (involving the $(\text{FeO})^{3+}$ species) followed by C(α)-H proton abstraction, and subsequent monooxygenation of the resulting carbon radical (Guengerich, Yun and Macdonald 1996). The C(α) hydroxylated species subsequently dissociates into the dealkylated metabolite and an aldehyde.

1.2.2 Cytochrome P450 heterogeneity and nomenclature

CYP enzymes play an essential role in the metabolism of xenobiotics and in the biosynthesis and catabolism of endogenous compounds in eukaryote and prokaryote species, including yeast, bacteria, plants and animals (Nebert, Wikvall and Miller 2013). As described earlier, CYP comprises a ‘superfamily’ of enzymes. The human genome includes a total of 115 *CYP* genes; 57 of these encode ‘active’ proteins while 58 are pseudogenes (Nelson et al. 2004; Rendic and Guengerich 2015; Sim and Ingelman-Sundberg 2010). The ‘active’ *CYP* genes encode functionally distinct proteins of approximately 500 amino acids. Human *CYP* genes have been classified in 18 families and 43 subfamilies based on the amino acid identity of the encoded proteins (Johnson and Stout 2013; Nelson et al. 1996; Nelson et al. 2004). Proteins exhibiting > 35% identity are classified in the same family, designated by an Arabic numeral (e.g. CYP2) while proteins sharing > 70% sequence identity are classified in the same subfamily, designated by a capital letter (e.g. CYP2C) (Johnson and Stout 2013). Individual proteins in a subfamily are identified by a number (e.g. CYP2C8). A classification of human CYP enzymes based on major substrate class is shown in Table 1.2. It is apparent that enzymes from CYP families 1, 2 and 3 are primarily responsible for the metabolism of drugs and non-drug xenobiotics. Of these, CYP 1A2, 2A6, 2B6,

2C8, 2C9, 2C19, 2D6, 2E1 and 3A4/5 contribute to the hepatic metabolism of over 95% of all drug and non-drug xenobiotic substrates (Backman et al. 2016; Zanger and Schwab 2013).

Table 1.2 Classification of human CYP enzymes based on major substrate class.

Steroids	Xenobiotics	Fatty acids	Eicosanoids	Vitamins	Unknown
1B1 ^a	1A1 ^a	2J2	4F2	2R1 ^a	2A7
7A1 ^a	1A2 ^a	2U1	4F3	24A1	2S1
7B1	2A6 ^a	4A11	4F8	26A1	2W1
8B1	2A13 ^a	4B1	5A1	26B1	4A22
11A1 ^a	2B6 ^a	4F11	8A1 ^a	26C1	4F22
11B1	2C8 ^a	4F12		27B1	4X1
11B2 ^a	2C9 ^a	4V2		27C1	4Z1
17A1 ^a	2C18				20A1
19A1 ^a	2C19 ^a				
21A2 ^a	2D6 ^a				
27A1	2E1 ^a				
39A1	2F1				
46A1 ^a	3A4 ^a				
51A1 ^a	3A5 ^a				
	3A7				
	3A43				

^a X-ray crystal structure(s) reported for human enzyme

Reproduced with permission from Guengerich, FP, Waterman, MR and Egli, M (2016), 'Recent structural insights into cytochrome P450 function', Trends in Pharmacological Sciences, 37 (8): 625-640. Copyright (2016) Elsevier.

1.2.3 Cytochrome P450: membrane topology and structure

The first X-ray crystal structure solved for a CYP enzyme was that of the soluble bacterial camphor monooxygenase from *Pseudomonas putida* (CYP101 or P450cam) (Poulos et al. 1985). Given the difficulties associated with the heterologous expression of a membrane bound CYP protein suitable for crystallisation, the first X-ray crystal structure of a mammalian CYP (*viz.* rabbit CYP2C5) was not solved until fifteen years later (Williams et al. 2000). However, approaches for the modification, expression and crystallisation of microsomal CYP enzymes advanced rapidly after the publication of the CYP2C5 structure (Johnson and Stout 2005), and X-ray crystal structures are now available for more than 20 human CYP proteins, including the major drug metabolising enzymes in CYP families 1, 2 and 3 (see Table 1.3).

An N-terminal leader sequence targets eukaryotic CYP proteins to the membrane (Johnson and Stout 2013). The leader sequence includes a hydrophobic transmembrane helix, which ‘anchors’ the protein to the cytosolic face of the membrane (Figure 1.2). Interactions with largely hydrophobic helices on the surface of microsomal CYP proteins also assist binding to the membrane of the endoplasmic reticulum. As described above, the iron of the heme prosthetic group of CYP enzymes is responsible for mono-oxygenation of the substrate. Substrates bind in the active site cavity above the plane of the heme (Figure 1.3) (Johnson and Stout 2013; Nair, McKinnon and Miners 2016a). Binding of the heme iron atom within the active site occurs by coordination with the thiol (-SH) group of a conserved cysteine. In the case of CYP2C8 (shown in Figure 1.3), and CYP2C9 and CYP2C19, the cysteine at position 435 provides the thiol group for heme binding (Schoch et al. 2004).

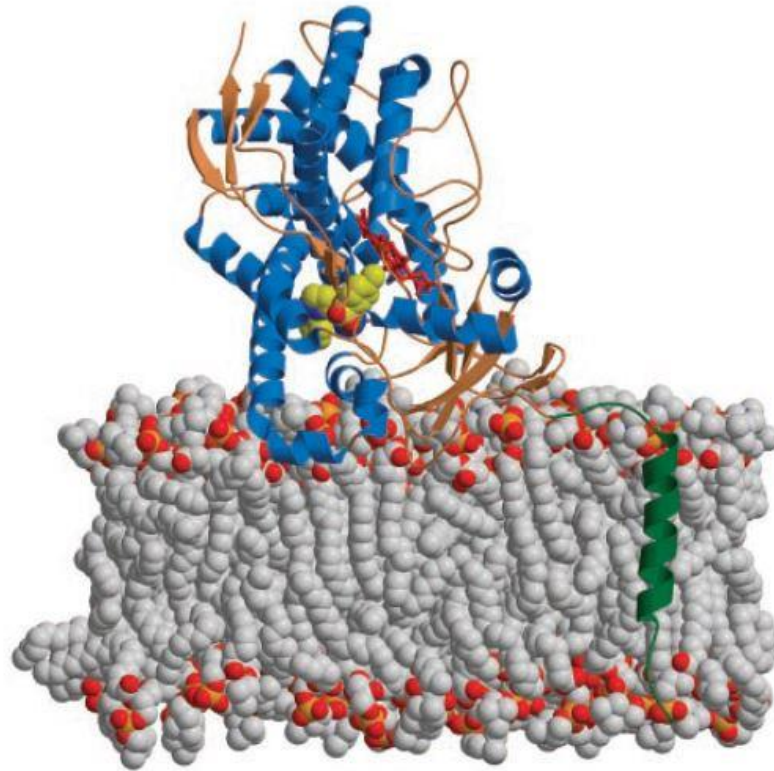


Figure 1.2 Attachment of CYP2C5 to the microsomal membrane.

The N-terminal transmembrane helix is shown in dark green. Carbons of the phospholipid bilayer are illustrated in grey.

Reproduced with permission from Johnson, EF (2003), 'The 2002 Bernard B. Brodie award lecture deciphering substrate recognition by drug-metabolizing cytochromes P450', Drug Metabolism and Disposition, 31 (12): 1532-1540. Copyright (2003) the American Society for Pharmacology and Experimental Therapeutics.

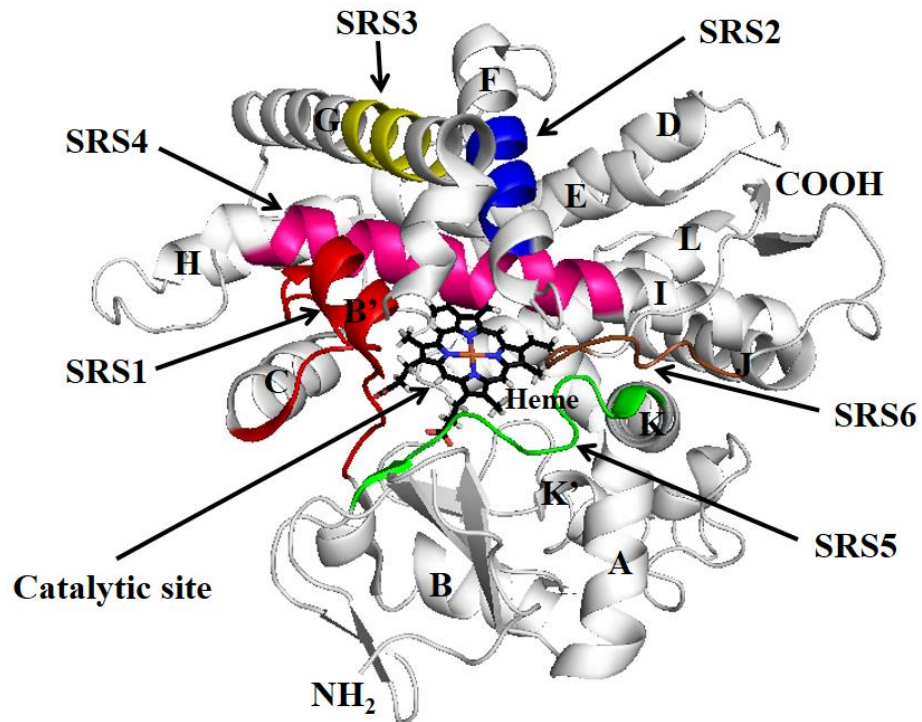


Figure 1.3 X-ray crystal structure of CYP2C8 (PDB - 1PQ2).

Figure modified from Schoch et al. (2004). Arrows point to substrate recognition sites (SRS) and the heme group. Helices are identified by a capital letter and β -sheets by the flat directional arrows (in dark grey). NH_2 shows the N-terminus, and COOH the carboxyl terminus.

The secondary structure and folding pattern of both eukaryotic and prokaryotic CYP proteins are highly conserved. CYP proteins contain twelve helices, designated A to L, and four β -sheets, the latter located near the N-terminus (Figure 1.3) (Johnson and Stout 2013). The heme moiety lies between helix I and helix L. The catalytic domain of CYP enzymes, which comprises approximately 460 residues, resembles a triangular prism (Figure 1.3). Six substrate recognition sites (SRS 1 to 6) identify the active (substrate-binding) site (Gotoh 1992), which, as indicated above, is located above the heme prosthetic group. Greatest amino acid sequence dissimilarity between CYP proteins occurs in the SRSs, which contributes to the different substrate and inhibitor selectivities observed for CYP enzymes (discussed in subsequent sections). Also of importance in this regard, active site volumes vary substantially between CYP proteins, due largely to the flexibility of helices B-C and F-G (Johnson and Stout 2013; Nair, McKinnon and Miners 2016a). For example, the active site volumes of unliganded CYP1A2, CYP2A6 and CYP2E1 range from 190 to 375 \AA^3 (Porubsky, Battaile and Scott 2010; Sansen et al. 2007; Yano et al. 2005), whereas those of unliganded CYP3A4 and CYP2C8 are 950 \AA^3 and 1,438 \AA^3 , respectively (Schoch et al. 2004; Yano et al. 2004). This allows both CYP2C8 and CYP3A4 to metabolise large substrates. For example, paclitaxel (molecular mass 854 Da) is preferentially metabolised by CYP2C8, with a lesser contribution of CYP3A4, while cyclosporine (molecular mass 1,202 Da) is preferentially metabolised by CYP3A4. By contrast, CYP2E1, which has an active site volume of less than 200 \AA^3 in the unliganded state (Porubsky, Battaile and Scott 2010), metabolises small molecules (e.g. benzene, ethanol, enflurane, halothane). The differences that occur in the architectures of the active sites of CYP proteins with respect to shape, size and the physicochemical properties of the amino acids involved in substrate binding, together determine enzyme

substrate and inhibitor selectivity.

However, and as alluded to above, there is increasing evidence demonstrating that CYP proteins are highly flexible or ‘plastic’ (Guengerich, Waterman and Egli 2016; Johnson and Stout 2013; Nair, McKinnon and Miners 2016a). Both X-ray crystal structures with co-crystallised ligand(s) and Molecular Dynamics Simulations (MDS) indicate that expansion of the active site can occur on substrate/inhibitor binding, even to the point of accommodating two substrate molecules. For example, X-ray crystal structures of CYP3A4 demonstrate that the active site volume can increase from 950 Å³ in the unliganded state up to 2,000 Å³ with bound erythromycin (Ekroos and Sjögren 2006; Yano et al. 2004). This adds an additional level of complexity in the understanding of ligand binding.

1.2.4 Substrate selectivities of human cytochrome P450 enzymes

It is believed that CYP enzymes have the capacity to metabolise a vast number of structurally diverse xenobiotics, contributing to the metabolism of approximately 75% of clinical drugs eliminated by biotransformation (Guengerich, Waterman and Egli 2016). This versatility arises from the existence of multiple CYP enzymes. However, as indicated in the previous section, the individual xenobiotic metabolising CYP enzymes exhibit distinct substrate (and inhibitor) selectivities due to the size and architecture of the active site, and the physicochemical properties of the amino acids involved in ligand recognition and binding. Figure 1.4 summarises the contribution of individual CYP enzymes to human drug metabolism. Not surprisingly, given its large, flexible and hydrophobic active site, CYP3A4 (together with the closely related CYP3A5, which shows similar substrate selectivity) is the main enzyme involved human drug metabolism, followed by CYP2C enzymes and CYP2D6.

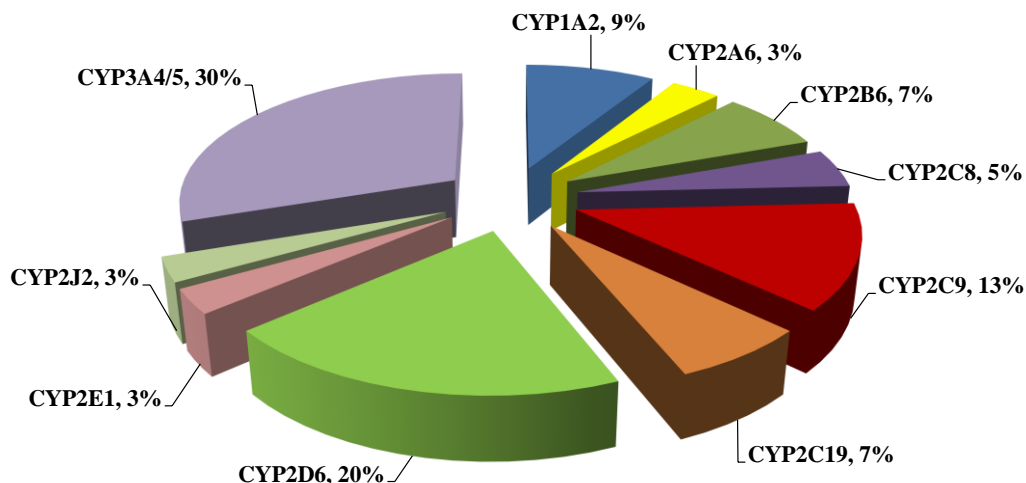


Figure 1.4 Proportion of clinically used drugs metabolised by the individual CYP enzymes.

Adapted with permission from Zanger, UM and Schwab, M (2013), 'Cytochrome P450 enzymes in drug metabolism: Regulation of gene expression, enzyme activities, and impact of genetic variation', Pharmacology and Therapeutics, 138 (1): 103-141. Copyright (2013) Elsevier.

Representative substrates of the individual drug metabolising enzymes are shown in Table 1.3. As discussed previously, the large active sites of CYP2C8 and CYP3A4 are able to accommodate large substrates, and the existence of multiple binding domains within the CYP3A4 active site further increases the scope of substrates metabolised and the ability to simultaneously bind two ligand molecules (Ekroos and Sjögren 2006; Galetin, Clarke and Houston 2002; Kenworthy et al. 2001; Williams et al. 2004b). The nature of the active site also determines the chemical classes of drugs that are metabolised by each enzyme. For example, CYP2C9 preferentially metabolises weakly acidic compounds (Miners and Birkett 1998). Within the CYP2C9 active site, the carboxylate (or other acidic) group on the substrate forms a salt-bridge with Arg108, facilitating substrate binding in a catalytically favourable orientation (Wester et al. 2004). Substrate binding is further stabilised by hydrogen bonding interactions between Arg108 and Asn289 and Asp293, which stabilises the conformation of

Arg108 in the active site. By contrast, the closely related enzyme CYP2C19 lacks the ability to metabolise the characteristically acidic substrates of CYP2C9, even though Arg108 is conserved between the two enzymes. However, CYP2C19 has the hydrophobic Ile instead of the polar Asn at position 289, affecting the conformation of Arg108 adopted in the active site (Reynald et al. 2012). Similarly, while CYP2C8, CYP2C9 and CYP2C19 show high sequence identity, active site volumes differ. The higher active site volume of CYP2C8 (1,438 Å³), which as discussed previously allows the binding of larger substrates, arises from amino acids with smaller side-chain volumes at positions 100, 266 and 476 that serve to ‘open up’ the active site (Reynald et al. 2012).

Although CYP enzymes exhibit distinct substrate preferences, overlap in substrate selectivity is not uncommon. Consequently, multiple enzymes may contribute to the metabolism of a given drug, either along the same or different pathways. For example, while glimepiride 6β- and 7β- hydroxylation are catalysed almost exclusively by CYP2C9, both CYP2C9 and CYP2C19 contribute to tolylmethyl hydroxylation (Elliot et al. 2007). Paclitaxel 6α-hydroxylation, the main clearance pathway, is catalysed by CYP2C8 whereas the 3’-phenyl hydroxylation pathway is mediated by CYP3A4 (Foti and Fisher 2003). These examples also serve to demonstrate that regio- and stereo-selective metabolism may differ between CYP enzymes.

Despite the frequently overlapping substrate selectivity, many metabolic pathways are CYP enzyme selective and this permits certain drugs to be used as substrate ‘probes’ for the investigation of CYP enzyme activity *in vitro* and *in vivo*. For example, caffeine (N3-demethylation) and phenacetin (O-deethylation) (CYP1A2); amodiaquine (N-deethylation) and paclitaxel (6α-hydroxylation) (CYP2C8); losartan (carboxylation), tolbutamide (tolylmethyl hydroxylation) and S-warfarin (6- and 7- hydroxylation)

(CYP2C9); S-mephenytoin (4'-hydroxylation) and omeprazole (5-hydroxylation) (CYP2C19); dextromethorphan (O-demethylation, CYP2D6); and midazolam (1-hydroxylation) and testosterone (6 β -hydroxylation) (CYP3A4/5) may be employed to measure activities of the respective enzymes in HLM and human hepatocytes (Daly, Rettie and Miners 2018; Flockhart 1995; Kronbach et al. 1989; Polasek et al. 2004; Polasek et al. 2006; Tassaneeyakul et al. 1994; Tassaneeyakul et al. 1993; Yu and Haining 2001; Zanger and Schwab 2013). Combinations of a number of these compounds (caffeine – losartan, tolbutamide or warfarin – omeprazole – dextromethorphan - midazolam) are also employed in so-called 'cocktails' to assess factors that influence CYP enzyme activities in humans *in vivo* (Fuhr, Jetter and Kirchheiner 2007).

Table 1.3 Representative substrates of cytochrome P450 enzymes^a.*Adapted from Zanger and Schwab (2013).*

Enzyme	Representative substrates
CYP1A2	Axitinib, caffeine, clozapine, duloxetine, lignocaine, mexiletine, phenacetin, tacrine, theobromine, theophylline, tizanidine
CYP2A6	Coumarin, nicotine
CYP2B6	Bupropion, cyclophosphamide, efavirenz, ifosfamide, ketamine
CYP2C8	Amodiaquine, chloroquine, montelukast, paclitaxel, repaglinide, rosiglitazone (see also Table 1.4)
CYP2C9	Angiotensin II blockers (irbesartan, losartan), NSAIDs (celecoxib, diclofenac, ibuprofen, naproxen, piroxicam), oral hypoglycaemic agents (chlorpropamide, glibenclamide, gliclazide, glipizide, tolbutamide), others (dapson, fluvastatin, phenytoin, toseamide, S-warfarin)
CYP2C19	Proton pump inhibitors (lansoprazole, omeprazole, pantoprazole, rabeprazole), antidepressants (citalopram, sertraline), others (clopidogrel, diazepam, hexobarbitone, mephenytoin, proguanil, voriconazole)
CYP2D6	Antidepressants (amitriptyline, clomipramine, desipramine, fluoxetine, imipramine, nortriptyline, paroxetine, venlafaxine), antipsychotics (risperidone, thioridazine), β -blockers (bufuralol, carvedilol, S-metoprolol, propafenone, timolol), others (codeine, dextromethorphan, ondansetron, perhexiline, tamoxifen, tramadol)
CYP2E1	General anaesthetics (enflurane, halothane, isoflurane, methoxyflurane, sevoflurane), others (benzene, ethanol)
CYP3A4/5	Antiarrhythmics (amiodarone, quinidine), antihistamines (astemizole, chlorpheniramine), antiretrovirals (indinavir, ritonavir, saquinavir), benzodiazepines (alprazolam, midazolam, triazolam), calcium channel blockers (diltiazem, felodipine, nifedipine, nisoldipine, nitrendipine, verapamil), HMG-CoA reductase inhibitors (atorvastatin, lovastatin, simvastatin), immunomodulators (cyclosporine, tacrolimus), macrolide antibiotics (clarithromycin, erythromycin), protein kinase inhibitors (afatinib, crizotinib, dasatinib, erlotinib, gefitinib, ibrutinib, lapatinib, palbociclib, sunitinib, trametinib, vemurafenib, and others), others (antineoplastic vinca alkaloids, carbamazepine, cisapride, methadone, sildenafil)

^a The Table shows the main enzyme involved in the metabolism of the listed drugs. Other CYP enzymes may contribute to a lesser extent.

1.3 Cytochrome P450 2C8 (CYP2C8)

1.3.1 General background

Cytochrome P450 2C8 (CYP2C8) is the P450 enzyme that is the focus of this thesis. CYP2C8 is one of four members of the human CYP2C subfamily, the others being CYP 2C9, 2C18 and 2C19. Except for CYP2C18, the CYP2C proteins are expressed in liver and all contribute to hepatic drug metabolism (see Table 1.3) (Zanger and Schwab 2013). The role of CYP2C8 in xenobiotic metabolism has received increasing attention over the last decade or so and it is now known that CYP2C8 participates in the biotransformation of more than 100 drugs (Rendic and Guengerich 2015; Totah and Rettie 2005; Zanger and Schwab 2013). Despite the fact CYP2C8 shares over 75% amino acid sequence identity with CYP2C9 and CYP2C19 (Johnson et al. 2014), the three enzymes have markedly different (although sometimes overlapping) substrate selectivities (Table 1.3). As alluded to in Section 1.2.4, this may be rationalised in terms of the differences in the active site volumes and architectures of the three proteins. In particular, CYP2C8 has a very large active site (1,438 Å³) with an unusual trifurcated geometry that permits the binding of large and structurally diverse compounds (Schoch et al. 2008; Schoch et al. 2004). Substrates (and inhibitors) may completely (e.g. montelukast) or partially (e.g. troglitazone) occupy the active site cavity (Schoch et al. 2008). Of note, the distal part of the active site contains a number of polar amino acids (Ser, Thr, Asn) that are capable of hydrogen binding to substrates with polar functional groups and this important for the unique ability of CYP2C8 to bind and metabolise glucuronide conjugates (see following section and Chapter 5).

1.3.2 Substrate selectivity

Backman and colleagues (2016) have recently reviewed the xenobiotic substrate selectivity of CYP2C8 in detail. Drugs were classified according to the contribution of CYP2C8 to overall metabolism; major (> 70% contribution of CYP2C8), intermediate (20 – 70% contribution of CYP2C8), and minor (< 20% contribution of CYP2C8). Table 1.4 shows major and intermediate substrates of CYP2C8. As indicated previously, it is apparent that CYP2C8 catalyses the oxidative metabolism of structurally diverse drugs from multiple therapeutic classes. Interestingly, there are relatively few (*viz.* eight) ‘major’ substrates, but many more ‘intermediate’ (*viz.* thirty) and ‘minor’ (*viz.* one hundred and thirty five) substrates. Many drugs metabolised by CYP2C8 are also substrates and inhibitors of CYP3A4/5, an observation first reported by this laboratory (Ong et al. 2000). This is a not an unsurprising finding given the large active sites of both enzymes. By way of example, and as stated in Section 1.2.4, paclitaxel 6 α -hydroxylation, the main clearance pathway, is catalysed by CYP2C8 whereas the 3’-phenyl hydroxylation pathway is mediated by CYP3A4. Importantly, paclitaxel 6 α -hydroxylation is the recommended ‘probe’ substrate and pathway for the assessment of CYP2C8 activity *in vitro* (European Medicines Agency (EMA), 2012; Food and Drug Administration (FDA) 2012), and it has been widely used in reaction phenotyping and DDI studies using HLM and hepatocytes as the enzyme source, for example Foti et al. (2009); Frank and Unger (2006); Kudo et al. (2017); Kudo et al. (2016); Polasek et al. (2004); Sim et al. (2015) and Wattanachai et al. (2011).

Table 1.4 Drugs that are metabolised by CYP2C8 to a major (> 70%) or intermediate (20 – 70%) extent.

Therapeutic class	Drug	Metabolic pathway(s) catalysed by CYP2C8
Antiacne agent	Isotretinoin (13- <i>cis</i> -retinoic acid)	4-hydroxylation
Antianemic agent	Daprodustat*	N/A
Antiarrhythmic agents	Amiodarone	N-deethylation
Antiasthmatic agents	Montelukast*	36-hydroxylation (M6), 25-hydroxylation (M3), M4 formation
	Olodaterol	O-deethylation
	Vidupiprant	t-butyl hydroxylation (M2), cyclopropyl hydroxylation (M3)
Anticancer agents	Enzalutamide*	Hydroxylation (M6) N-demethylation (M2)
	9cUAB30	M1-M5 formation
	Dabrafenib	Hydroxylation
	Fenretinide	4'-hydroxylation, 4'-oxidation
	Imatinib	N-demethylation
	Irosustat	M9 and M13 formation
	Paclitaxel	6 α -hydroxylation
	Tazarotenic acid	Sulfoxidation
	Tozasertib	N-demethylation
Antidepressant agents	R/S-Fluoxetine	N-demethylation
Antidiabetic agents	Pioglitazone*	Hydroxylation (M-IV, III and XI)
	Repaglinide*	M4, M2, M1 and M0-OH formation
	Rosiglitazone	p-hydroxylation, N-demethylation
	Troglitazone	Quinone metabolite formation
	R483	M1 and M4 formation

Table 1.4 Drugs that are metabolised by CYP2C8 to a major (> 70%) or intermediate (20 – 70%) extent (cont.).

Therapeutic class	Drug	Metabolic pathway(s) catalysed by CYP2C8
Antihypertensive agents	Treprostinil	N/A
	R/S-Verapamil	N-dealkylation, N-demethylation, O-demethylation
Anti-inflammatory agents	R-Ibuprofen	2-hydroxylation, 3-hydroxylation
Antimalarial agents	Amodiaquine*	N-deethylation
	Chloroquine	N-deethylation

*Major contribution of CYP2C8 to metabolism (> 70%)

N/A, not available

Adapted with permission from Backman, JT, Filppula, AM, Niemi, M and Neuvonen, PJ (2016), 'Role of cytochrome P450 2C8 in drug metabolism and interactions', Pharmacological Reviews, 68 (1): 168-241. Copyright (2016) the American Society for Pharmacology and Experimental Therapeutics. Some of the data included in the original table was obtained from the University of Washington Metabolism and Transport Drug Interaction Database (accessed May – September, 2015).

Of particular relevance to this thesis, CYP2C8 has the capacity to metabolise the glucuronide conjugates of several drugs (Backman et al. 2016; Ma et al. 2017). The ability of CYP2C8 to metabolise glucuronide conjugates was first identified in 2002 when Kumar et al. described the CYP2C8 catalysed 4'-hydroxylation of diclofenac acyl glucuronide (Kumar et al. 2002). Since that time, it has additionally been demonstrated that CYP2C8 metabolises the following glucuronides: clopidogrel acyl glucuronide (site of metabolism not identified) (Tornio et al. 2014); desloratadine N-glucuronide (3-hydroxylation) (Kazmi et al. 2015a); estradiol 17- β -glucuronide (2-hydroxylation); gemfibrozil acyl glucuronide (benzylic oxidation) (Ogilvie et al. 2006); licofelone acyl glucuronide (6-methyl hydroxylation) (Albrecht et al. 2008); Lu AA34893 carbamoyl glucuronide (site of metabolism not identified) (Kazmi et al. 2010); MRL-C acyl glucuronide (hydroxylation, position not identified); and sipoglitazar acyl glucuronide (O-dealkylation) (Nishihara et al. 2012). The structural features of CYP2C8 that confer the binding of glucuronide conjugates are discussed in detail in Chapter 5. Importantly, and as discussed subsequently (Section 1.7.3 and Chapter 5), several glucuronides (e.g. clopidogrel and gemfibrozil acyl glucuronides) are potent mechanism-based inhibitors of CYP2C8 (Ogilvie et al. 2006; Tornio et al. 2014).

1.4 UDP-Glucuronosyltransferases (UGTs)

1.4.1 The glucuronidation reaction

Glucuronidation refers to the covalent linkage (or conjugation) of an acceptor functional group on the substrate (or aglycone) with glucuronic acid, which is derived from the co-factor UDP-glucuronic acid (abbreviated as UDP-GA or UDP-GlcUA) (Miners and Mackenzie 1991; Radomska-Pandya et al. 1999). UDP-GA is biosynthesised from α -D-glucose 1-phosphate in a two stage pathway sequentially involving UDP-glucose pyrophosphorylase and UDP-glucose dehydrogenase (Dutton 1980) which results in oxidation of the $-\text{CH}_2\text{-OH}$ group at position 6 to form the corresponding carboxylic acid ($-\text{COOH}$). The glucuronidation reaction follows a second order nucleophilic substitution ($\text{S}_{\text{N}}2$) mechanism (Figure 1.5). Thus, there is inversion of configuration of the anomeric C1 atom of resulting in the formation of a β -D-glucuronide conjugate (Figure 1.5). Glucuronidation reactions are catalysed by UGT; there are no known examples of 'spontaneous' non-enzymatic glucuronidation. An N-terminal domain His that is conserved in most UGT enzymes functions as the catalytic base in glucuronidation reactions that require deprotonation of the acceptor functional group (Radomska-Pandya et al. 1999 and subsequent discussion).

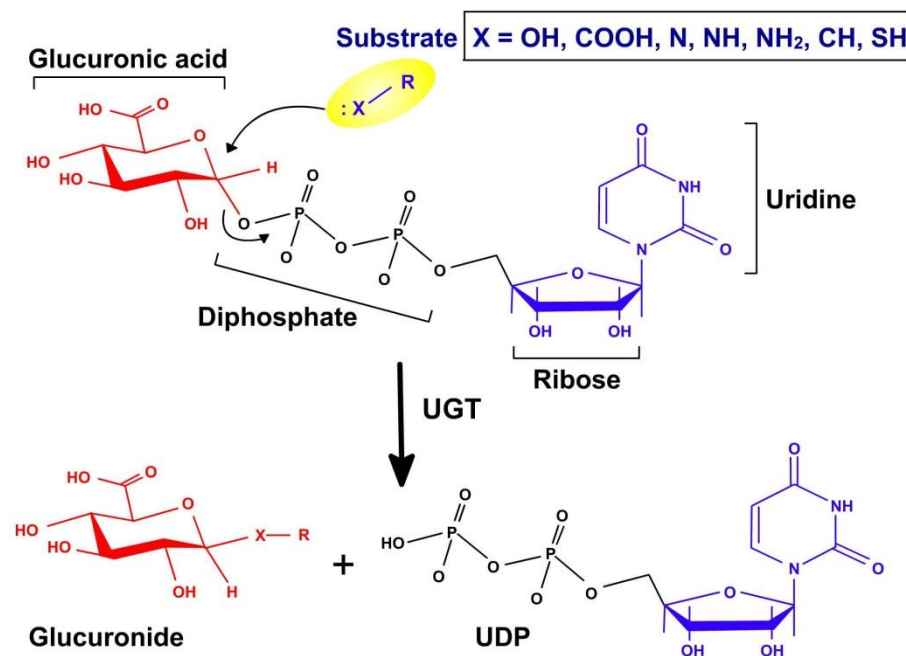


Figure 1.5 The glucuronidation reaction.

Reproduced with permission from Zhou, J and Miners, JO (2014), 'Enzyme kinetics of uridine diphosphate glucuronosyltransferases (UGTs)', In *Enzyme Kinetics in Drug Metabolism: Fundamentals and Applications*, eds S Nagar, UA Argikar and DJ Tweedie, Chapter 11: 203-228, Humana Press, New Jersey. Copyright (2014) Springer Nature.

Compounds that are glucuronidated are typically lipophilic but, as shown in Figure 1.5, necessarily contain a nucleophilic acceptor functional group. Functional groups that are glucuronidated include hydroxyl (aliphatic and phenolic), carboxylate, amine (primary, secondary, tertiary and aromatic N-heterocyclic), and thiol (Foti and Fisher 2012; Radomska-Pandya et al. 1999; Rowland, Miners and Mackenzie 2013; Tukey and Strassburg 2000). Interestingly, compounds with an 'acidic' carbon atom (e.g. a C-H bond adjacent to electron withdrawing groups) may also undergo glucuronidation, as occurs with phenylbutazone and sulfinpyrazone (Kerdpin et al. 2006). Since many drugs contain a hydroxyl, carboxylate or amine group, glucuronidation is a common metabolic pathway in drug metabolism. In terms of scope of metabolism, UGT is the second most important drug metabolising enzyme after CYP and contributes to the metabolism of drugs from almost all therapeutic classes (e.g. analgesics, anticancer

drugs, anticoagulants, anticonvulsants, antidepressants, antihypertensives, antimicrobials, diuretics, hypnotic-anxiolytic agents, hypolipidaemic agents, NSAIDs, uricosuric agents, etc) (Foti and Fisher 2012; Kiang, Ensom and Chang 2005; Miners and Mackenzie 1991; Stingl et al. 2014). In addition, UGT metabolises a large number of non-drug xenobiotics (dietary chemicals (e.g. flavonoids) and environmental contaminants, including some carcinogens (e.g. nitrosamines, hydroxylated polycyclic aromatic hydrocarbons) as well as endogenous compounds (e.g. bilirubin, steroid hormones (e.g. testosterone and estradiol), serotonin, and fatty acids and eicosanoids (e.g. arachidonic acid and 20-HETE)) (Foti and Fisher 2012; Hu et al. 2016; Tukey and Strassburg 2000). Further, UGT metabolises the hydroxylated and carboxylated products from functionalisation reactions, a property that was instrumental in the development of the concept of 'Phase I' and 'Phase II' metabolism (Josephy, Guengerich and Miners 2005).

Glucuronidation is normally considered a 'detoxification' reaction. Although most glucuronides lack biological activity, there are examples of drug glucuronides that are pharmacologically or toxicologically active. Morphine 6-glucuronide is a potent opioid μ -receptor agonist that contributes significantly to analgesia in patients administered morphine (Osborne et al. 1990), while morphine 3-glucuronide is believed to contribute to the excitatory effects of morphine (Milne, Nation and Somogyi 1996). With respect to toxicity, several carboxylic acid-containing drugs (NSAIDs) form inherently reactive acyl glucuronides, which may form adducts with intra- and extra-cellular proteins (Regan et al. 2010). Furthermore, not all glucuronides are not metabolically inert, as originally believed. As discussed in Section 1.3.2, several glucuronide conjugates serve as substrates for CYP2C8.

1.4.2 UDP-Glucuronosyltransferase heterogeneity and nomenclature

Like CYP, and consistent with its substrate diversity, UGT exists as an enzyme superfamily (Mackenzie et al. 2005; Miners et al. 2004; Rowland, Miners and Mackenzie 2013). The broader human UDP-glycosyltransferase family (also abbreviated UGT) contains 22 genes that encode active proteins. As described previously for CYP, the UGTs are classified into families and subfamilies based on amino sequence identity (which reflects divergent evolution) (Mackenzie et al. 2005; Mackenzie, Gardner-Stephen and Miners 2010). Enzymes sharing $\geq 45\%$ sequence identity are classified in the same family (designated by an Arabic numeral), and enzymes sharing $\geq 60\%$ sequence identity are classified in the same subfamily (designated by a capital letter). For example, UGT1A1 is the first member of UGT family 1, subfamily A. Human UGTs are classified in four families (1, 2, 3 and 8) and five subfamilies (1A, 2A, 2B, 3A and 8A) (Figure 1.6).

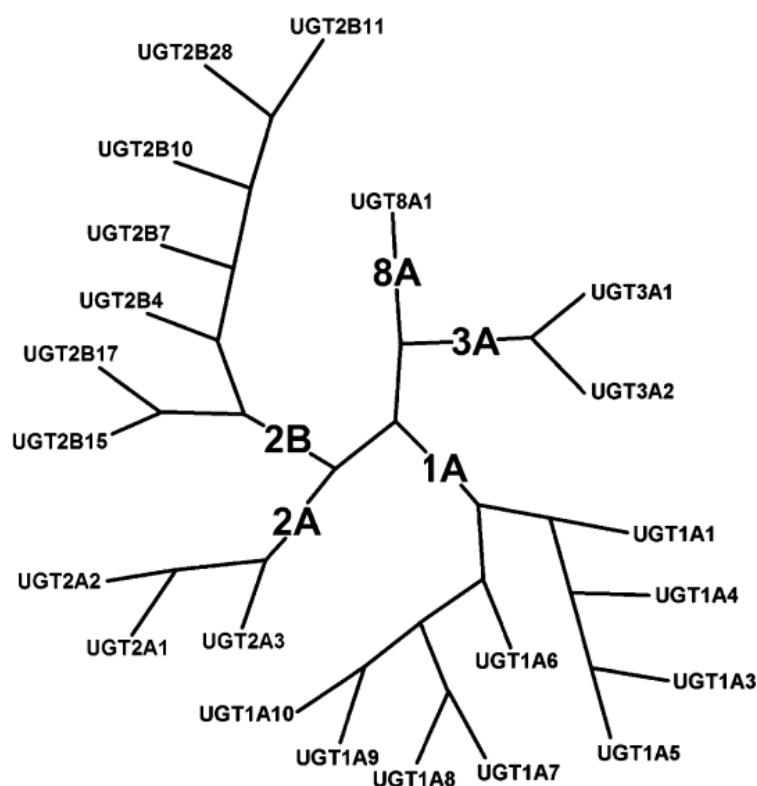


Figure 1.6 Dendrogram showing relationships between human UGT families based on the similarity of amino acid sequence.

Reproduced with permission from Rowland, A, Miners, JO and Mackenzie, PI (2013), 'The UDP-glucuronosyltransferases: Their role in drug metabolism and detoxification', The International Journal of Biochemistry and Cell Biology, 45 (6): 1121-1132. Copyright (2013) Elsevier.

The human UGT family 1, 2, 3 and 8 genes are located on chromosomes 2q37, 4q13, 5p13.2 and 4q26, respectively (Mackenzie et al. 2005). The UGT1 gene locus is shown in Figure 1.7. The individual UGT1A proteins are encoded by a transcript generated from splicing a unique first exon (A1, A3, A4, A5, A6, A7, A8, A9 or A10) to four downstream exons (Mackenzie et al. 2005). The unique first exon encodes the N-terminal domain of 285 to 289 amino acids, while the common exons (2 to 5) encode an identical C-terminal domain of 246 residues. The five unique A2P, A11P, A12P and A13P exons do not express active protein and are designated as pseudogenes. Exon sharing similarly occurs with the UGT2A1 and UGT2A2 genes, but UGT2A3, all UGT2B enzymes, and UGT 3A1, 3A2 and 8A1 are encoded by discrete genes of five to seven exons (Mackenzie et al. 2005; Mackenzie, Gardner-Stephen and Miners 2010). These UGTs therefore show differences in amino acid sequence across the entire protein. Five UGT2B pseudogenes have been identified; 2B24P, 2B25P, 2B26P, 2B27P and 2B29P.



Figure 1.7 UGT1A exon arrangement.

Reproduced with permission from Mackenzie, PI, Bock, KW, Burchell, B, Guillemette, C, Ikushiro, S-i, Iyanagi, T, Miners, JO, Owens, IS and Nebert, DW (2005), 'Nomenclature update for the mammalian UDP glycosyltransferase (UGT) gene superfamily', Pharmacogenetics and Genomics, 15 (10): 677-685. Copyright (2005) Wolters Kluwer Health, Inc.

Enzymes of the UGT 1A, 2A and 2B subfamilies primarily utilise UDPGA as the cofactor, that is catalyse glucuronidation reactions (Meech et al. 2012). In contrast, UGT3A1 and UGT3A2 catalyse glucosidation, galactosidation and/or N-

acetylglucosamination reactions using UDP-glucose (UDP-Glc), UDP-galactose and UDP-N-acetylglucosamine as the respective cofactors (Mackenzie et al. 2011; Mackenzie et al. 2008). Available evidence indicates that UGT8A1 functions exclusively as a UDP-galactose ceramide galacosyltransferase and, like the UGT3A enzymes, appears not to have a significant role in drug metabolism (Meech et al. 2012). Although, as indicated above, the main function of UGT 1A, 2A and 2B enzymes is glucuronidation, several enzymes also have the ability to catalyse other glycosidation reactions (see Meech et al. 2012 for a summary). By way of example, UGT2B7 catalyses both the glucuronidation and glucosidation of several compounds, including morphine (Chau et al. 2014). However, glucuronidation dominates over glucosidation because UDPGA has a higher binding affinity (lower K_m) than UDP-Glc.

1.4.3 UDP-Glucuronosyltransferase tissue expression and membrane topology

As discussed in Section 1.1, most UGT enzymes are expressed in the liver; UGT 1A5, 1A7, 1A8, 1A10, 2B11 and 2A1 are the only family 1 and 2 enzymes that are not expressed in this organ (Court et al. 2012; Rowland, Miners and Mackenzie 2013). Of the hepatic enzymes, mRNA expression levels differ markedly, although relationships between mRNA expression and activity appear not have been characterised (Rowland, Miners and Mackenzie 2013). Human liver microsomal UGT 1A1, 1A3, 1A4, 1A6, 1A9, 2B4, 2B7 and 2B15 protein contents have been quantified by liquid chromatography – mass spectrometry (Achour et al. 2017; Fallon et al. 2013). As with mRNA expression, wide inter-liver variability in protein expression is observed. UGT protein abundances measured using stable-isotope labelled peptides correlated reasonably well with activities, with r^2 values ranging from 0.34 to 0.79. Interestingly, the correlations were generally poorer than abundance – activity relationships reported for UGT proteins expressed in kidney (Knights et al. 2016a). It is noteworthy,

however, that hepatic UGT enzyme abundance data varied substantially between proteomic studies and this may lead to spurious abundance – activity relationships (Achour et al. 2017; Fallon et al. 2013).

UGT 1A7, 1A8 and 1A10 are mainly expressed in the gastrointestinal tract (small intestine, colon and, to a lesser extent, stomach) and may therefore contribute to pre-hepatic metabolism, although there appears to be no data supporting a role of these enzymes in the pre-hepatic metabolism of specific drugs *in vivo*. Real-time PCR data suggests that almost all of the hepatically expressed enzymes of the 1A and 2B subfamilies (*viz.* 1A1, 1A3, 1A4, 1A6, 1A9, 2B4, 2B7, 2B15 and 2B17) additionally occur in the gastrointestinal tract (Rowland, Miners and Mackenzie 2013). Despite identification of mRNA transcripts for numerous UGT enzymes in human kidney, recent proteomic data indicates that UGT 1A6, 1A9 and 2B7 are the only renally-expressed proteins (Knights et al. 2016a; Margaillan et al. 2015). These data are consistent with the generally held view that mRNA is not necessarily predictive of protein expression. Mean contents of UGT1A6, UGT1A9 and UGT2B7 in human kidney were reported as 4.7, 61.3 and 37.6 pmol/mg protein, respectively (Knights et al. 2016a). *In vitro* – *in vivo* extrapolation suggests that the kidney may contribute significantly to the systemic clearances of UGT1A9 substrates (Gill, Houston and Galetin 2012; Knights et al. 2016a; Scotcher et al. 2017). More broadly, UGT 1A6, 1A9 and 2B7 may all modulate the intra-renal exposure and response to drugs and physiological mediators (e.g. arachidonic acid) that are metabolised by these enzymes (Miners et al. 2017b). mRNA expression suggests that UGT 1A and 2B subfamily enzymes are variably expressed in numerous other tissues, including adrenals, bladder, brain, breast, lung, ovary, placenta, prostate, testes and thyroid, (Court et al. 2012; Ohno and Nakajin 2009). Paradoxically, real time PCR failed to detect expression of

UGT2B11, an enzyme of unknown function, in any tissue (Ohno and Nakajin 2009).

As noted previously, UGT3A1 and UGT3A2 catalyse glycosidation reactions other than glucuronidation. Reverse transcription PCR identified UGT3A1 expression in liver and kidney, and UGT3A2 expression in the kidney, testis and thymus (Mackenzie et al. 2011; Mackenzie et al. 2008).

Available evidence indicates that UGT proteins are localised in the smooth endoplasmic reticulum of cells, with the majority of the protein protruding into the lumen (Radomska-Pandya et al. 1999; Rowland, Miners and Mackenzie 2013). The currently accepted topology model is shown in Figure 1.8. It has also been suggested that some UGTs may occur in the nuclear compartment of cells, but this may represent an experimental artefact since the outer nuclear membrane is continuous with the smooth endoplasmic reticulum. UGT proteins are targeted to the endoplasmic reticulum by an N-terminal signal peptide of 25 amino acids, which is cleaved following insertion into the membrane to produce a mature protein of approximately 500 residues (Mackenzie and Owens 1984). The UGT protein is anchored to the endoplasmic reticulum by a conserved lipophilic 17 amino acid transmembrane domain and via a hydrophobic interaction with a second region of the lumenally oriented protein (Mackenzie and Owens 1984; Miners et al. 2004) (Figure 1.8). Given the luminal orientation of UGT proteins, access of the charged cofactor (UDPGA) required for glucuronidation reactions is facilitated by transport proteins. Kinetic studies indicate the involvement of two UDPGA transporters; a high affinity, low capacity transporter and a low affinity, high capacity transporter (Rowland, Mackenzie and Miners 2015). Transfer of substrate (the aglycone) into the lumen presumably occurs mainly by passive diffusion, although transporters are likely to be involved in the uptake of more polar compounds. Similarly, efflux of glucuronide conjugates from

the luminal compartment presumably involves transporters, but these are yet to be identified definitively.

As a result of the luminal orientation of the enzyme active site, UGT activity studies with microsomes as the enzyme source require microsomal ‘activation’ for optimal glucuronidation activity. Activation may be achieved by physical disruption (e.g. sonication) or treatment with a detergent or alamethicin (Boase and Miners 2002; Kilford et al. 2009; Knights et al. 2016a; Miners 2002; Walsky et al. 2012). Detergents disrupt the microsomal membrane facilitating entry of UDPGA, however, careful optimisation of the detergent concentration is required to avoid disruption of the UGT – membrane interaction and subsequent loss of activity (Miners et al. 1990). By contrast, alamethicin is a pore-forming agent that appears to minimally affect the UGT – membrane interaction (Boase and Miners 2002; Fisher et al. 2000). Furthermore, alamethicin treatment of HLM appears to not affect CYP enzyme activity detrimentally (Fisher et al. 2000).

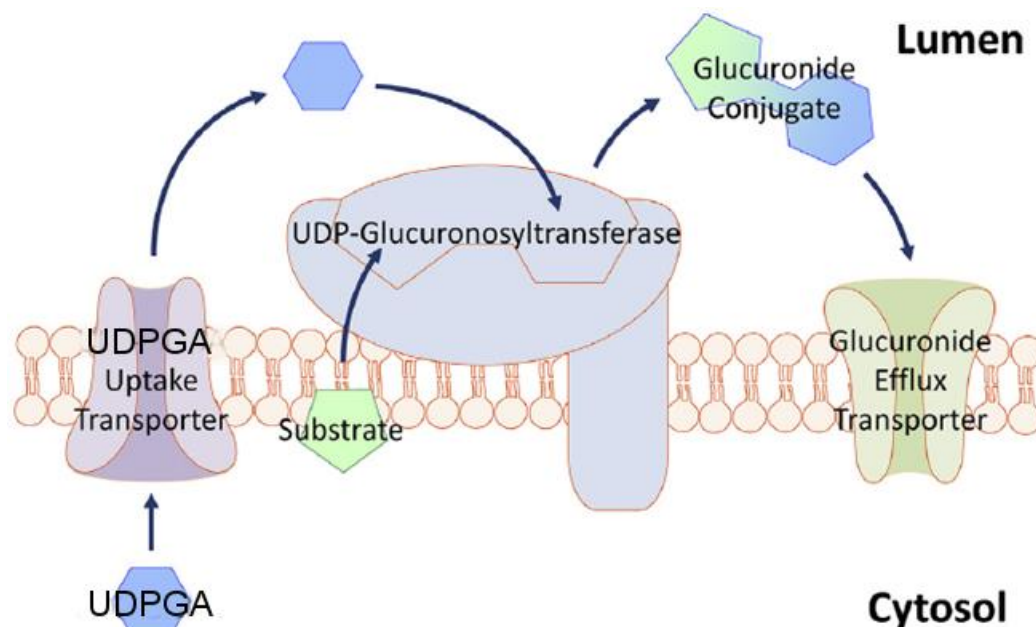


Figure 1.8 UDP-Glucuronosyltransferase topology model.

Reproduced with permission from Rowland, A, Miners, JO and Mackenzie, PI (2013), 'The UDP-glucuronosyltransferases: Their role in drug metabolism and detoxification', *The International Journal of Biochemistry and Cell Biology*, 45 (6): 1121-1132. Copyright (2013) Elsevier.

1.4.4 UDP-Glucuronosyltransferase structure-function

In comparison to cytochrome P450, knowledge of UGT structure-function is less advanced, mainly due to the lack of a full length UGT protein X-ray crystal structure. However, it is widely accepted that UDPGA binding occurs in a conserved region of the C-terminal domain, while substrate (aglycone) binding occurs in the N-terminus of UGT proteins (Mackenzie, Gardner-Stephen and Miners 2010). The so-called cofactor binding signature sequence occurs between positions 354 - 357 and 397 - 400 of human UGT 1A, 2A and 2B proteins (Figure 1.9) (Nair et al. 2015). Residues within the signature sequence differentially interact with the phosphate groups and the uracil, ribose and sugar rings of the UDP-sugars that act as cofactors for glycosidation reactions catalysed by human UGT 1, 2, 3 and 8 family enzymes (Nair et al. 2015).

Despite the lack of an X-ray crystal structure for a full-length human UGT protein, Miley et al. (2007) reported a crystal structure for the C-terminal domain (residues 285 - 451) of UGT2B7. Although it was not possible to co-crystallise the C-terminal domain of UGT2B7 and UDPGA, the cofactor docked well within the signature sequence region of the crystal structure (Miley et al. 2007). The partial UGT2B7 X-ray crystal structure has proved valuable for generating homology models to explore the interactions of different UDP-sugars with human UGT proteins (for example: Chau et al. 2014; Nair et al. 2015). Experimental evidence further supports the involvement of the C-terminal domain in cofactor but not aglycone binding. For example, exchanging 232 residues of the C-terminal domains of the rat enzymes UGT2B2 and UGT2B3 provided active enzymes with unaltered substrate selectivities (Mackenzie 1990). Broadly similar results were obtained when 230 residues of the C-terminal domains of the human enzymes UGT2B4 and UGT2B7 were exchanged (Ritter et al. 1992).

```

UGT1A1  354WLPQNDLLGHPMTRAFITHAGSHGVYESICNGVPMVMMPLFGDQ397
UGT2A1  354WIPQNDLLGHPKTKAFITHGGTNGIYEAIYHGVPVMGVPMFADQ397
UGT2A3  354WIPQNDLLGHPKTKAFITHGGMNGIYEAIYHGVPVMGVPIFGDQ397
UGT2B4  356WIPQNDLLGHPKTRAFITHGGANGIYEAIYHGIPMVGVPPLFADQ399
UGT2B7  356WIPQNDLLGHPKTRAFITHGGANGIYEAIYHGIPMVGIPPLFADQ399
UGTB10  355WIPQNDLLGHPKTRAFITHGGANGIYEAIYHGIPMVGIPPLFFDQ398
UGTB11  356WIPQNDLLGHPKTRAFITHGGANGIYEAIYHGIPMVGIPPLFFDQ399
UGTB15  357WLPQNDLLGHPKTKAFITHGGTNGIYEAIYHGIPMVGIPPLFADQ400
UGTB17  357WLPQNDLLGHPKTKAFITHGGTNGIYEAIYHGIPMVGIPPLFADQ400
UGTB28  356WIPQNDLLGLPKTRAFITHGGANGIYEAIYHGIPMVGIPPLFWDQ399
UGT3A1  351WLPQSDLLAHPsirLfvTHGGQNSVMEAIRHGVPMVGLPVNGDQ394
UGT3A2  351WLPQSDLLAHPsirLfvTHGGQNSIMEAIQHGVPMVGIPPLFGDQ394
UGT8A1  340WLPQNDLLGHskIKaFLSHGGLNSIFETIYHGVPVVGIPPLFGDH383

```

Figure 1.9 Signature sequence of human UDP-glucuronosyltransferase enzymes.

Only the sequence for UGT1A1 is shown since all UGT1A enzymes share an identical C-terminal domain, as do UGT2A1 and UGT2A2.

Reproduced with permission from Nair, PC, Meech, R, Mackenzie, PI, McKinnon, RA and Miners, JO (2015), 'Insights into the UDP-sugar selectivities of human UDP-glycosyltransferases (UGT): A molecular modeling perspective', Drug Metabolism Reviews, 47 (3): 335-345. Copyright (2015) Taylor & Francis.

Just as it is accepted that the C-terminal domain of UGT proteins is associated with cofactor binding, there is overwhelming evidence showing that aglycone binding occurs in the N-terminal half of UGT proteins. The notion that aglycone binding occurs in the N-terminal domain also follows logically from the fact that the sequences of the C-terminal half of UGT1A proteins are identical. If aglycone binding occurred in the C-terminal domain of UGT1A enzymes it would be expected that they would have identical or very similar substrate selectivities, which is not the case (see following section). Sequence dissimilarity is also greater in the N-terminal domain (compared to the C-terminal domain) of UGT2B proteins (Mackenzie et al. 2005), and chimeragenesis studies have linked aglycone binding to the N-terminal domain of UGT2B enzymes. As indicated above, exchanging the C-terminal domains of UGT2B2 and UGT2B3 and of UGT2B4 and UGT2B7 did not alter substrate selectivity (Mackenzie 1990; Ritter et al. 1992). Further, a UGT2B7-15-7 chimera that

incorporated residues 61 to 194 of UGT2B15 exhibited the characteristic substrate selectivity of UGT2B15 while lacking activity towards UGT2B7 substrates (Lewis et al. 2007). Exchanging the first 44 residues of UGT1A3 and UGT1A4 similarly demonstrated that this region determined the differing substrate selectivities of these enzymes (Kubota et al. 2007), which is discussed further below.

In addition to the data from chimeragenesis experiments, site-directed mutagenesis has been employed to identify individual N-terminal amino acids that influence the substrate selectivities of numerous human UGT enzymes (Barre et al. 2007; Dubois et al. 1999; Fujiwara et al. 2009; Kerdpin et al. 2009; Korprasertthaworn et al. 2012; Kubota et al. 2007; Martineau, Tchernof and Bélanger 2004; Xiong et al. 2006). By way of example, the Ser121Tyr substitution in UGT2B17 abolishes androsterone 3 α -glucuronidation, but not the 17 β -glucuronidation of dihydrotestosterone and testosterone (Dubois et al. 1999). Substrate-dependent effects have also been demonstrated for mutations at positions 33 and 37 of UGT1A9 (Korprasertthaworn et al. 2012).

Although UGT1A3 and UGT1A4 share 93.4% sequence identity, they exhibit markedly different substrate selectivities. UGT1A4 is just one of two enzymes, the other being UGT2B10, that glucuronidates tertiary amines to form a quaternary ammonium glucuronide, while lacking the ability to glucuronidate planar phenols such as 4-methylumbelliferone (4MU) and 1-naphthol (1NP). Conversely, UGT1A3 has the capacity to glucuronidate 4MU and 1NP, but not tertiary amines. As noted above, the unique substrate selectivities of these two enzymes were shown to be associated with the first 44 residues (Kubota et al. 2007). Site-directed mutagenesis demonstrated that Pro-40 of UGT1A4 was essential for the N-glucuronidation of the tertiary amines lamotrigine and trifluoperazine, while His-40 of UGT1A3 was important for planar

phenol glucuronidation (Kubota et al. 2007). The His residue that occurs at position 40 of UGT1A3 is conserved in all UGT1A and UGT2B proteins except UGT1A4 and UGT2B10; the latter has a Leu at position 34, which aligns with position 40 of UGT1A4. Substitution of the conserved His of UGT 1A1, 1A6 and 1A9 with Pro resulted in enzymes that glucuronidated lamotrigine, but planar phenol glucuronidation was abolished (Kerdpin et al. 2009). Conversely, substitution of Leu-34 of UGT2B10 with His conferred the ability to glucuronidate 4MU and 1NP (Kerdpin et al. 2009). These observations are consistent with the hypothesis that the conserved N-terminal His acts as the catalytic base necessary for proton abstraction in the glucuronidation of hydroxyl-containing substrates and presumably primary and secondary amines (Radomska-Pandya et al. 1999). The mechanism by which Pro-40 of UGT1A4 and Leu-34 of UGT2B10 facilitate tertiary amine glucuronidation, which does not involve proton abstraction, is unknown. Taken together, however, the chimeragenesis and site-directed mutagenesis data indicate that, as with cytochrome P450, individual amino acids can play an essential role in UGT-catalysed glucuronidation, either through involvement in the catalytic mechanism or in substrate binding.

1.4.5 UDP-Glucuronosyltransferase enzyme substrate selectivity

Hepatically-expressed UGT 1A and 2B subfamily enzymes are the focus of the glucuronidation studies performed in this thesis, as these are of greatest importance in human drug metabolism. Most UGT 1A and 2B subfamily enzymes have the capacity to glucuronidate low molecular weight phenols, such as 4MU and 1NP (Uchaipichat et al. 2004). Indeed, only UGT 1A4 and 2B10 (see preceding section) lack activity towards these compounds, while UGT 2B4 and 2B28 exhibit relatively low activity (Lévesque et al. 2001; Uchaipichat et al. 2004). However, enzyme substrate selectivity

increases with structural complexity, presumably due to steric, electrostatic, and hydrophobic interactions (Miners, Mackenzie and Knights 2010a). Except for tertiary amine glucuronidation by UGT1A4 and UGT2B10 and the apparently unique ability of UGT1A9 to glucuronidate compounds with an acidic carbon atom (namely the acidic carbon atom of the pyrazolidene ring of phenylbutazone and sulfinpyrazone (Kerdpin et al. 2006)), the chemical nature of the nucleophilic acceptor functional group appears not to be a major determinant of enzyme substrate selectivity. As described above, most UGTs are able to metabolise phenols (and aliphatic alcohols), and several UGTs (e.g. UGT 1A1, 1A3, 1A9 and 2B7) glucuronidate carboxylic acids, which are typically charged at physiological pH. Pharmacophore models suggest that the chemical environment adjacent to the site of glucuronidation influences enzyme selectivity (Sorich et al. 2004).

Table 1.5 summarises the substrate selectivities of the major drug-metabolising human UGTs (Foti and Fisher 2012; Kiang, Ensom and Chang 2005; Miners and Mackenzie 1991; Miners, Mackenzie and Knights 2010a; Stingl et al. 2014).

Table 1.5 Representative substrates of human UGT enzymes.

UGT	Representative substrates
UGT1A1	Bilirubin, β -estradiol, ethinylestradiol, etoposide, niflumic acid, raloxifene, raltegravir, SN-38 (the active metabolite of irinotecan), tranilast
UGT1A4	Amitriptyline, 1-hydroxymidazolam, lamotrigine, olanzapine, posaconazole, trifluoperazine (all N-glucuronidation)
UGT1A6	Deferiprone, paracetamol, serotonin
UGT1A9	Canagliflozin, dapagliflozin, edaravone, frusemide, mycophenolic acid, NSAIDs ^a , phenylbutazone, propofol, regorafenib, retigabine, sorafenib, sulfinpyrazone
UGT2B7	Aldosterone, chloramphenicol, clofibric acid, codeine, dimethylxanthene-4-acetic acid, efavirenz, epirubicin, gemfibrozil, morphine, naloxone, NSAIDs ^a (e.g. diclofenac, flurbiprofen, indomethacin, ketoprofen, naproxen), PR-104A, valproic acid, zidovudine
UGT2B15	Lorazepam, phenolphthalein, S-oxazepam, sipoglitazar, temazepam
UGT2B17	Testosterone, dihydrotestosterone, vorinostat

^a *The acyl glucuronidation of most NSAIDs, and some other carboxylic acids (e.g. clofibric acid, gemfibrozil), by HLM exhibits high- and low- affinity components. UGT2B7 is generally the enzyme responsible for the high affinity reaction, while UGT1A9 is frequently responsible for the low affinity reaction, although there are exceptions (Miners, Mackenzie and Knights 2010a).*

Other hepatically-expressed UGTs are also known to contribute to drug glucuronidation. Early studies suggested that UGT1A3 and UGT1A4 share overlapping substrate selectivities with respect to amine-containing compounds (Green and Tephly 1998). However, while it appears that UGT1A3 is able to glucuronidate primary amines (Green et al. 1998), a later investigation demonstrated that this enzyme lacks activity towards tertiary amines (Kubota et al. 2007). It should be noted that many of the early studies characterising UGT enzyme substrate selectivity typically employed a non-specific radiometric TLC assay for the

measurement of glucuronide formation, which probably accounts for the discrepancies between the earlier and more recent studies that utilise HPLC and LC-MS for metabolite identification and quantification. Other drugs glucuronidated by UGT1A3 include fimasartan and telmisartan (Jeiri et al. 2011; Jeong et al. 2015). It has also been reported that UGT1A3 exhibits low activity towards several carboxylic acid-containing drugs (Kiang, Ensom and Chang 2005).

As indicated previously, UGT2B10, like UGT1A4, catalyses the N-glucuronidation of aliphatic tertiary amines to form a quaternary ammonium glucuronide. UGT2B10 also glucuronidates substrates with an aromatic N-heterocyclic group (Kaivosaaari, Finel and Koskinen 2011). The role of UGT2B10 in drug and chemical metabolism is discussed in detail in Section 3.1. Accumulating evidence suggests that the contribution of UGT2B10 to N-glucuronidation may be more important than that of UGT1A4.

UGT2B4 shares overlapping substrate selectivity with UGT2B7, especially with respect to hydroxy-steroids (Jin, Mackenzie and Miners 1997). However, the activity of UGT2B4 is generally an order of magnitude lower than that of UGT2B7. Overlapping substrate selectivity between UGT2B4 and UGT2B7 has also been reported for several drugs, including carvedilol, codeine, zidovudine, and some NSAIDs (Stingl et al. 2014). Generally the contribution of UGT2B4 is much lower than that of UGT2B7, although both enzymes appear to contribute equally to codeine 6-glucuronidation (Raungrut et al. 2010).

1.5 Inter-individual variability in drug metabolism

Wide inter-individual variability in metabolic drug clearance is a well-accepted feature of many drugs metabolised by CYP and UGT enzymes (Foti and Fisher 2012; Guillemette, Lévesque and Rouleau 2014; Lin and Lu 2001; Miners and Mackenzie 1991; Miners et al. 2004; Rowland, Miners and Mackenzie 2013; Zanger and Schwab 2013). Variability typically arises from differences in the activities of the individual enzymes involved in drug metabolism, and is most pronounced when a single enzyme is responsible for metabolic clearance. As indicated in Section 1.1, inter-individual variability in metabolic clearance often requires dose adjustment to avoid drug-related toxicity or loss of efficacy, especially for drugs with a narrow therapeutic index. Discussion of the various factors that lead to variability in drug metabolising enzyme activity is not warranted in the context of this thesis, but include: age, cigarette smoking, diet, disease states (e.g. hepatic and renal impairment, heart failure), drug-drug interactions, ethnicity, gender, and genetic polymorphism and epigenetics. However, drug-drug interactions (DDIs) arising from inhibition of UGT enzymes and inhibition of CYP2C8 by glucuronide conjugates is the common theme of the research described in thesis and hence a more detailed discussion of DDIs follows.

1.6 Drug-drug interactions

A DDI occurs when the response to a drug (the ‘victim’ or ‘object’ drug) is modified by a co-administered drug (the ‘perpetrator’). DDIs may arise from multiple mechanisms (Snyder, Polasek and Doogue 2012). A behavioural DDI results from modification of a patient’s behaviour due to one drug to alter compliance with another drug. An example is improvement of depressive symptoms (due to an antidepressant

drug) improving mood and subsequently compliance with other medications. Pharmaceutical DDIs, or *in vitro* incompatibility interactions, arise from inappropriate mixing of formulations (e.g. sodium thiopentone and vecuronium) prior to administration. Pharmacodynamic DDIs occur when co-administered drugs have added or opposing effects at the same (e.g. morphine and naloxone) or different receptors (e.g. sildenafil and glyceryl trinitrate) or physiological systems (e.g. the diuretic furosemide and the cardiac glycoside digoxin). Pharmacokinetic DDIs occur from the altered absorption, distribution, metabolism/transport (inhibition or induction), and/or excretion of a drug. The outcome of a pharmacokinetic DDI is altered systemic concentration of the victim drug and time course of effect. DDIs arising from inhibition of drug metabolising enzymes are the focus of this thesis.

It has been suggested that up to 10 to 20% of adverse drug reactions that result in hospitalisation of patients is due to a DDI (Snyder, Polasek and Doogue 2012). Moreover, most of the DDIs are avoidable from a knowledge of the pharmacological effects of the co-administered drugs and DDI mechanisms (Pirmohamed et al. 2004). It is likely that the incidence of serious DDIs may increase into the future due to the ageing population and ongoing trend towards polypharmacy (Björkman et al. 2002; Qato et al. 2008).

1.6.1 Inhibitory drug-drug interactions

As noted above, the focus of this thesis is DDIs caused by inhibition of drug metabolising enzymes, particularly UGTs and CYP2C8. Impairment of enzyme activity results in a higher systemic concentration of the victim drug due to decreased hepatic clearance (low hepatic clearance drug) or increased bioavailability (high hepatic clearance drug). By contrast, pharmacokinetic DDIs arising from induction of metabolism result in a lower systemic concentration of the victim drug and potential

loss of efficacy. Inhibitory DDIs are considered to be a significant cause of adverse drug reactions. In this regard, it has been suggested that many inhibitory DDIs are ‘silent’ since only the most obvious are recorded (Rowland-Yeo and Tucker 2016). Inhibitory DDIs are often difficult to identify as they are not defined by the pharmacological actions of the drug, and are not always predictable from the known enzymology of drug metabolism. It is well established in the cytochrome P450 DDI literature that the perpetrator is not always a substrate of the inhibited enzyme (e.g. potent inhibition of CYP2D6 activity by the predominantly CYP3A substrates quinine and quinidine), and similar considerations apply to DDIs arising from altered glucuronidation activity. Fluconazole undergoes glucuronidation to a negligible extent *in vivo* but causes clinically significant inhibition of zidovudine glucuronidation in HIV patients treated with these drugs (see subsequent discussion). Moreover, inhibitory DDIs represent a potential economic loss and marketing disadvantage to the pharmaceutical industry; several drugs (e.g. astemizole, cisapride, mibefradil and terfenadine) have been withdrawn from the market due to DDIs that resulted in cardiac toxicity (Rowland-Yeo and Tucker 2016).

1.6.2 Drug-drug interactions arising from inhibition of cytochrome P450 enzymes

Using a criterion-based approach, Polasek et al. (2011) identified ‘strong’ and ‘moderate’ perpetrators of inhibitory DDIs due to inhibition of CYP enzymes. These are shown in Table 1.6, below. The Table lists only drugs marketed in Australasia, although Polasek et al. also refers to drugs implicated as perpetrators of DDIs that are not available in Australasia. (Many of these (e.g. sulfaphenazole) are also unavailable in most western countries, including the USA and European countries.) A doubling of the AUC of the victim drug was taken as the criterion for classification of a perpetrator.

However, this criterion ignores the importance of interactions where the victim is a narrow therapeutic drug. For example, a 30% increase in the AUC of warfarin could result in significant toxicity. A strong inhibitor was identified as one that increased the AUC of the victim drug ≥ 5 -fold (corresponding to $\geq 80\%$ decrease in systemic clearance), and a moderate inhibitor as one that increased the AUC between 2- and 5-fold (i.e. 50% to 80% decrease in systemic clearance). Polasek et al. (2011) further highlighted that the effect of a perpetrator may vary from victim drug to victim drug. In the case of CYP2C8, clopidogrel and gemfibrozil glucuronides are shown as the perpetrators, since the parent drugs require glucuronidation for inhibition (see Section 1.3.2 and Chapter 5).

It is evident from Table 1.6 that several inhibitors are relatively selective, but others are non-selective inhibitors of CYP enzymes. For example, the clopidogrel and gemfibrozil glucuronides inhibit only CYP2C8, and quinine and quinidine cause significant interactions only with CYP2D6 even though they are metabolised by CYP3A (Zhang et al. 1997). By contrast, fluvoxamine and fluconazole significantly inhibit several CYP enzymes. This presumably reflects the different architectures and chemical characteristics of the various CYP enzymes.

Table 1.6 Representative strong and moderate perpetrators of DDIs arising from inhibition of cytochrome P450 enzymes in humans.

Adapted with permission from Polasek, TM, Lin, FPY, Miners, JO and Doogue, MP (2011), 'Perpetrators of pharmacokinetic drug–drug interactions arising from altered cytochrome P450 activity: A criteria-based assessment', British Journal of Clinical Pharmacology, 71 (5): 727-736. Copyright (2011) John Wiley and Sons. Additional data are from Backman et al. (2016).

CYP enzyme	Inhibitors
CYP1A2	Ciprofloxacin, ethinyestradiol, fluvoxamine, interferon α -2b
CYP2C8	Clopidogrel glucuronide, gemfibrozil glucuronide, montelukast, trimethoprim
CYP2C9	Fluconazole
CYP2C19	Clarithromycin, fluconazole, fluoxetine, fluvoxamine, moclobemide, moriconazole, ticlopidine
CYP2D6	Bupropion, cinacalcet, doxepin, duloxetine, flecainide, fluoxetine, fluvoamine, moclobemide, paroxetine, perhexiline, quinidine, quinine, terbinafine
CYP3A	Aprepitant, atazanavir, cimetidine, clarithromycin, cyclosporine, diltiazem, erythromycin, fluvoxamine, grapefruit juice, imatinib, indinavir, itraconazole, ketoconazole, lopinavir, posaconazole, ritonavir, saquinavir, verapamil, voriconazole

The overall hepatic clearance of a drug represents the combination of three processes; cellular uptake and efflux back into the systemic circulation, metabolism, and biliary excretion (Benet 2009; Giacomini et al. 2010; Giacomini and Huang 2013; Patilea-Vrana and Unadkat 2016; Ronaldson et al. 2016; Shi and Li 2014; Yoshida, Maeda and Sugiyama 2013; Zhang, Zhang and Huang 2009). For highly lipophilic drugs that are freely membrane permeable, hepatic clearance is dependent on intrinsic metabolic clearance (along with liver blood flow and fraction of the drug unbound in blood). For more polar drugs, hepatic uptake and efflux transporters can assume importance and may be rate-limiting in hepatic clearance. This phenomenon is known as transport –

metabolism interplay and although it is recognised as being of increasing relevance, it is outside of the scope of this thesis.

1.6.3 Drug-drug interactions arising from inhibition of UDP-glucuronosyltransferase enzymes

In contrast to CYP-catalysed drug biotransformation, there are fewer reports of clinically relevant inhibitory DDIs arising from inhibition of UGT enzymes. Williams and colleagues (2004a) proposed that DDIs arising from inhibition are uncommon because inhibitor constants (K_i , described later) are high and unbound drug concentrations ($[I]_u$) of glucuronidated drugs are frequently low (due to high plasma protein binding), leading to low $[I]_u/K_i$ ratios. However, there is no enzymatic basis to support the hypothesis that glucuronidated compounds should universally have high K_i values, and hence DDIs should always be considered as a possibility. In fact, this laboratory recently reported that regorafenib and sorafenib inhibit UGT1A1 with K_i values in the low nanomolar range (Miners et al. 2017a). Furthermore, the Food and Drug Administration (FDA) recognised the potential for DDIs arising from altered UGT activity and recommends that new chemical entities are screened for interactions arising from altered drug (or endogenous compound) glucuronidation (Food and Drug Administration (FDA) 2012). In this respect, the physicochemical properties of drug molecules have changed substantially in recent years (Walters et al. 2011). They are getting larger (higher molecular mass), more lipophilic and complex, and contain more hydrogen bond donors and acceptors. While oxidative metabolism by enzymes such as CYP3A, which has a large active site, is likely to remain an important mechanism of drug elimination, the changing properties of drug molecules favour an increasing contribution of glucuronidation (and transport). Notable examples are the protein kinase inhibitors regorafenib and sorafenib (Miners et al. 2017a).

DDIs due to inhibition of human UGT enzymes have been summarised previously (Miners et al. 2010b). These include interactions with valproic acid (lamotrigine, lorazepam and zidovudine) and probenecid (paracetamol, clofibric acid, lorazepam and zidovudine) as perpetrators. Other examples cited by Miners et al. (2010b) include the fluconazole – zidovudine and lopinavir/ritonavir – SN38 interactions. Atovaquone is additionally known to inhibit zidovudine glucuronidation in patients (Lee et al. 1996); methadone, which is not glucuronidated, has been reported to inhibit codeine clearance via 6-glucuronidation (Gelston et al. 2012), a reaction catalysed by UGT2B4/2B7; and propranolol reduces paracetamol clearance via glucuronidation (Baraka et al. 1990). Interestingly, the methadone – codeine interaction was predicted from *in vitro* experiments (Raungrut et al. 2010). Atazanavir, administered alone or in combination with ritonavir, is also known to markedly reduce the clearance of buprenorphine via 3-glucuronidation (McCance-Katz, Sullivan and Nallani 2010). Decreases in the clearances (total or via glucuronidaion) of the victim drugs ranged from approximately 25% to 65%.

In addition to DDIs, a number of drugs are known to inhibit the UGT1A1-catalysed glucuronidation of bilirubin, leading to hyperbilirubinemia as an adverse effect. These are often referred to as drug-endobiotic interactions. Atazanavir is known to impair bilirubin glucuronidation in HIV patients (Zhang et al. 2005), and this may result in discontinuation of therapy (Leger et al. 2018). It has also been demonstrated that indinavir (Boyd et al. 2006), and regorafenib and sorafenib (Miners et al. 2017b) cause hyperbilirubinemia due inhibition of UGT1A1.

1.7 Enzyme kinetics and mechanisms of inhibition of drug metabolising enzymes

1.7.1 Enzyme kinetics

Most CYP- and UGT- catalysed drug metabolism reactions using HLM and recombinant proteins exhibit hyperbolic kinetics (Houston and Kenworthy 2000; Miners, Mackenzie and Knights 2010a), that is a plot of rate of product formation ('velocity') versus substrate concentration is hyperbolic in shape. Hyperbolic kinetics may be modelled using the Michaelis-Menten equation.

Equation 1.2,

$$v = \frac{V_{\max} \times [S]}{K_m + [S]}$$

where v is the rate of product formation, K_m is the Michaelis constant, V_{\max} is the maximal velocity, and $[S]$ is the substrate concentration. The K_m corresponds to the value of $[S]$ at half maximal velocity (V_{\max}). Although the K_m has no mechanistic meaning (Houston and Kenworthy 2000), it generally reflects binding affinity; the lower the K_m , the higher the binding affinity and *vice versa*. The ratio of V_{\max} to K_m gives the intrinsic clearance, Cl_{int} .

Equation 1.3,

$$Cl_{\text{int}} = \frac{V_{\max}}{K_m}$$

The Cl_{int} is a pivotal parameter for *in vitro* – *in vivo* extrapolation, since it provides a measure of intrinsic metabolic capacity (Houston and Kenworthy 2000). Experimental data may be shown as a velocity versus $[S]$ plot or as a linear transformation, most commonly the Eadie-Hofstee plot (velocity versus velocity/ $[S]$) and the Lineweaver-

Burk (1/velocity versus 1/[S]) plot (Figure 1.10). Presentation of experimental data as an Eadie-Hofstee plot is of value for the visual detection of deviation from hyperbolic kinetics (so-called atypical kinetics) (Miners, Mackenzie and Knights 2010a).

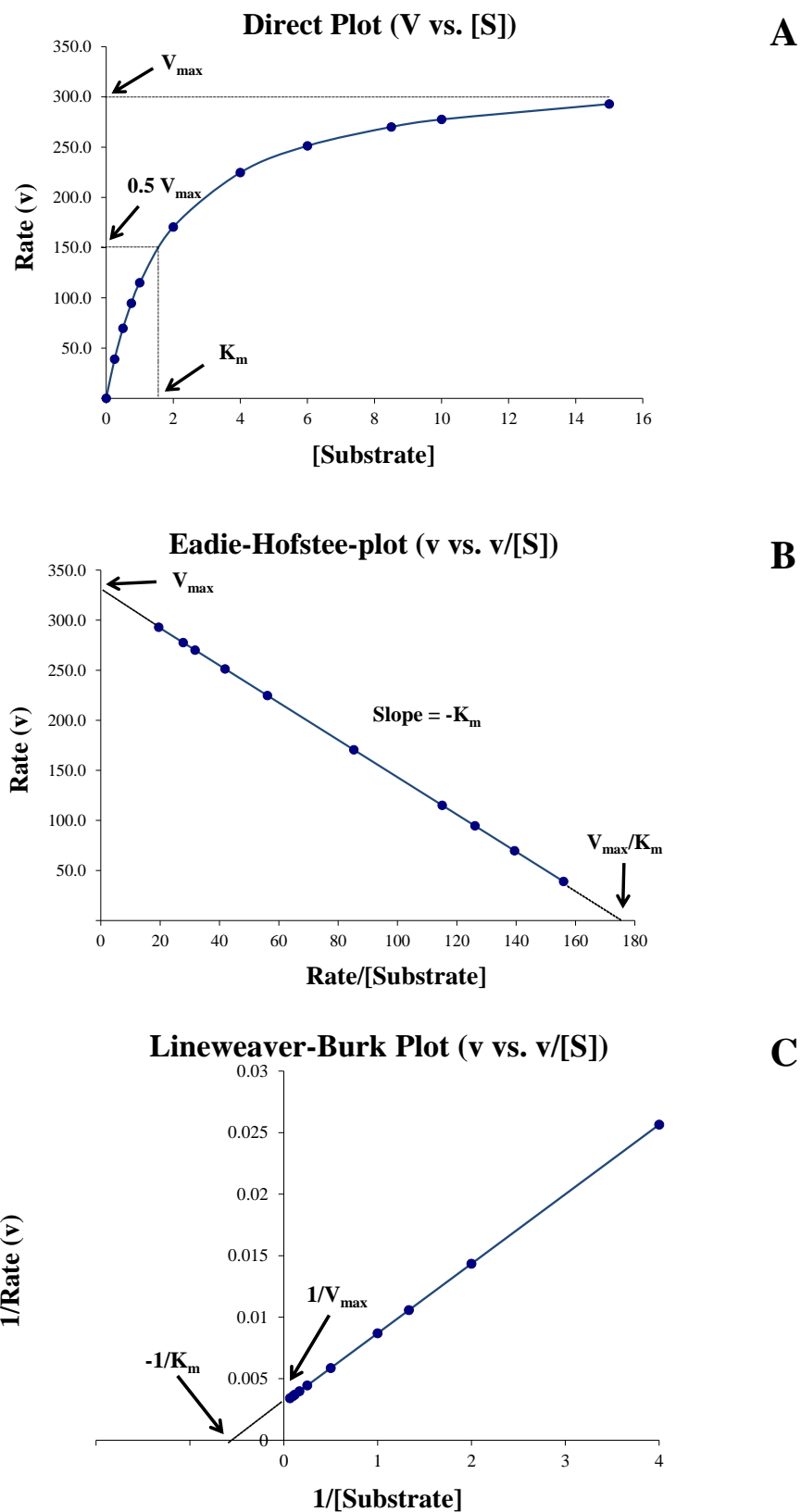


Figure 1.10 Graphical representations of hyperbolic kinetics.

Panel A, untransformed plot (velocity versus [S]); Panel B, Eadie-Hofstee plot; Panel C, and Lineweaver-Burk plot.

Although most drug metabolism reactions exhibit hyperbolic kinetics, the occurrence of non-hyperbolic (atypical) kinetics is well established (Houston and Kenworthy 2000; Miners, Mackenzie and Knights 2010a). Common examples include the involvement of two (or more) enzymes in metabolite formation, substrate inhibition, and positive (autoactivation) and negative cooperativity (see Figure 1.11). Atypical kinetic data are usually analysed empirically, by fitting relevant equations to experimental data; these include the Hill equation (positive and negative cooperativity), the substrate inhibition equation, and the 2-enzyme Michaelis-Menten equation. These equations are given in numerous publications (e.g. Houston and Kenworthy, 2000) and enzyme kinetics textbooks (e.g. Segel, 1993).

Equation 1.4, substrate inhibition equation:

$$v = 1 + \left[\left(\frac{K_m}{[S]} \right) + \left(\frac{[S]}{K_{si}} \right) \right]$$

where K_{si} is the inhibition constant resulting from substrate-enzyme interaction.

Equation 1.5, Hill equation:

$$v = \frac{V_{max} \times [S]^n}{S_{50}^n + [S]^n}$$

where n is the Hill coefficient reflecting sigmoidal degree.

Equation 1.6, two enzyme Michealis-Menten equation:

$$v = \frac{V_{max1} \times [S]}{K_{m1} + [S]} + \frac{V_{max} \times [S]}{K_{m2} + [S]}$$

It is noteworthy that Cl_{int} cannot be calculated for reactions that exhibit cooperativity (unless the Hill coefficient, n , is close to unity). The corresponding parameter for

positive cooperative (autoactivation) kinetics is the maximal clearance, Cl_{max} (Houston and Kenworthy 2000). The application of mechanistic models that assume the existence of multiple substrate binding sites provides an alternative approach to the use of empirical equations. Multi-site kinetic models that assume the existence of two equivalent or non-equivalent substrate binding sites have been employed to explore the mechanistic basis of substrate inhibition and positive and negative cooperativity for substrates of both human CYP (Houston and Galetin 2005; Houston and Kenworthy 2000) and UGT (Stone et al. 2003; Uchaipichat et al. 2004; Zhou, Tracy and Remmel 2010) enzymes.

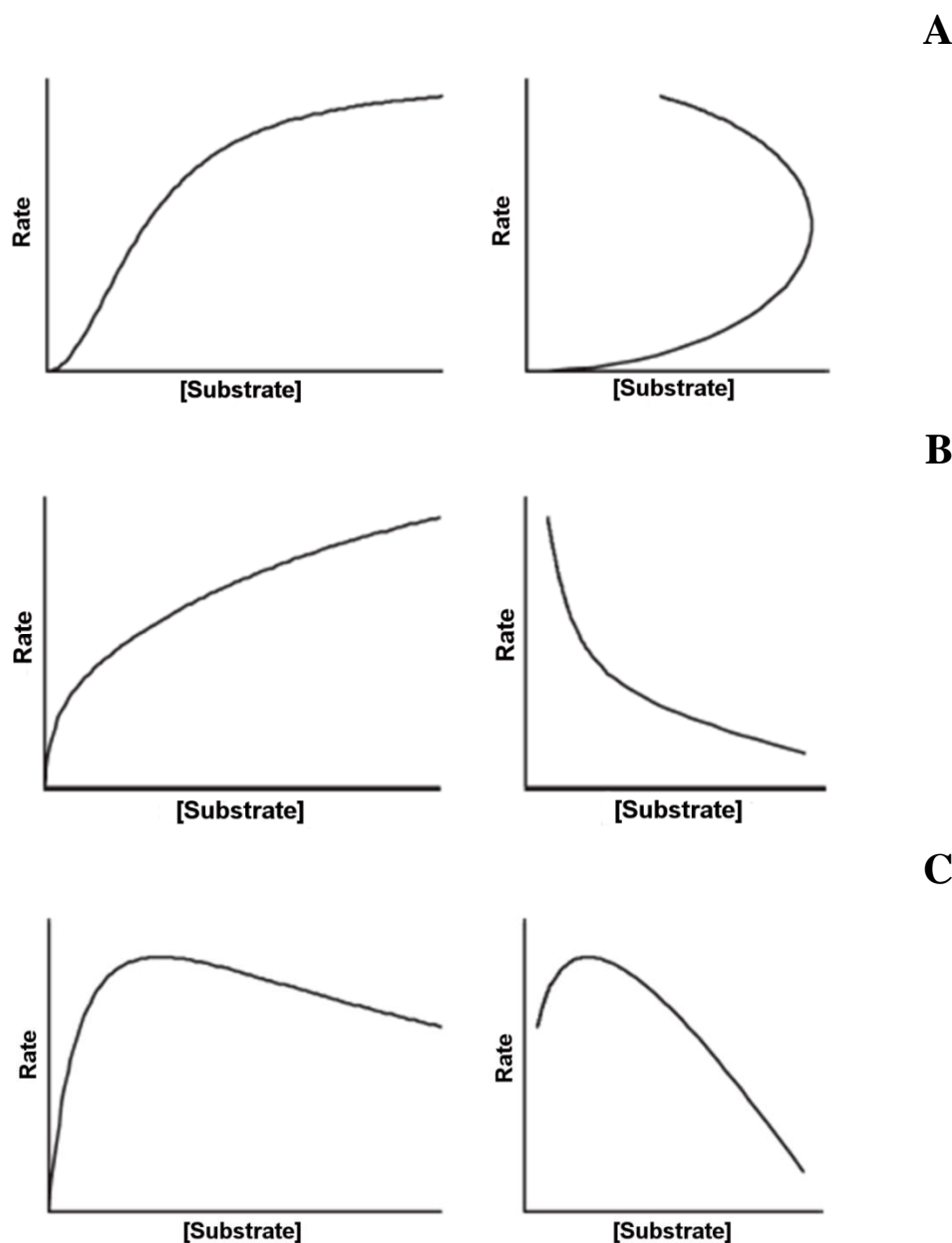


Figure 1.11 Simulations of direct and Eadie-Hofstee plots for atypical kinetics.

Homotropic positive cooperativity (Panel A), two-enzyme Michaelis-Menten kinetics/homotropic negative cooperativity (Panel B,) and substrate inhibition (Panel C).

Reproduced with permission from Miners, JO, Mackenzie, PI and Knights, KM (2010a), 'The prediction of drug-glucuronidation parameters in humans: UDP-Glucuronosyltransferase enzyme-selective substrate and inhibitor probes for reaction phenotyping and in vitro – in vivo extrapolation of drug clearance and drug-drug interaction potential', Drug Metabolism Reviews, 42 (1): 196-208. Copyright (2010) Taylor & Francis.

1.7.2 The kinetics of drug metabolising enzyme inhibition *in vitro*

The critical parameter for the characterisation of most types of enzyme inhibition *in vitro* is the inhibitor (or inhibition) constant, K_i . The K_i is the dissociation constant for the various types of enzyme (E) – inhibitor (I) complexes associated with different mechanisms of inhibition (see below). For example, the K_i for competitive inhibition, where binding of the inhibitor precludes substrate binding, is $K_i = ([E] \times [I])/[EI]$, where the square brackets indicate concentration. Evidence from *in vitro* studies indicates that the majority of inhibitory DDIs arise from competitive inhibition where, as noted above, the inhibitor competes reversibly with binding of the substrate (S) in the enzyme active site. Both enzyme-substrate (ES) and enzyme-inhibitor (EI) complexes form, but ES dissociates to produce the expected metabolite.

Equation 1.7, competitive inhibition:

$$v = \frac{V_{\max} \times [S]}{K_m(1 + [I]/K_i) + [S]}$$

where terms have been defined previously. As expected from the nature of competitive inhibition, a competitive inhibitor increases the apparent K_m for the substrate, without affecting V_{\max} . The extent of inhibition observed experimentally for a competitive inhibitor depends on [I], [S], K_m and K_i (Segel 1993). K_i is the dissociation constant for the EI complex, as shown above. At any given substrate concentration, the degree of inhibition increases as the value of $[I]/K_i$ increases. Most competitive inhibitors are alternate substrates for the enzyme, although this is not always the case. As stated earlier, although metabolised by CYP3A (Zhang et al. 1997), quinine and quinidine are competitive inhibitors of CYP2D6.

Non-competitive inhibition is generally considered to arise from the independent, random and reversible binding of S and I at different sites on the enzyme; S can bind

to E and to EI, and *vice versa* I can bind to E and ES (Segel 1993). However, the EI and EIS complexes are inactive. Since the EIS species will exist at all values of I, V_{\max} is decreased in non-competitive inhibition whereas K_m is unaffected.

Equation 1.8, non-competitive inhibition:

$$v = \frac{V_{\max} \times [S]}{(1 + [I]/K_i)(K_m + [S])}$$

In uncompetitive inhibition, I binds reversibly to the EI complex but not to the enzyme itself. The ESI complex is inactive but, since inhibitor binding is reversible, it dissociates to ES (Segel 1993). V_{\max} and apparent K_m are both decreased to the same extent in uncompetitive inhibition.

Equation 1.9, uncompetitive inhibition:

$$v = \frac{V_{\max} \times [S]}{K_m + [S] \left(1 + \frac{[I]}{K_i}\right)}$$

Mixed (competitive – non-competitive) inhibition has also been observed for inhibition of drug metabolising enzymes. The equation for mixed inhibition includes two inhibitor constants; K_i (for the EI complex) and K_i' (for the EIS complex). K_i and K_i' are related by a factor α , such that $K_i' = \alpha K_i$ (where $\alpha > 1$; EI has a lower affinity for S than does E) (Segel 1993).

Equation 1.10, mixed (competitive – non-competitive) inhibition:

$$v = \frac{V_{\max} \times [S]}{K_m(1 + [I]/K_i) + [S]\left(1 + \frac{[I]}{K_i'}\right)}$$

Like enzyme kinetic data, inhibition data are analysed by fitting the various equations to experimental data. However, visual inspection of inhibition plots (e.g. the Dixon plot, which graphs $1/v$ versus $[I]$ at several substrate concentrations; see Figure 1.12.

below) is also of value for differentiating types of inhibition.

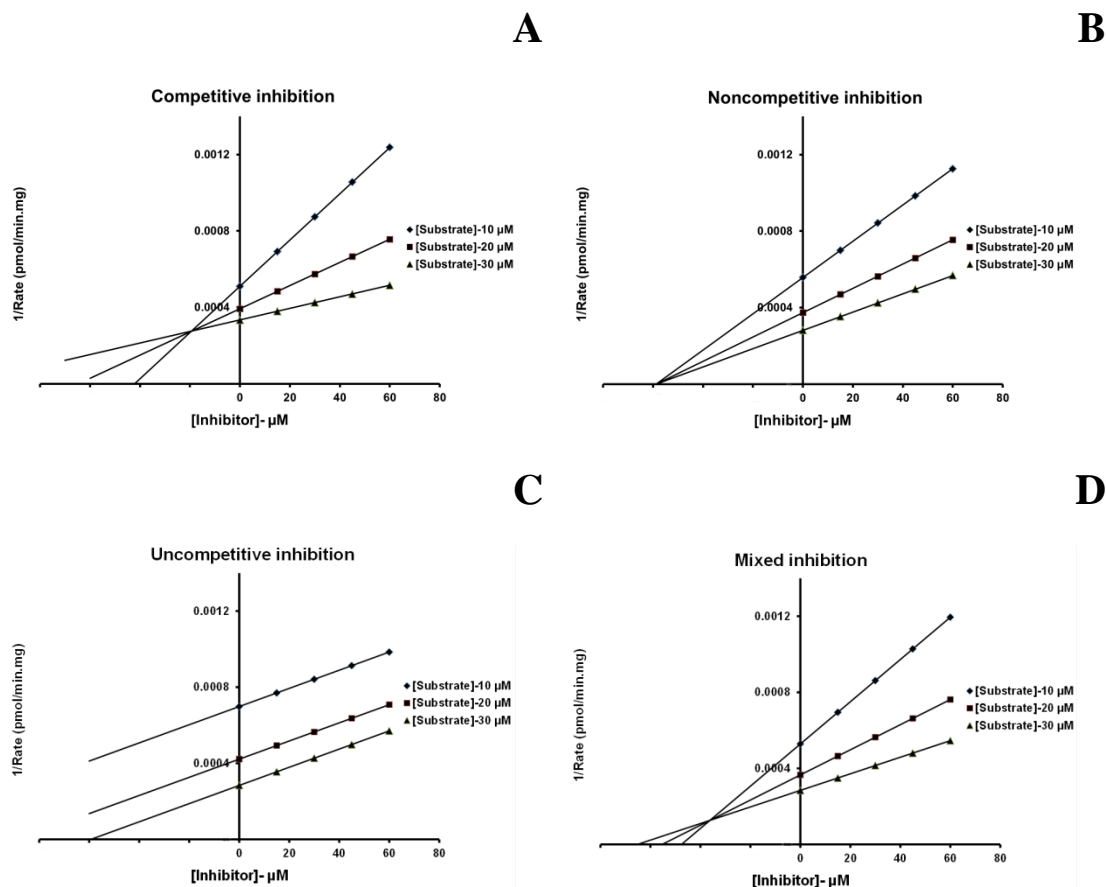


Figure 1.12 Dixon plots for competitive (panel A), non-competitive (panel B), uncompetitive (panel C) and mixed (panel D) inhibition.

An alternative approach to conducting ‘formal’ kinetic studies, such as those illustrated in Figure 1.12 above, is to estimate the K_i from an IC_{50} value (i.e. the inhibitor concentration causing half-maximal inhibition). It can be demonstrated that $K_i = \text{IC}_{50}/2$ (when $[\text{S}] = K_m$) for competitive inhibition, but $K_i = \text{IC}_{50}$ for non-competitive and uncompetitive inhibition (Cheng and Prusoff 1973). However, use of these relationships requires knowledge of the mechanism of inhibition and, as noted above, for competitive inhibition experiments must be performed at a substrate concentration that corresponds to the K_m for the reaction and enzyme system. Thus, the kinetic parameters for the ‘probe’ substrate must be known. However, in the case of HLM,

human hepatocytes and recombinant enzymes, the K_m can vary from liver to liver, batch to batch, and between expression systems.

1.7.3 Mechanism-based inhibition

Mechanism-based inhibition (or inactivation) (MBI) occurs when a substrate is converted to a metabolite that, prior to its release from the catalytic site, inactivates the enzyme (Silverman 1988). MBI is time-dependent, and is therefore also referred to as time-dependent inhibition (TDI). Loss of activity *in vivo*, but not necessarily *in vitro*, is irreversible (see below) (Polasek and Miners 2007). Restoration of enzyme activity requires the biosynthesis of new protein. Thus, DDIs that arise from MBI can be severe and prolonged in duration. Figure 1.13 illustrates the reaction scheme for MBI (Grimm et al. 2009).

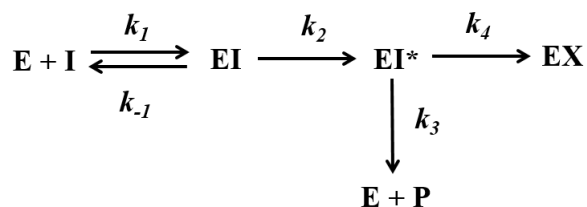


Figure 1.13 Reaction scheme for MBI.

E is the CYP enzyme, *I* is the inhibitor (inactivator), *EI* is enzyme-inhibitor complex, *EI** is enzyme-reactive metabolite complex, *EX* is the inactivated enzyme, and *P* is product (metabolite) produced by the enzyme.

Reproduced with permission from Grimm, SW, Einolf, HJ, Hall, SD, He, K, Lim, H-K, Ling, K-HJ, Lu, C, Nomeir, AA, Seibert, E and Skordos, KW (2009), 'The conduct of in vitro studies to address time-dependent inhibition of drug-metabolizing enzymes: A perspective of the pharmaceutical research and manufacturers of America', Drug Metabolism and Disposition, 37 (7): 1355-1370. Copyright (2009) the American Society for Pharmacology and Experimental Therapeutics.

There appear to be no reports of DDIs due to MBI of UGT enzymes, even though some acyl glucuronides are inherently reactive and form adducts with non-UGT proteins (Regan et al. 2010). By contrast, there are numerous reports of MBI involving CYP

enzymes, for example Hollenberg, Kent and Bumpus (2008); Kalgutkar, Obach and Maurer (2007); Obach, Fahmi and Walsky (2010); Obach, Walsky and Venkatakrishnan (2007), and Zhou and Zhou (2009). Indeed, MBIs of almost all of the major drug metabolising human CYP enzymes have been reported *in vitro* and/or *in vivo*. Selected examples include: furafylline (CYP1A2); methoxsalen (CYP2A6); ticlopidine (CYP2B6); tienilic acid (CYP2C9); ticlopidine (CYP2C19); paroxetine (CYP2D6); disulfiram (CYP2E1); and clarithromycin, delavirdine, erythromycin, mibefradil, ritonavir, and troleandomycin (CYP3A).

Of relevance to this thesis, MBI of CYP2C8 has also been described (Backman et al. 2016; Tornio et al. 2014; Tornio et al. 2017). Clinically relevant DDIs have been described for clopidogrel and gemfibrozil. In particular, co-administration of gemfibrozil results in a more than doubling of the AUCs of the CYP2C8 substrates cerivastatin, dasabuvir, montelukast, pioglitazone and repaglinide (Backman et al. 2016). Transport – metabolism plays a role in the interactions with cerivastatin and repaglinide. Time-dependent inhibition of CYP2C8 is not due directly to clopidogrel and gemfibrozil, but rather the glucuronides of these drugs. This is described in detail in Chapter 5.

Mechanisms of MBI of CYP enzymes are illustrated in Figure 1.14. The inactivating species can (Grimm et al. 2009; Polasek and Miners 2007):

- 1) Form a stable adduct with a nucleophilic amino acid(s) in the active site (protein alkylation or arylation). The modified amino acid(s) may be involved in substrate binding or electron transfer. Examples include reactive metabolites formed from furafylline and tienilic acid that inhibit CYP1A2 and CYP2C9, respectively.

- 2) React with a heme nitrogen atom(s) (heme alkylation or arylation), for example the acetylene-containing 17 α -ethinylestradiol and gestodene inhibition of CYP3A.
- 3) Form a coordination complex with the heme iron, producing a metabolite-intermediate complex (MIC). A well characterised example is the conversion of macrolide antibiotics (e.g. clarithromycin and erythromycin), which are alkylamines, to a nitroso species that forms a nitroso – iron complex.

More recently, Orr et al. (2012) described inactivation that combines mechanisms (1) and (2), whereby binding of inactivator to the heme leads to degradation of the heme – inactivator complex, generating fragments that react with the apoprotein. Although all of the mechanisms referred to above are considered as MBI according to the definition of Silverman (1988), only mechanisms (1) and (2) are truly irreversible (Polasek and Miners 2007). Covalent binding inactivates the enzyme. By contrast, heme – iron complex formation is referred to as quasi-irreversible because catalytically active enzyme can be regenerated, as least *in vitro*. Where MIC occurs, active enzyme can be regenerated, most commonly using potassium ferricyanide to oxidise the iron back to the ferric state (Polasek and Miners 2007).

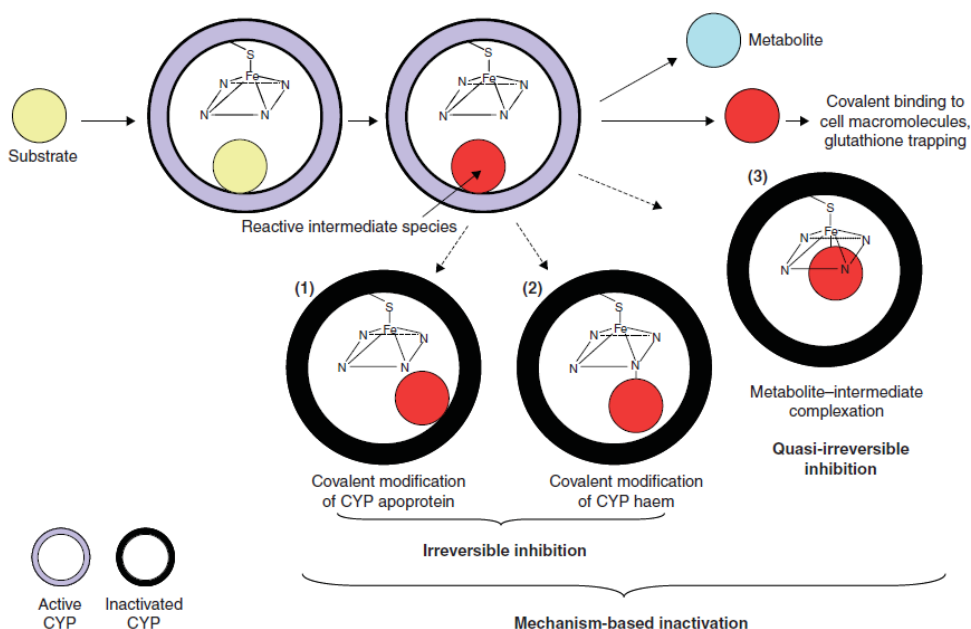


Figure 1.14 Mechanisms of mechanism-based inactivation.

Reproduced with permission from Polasek, TM and Miners, JO (2007), 'In vitro approaches to investigate mechanism-based inactivation of CYP enzymes', *Expert Opinion on Drug Metabolism and Toxicology*, 3 (3): 321-329. Copyright (2007) Taylor & Francis.

The maximal rate of inactivation (k_{inact}) and the inactivator concentration required for half maximal inactivation (K_I) are the key parameters used to describe MBI experimentally, and are additionally required for *in vitro* – *in vivo* extrapolation to predict the magnitude of DDIs involving MBI (Li et al. 2005; Obach, Walsky and Venkatakrishnan 2007). The most commonly employed approach to investigate MBI *in vitro*, the so-called two-step dilution assay, is shown schematically in Figure 1.15 (Obach, Walsky and Venkatakrishnan 2007; Polasek and Miners 2007). HLM and recombinant CYP proteins are generally used as the enzyme source (Houston and Galetin 2010). In the initial inactivation assay, a high concentration of the enzyme source is pre-incubated with a range of concentrations of the inactivating drug ([I]) plus NADPH for various times. This is followed by the activity assay, where individual samples are diluted into a second incubation

mixture that contains a saturating concentration of a selective ‘probe’ drug for the enzyme of interest to obtain plots of activity remaining versus incubation time (Figure 1.15, panel A). Values of k_{obs} are obtained as the negative slopes of the plots of the natural logarithm of the decrement in activity remaining versus incubation time. The relationship between k_{obs} , k_{inact} and K_I is shown in Equation 1.11. k_{inact} and K_I can be calculated from a direct plot between k_{obs} [I] (Figure 1.15, Panel B) or from the double reciprocal plot (Figure 1.15, Panel C) (Kitz and Wilson 1962; Zhou and Zhou 2009).

Equation 1.11,

$$k_{\text{obs}} = k_{\text{obs},[\text{I}]=0} + \frac{k_{\text{inact}} \cdot [\text{I}]}{K_I + [\text{I}]}$$

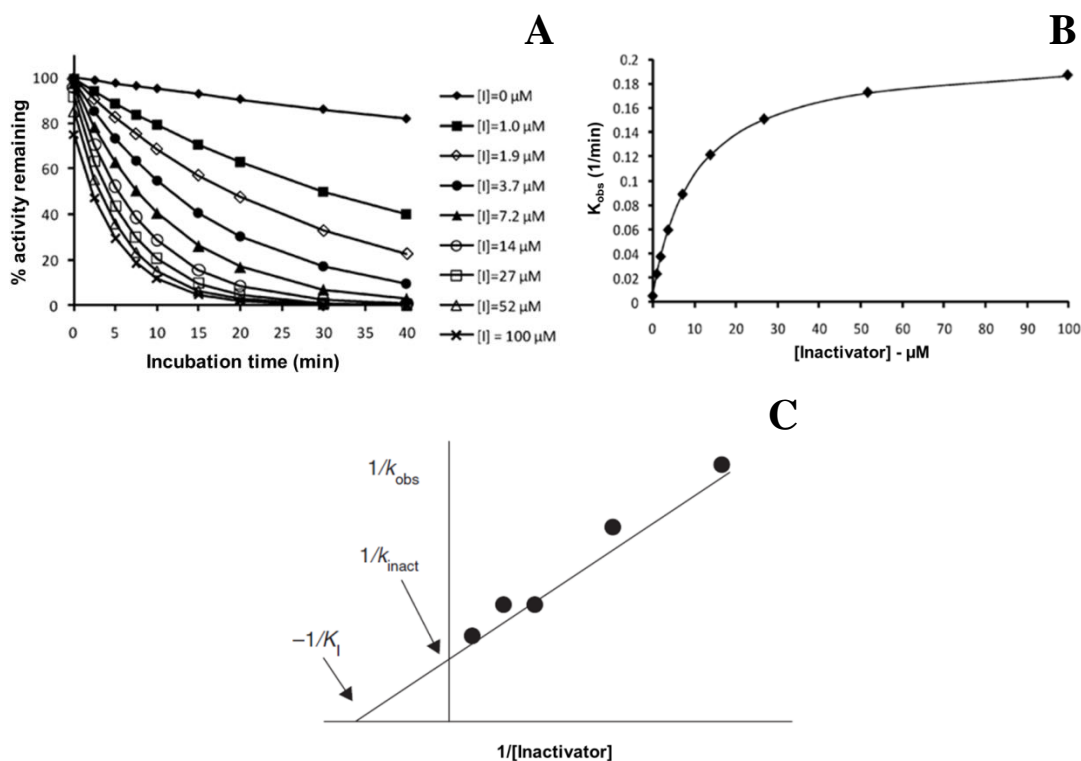


Figure 1.15 Plots of a CYP TDI experiment to generate k_{inact} and K_I values.

Plots of the loss of CYP activity versus time (Panel A), k_{obs} versus inactivator concentration (Panel B), and $1/k_{obs}$ versus $1/[I]$ (Panel C). Plots shown in Panels B and C may both be used for the estimation of k_{inact} and K_I .

Reproduced with permission from Orr, ST, Ripp, SL, Ballard, TE, Henderson, JL, Scott, DO, Obach, RS, Sun, H and Kalgutkar, AS (2012), 'Mechanism-based inactivation (MBI) of cytochrome P450 enzymes: Structure–activity relationships and discovery strategies to mitigate drug–drug interaction risks', *Journal of Medicinal Chemistry*, 55 (11): 4896-4933. Copyright (2012) American Chemical Society.

With respect to Figure 1.13, k_{inact} is described by the rate constants k_2 , k_3 and k_4 (Silverman 1988):

Equation 1.12,

$$k_{inact} = (k_2 \times k_3)/(k_2 + k_3 + k_4)$$

while K_I is described by the rate constants k_1 , k_{-1} , k_2 and k_4 .

Equation 1.13,

$$K_I = (k_{-1} + k_2)/k_1 \times (k_3 + k_4)/(k_2 + k_3 + k_4)$$

The IC₅₀ shift method provides a somewhat simpler alternative to the two-step dilution assay (Grimm et al. 2009; Li et al. 2011; Obach, Walsky and Venkatakrishnan 2007; Parkinson et al. 2011; Perloff et al. 2009; Sekiguchi et al. 2009), and was adopted in this thesis to characterise the mechanism of inhibition of CYP2C8 by glucuronide conjugates. The method is described in Chapter 5. Briefly, in the IC₅₀ shift method the enzyme source is pre-incubated with a range of concentrations of the inhibitor in the presence and absence of NADPH for a specified time. After this time, enzyme activity is measured using a ‘probe’ substrate, using either a dilution or non-dilution approach. Where MBI occurs, there will be a shift to the left in the IC₅₀ (Figure 1.16). An increase in the IC₅₀ ratio ($IC_{50} (-NADPH) / IC_{50} (+NADPH) \geq 1.5$) is usually taken as the cut-off value for TDI when HLM are used as the enzyme source (Berry and Zhao 2008; Grimm et al. 2009).

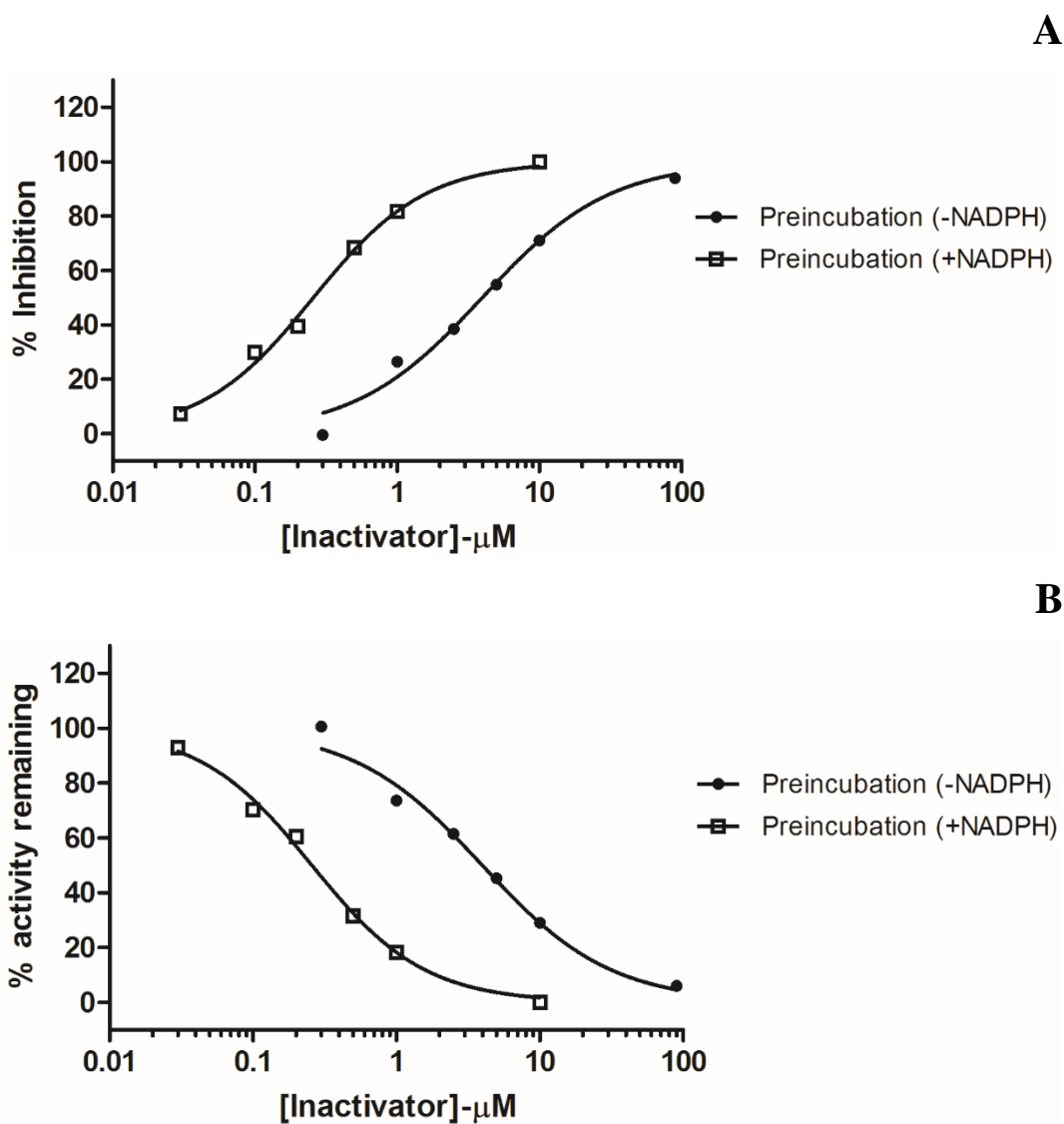


Figure 1.16 Plots of time-dependent inactivation from IC_{50} shift experiments.

Inhibition data are shown as percent inhibition (Panel A) and percent remaining activity (Panel B).

The K_I to k_{inact} ratio can be determined from the IC_{50} using the expression (Parkinson et al. 2011):

Equation 1.14,

$$IC_{50}^t = \ln 2 \left(\frac{K_I}{k_{inact} \times t} \right) \left(1 + \frac{[S]}{K_m} \right)$$

where IC_{50}^t is the ‘shifted’ IC_{50} from time-dependent inhibition studies, t is the pre-incubation time in the presence of inhibitor and NADPH, and $[S]/K_m$ is the ratio of the concentration of the ‘probe’ substrate relative to its K_m .

An even simpler approach, referred to as the single point inactivation method, has been shown to distinguish TDIs from non-inactivators (Obach, Walsky and Venkatakrishnan 2007). As the name suggests, the method employs a single concentration of the putative inactivator. This approach appears to be of most value for the screening for TDI in drug discovery/pre-clinical development where hundreds of compounds might be investigated.

1.8 *In vitro* – *in vivo* extrapolation (IV-IVE)

In its broadest sense, *in vitro* – *in vivo* extrapolation (IV-IVE) refers to the prediction of *in vivo* drug elimination parameters, or factors that alter drug elimination (e.g. metabolic clearance or an inhibitory DDI) from *in vitro* data. As described by Miners, Mackenzie and Knights (2010a), IV-IVE may be broadly classified as qualitative or quantitative. Qualitative prediction of factors likely to alter drug metabolic clearance *in vivo* is possible when the enzyme(s) responsible for the metabolism of the drug is known. Procedures for identification of the enzyme(s) that contribute to the metabolism of any given drug or chemical, a process referred to as ‘reaction phenotyping’ (Rodrigues 1999), are well established for both CYP- and UGT-

catalysed drug biotransformation. If factors that alter enzyme activity *in vivo* (e.g. age, ethnicity, DDIs, disease states, genetic polymorphism, etc) are known, then populations susceptible to altered drug clearance may be predicted (Figure 1.17) (Miners, Mackenzie and Knights 2010a; Miners, Veronese and Birkett 1994). As the term implies, qualitative IV-IVE refers to the use of *in vitro* data to predict actual values of ADME parameters (absorption, distribution, metabolism and excretion) *in vivo*.

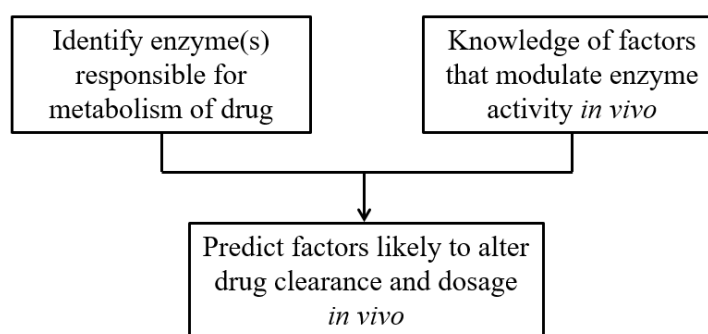


Figure 1.17 Qualitative IV-IVE.

Adapted with permission from Miners, JO, Mackenzie, PI and Knights, KM (2010a), 'The prediction of drug-glucuronidation parameters in humans: UDP-Glucuronosyltransferase enzyme-selective substrate and inhibitor probes for reaction phenotyping and in vitro – in vivo extrapolation of drug clearance and drug-drug interaction potential', Drug Metabolism Reviews, 42 (1): 196-208. Copyright (2010) Taylor & Francis.

1.8.1 Reaction phenotyping

General methods for reaction phenotyping are described in Miners et al (1994 and 2010a) and Zientek and Youdim (2015). The most powerful approach for the identification of the CYP or UGT enzyme responsible for the metabolism of any given compound is determination of the reduction in metabolism by enzyme selective chemical inhibitors with HLM or hepatocytes as the enzyme source. Antibody inhibitors may also be employed, but these tend to be more expensive and selectivity is sometimes questionable. The extent of the decrease in metabolism caused by the

inhibitor gives the contribution of that enzyme to overall metabolism by CYP or UGT. For example, if hecogenin, a highly selective inhibitor of UGT1A4, abolished the glucuronidation of the test drug by HLM then it could be concluded that UGT1A4 was solely responsible for the metabolism that drug. Enzyme inhibition studies are usually complemented by investigating the metabolism of the test drug by ‘batteries’ of recombinant CYP or UGT enzymes. Alternative approaches for reaction phenotyping include demonstration of: (i) a highly significant correlation between the rates of metabolism of the test drug and an enzyme-selective probe substrate (or immunoreactive protein content) for microsomes or hepatocytes from a ‘panel’ of livers; and (ii) competitive inhibition of an enzyme-selective substrate by the test drug, with concordance between the K_i and K_m values of the test drug.

As described in Section 1.2.4, CYP-enzyme selective substrate probes suitable for reaction phenotyping are available. CYP-enzyme selective inhibitors have also been characterised (El-Sherbeni and El-Kadi 2017; Miners, Veronese and Birkett 1994; Zientek and Youdim 2015), and include: furafylline (CYP1A2); tranlylcypromine (CYP2A6); 2-phenyl-2-(1-piperdiny)propane (CYP2B6); montelukast (CYP2C8); sulfaphenazole (CYP2C9); N-3-benzyl-phenobarbitone (CYP2C19); quinine and quinidine (CYP2D6); CYP3cide (CYP3A4); and ketoconazole (CYP3A4/5). 1-Aminobenzotriazole is a non-selective MBI of most CYP enzymes, and may be used assess the overall involvement of CYP in drug biotransformation (Zientek and Youdim 2015).

Reaction phenotyping of drug glucuronidation was undertaken in this thesis (Chapter 3). Selective substrates and inhibitors have been reported for most of the major drug metabolising human UGT enzymes, and these are shown in Table 1.7 (Bichlmaier et al. 2007; Lapham et al. 2012; Miners et al. 2017a; Miners, Mackenzie and Knights

2010a; Zientek and Youdim 2015). It should be noted, however, that claims of selectivity are, in some cases, based on incomplete evidence, for example hexafluoro-1 α ,5-dihydroxyvitamin D and buprenorphine as probes for UGT1A3, and troglitazone as a UGT1A6 inhibitor (Miners, Mackenzie and Knights 2010a). Despite being one of the most important UGT enzymes in terms of substrate diversity, there is no readily available highly selective inhibitor of UGT2B7. Apart from UGT2B7, fluconazole also inhibits UGT2B4 and UGT2B10 (see Chapter 3). Although there is evidence to suggest that iso-longifolol may be a selective inhibitor of UGT2B7 (Bichlmaier et al. 2007), this compound is no longer available from the supplier (M Finel, personal communication to JO Miners).

While outside of the scope of this thesis, substrate and inhibitor probes are also available for most transporters relevant to drug disposition.

Table 1.7 Representative selective substrates and inhibitors of hepatically-expressed human UDP-glucuronosyltransferase enzymes for reaction phenotyping.

UGT enzyme	Substrates	Inhibitors
1A1	β -Estradiol (3-glucuronidation), etoposide, SN-38	Atazanavir, regorafenib, sorafenib
1A3	Hexafluoro-1 α ,5-dihydroxyvitamin D	Buprenorphine
1A4	1'-Hydroxymidazolam, trifluoperazine	Hecogenin
1A6	Deferiprone, serotonin	Troglitazone
1A9	Mycophenolic acid (phenolic glucuronidation), propofol, sulfinpyrazone	Digoxin, niflumic acid, tranilast
2B7	6 α -Hydroxyprogesterone, morphine (3- and 6-glucuronidation), zidovudine	Fluconazole, iso-longifolol
2B10	Cotinine	Desloratadine
2B15	S-Oxazepam	-

1.8.2 Quantitative prediction of hepatic metabolic clearance and inhibitory drug-drug interaction potential

IV-IVE approaches that predict hepatic metabolic clearance and inhibitory DDI potential have found widespread acceptance over the last two decades, especially in pre-clinical drug development. Theoretical considerations relevant to metabolic clearance prediction have been detailed in several reviews, for example Houston (1994) and Iwatsubo et al. (1997). The experimental approach adopted is shown schematically in Figure 1.18. HLM and human hepatocytes are typically used as the enzyme source. Cl_{int} values, obtained from *in vitro* kinetic studies, are summed and scaled to a ‘whole liver’ intrinsic clearance using scaling factors that account for microsome yield (per gram of liver) or hepatocellularity (number of hepatocytes per gram of liver) and liver weight (Barter et al. 2007). Recombinant human and CYP and UGT enzymes may also be employed if the enzyme protein contents of the recombinant preparation (e.g. Supersomes) and HLM are known from proteomic studies, or alternatively using an intersystem scaling factor (Proctor, Tucker and Rostami-Hodjegan 2004) or relative activity factor (Venkatakrishnan, Von Moltke and Greenblatt 1998). Hepatic metabolic clearance (and hence extraction ratio, as $E_H = Cl_H/Q_H$) can subsequently be determined using equations for mathematical models of hepatic clearance. The equation shown in Figure 1.18 is for the well-stirred model of hepatic clearance, although equations for the parallel tube and dispersion models have also been used for CYP- and UGT- catalysed drug metabolism (for example, Boase and Miners (2002); Ito and Houston (2004)). However, differences in predictions observed between the models are generally small and the equation for the well-stirred model is almost invariably used for IV-IVE.

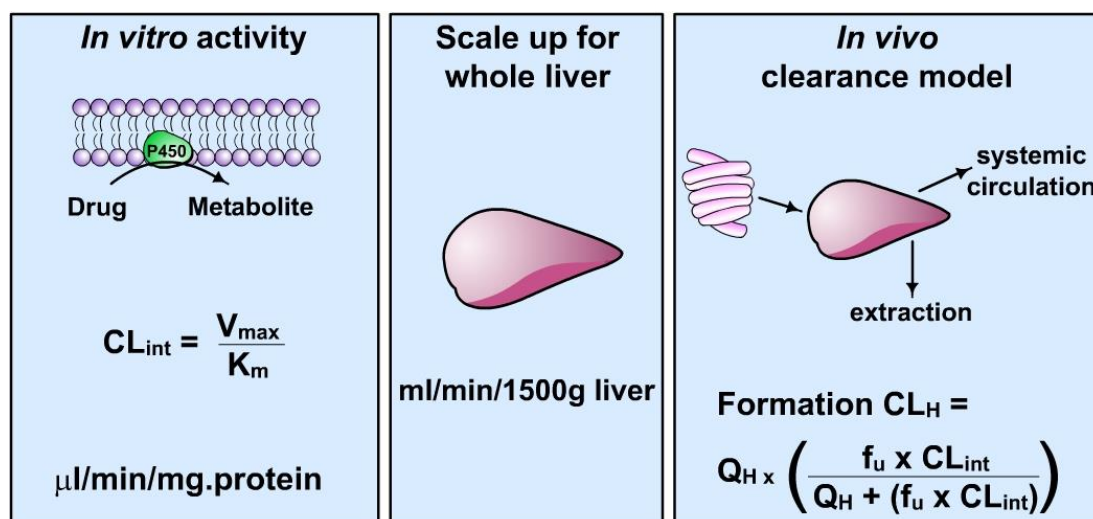


Figure 1.18 Scheme for the extrapolation of *in vitro* intrinsic clearance to hepatic metabolic clearance.

The equation for the well-stirred model of hepatic clearance is given in panel 3; Q_H = hepatic blood flow and f_u = fraction of the drug unbound in blood.

Reproduced with permission from Miners, JO (2002), 'Evolution of drug metabolism: Hitchhiking the technology bandwagon', *Clinical and Experimental Pharmacology and Physiology*, 29 (11): 1040-1044. Copyright (2002) John Wiley and Sons.

IV-IVE approaches to predict the magnitude of a DDI arising from inhibition of drug metabolising enzymes is of particular relevance to this thesis. The key experimental parameter for DDI prediction is the inhibitor (or inhibition) constant, K_i (Section 1.7.2). The magnitude of a DDI is given by the ratio of the areas under the plasma concentration – time curve (AUC) of the victim drug when administered with and without the inhibitor (perpetrator). If other clearance pathways (e.g. renal, biliary) are unaffected by the perpetrator and inhibition arises from competitive or non-competitive inhibition of a single enzyme, the AUC-ratio (or ratios of hepatic CL_{int}) is given by the following expression (Houston and Galetin 2010; Ito et al. 1998; Miners, Mackenzie and Knights 2010a):

Equation 1.15, AUC-ratio:

$$\frac{AUC_i}{AUC} = \frac{Cl}{Cl_{int(i)}} = \frac{1}{\frac{f_m}{1 + \frac{[I]}{K_i}} + (1 - f_m)}$$

where f_m is the fraction of hepatic metabolic clearance mediated by the inhibited enzyme and $[I]$ is the inhibitor concentration available to the enzyme. When multiple metabolic pathways/enzymes are inhibited, each of the two terms of the denominator are summed. Alternatively, the equation can be re-written as the so-called mechanistic equation for the AUC-ratio (Houston and Galetin 2010):

Equation 1.16, mechanistic equation:

$$\frac{AUC_i}{AUC} = \frac{Cl}{Cl_{int(i)}} = 1 + \Sigma \frac{[I]}{K_i}$$

If hepatic metabolic clearance is due to just one enzyme ($f_m = 1$) the above equations simplify to:

Equation 1.17, single enzyme/inhibition pathway AUC-ratio:

$$\frac{AUC_i}{AUC} = \frac{Cl}{Cl_{int(i)}} = 1 + \frac{[I]}{K_i}$$

As indicated in previous Sections, several drug metabolising enzymes are expressed in the gastrointestinal tract and inhibition of intestinal enzymes may be of importance in DDIs following oral drug administration. Where this occurs, an additional term (F_G'/F_G) is included in equation 1.15; here F_G is the fraction of the administered dose avoiding intestinal metabolism (Galetin, Gertz and Houston 2008). Alternatively a mechanistic equation that describes inhibition of intestinal metabolism (Cl_{intG})/($Cl_{intG'}$) may be combined with the mechanistic equation (1.16) for inhibition of hepatic enzymes (Houston and Galetin 2010). An important example is intestinal CYP3A,

which is inhibited by a number of drugs and other compounds (including grapefruit juice) (Table 1.6). As indicated in Section 1.4.3, numerous UGT enzymes are expressed in the gastrointestinal tract. However, their contribution to pre-hepatic drug metabolism is poorly understood and potential effects of inhibitors of intestinal UGTs are ignored in IV-IVE.

Wherever possible, the concentration of inhibitor available to the enzyme in equations 1.15. to 1.17 above is determined as the hepatic input concentration (Ito et al, 1998):

Equation 1.18, hepatic input concentration:

$$[I_{\text{inlet}}] = [I_{\text{max}}] + \frac{k_a \times F_a \cdot F_g \times D}{Q_H}$$

where $[I_{\text{max}}]$ is a maximum unbound concentration of drug, k_a is the absorption rate constant, F_a is the fraction absorbed from the gastrointestinal tract, F_g is the fraction of the absorbed dose escaping metabolism in the intestine, D is the inhibitor dose and Q_H is hepatic blood flow. Importantly, however, k_a and $F_a \cdot F_g$ are frequently unavailable, especially for new drugs. As alternatives, up to late 2017 the FDA and EMA recommended use of the mean total (unbound plus bound) and unbound maximum concentration of the drug (C_{max}) in plasma at the highest recommended dose, respectively (European Medicines Agency (EMA) 2012; Food and Drug Administration (FDA) 2012). In late 2017, however, the FDA updated its DDI Guidance to use the maximal unbound plasma concentration of the interacting drug (FDA 2017).

A relationship similar to that given for reversible inhibition in equation 1.15 is used to model MBI (Galetin, Gertz and Houston 2008):

Equation 1.19, AUC ratio for MBI:

$$\frac{AUC_i}{AUC} = \frac{1}{\left(\frac{f_m}{1 + \left(\frac{k_{inact} \cdot [I]}{k_{deg} \cdot (K_I + [I])} \right)} \right) + (1 - f_m)}$$

Symbols have been described earlier except for k_{deg} , which is the rate constant for degradation of the inactivated enzyme. As with equations for reversible inhibition, equation 1.18 requires modification (summation) where multiple enzymes are inactivated and inclusion of the factor F_G'/F_G when simultaneous inactivation of an intestinal enzyme (especially CYP3A) occurs (Galetin, Gertz and Houston 2008).

1.8.3 Experimental factors affecting the prediction accuracy of *in vitro* – *in vivo* extrapolation.

Early studies of IV-IVE for hepatic metabolic clearance and DDI prediction indicated a trend towards under-prediction, ranging from approximately 50% to as much as 1- to 2- orders of magnitude, for substrates and inhibitors of both CYP and UGT (for example Hallifax, Foster and Houston (2010); Hallifax and Houston (2009); Miners et al. (2006) and Uchaipichat et al. (2006a)). It is known that numerous experimental and data analysis considerations contribute to the under-prediction (Houston and Galetin 2010; Miners, Mackenzie and Knights 2010a).

Several of the factors affecting IV-IVE accuracy are generic to both clearance and DDI prediction. Experimental factors include (Boase and Miners 2002; Miners, Mackenzie and Knights 2010a): incubation buffer type and pH; inclusion of organic solvents for substrate and/or inhibitor solubilisation in the incubation medium (Busby, Ackermann and Crespi 1999; Uchaipichat et al. 2004); and the addition of bovine serum albumin (BSA) to incubations (see later discussion). Some experimental factors are specific to drug glucuronidation, particularly the requirement for activation of HLM for removal

of ‘latency’ (see Section 1.4.3). Activation of HLM by the pore-forming agent alamethicin is the method of choice (Boase and Miners 2002; Fisher et al. 2000; Kilford et al. 2009; Knights et al. 2016a; Walsky et al. 2012). By contrast, alamethicin has no effect on the activities of UGT enzymes expressed in insect cells (e.g. Supersomes) (Walsky et al. 2012), while sonication of HEK293 cells expressing UGT enzymes (to produce cell lysate) results in activation precluding the need for treatment with alamethicin (Miners, Mackenzie and Knights 2010a). Incubations for the characterisation of drug glucuronidation kinetics are typically performed at saturating cofactor (UDPGA) concentration (5 mM) (Miners, Mackenzie and Knights 2010a), with inclusion of $MgCl_2$ (4 – 10 mM) to sequester UDP formed during the glucuronidation reaction (Boase and Miners 2002; Walia et al. 2017). Since acyl glucuronides may hydrolyse under alkaline conditions, it has been recommended that incubations of carboxylic acid containing substrates (or inhibitors) should be performed at pH 6.8 (Miners, Mackenzie and Knights 2010a).

Model selection for the calculation of *in vitro* kinetic constants, for example recognition of atypical kinetics and the mechanism of inhibition, is critical (Houston and Galetin 2010; Miners, Mackenzie and Knights 2010a). Similarly, accounting for the non-specific binding of substrate and inhibitor to the enzyme source (HLM, hepatocytes, recombinant protein preparations) is essential. If binding to incubation components is not taken into account then K_m and K_i are over-estimated, leading to under-estimation of *in vivo* metabolic clearance and inhibitory DDI potential (Hallifax and Houston 2009; McLure, Miners and Birkett 2000; Miners, Mackenzie and Knights 2010a; Obach 1999; Riley, McGinnity and Austin 2005). Microsomal binding is most extensive for lipophilic organic bases, and negligible for most organic acids (Austin et al. 2002; Nair, McKinnon and Miners 2016b). Accounting for the contribution(s) of

organs other than the liver to drug metabolism (and transport) is additionally important for both clearance and DDI prediction. By way of example, UGT1A9 is expressed to a significant extent in the kidney and failure to account for glucuronidation by renal UGT1A9 can result in under-estimation of clearance via glucuronidation for reactions catalysed by this enzyme (Gill, Houston and Galetin 2012; Knights et al. 2016a). High expression of CYP3A occurs in the gastrointestinal tract and prediction of DDIs arising from inhibition of this enzyme should account for impaired intestinal metabolism (Galetin, Gertz and Houston 2008; Houston and Galetin 2010). As shown in equation 1.15 and 1.18, prediction of DDI potential requires knowledge of the contribution of the inhibited pathway (f_m) to clearance, and relatively small changes in this parameter can result in significant changes to the predicted AUC-ratio, for interactions arising from both reversible inhibition and TDI (Brown et al. 2005; Galetin et al. 2006; Ito et al. 2005). Also as shown previously (equation 1.17, Section 1.8.2), the hepatic inlet unbound concentration of inhibitor (perpetrator) is recommended for DDI prediction. However, values of k_a and $F_a \cdot F_g$ are frequently unavailable. Under these circumstances, the FDA recommends values of 0.1 min^{-1} and 1 (Food and Drug Administration (FDA) 2012), respectively. Alternatively, up to late 2017, it was recommended that [I] can be estimated as either the total or unbound concentration of inhibitor in plasma (European Medicines Agency (EMA) 2012; Food and Drug Administration (FDA) 2012), although as noted earlier the FDA updated its Guidance in late 2017 to use the maximal unbound inhibitor concentration (Food and Drug Administration (FDA) 2017). Assuming gastric emptying is rate-limiting for absorption, a k_a of 0.1 min^{-1} represents the maximum possible value for this parameter (Ito et al. 1998). Clearly, the value of [I] adopted will influence the estimated magnitude of an inhibitory DDI.

Studies in this and other laboratories has demonstrated that addition of BSA to

incubations of HLM and recombinant enzymes provides values of Cl_{int} and K_i that give more accurate estimates of metabolic clearance and DDI potential. The so-called ‘albumin effect’ has been demonstrated for several hepatically expressed enzymes, including CYP 1A2, 2C8 and 2C9, and UGT 1A9, 2B4, 2B7 and 2B10 (Gill, Houston and Galetin 2012; Lapham et al. 2016; Manevski et al. 2011; Raungrut et al. 2010; Rowland et al. 2008a; Rowland et al. 2007; Rowland et al. 2008b; Uchaipichat et al. 2006b; Walsky et al. 2012; Wattanachai et al. 2012). Amongst the UGTs, the greatest effect of albumin on *in vitro* Cl_{int} occurs with UGT 1A9 and 2B7. Multiple studies have shown that the *in vitro* Cl_{int} for substrates of UGT2B7, most commonly with the prototypic substrate zidovudine, using HLM as the enzyme source increases between approximately 4- to 10- fold when incubations are performed in the presence of 1 – 2% (w/v) BSA (Gill, Houston and Galetin 2012; Kilford et al. 2009; Lapham et al. 2016; Manevski et al. 2011; Rowland et al. 2007; Walsky et al. 2012). The increase in Cl_{int} appears to occur predominantly from a decrease in K_m , although some studies have also reported an increase in V_{max} . An increase in Cl_{int} is additionally observed when human kidney and intestinal microsomes and recombinant UGT2B7 are used as the enzyme source, although the magnitude of the effect of BSA varies with recombinant protein expression system. BSA also increases the human liver microsomal Cl_{int} of UGT1A9 substrates, most commonly using propofol as the probe substrate (Gill, Houston and Galetin 2012; Kilford et al. 2009; Lapham et al. 2016; Manevski et al. 2011; Rowland et al. 2008b; Walsky et al. 2012). Like UGT2B7, the magnitude of the effects of BSA tends to vary between studies, with increases in the *in vitro* Cl_{int} ranging from approximately 4.5- to 12- fold. Although all studies that measured metabolite formation reported a decrease in K_m , V_{max} was variably found to be unchanged, increased, or even decreased. Also similar to UGT2B7, an increase in

Cl_{int} is observed when human kidney and intestinal microsomes and recombinant UGT1A9 are used as the enzyme source. An effect of BSA on *in vitro* Cl_{int} has also been reported for substrates of CYP 1A2, 2C8 and 2C9 (Rowland et al. 2008a; Wattanachai et al. 2011; Wattanachai et al. 2012). The largest effect, an approximate 5-fold increase in *in vitro* Cl_{int} , was found for human liver microsomal phenytoin hydroxylation, a reaction catalysed by CYP2C9 (Rowland et al. 2008a).

The mechanism of the ‘BSA effect’ appears to be sequestration of long-chain unsaturated fatty acids released from membranes of the enzyme source that are released during the course of a reaction. For example, arachidonic, linoleic and oleic acids have all been shown to inhibit UGT1A9, UGT2B7, CYP2C8 and CYP2C9-catalysed reactions *in vitro*, and addition of BSA to the incubation medium reverses the inhibition (Rowland et al. 2008a; Rowland et al. 2007; Wattanachai et al. 2011). The extent of inhibition varies with the enzyme source (HLM and recombinant enzymes expressed in different cell lines, *viz.* mammalian vs. insect vs. *E. coli*) presumably because membrane fatty acids (type and content) differ between species (Rowland et al. 2008a; Rowland et al. 2007; Wattanachai et al. 2011).

Experimental variables also appear to contribute to differences reported in the magnitude of the BSA effect (i.e. Cl_{int} increase and K_i decrease), especially the relative effects on K_m and V_{max} observed between studies. It is essential that fatty acid free BSA (or human serum albumin) is employed, since bound inhibitory fatty acids can be released from ‘crude’ albumin preparations (Rowland et al. 2007; Rowland et al. 2008b). Further, the effect of albumin is concentration-dependent. At least with UGT1A9 and UGT2B7, the maximal increase in Cl_{int} occurs for BSA concentrations between 1% and 2% (w/v); smaller increases (or no effect) are observed at lower concentrations (Lapham et al. 2016; Rowland et al. 2007; Rowland et al. 2008b). The

variable effect of BSA and substrate-dependent changes in Cl_{int} reported by some authors may be due to the use of a low BSA concentration (0.1%, w/v) (Manevski et al. 2011; Manevski et al. 2013), resulting in sub-optimal sequestration of fatty acids. Clearly, albumin binding of substrate and inhibitor, not just non-specific binding, must be measured and corrected for in the calculation of *in vitro* kinetic parameters. In this regard, addition of BSA to incubations may not be practical for highly albumin bound compounds. Here, the use of intestinal fatty acid binding protein provides an alternative (Rowland et al. 2009), although this protein is not commercially available.

In the case of drug glucuronidation, the use of optimised incubation conditions, particularly alamethicin-activation and inclusion of BSA, and accounting for non-specific binding and extra-hepatic metabolism greatly improves the IV-IVE prediction accuracy of metabolic clearance and the magnitude of inhibitory DDIs (Gill, Houston and Galetin 2012; Kilford et al. 2009; Lapham et al. 2016; Raungrut et al. 2010; Rowland et al. 2007; Rowland et al. 2008b; Uchaipichat et al. 2006b). For example, metabolic clearance for about half of the drugs investigated by Gill, Houston and Galetin (2012) was predicted within 50% of known *in vivo* values, while the magnitude of the valproic acid – lamotrigine, fluconazole – zidovudine and methadone – codeine interactions was predicted within 25% of the known decrement in victim drug clearance (Gill, Houston and Galetin 2012; Kilford et al. 2009; Raungrut et al. 2010; Rowland et al. 2006a; Uchaipichat et al. 2006b). Addition of BSA to incubations may also improve metabolic clearance prediction for drugs metabolised by some CYP enzymes, and for drugs metabolised by both CYP and UGT enzymes (Kilford et al. 2009; Rowland et al. 2008a). However, a bias towards under-prediction in metabolic clearance and DDI potential still occurs for numerous drugs (Hallifax, Foster and Houston 2010). It is possible that transport-metabolism interplay contributes to the

bias, especially where transporter mediated hepatic uptake is involved, for example Brown et al. (2010).

1.8.4 Physiologically-based pharmacokinetic modelling

As described previously, metabolic clearance and the magnitude of a DDI *in vivo* can be estimated from *in vitro* data using IV-IVE approaches based on equations for ‘static’ models, for example equations 1.15, 1.16 and 1.17. The *in vitro* data are generated from recombinant enzymes, or hepatocytes or HLM from a limited number of livers, and mean values are used for extrapolation. Given the many factors that influence enzyme activity in humans (Section 1.8), IV-IVE based on the *in vitro* kinetic parameters generated provide limited insights into population variability and the importance of individual covariates (e.g. age, disease states, ethnicity, genetic polymorphism) in drug pharmacokinetics and response in different patient populations. To overcome this limitation, which is of particular relevance in drug discovery and development and during regulatory review (Huang and Rowland 2012), physiologically-based pharmacokinetic (PBPK) modelling approaches, based on *in vitro* data, have been developed over the last twenty years to simulate pharmacokinetic profiles following oral and intravenous drug administration (Rostami-Hodjegan and Tucker 2007; Rowland, Peck and Tucker 2011). Importantly, these models permit the simulation of covariates, including DDIs, which influence drug pharmacokinetics in different patient populations.

As described by Jones et al. (2015), “A PBPK model is a mathematical model that integrates drug data and data on species physiology (system data) to simulate the pharmacokinetic profile of a drug in plasma and tissues”. The ‘compartments’ of a PBPK model include organs (liver, kidney, gastrointestinal tract, lungs, etc) connected by the circulation (Rowland, Peck and Tucker 2011). The compartments are

characterised by tissue blood flow and volume/weight. Drug related parameters include physicochemical parameters (e.g. logP, pK_a and compound type features (acid, base, neutral)), and parameters related to kinetics (e.g. Cl_{int}, plasma protein binding, blood:plasma partitioning, *in vitro* scaling factors, and K_i (for the modelling of DDIs)) (Rostami-Hodjegan and Tucker 2007). The availability of software programs that allow solution of the differential equations that describe the PBPK model has been a critical factor for the increasing use of this approach. Commercial software include the Simcyp simulator, GastroPlus, PK-Sim and Cloe Predict (Rowland, Peck and Tucker 2011).

PBPK modelling was not employed in this thesis to model potential DDIs arising from inhibition of UGT2B10 (Chapter 3) and the inhibition of UGT enzymes by SGLT2 inhibitors (Chapter 4). The principal aim of this work was simply to identify potential interactions, rather than identify ‘at risk’ populations and the time course of inhibition, and a static model (using equations described in Section 1.8.3) was considered appropriate for this purpose. In addition, when these studies were performed approximately 3 years ago, the Simcyp simulator (which is now available in this Department) was not fully developed for the characterisation of DDIs arising from inhibition of UGT enzymes. Interestingly, however, a comparison of static and dynamic (Simcyp) modelling of 35 DDIs arising from inhibition of CYP3A demonstrated similar predictivity (Guest et al. 2011).

1.9 Research aims

The overarching theme of the studies described in this thesis is the *in vitro* characterisation of DDIs. Two studies characterised potential DDIs arising from the inhibition of UGT enzymes while the third investigated the molecular basis of the inhibition of cytochrome P450, specifically CYP2C8, by glucuronide conjugates.

The studies detailed in Chapter 3 primarily sought to characterise the inhibition of UGT2B10 by 34 amine-containing antidepressant and antipsychotic drugs and identify potential perpetrators of DDIs. Secondary aims were to: (i) confirm cotinine as a UGT2B10-selective substrate and desloratadine as a UGT2B10-selective inhibitor (for use in reaction phenotyping); and (ii) identify, using molecular modelling approaches, the structural features of compounds required for inhibition of UGT2B10.

The theme of DDIs arising from inhibition of UGT was continued in Chapter 4, which aimed to characterise the inhibition of human UGT enzymes by the sodium glucose transporter 2 (SGLT2) inhibitors canagliflozin, dapagliflozin and empagliflozin to assess their DDI potential. These drugs are the first three SGLT2 inhibitors approved for the treatment of type 2 diabetes, and are used widely for this purpose.

The aim of the final experimental chapter (Chapter 5), was to characterise the molecular basis of the inhibition of CYP2C8 by glucuronide conjugates using protein homology modelling, site-directed mutagenesis and enzyme kinetic approaches. Three glucuronides were investigated; the prototypic CYP2C8 time-dependent inhibitor gemfibrozil acyl glucuronide, and two glucuronides known to be metabolised by CYP2C8, diclofenac acyl glucuronide and estradiol 17- β -glucuronide.

CHAPTER 2

MATERIALS AND GENERAL METHODS

2.1 Materials and Equipment

Drugs, non-drug chemicals, reagents, enzymes, buffers, kits and equipment used for the various procedures employed in this thesis are documented in Tables 2.1 to 2.4, and software in Table 2.5. Chemicals were typically of analytical reagent grade.

Table 2.1 Drugs and metabolites used in enzyme activity assays and for protein expression.

Drug/metabolite	Supplier
Amitriptyline hydrochloride, aripiprazole, chlorpromazine hydrochloride, citalopram hydrobromide, clomipramine hydrochloride, clozapine, codeine, desipramine hydrochloride, desvenlafaxine hydrochloride, diclofenac sodium salt, diethylstilbestrol, doxepin hydrochloride, β -estradiol, β -estradiol 3- β -D-glucuronide, β -estradiol 17- β -D-glucuronide, fluphenazine hydrochloride, fluvoxamine maleate, gemfibrozil, hecogenin, imipramine hydrochloride, 4-methylumbelliferone sodium salt, 4-methylumbelliferone- β -D-glucuronide, mirtazapine, S-(-)-nicotine, niflumic acid, norclomipramine hydrochloride, nortriptyline hydrochloride, perphenazine, phenylbutazone, protriptyline hydrochloride, propofol, R-(-)-selegiline hydrochloride, thioridazine hydrochloride, tranlycypromine hydrochloride, trimipramine hydrochloride	Sigma Aldrich, Sydney, NSW, Australia
Ampicillin sodium salt, chloramphenicol	Astral Scientific, Sydney, NSW, Australia
Canagliflozin, dapagliflozin, duloxetine hydrochloride, empagliflozin	Selleck Chemicals, Houston, Texas, USA
Codeine 6-O-glucuronide, cotinine N- β -D-glucuronide, desloratadine, diclofenac acyl glucuronide, fluoxetine hydrochloride, loratadine, olanzapine, 6 α -hydroxy paclitaxel, phenelzine sulfate, quetiapine hemifumarate, sertraline hydrochloride	Toronto Research Chemicals, North York, ON, Canada
S-(-)-Cotinine, haloperidol, paroxetine, venlafaxine hydrochloride	Cayman Chemical, Ann Arbor, MI, USA
Desmethylnortriptyline hydrochloride	Roche Pharmaceuticals, Grenzacherstrasse, Basle, Switzerland

Table 2.1 Drugs and metabolites used in enzyme activity assays and for protein expression (cont.).

Drug/metabolite	Supplier
Didesmethylimipramine hydrochloride	Ciba-Geigy AG Pharmaceutical company, Basel, Baslestadt, Switzerland
Fluconazole, lamotrigine N2- β -D-glucuronide	Pfizer, Sydney, NSW, Australia
Gemfibrozil acyl glucuronide	XenoTech, LLC, Lenexa, Kansas, USA
Itraconazole, ketoconazole	Janssen Research Foundation, Beerse, Antwerp, Belgium
Lamotrigine	The Wellcome Foundation Ltd, Beckenham, London, UK
Loxapine	Alexza Pharmaceutical Inc., Mountain View, CA, USA
Mianserin hydrochloride	Akzo Pharmaceutical Division, Arnhem, Gelderland, the Netherlands
Paclitaxel	LC Laboratories, Woburn, MA, USA

Table 2.2 Chemicals and reagents used in experimental procedures.

Chemical/reagent	Supplier
Acetic acid (glacial), copper sulfate, Folin–Ciocalteu reagent	BDH Laboratory Supplies, Poole, Dorset, England
Acetonitrile, ammonium acetate, dimethyl sulfoxide, magnesium sulfate, methanol	Merck, Darmstadt, Hesse, Germany
Acrylamide (30%), nitrocellulose membrane, Precision Plus Protein™ WesternC™ Standards, Precision Protein™ Strep Tactin-HRP conjugate	BioRad, Sydney, NSW, Australia
Agar, tryptone (BSE-free), yeast extract (Yeastolate)	US Biological, Technology Way Salem, MA, USA
Agarose MB (Biotechnology grade)	Stennick Scientific, Adelaide, SA, Australia
Anti-rabbit IgG-HRP conjugated (secondary antibodies)	Jackson ImmunoResearch Laboratories, Inc, Chester, PA, USA
Bacto® peptone	DIFCO Laboratories, Detroit, MI, USA
Calcium chloride, manganese chloride, potassium acetate, tri-sodium citrate, sodium tartrate	Ajax Chemicals, Sydney, NSW, Australia
CYP2C8 antibody	Abcam, Melbourne, Vic, Australia
δ-Aminolevulinic acid, bovine serum albumin (BSA; essentially fatty acid free), cytochrome C (from horse heart), DL-dithiothreitol (DTT), glycerol, isopropyl β-D-1-thiogalactopyranoside, lysozyme (from chicken egg white), mineral oil, MOPS, β-nicotinamide adenine dinucleotide 2'-phosphate reduced tetrasodium salt hydrate (NADPH), NZ amine (casein hydroxylase), 1-octanesulfonic acid sodium salt, phenylmethylsulfonyl fluoride, rubidium chloride, Tween-20, N,N,N',N'-tetramethylethylenediamine (TEMED), UDP-glucuronic acid (trisodium salt)	Sigma Aldrich, Sydney, NSW, Australia
Dulbecco's modified eagle medium powder	Invitrogen, Erie, NY, USA
DH5a <i>Escherichia coli</i> (<i>E. coli</i>) cells	Life Technologies, Melbourne, Vic, Australia
Ethanol (absolute), perchloric acid (11.6 M), potassium dihydrogen orthophosphate, di-potassium hydrogen orthophosphate, sodium chloride, sucrose	Chem-Supply, Adelaide, SA, Australia
Ethylenediaminetetraacetic acid (EDTA) disodium salt, magnesium acetate	BDH Chemicals, Melbourne, Vic, Australia
GelRed™ DNA stain (10,000x in water)	Fisher Biotec, Perth, WA, Australia

Table 2.2 Chemicals and reagent used in experimental procedures (cont.).

Chemical/reagent	Supplier
Magnesium chloride, sodium hydroxide	Merck, Melbourne, Vic, Australia
Orthophosphoric acid (14.6 M)	Merck, Boston, MA, USA
Potassium cyanide	Fluka Biochemika, Ronkokoma, NY, USA
Potassium hydroxide	APS Ajax Finechem, Sydney, NSW, Australia
Protease inhibitor cocktail tablet	Roche Diagnostics, Mannheim, BW, Germany
RNase, Coomassie dye	Thermo Fisher Scientific, Lombard, IL, USA
Skim milk powder	Fonterra Food Service, Melbourne, Vic, Australia
Sodium carbonate	APS, Sydney, NSW, Australia
Spectra/Por 4 dialysis membrane (12-14 kDa)	Spectrum Laboratories, Inc, Rancho Dominguez, CA, USA
Tris free-base	Astral Scientific, Sydney, NSW, Australia

Table 2.3 Enzymes, buffers and kits used in incubations and molecular biology procedures.

Enzyme/buffer/kit	Supplier
Antarctic phosphatase, antarctic phosphatase reaction buffer, CutSmart® buffer, 1 kb DNA ladder, NEB buffer 2.1, Phusion® High-Fidelity DNA Polymerase, Phusion® High Fidelity reaction buffer, restriction enzymes (BamHI, DpnI, HindIII, NdeI, XhoI), T4 DNA ligase, T4 DNA ligase buffer	New England BioLabs, Hitchin, Herts, UK
dNTPs (dATP, dCTP, dGTP, dTTP), isolate II plasmid Mini Kit, isolate II PCR and Gel Kit	Bioline, Sydney, NSW, Australia
Lysozyme (chicken egg)	Sigma Aldrich, Sydney, NSW, Australia
Rapid equilibrium dialysis (RED) device inserts, reusable RED base plate, SuperSignal West Pico Chemiluminescent Substrate	Thermo Fisher Scientific, Rockford, IL, USA

Table 2.4 Equipment used in experimental procedures.

Equipment	Supplier
Bacterial incubator	Scientific Equipment Manufacturers, Adelaide, SA, Australia
Capsulefuge	TOMY, Brisbane, QLD, Australia
Cary 300 Conc UV-VIS spectrophotometer	Varian Australia Pty, Ltd., Melbourne, Vic, Australia
DNA Thermal Cycler 480	Perkin Elmer, Waltham, MA, USA
Dianorm apparatus	Dianorm, Munich, Germany
Gel Doc™ EZ imager, horizontal electrophoresis systems (PowerPac™ basic power supply, gel bath, gel setting tray and comb), BIORAD Mini-PROTEAN® III Electrophoresis and Mini Trans-Blot® Cell	BIO-RAD Life Science, Sydney, NSW, Australia
Gene Genius Bio Imaging System	Syngene, Frederick, MD, USA
GeneQuant II, RNA/DNA calculator	Pharmacia Biotech, Boston, MA, USA
Heraeus Megafuge 1.0 R	Thermo Fisher Scientific, Rockford, IL, Australia
HPLC series 1100 with auto-injector and UV-VIS detector	Agilent Technologies, Melbourne, Vic, Australia
Innova® 4330 refrigerated shaking incubator	New Brunswick Scientific, Enfield, CT, USA
J2-21M/E centrifuge, L8-70M ultracentrifuge, microfuge® 18 bench top centrifuge	Beckman Instrument, Munich, Bavaria, Germany
LAS-400 Imager (chemiluminescence)	Fuji Film, Sydney, NSW, Australia
MiVac Sample concentrator	Genevac, Ipswich, Suffolk, UK
Orbital shaking incubator	Adelab Scientific, Adelaide, SA, Australia
pH meter (PPS 901-PH)	Stennick Scientific, Adelaide, SA, Australia
Robocycler® Gradient96 Stratagene	Stratagene, La Jolla, CA, USA
Sigma Laboratory Centrifuge 4K15	Sigma, Mannheim, Baden-Württemberg, Germany

Table 2.4 Equipment used in experimental procedures (cont.).

Equipment	Supplier
VC505 Ultrasonic processor (Sonics Vibra cell™)	Sonics and Materials Inc., Newtown, CT, USA
Shaking water bath	Ratek Instruments, Melbourne, Vic, Australia

Table 2.5 Software used for data analysis, molecular modeling and oligonucleotide design.

Software	Supplier
Enzfitter® version 2.1	Biosoft, Great Shelford, Cambridge, UK
GraphPad Prism version 7.01	GraphPad Software, Inc, La Jolla, CA, USA
IBM-SPSS version 22	IBM, Armonk, NY, USA
OMEGA version 2.5.1.4	Openeye Scientific Software, Santa Fe, NM, USA
SYBYL-X version 2.1.1	TRIPOS, St Louis, MO, USA
Vector NTi version 11.5	Invitrogen, Melbourne, Vic, Australia

2.2 Methods

2.2.1 Recombinant human UGTs and human liver microsomes (HLM)

Human UGT 1A1, 1A3, 1A4, 1A6, 1A7, 1A8, 1A9 and 1A10 cDNAs were stably expressed in a human embryonic kidney cell line (HEK293T) according to the procedure of Uchaipichat et al. (2004). Briefly, after growth to at least 80% confluence, cells were harvested and washed in phosphate-buffered saline and then lysed by sonication using a Vibra Cell VCX 130 Ultrasonics Processor (Sonics and Materials, Newtown, CT, USA). Lysates were centrifuged at 12,000 g for 1 min at 4°C. The supernatant fraction was separated and stored in phosphate buffer (0.1 M, pH 7.4) at -80°C until use. Since expression of UGT2B subfamily enzymes (*viz.* 2B4, 2B7, 2B10, 2B15 and 2B17) in HEK293 cells is low, commercially sourced Supersomes™ (Corning) expressing these proteins were used for UGT enzyme activity and inhibition studies.

Corning® UltraPool™ HLM 150 were purchased from BD Biosciences (San Jose, CA, USA). The HLM pool comprised of microsomes from 150 donors (equal number of male and female donors) at a microsomal protein concentration of 20 mg/ml. All donors were Caucasian, with an age range of 18 to 82 years old.

2.2.2 1-Naphthol (1NP) glucuronidation by recombinant UGT2B10

Incubation conditions. Incubations, in a total volume of 100 µl, contained 1NP, UGT2B10 (expressed in Supersomes), phosphate buffer (0.1 M, pH 7.4) and MgCl₂ (4 mM). Following a 5 min pre-incubation at 37°C, reactions were initiated by the addition of UDPGA (final concentration 5 mM) and continued for 120 min. Reactions were terminated with of HClO₄ (11.6 M, 1 µl) and cooling on ice for 10 min. Protein was precipitated by centrifugation (5,000 g) at 4°C for 10 min.

Quantification. 1NP glucuronide formation was quantified following the method of Udomuksorn et al. (2007). An aliquot of the supernatant fraction from incubations was injected into an Agilent 1100 series HPLC (Agilent Technologies, Sydney, Australia) fitted with a Waters Nova-Pak[®], C-18 column (3.9 x 150 mm, 4 µm particle size; Waters, Sydney, NSW, Australia). Analytes were separated by gradient elution employing the following mobile phases: A, 10 mM triethylamine and 10% acetonitrile in distilled water, adjusted to pH 2.5 with 11.6 M HClO₄; and B, acetonitrile). Initial conditions were 86% phase A – 14% phase B for 4 min, after which time the proportion of phase A was reduced to 36% over 1 min. The mobile phase was delivered at a flow rate of 1 ml/min and 1NP glucuronide was detected by UV absorbance at 230 nm. Retention times of 1NP glucuronide and 1NP were 4.8 and 6.8 min, respectively. 1NP glucuronide formation was quantified by reference to a 1NP glucuronide standard curve prepared using five concentrations from 0.5 to 2 µM ($r^2 > 0.99$).

2.2.3 Measurement of recombinant UGT enzyme activities, with and without inhibitors

Activities of UGT 1A1, 1A3, 1A6, 1A7, 1A8, 1A9, 1A10, 2B7, 2B15 and 2B17 (\pm inhibitor) were measured using the non-selective substrate 4-methylumbelliferone (4MU) as the probe. Incubations were performed at a 4MU concentration corresponding to the K_m (or S_{50}) for each UGT enzyme (Uchaipichat et al. 2004). 4MU and protein (HEK293 cell lysate or Supersome) concentrations and incubation times are given in Table 2.6. Activities of UGT1A4 and UGT2B4 were determined using lamotrigine (LTG) and codeine (COD) as the respective substrate probes at concentrations corresponding to the K_m for each enzyme/substrate pair (Table 2.6; Rowland et al. 2006; Raungrut et al. 2010). Incubation conditions for the measurement of cotinine (COT) N-glucuronidation by UGT2B10 were developed during the course

of this thesis (Section 2.2.3.6). Where included, concentrations of organic solvents (required for the dissolution of substrate and/or inhibitor) present in incubations did not exceed 1% v/v, which has a negligible or minor effect on UGT enzyme activity (Uchaipichat et al. 2004).

Calibration curves for all assays were linear ($r^2 > 0.99$) over the respective concentration ranges and assay within- and between-day coefficients of variation for substrate concentrations that spanned the K_m (or S_{50}) for each enzyme were $< 5\%$ and 10% , respectively. Positive control inhibitors (Table 2.6) were included in all inhibition screening experiments (Chapters 3 and 4). The magnitude of the inhibition of each positive control inhibitor was as expected from previous studies in this laboratory (Miners et al. 2011; Raungrut et al. 2010; Uchaipichat et al. 2006a; Uchaipichat et al. 2004; Uchaipichat et al. 2006b).

As for the 1NP glucuronidation assay described above, all HPLC procedures documented in the following sections were performed using an Agilent 1100 series HPLC (Agilent Technologies, Sydney, Australia), which consisted of an auto-injector, dual pump solvent delivery system and variable wavelength ultraviolet – visible (UV-VIS) detector. The mobile phase flow rate for all assays was 1 ml/min.

Table 2.6 Protein concentrations, incubation times, probe substrate (4-methylumbelliferone, 4MU; lamotrigine; LTG; codeine, COD; cotinine, COT) concentrations and positive control inhibitors used for the measurement of recombinant UGT enzyme activities.

Recombinant UGT enzyme	Protein (mg/ml)	Incubation time (min)	Probe substrate (μM)	Positive control inhibitor (μM)	Reference
1A1	0.33	120	4MU (100)	Niflumic acid (100)	Miners et al. (2011)
1A3	0.167	75	4MU (1000)	Phenylbutazone (500)	Uchaipichat et al. (2006a)
1A4	0.5	75	LTG (1500)	Hecogenin (10)	Uchaipichat et al. (2006a)
1A6	0.0025	30	4MU (100)	Phenylbutazone (500)	Uchaipichat et al. (2006a)
1A7	0.0083	10	4MU (15)	Phenylbutazone (500)	Uchaipichat et al. (2006a)
1A8	0.05	30	4MU (750)	Phenylbutazone (500)	Uchaipichat et al. (2006a)
1A9	0.025	15	4MU (10)	Niflumic acid (2.5)	Miners et al. (2011)
1A10	0.208	30	4MU (30)	Phenylbutazone (500)	Uchaipichat et al. (2006a)
2B4	1	120	COD (2000)	Fluconazole (2500)	Raungrut et al. (2010)
2B7	0.2	90	4MU (350)	Fluconazole (2500)	Uchaipichat et al. (2006b)
2B10	1	120	COT (2800)	Desloratadine (10)	Result from Chapter 3 and Kazmi et al. (2015b)
2B15	0.5	90	4MU (300)	Diclofenac (500)	Uchaipichat et al. (2004)
2B17	0.5	120	4MU (1000)	Diclofenac (500)	Uchaipichat et al. (2004)

2.2.3.1 4-Methylumbelliferone (4MU) glucuronidation

Incubation conditions. Incubation mixtures, in a total volume of 200 μ l, contained 4MU (\pm inhibitor), enzyme protein (HEK293 cell lysate or Supersome), phosphate buffer (0.1 M, pH 7.4) and $MgCl_2$ (4 mM). The incubation mixtures were pre-incubated at 37°C for 5 min and then reactions were initiated by the addition of UDPGA (final concentration 5 mM). After the specified incubation time for each enzyme (Table 2.6), reactions were terminated with $HClO_4$ (11.6 M, 2 μ l) and cooling on ice. The precipitated protein was subsequently centrifuged (5,000 g) at 4°C for 10 min. An aliquot of the supernatant fraction was analysed by HPLC.

Quantification. 4MU glucuronide formation was quantified according to Lewis et al. (2007) using a Waters Nova-Pak[®], C-18 column (3.9 x 150 mm, 4 μ m particle size). Separation was achieved by gradient elution using mobile phases A (10 mM triethylamine and 10% acetonitrile in distilled water, adjusted to pH 2.5 with 11.6 M $HClO_4$) and B (acetonitrile). Initial conditions were 96% phase A - 4% phase B held for 3 min, followed by an increase in the proportion of phase B and to 30%, which was similarly held for 3 min. After this time, the proportion of phase B was increased linearly to 70% over 2.5 min. Column eluent was monitored by UV absorbance at 316 nm. Under these conditions, the retention times of 4MU glucuronide and 4MU were 3.9 and 5.9 min, respectively. The 4MU glucuronide calibration curve included 5 concentrations between 1 and 10 μ M for all enzymes except UGT 1A10, 2B7, 2B15 and 2B17 (1 to 25 μ M).

2.2.3.2 Lamotrigine (LTG) glucuronidation

Incubation conditions. As previously reported by Rowland et al. (2006a), incubations were conducted in a total volume of 200 μ l and contained LTG (prepared in 1 M H_3PO_4

containing 10% acetonitrile) \pm inhibitor, KOH (1 M, 37.2 μ l), HEK293 cell lysate expressing recombinant UGT1A4 (1 mg/ml) and MgCl₂ (4 mM). After a 5 min pre-incubation at 37°C, reactions were initiated with UDPGA (final concentration 5 mM) and then continued for 75 min. Reactions were terminated with HClO₄ (11.6 M, 2 μ l) and cooling on ice for 10 min. Samples were centrifuged (5,000 g) at 4°C for 10 min and an aliquot of the supernatant fraction was transferred into an HPLC vial.

Quantification. LTG glucuronide was separated using a Zorbax Eclipse XBD-C8 column (4.6 x 150 mm, 5 μ m particle size, Agilent Technologies) with gradient elution employing the following mobile phases: A, 25 mM phosphate buffer containing 2 mM triethylamine and 5% acetonitrile; and B, acetonitrile. Initial conditions were 96% phase A - 4% phase B for 3 min, after which time phase B was increased linearly to 13% over 4 min and then held for 1 min. Subsequently the proportion of phase B was increased to 50% over 1 min and held for 2 min, before returning to starting conditions. Column eluent was monitored by UV absorbance at 254 nm. Under these conditions retention times of LTG glucuronide and LTG were 5.1 and 11.4 min, respectively. The LTG glucuronide calibration curve included 5 concentrations in the range 1 – 10 μ M.

2.2.3.3 Codeine (COD) glucuronidation

Incubation conditions. Incubations, in a total volume of 100 μ l, contained COD (\pm inhibitor), recombinant UGT2B4 (1 mg/ml of Supersome protein), phosphate buffer 0.1 M, pH 7.4) and MgCl₂ (4 mM). Following pre-incubation at 37°C for 5 min reactions were initiated by the addition of UDPGA (final concentration 5 mM) and incubations were continued for 120 min. The reaction was terminated by the addition of HClO₄ (11.6 M, 1.5 μ l) and cooling on ice for 10 min. Samples were centrifuged (14,000 g) at 4°C for 5 min, and an 80 μ l of the supernatant fraction was transferred to

an Eppendorf tube containing 1 μl of KOH (4 M). After cooling on ice for 10 min samples were centrifuged (14,000 g for 5 min) and the supernatant fraction was decanted for analysis by HPLC.

Quantification. COD 6-O- β -D glucuronide was separated using a Phenomenex[®] Synergi Hydro-RP 80A-C18 column (3.0 x 150 mm, 4 μm particle size; Phenomenex, Sydney, Australia) with gradient elution employing the following mobile phases: A, 2 mM triethylamine and 13.5% acetonitrile in distilled water (adjusted to pH 2.7 with 11.6 M HClO₄); and B, acetonitrile. Initial conditions were 100% phase A for 3.5 min, after which time phase B was increased to 60% for 1 min followed by a return to the starting conditions. Column eluent was monitored by UV absorbance at 205 nm. Under these conditions, the retention times of COD glucuronide and COD were 1.9 and 2.8 min, respectively. The COD glucuronide calibration curve included 5 concentrations in the range 1 – 5 μM .

2.2.3.4 β -Estradiol (EST) glucuronidation

Incubation conditions. Incubations, in a total volume of 200 μl , contained β -EST (see Section 4.2.2 for concentrations) with and without a flozin (Section 4.2.2), enzyme (recombinant UGT1A1 (0.25 mg/ml of HEK293 cell lysate) or HLM (0.25 mg/ml)), phosphate buffer (0.1 M, pH 7.4), and MgCl₂ (4 mM). Following a 5 min pre-incubation at 37°C, reactions were initiated by the addition of UDPGA (final concentration 5 mM) and incubations were continued for 30 min. Reactions were terminated by the addition of HClO₄ (11.6 M, 2 μl) and cooling on ice for 10 min. Samples were subsequently centrifuged (5,000 g) at 4°C for 10 min and an aliquot of the supernatant fraction was injected into the HPLC column for the measurement of β -EST 3- β -D glucuronide formation.

Quantification. β -EST 3- β -D-glucuronide was separated on a Waters Nova-Pak[®], C-18 column (3.9 x 150 mm, 4 μ m particle size) with gradient elution employing the following mobile phases: A, 10 mM triethylamine and 10% acetonitrile in distilled water; and B, acetonitrile. Initial conditions were 85.5% phase A - 14.5% phase B for 4 min, after which time the proportion of phase B was increased linearly to 22% over 3 min. Phase B was then increased to 64% over 0.5 min held for 0.5 min, before returning to the starting conditions. β -EST glucuronide and β -EST were monitored by UV absorbance at 220 nm. The respective retention times of β -EST 3- β -D-glucuronide and β -EST were 5.1 and 9.7 min. The calibration curve included 5 β -EST 3- β -D-glucuronide concentrations in the range 1 – 5 μ M.

2.2.3.5 Propofol (PRO) glucuronidation

Incubation conditions. Incubations contained PRO (see Section 4.2.2 for concentrations) in the presence and absence of a flozin (Section 4.2.2), enzyme (recombinant UGT1A9 (0.25 mg/ml of HEK293 cell lysate) or HLM (0.5 mg/ml), phosphate buffer (0.1 M, pH 7.4) and MgCl₂ (4 mM) in a total volume of 200 μ l. Reactions were pre-incubated at 37°C for 5 min, and then initiated by the addition of UDPGA (final concentration 5 mM). Reactions were performed for 15 min, and then terminated with 4 volumes of ice-cold 4% acetic acid in methanol and cooling on ice for 10 min. Samples were centrifuged (5,000 g) at 4°C for 10 min and an aliquot of the supernatant fraction was injected into the HPLC column for measurement of PRO glucuronide formation.

Quantification. PRO glucuronide was separated using a Waters Nova-Pak[®] C-18 column with gradient elution employing the following mobile phases: A, 20 mM KH₂PO₄ (adjusted to pH 4.6 with 1 M K₂HPO₄) containing 5% acetonitrile; and B,

acetonitrile. Initial conditions were 80% phase A - 20% phase B for 4.5 min, after which time the proportion of phase B was increased linearly to 75% over 0.5 min and held for 5.5 min. Analytes were detected by UV absorbance at 214 nm. The retention times of PRO glucuronide and PRO were 4.2 and 8.4 min, respectively. Standard curves were generated with PRO itself (five concentrations in the range 2.5 – 25 μ M) due to the unavailability of an authentic glucuronide standard.

2.2.3.6 Cotinine glucuronidation by recombinant UGTs and human liver microsomes

Incubation conditions. Incubations (100 μ l total volume) contained COT (see Chapter 3 for concentrations), Supersome or HEK293 lysate protein (1 mg/ml) or HLM (0.5 mg/ml), phosphate buffer (0.1 M, pH 7.4) and $MgCl_2$ (4 mM). The incubation mixtures were pre-incubated at 37°C for 5 min and then reactions were initiated by the addition of UDPGA (5 mM final concentration). Incubations were continued at 37°C for 120 min, after which time reactions were terminated by the addition of $HClO_4$ (11.6 M, 1 μ l). Samples were cooled on ice for 10 min and then centrifuged (5,000 *g*) at 4°C for 10 min. An aliquot of the supernatant fraction was transferred to an HPLC vial for injection onto the HPLC column.

Quantification. Cotinine N-glucuronide was separated using a Zorbax Eclipse XBD-C8 column (4.6 x 150 mm, 5 μ m particle size) (Agilent Technologies) and isocratic elution with a 96:4 mixture of mobile phases A (4 mM 1-octanesulfonic acid in distilled water adjusted to pH 2.7 with 11.6 M $HClO_4$) and B (acetonitrile). Column eluent was monitored by UV absorbance at 254 nm. The retention times of cotinine N-glucuronide and cotinine were 7 and 43 min, respectively. A representative chromatogram is shown in Figure 2.1. Cotinine N-glucuronide was quantified by

reference to a calibration curve prepared using an authentic standard. Calibration curve concentration ranges were 1 – 5 μM and 1 – 25 μM with recombinant UGT2B10 and HLM as the respective enzyme sources.

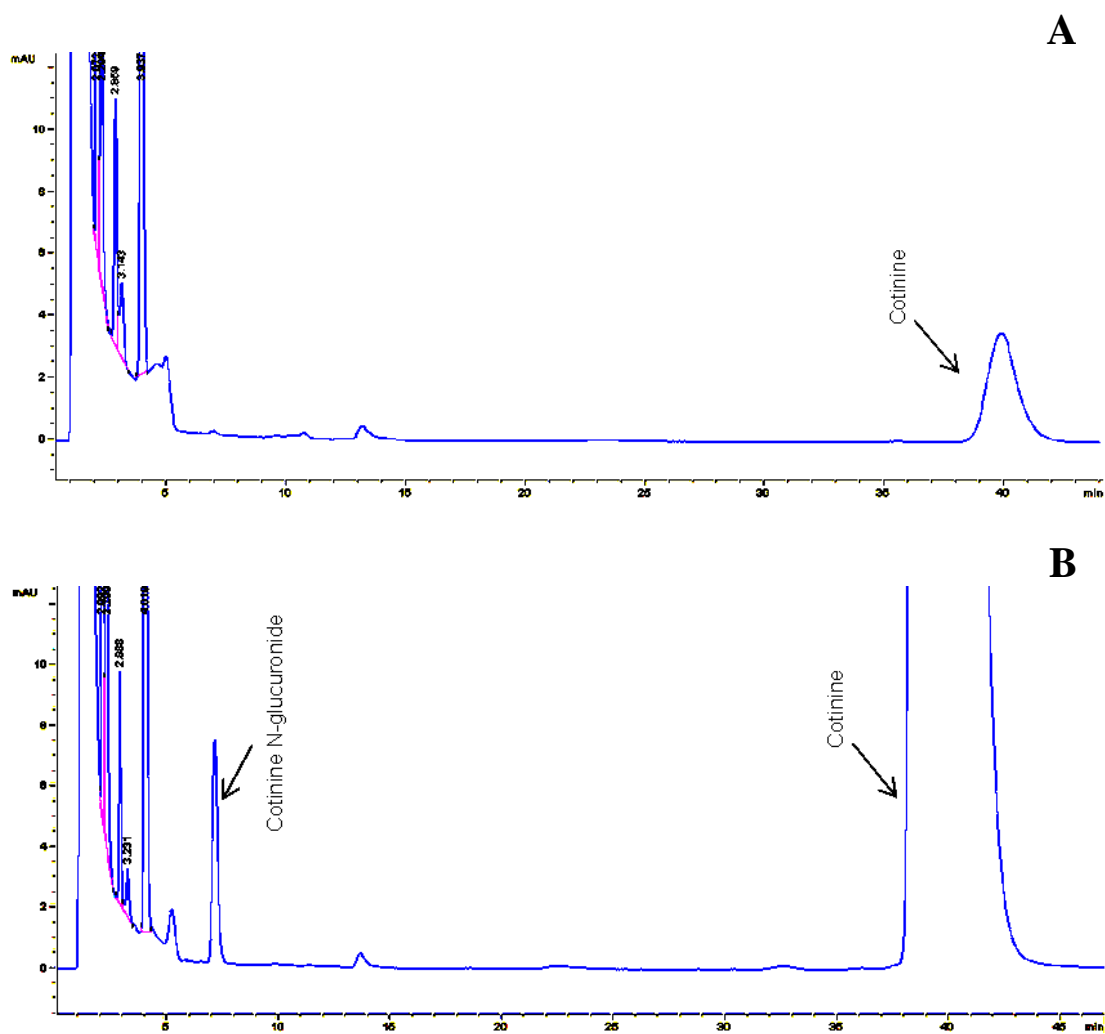


Figure 2.1 Representative chromatograms of cotinine and cotinine N-glucuronide.

Incubation of HLM with 0.25 mM cotinine in the absence of UDPGA (5 mM; Panel A) and 3 mM cotinine in the presence of UDPGA (5 mM; Panel B).

2.2.3.7 Linearity of cotinine N-glucuronidation by recombinant UGT2B10 with respect to protein concentration and incubation time

The cotinine glucuronidation assay was validated using HLM as the enzyme source to confirm linearity of cotinine glucuronide formation with respect to protein concentration (protein linearity) and incubation time (time linearity). For demonstration of protein linearity, cotinine N-glucuronide formation was measured at four HLM protein concentrations (0.25, 0.5, 0.75 and 1 mg/ml) at low, medium and high cotinine concentrations (0.25, 3 and 15 mM) following the method described in Section 2.2.3.6. The incubation time was 120 min. Demonstration of linearity with respect to incubation time was confirmed using four incubation times (60, 90, 120 and 150 min) at the same three COT concentrations employed for the protein linearity experiment. The HLM protein concentration present in incubations was 0.5 mg/ml. As shown in Figure 2.2, formation of cotinine N-glucuronide was linear ($r^2 > 0.98$) with respect to both HLM protein concentration and incubation time over the ranges investigated.

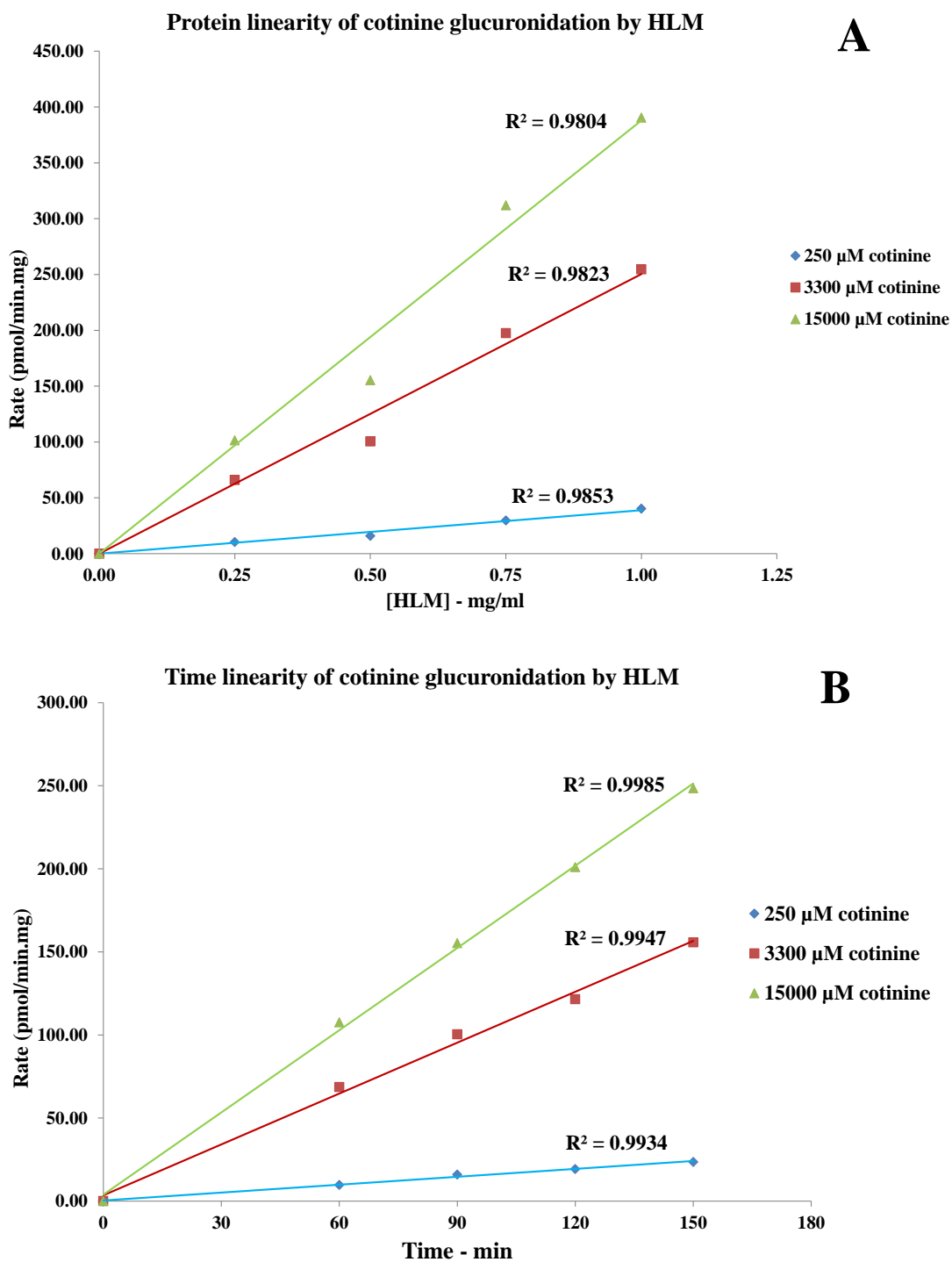


Figure 2.2 Linearity of protein concentration and incubation time for cotinine N-glucuronide formation by human liver microsomal UGT2B10.

Cotinine (0.25, 3 and 15 mM) was incubated with 0.25 – 1 mg/ml HLM for 120 min (Panel A) and with 0.5 mg/ml HLM from 60 to 150 min (Panel B).

2.2.3.8 Paclitaxel 6 α -hydroxylation by recombinant CYP2C8

Incubation procedure for the characterisation of paclitaxel (PAC) 6 α -hydroxylation kinetics. The method employed was as described in previous publications from this laboratory (Kerdpin et al. 2004; Polasek et al. 2004; Wattanachai et al. 2011), with minor modifications. Incubations, in a total volume of 200 μ l, contained of PAC (see Sections 5.2.2 and 5.3.3 for concentration ranges) and recombinant CYP2C8 (10 or 20 pmol/ml, see Section 5.2.2) in 0.1 M phosphate buffer (pH 7.4). The final concentration of DMSO, used to aid the dissolution of PAC in incubations, was 0.5%, which has only a minor effect on CYP2C8 activity (Busby, Ackermann and Crespi 1999). After pre-warming the incubation mixture to 37°C for 5 min, reactions were initiated by the addition of NADPH (1 mM final concentration) mixed with 5 mM MgCl₂. Following incubation at 37°C for 15 min, reactions were terminated with ice-cold acetonitrile (600 μ l) containing the assay internal standard (diethylstilbestrol, 0.05 μ g/ml). Protein was pelleted by centrifugation (5,000 g) at 4°C for 10 min. A 500 μ l aliquot of the supernatant fraction was evaporated to dryness using a miVac modular concentrator (Genevac, Suffolk, UK) over 30 min. The residue was reconstituted in 100 μ l of 25% acetonitrile in water and analysed by HPLC.

Inhibition of CYP2C8-catalysed paclitaxel 6 α -hydroxylation by glucuronide conjugates and their aglycones. Inhibition of CYP2C8 by glucuronides and their aglycones was characterised as the IC₅₀ and by the IC₅₀ ‘shift’ method, the latter to assess time-dependent inhibition from the comparison of IC₅₀ values determined from reactions pre-incubated in the absence and presence of NADPH (Grimm et al. 2009; Orr et al. 2012).

- An IC₅₀ was determined initially by co-incubation of PAC, inhibitor (see Section

5.2.3 for concentrations), recombinant CYP2C8 and NADPH. Following pre-incubation at 37°C for 5 min, reactions were initiated by the addition of NADPH and continued for 15 min. Reactions were terminated as described above and the decrease in PAC 6 α -hydroxylation activity was measured by HPLC. In the IC₅₀ shift method, recombinant CYP2C8 (2 or 4 pmol) and inhibitor (see Section 5.2.3 for concentrations) were pre-incubated in phosphate buffer (0.1 M, pH 7.4) at 37°C for 30 min, in the absence and presence of NADPH (1 mM plus MgCl₂, 5 mM). After this time, PAC and 1 mM NADPH (containing 5 mM MgCl₂) were added to mixtures lacking NADPH while PAC alone was added to the mixtures pre-incubated with added NADPH. Incubations were continued for 15 min at 37°C, and then terminated as described above.

Quantification of 6 α -hydroxy paclitaxel (6 α -OH PAC) formation. Analytes were separated using a Nova-Pak[®] C-18 column (3.9 x 150 mm, 4 μ m particle size) with gradient elution employing 0.002% glacial acetic acid in water containing 15% acetonitrile (mobile phase A) and acetonitrile (mobile phase B). Initial conditions were 78% phase A - 22% phase B. The proportion of phase B was increased from 22% to 37% according to a linear gradient over 15 min held for 0.4 min, and then increased to 72%. After 0.5 min the mobile phase composition was returned to starting conditions. Column eluent was monitored by UV absorbance at 230 nm. Retention times of 6 α -OH PAC, diethylstilbestrol and PAC were 12.7, 13.6 and 16.8 min, respectively. The calibration curve concentration range was 0.05 – 0.5 μ M.

2.2.4 Measurement of the non-specific binding of drugs to recombinant UGT enzyme sources, HLM and BSA using equilibrium dialysis

Most commonly, the non-specific binding of substrates and inhibitors to HLM and recombinant enzyme sources (\pm BSA, where included in incubations) was determined

using commercial rapid equilibrium dialysis (RED) devices with 8 kDa molecular weight cut-off cellulose membrane. The volume loaded in the sample (substrate or inhibitor with enzyme source in 0.1 M phosphate buffer, pH 7.4, \pm BSA) and buffer (0.1 M phosphate buffer, pH 7.4) chambers was as recommended by the supplier (RED device inserts, Thermo Fisher Scientific, USA). The RED devices were incubated at 37°C using an orbital shaking incubator. Control experiments, with either buffer or the protein source (buffer-buffer and protein-protein) in both chambers of the RED device, were performed to demonstrate attainment of equilibrium.

Where equilibrium was not achieved using the RED devices, binding was measured using conventional equilibrium dialysis according to the procedure of McLure, Miners and Birkett (2000). Dialysis was performed using Dianorm equilibrium dialysis cells (Dianorm, Munich, Germany) of 1.2 ml capacity per side, separated by Spectrapor number 4 dialysis membrane (molecular mass cut-off 12 – 14 kDa; Spectrum Medical Industries Inc, Los Angeles, CA, USA). As with experiments using RED devices, one cell contained the enzyme protein source (\pm BSA) and drug/inhibitor in phosphate buffer (0.1 M, pH 7.4), and the other phosphate buffer alone. The dialysis cell assembly was immersed in a water bath at 37°C and rotated at 12 rpm until equilibrium was achieved, typically 4 to 8 hr. As with the studies performed using RED devices, protein-protein and buffer-buffer control experiments were performed.

Following dialysis, the concentration of substrate or inhibitor present in each chamber of the RED device or each side of the dialysis cell was quantified by HPLC, as described in Chapter 3, Section 3.2.8 and Chapter 4, Section 4.2.3.

2.2.5 Bacterial culture, DNA manipulation and cytochrome P450 (CYP) expression

2.2.5.1 Preparation of competent cells for bacterial transformation

Manipulations of the wild-type and mutant CYP2C8 cDNAs (co-expressed with rat NADPH cytochrome P450 oxidoreductase (rCPR)) were carried out using DH5 α competent cells. DH5 α competent cells were prepared as described by Hanahan (1985). A 40% glycerol stock of DH5 α cells was streaked onto a Lauria-Bertani (LB) agar plate (Table 2.7) in the absence of antibiotic. The streaked plate was then placed in an incubator at 37°C for 16 hr. After this time, a single colony was isolated and subcultured in NZY⁺ broth (5 ml; Table 2.7) with orbital shaking (220 rpm; New Brunswick Scientific, Innova 4330) for 16 hr at 37°C. The subcultured DH5 α cells were then used to inoculate pre-warmed LB broth at 1:100 dilution in 500 ml conical flasks, which were maintained at 37°C with shaking (220 rpm), until an OD₆₀₀ of 0.3 – 0.5 absorbance units (AU) was attained. Cultures were subsequently transferred to sterile Falcon[®] tubes and chilled on ice for 10 min, and then centrifuged at 1,912 g for 10 min at 4°C. The pelleted bacteria were resuspended in 30 ml of RF1 solution (Table 2.8), incubated on ice for 45 min, and re-centrifuged at 5,311 g for 10 min at 4°C. The pellet of bacterial cells was resuspended in RF2 solution (Table 2.8) to provide a final volume of 8 ml. Resuspended cells were incubated on ice for 10 min, and then a 100 μ l aliquot was transferred into pre-chilled Eppendorf tubes (1.5 ml) using a sterile pipette tip. Tubes were immediately cooled in a dry ice - ethanol bath and then stored at -80°C until use.

Table 2.7 NZY⁺ broth and Lauria Bertani medium for bacterial culture.

Chemical/amount (g)
NZY⁺ broth (per litre)
NZ amine (10 g), yeast extract (5 g) and sodium chloride (5 g) were mixed in distilled water and the pH adjusted to 7.5 by the drop-wise addition of sodium hydroxide (0.1 M). The solution was autoclaved and supplemented (before use) with 1 M magnesium chloride (12.5 ml), 1 M magnesium sulfate (12.5 ml) and 20% glucose (20 ml). Finally, the mixture was filtered through a 0.2 µm membrane.
Lauria Bertani Medium (LB) (per litre)
Bacto-tryptone (10 g), yeast extract (5 g), sodium chloride (5 g) and sucrose (1 g) were mixed in 1 litre of distilled water. The pH was adjusted to 7.0 by the drop-wise addition of sodium hydroxide (10 M) before autoclaving.

Table 2.8 RF1 and RF2 preparation.

Chemical/amount (g)
RF1 solution
Rubidium chloride (12.1 g), manganese chloride (9.895 g), potassium acetate (2.944 g), calcium chloride (1.47 g) and 15% w/v glycerol were dissolved in distilled water and the pH was adjusted to 5.8 by a drop-wise addition of glacial acetic acid (10% v/v). Distilled water was added to a final volume of 1 litre and the solution was sterilised by filtration.
RF2 solution
MOPS (1.05 g), rubidium chloride (0.6 g), calcium chloride (5.51 g), 15 % w/v glycerol were dissolved in distilled water (500 ml) and the solution was sterilised by filtration.

2.2.5.2 Wild type human CYP2C8 and rat oxidoreductase (rCPR) cDNA construct

High expression levels of human CYP2C8 protein in *E. coli* was facilitated by modification of the N-terminus of the CYP2C8 cDNA, as established previously in this laboratory (Boye et al. 2004). The first 18 amino acids of the CYP2C8 cDNA were replaced by the leader sequence (MALLLAVFL) of bovine CYP17A (17α-

hydroxylase), and then the CYP2C consensus sequence (GLSCLLLLS) was connected to the leader sequence. The 17 α -CYP2C8 cDNA was constructed in the pCW ori (+) plasmid (Figure 2.3, Panel A).

CYP2C8 mutants were generated using pBlueScript II SK (+) (pBS II SK (+), Figure 2.3, Panel B) containing the 17 α -CYP2C8 cDNA. XhoI and HindIII restriction sites were added into the 17 α -CYP2C8 primers for cloning purposes. The forward and reverse primers were 5' AACCGC**CTCGAGG**AGAGGTCATATGGCTCTGTTATT AGC 3' and 5' CATGTTTGACAGCTTATCATCGATA**AGCTTTT**CAGACAGG 3', respectively. The recognition sites for these restriction enzymes are shown in bold type.

The N-terminus of rat CPR (rCPR) was additionally modified. The OmpA signal sequence (MKKTAIAIAVALAGFATVAQA) was fused upstream of the cDNA encoding rCPR. The Omp-rCPR expression construct was generated in the bacterial expression plasmid pACYP184, as previously reported by this laboratory (Boye et al. 2004) (Figure 2.3, Panel C).

The PCR product containing the 1,526 bp wild-type pCW17 α -CYP2C8 construct (see below, Section 2.2.5.3) was ligated into pBS II SK(+). 17 α -CYP2C8 and pBS II SK(+) were digested with XhoI and HindIII (1:2 vector to insert ratio). The ligation product was transformed into DH5 α *E. coli* cells. Colonies were randomly picked and analysed for pBS17 α -CYP2C8 by digestion with XhoI and HindIII (Figure 2.3, Panel D). The pBS17 α -CYP2C8 DNA sequence was confirmed by sequencing both strands (ABI 3130-XL DNA sequencer; Applied Biosystems, Victoria, Australia). This plasmid was subsequently used for site-directed mutagenesis.

2.2.5.3 *Polymerase chain reaction (PCR) conditions for wild-type CYP2C8 and CYP2C8 mutants*

PCR of wild-type CYP2C8 and CYP2C8 mutants was performed using the thermal cycler and chemicals given in Tables 2.3 and 2.4.

The primers containing the XhoI and HindIII recognition sites were used to produce 17 α -CYP2C8 fragments for mutagenesis (Figure 2.3, Panel E). PCR mixtures (25 μ l) contained Phusion[®] HF polymerase buffer (5x, 5 μ l), Phusion[®] HF polymerase (2 unit/ μ l, 0.25 μ l), DMSO (100%, 1.25 μ l), parenteral template (pCW17 α -CYP2C8, 10 ng/ μ l), XhoI and HindIII CYP2C8 primer (10 μ M, 1.25 μ l), and dNTPs (10 mM each, 0.5 μ l). Mineral oil (2 drops) was added to the surface of PCR mixtures to minimise evaporation. The initial PCR conditions were 98°C for 30 sec, followed by 35 amplification cycles, and then a denaturation step at 98°C for 10 sec following annealing step with gradient temperature 56 - 67°C for 30 sec and extension step at 72°C for 1 min. All PCR products were completely extended at 72°C for 5 min. After PCR completion, mixtures were cooled at 6°C until used.

As described in Chapter 5, eight single and 6 multiple CYP2C8 mutants were generated: Asn99Ala, Ser100Ala, Ser103Ala, Thr107Ala, Thr107Val, Ser114Ala, Gln214Ala, Gln214Leu, Ser100Ala-Ser103Ala, Ser103Ala-Thr107Val, Ser100Ala-Ser103Ala-Thr107Val, Ser100Ala-Ser103Ala-Thr107Val-Ser114Ala, Ser100Ala-Ser103Ala-Thr107Val-Ser114Ala-Gln214Ala, and Ser100Ala-Ser103Ala-Thr107Val-Ser114Ala-Gln214Leu.

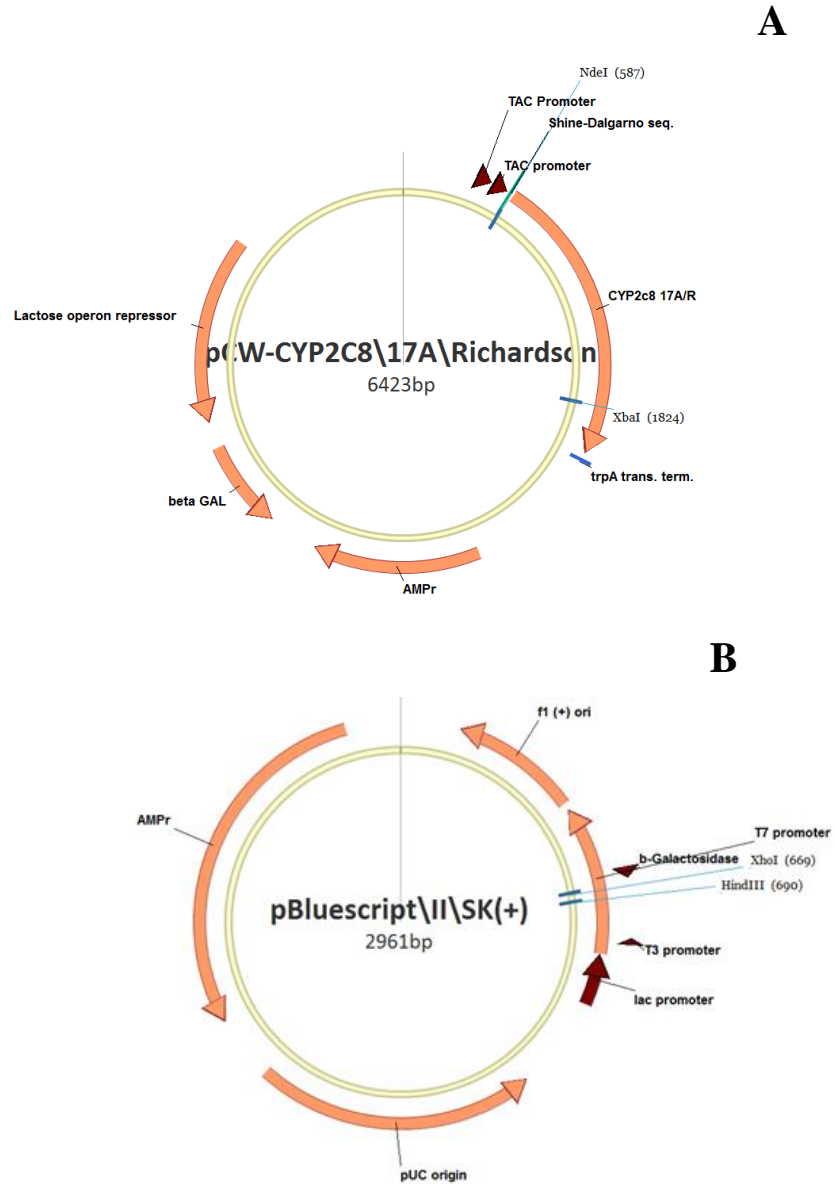
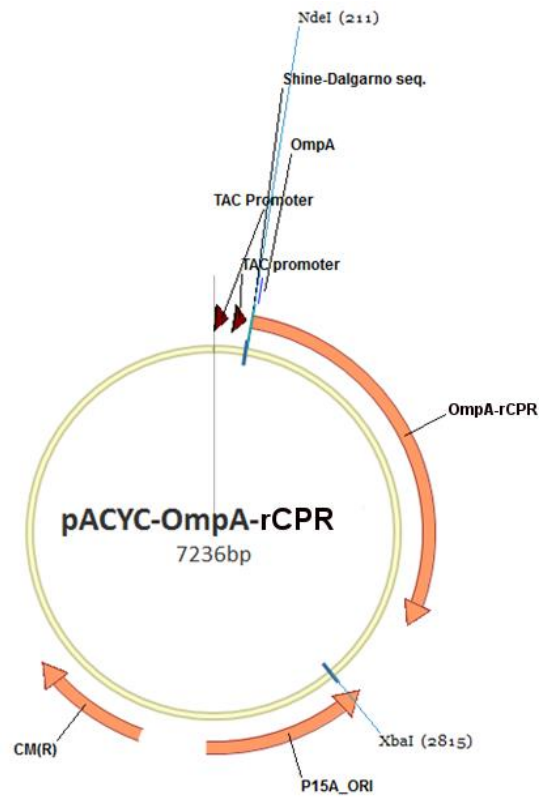


Figure 2.3 Plasmids used in molecular biology experiments.

pCW17 α -CYP2C8 (wild-type) (Panel A), pBS II SK (+) (Panel B), pACYC-OmpA-rCPR (Panel C), pBS17 α -CYP2C8 (Panel D), 17 α -CYP2C8 (XhoI/HindIII) (Panel E), and pCW ori (+) (Panel F). Restriction sites are shown.

C



D

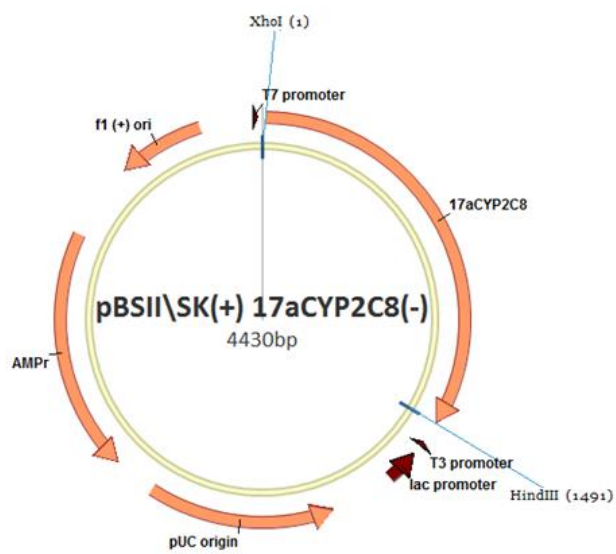


Figure 2.3 Plasmids used in molecular biology experiments (cont.).

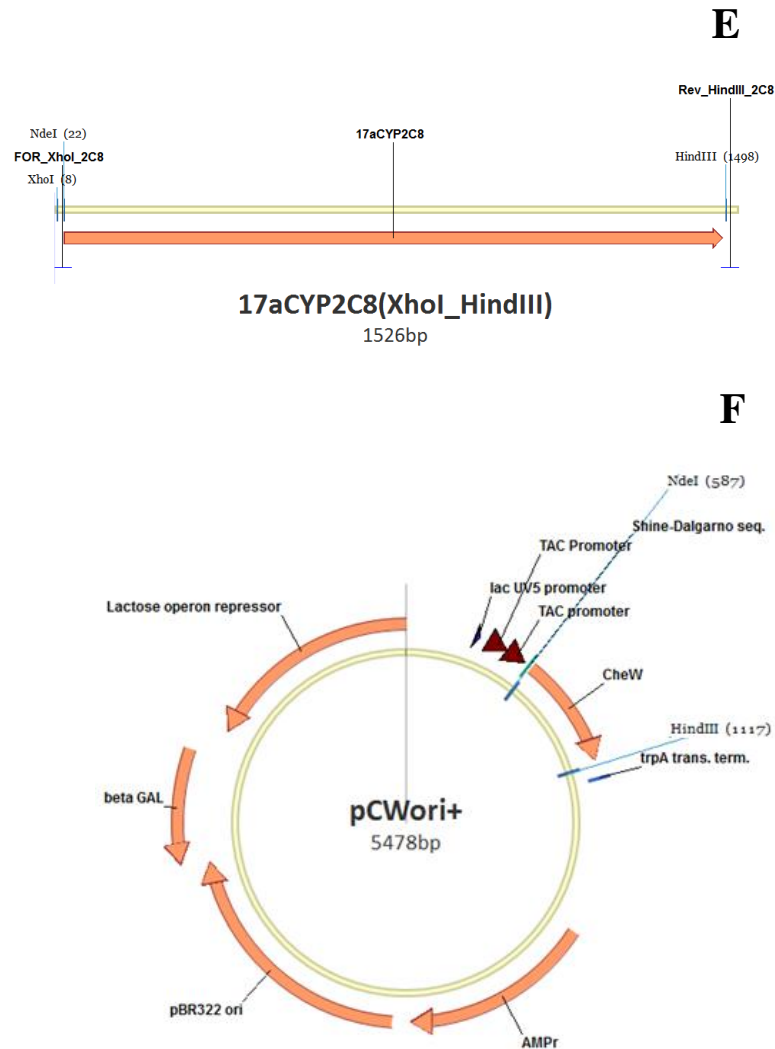


Figure 2.3 Plasmids used in molecular biology experiments (cont.).

Primers and templates used for site-directed mutagenesis are shown in Table 2.9. PCR mixtures (50 μ l) contained Phusion[®] HF polymerase buffer (5x, 10 μ l), Phusion[®] HF polymerase (2 unit/ μ l, 1 μ l), DMSO (100%, 2.5 μ l), DNA template (50 ng/ μ l, 2 μ l), forward and reverse mutagenesis primers (100 ng/ μ l, 1.25 μ l), and dNTPs (10 mM each, 1 μ l), with 2 drops of mineral oil added to the surface. A negative control reaction was incorporated in all PCR runs using nuclease-free water instead of DNA template. The PCR amplification protocol was essentially as described in the instruction manual of the QuikChange[®] Site-Directed Mutagenesis Kit, with minor modifications in primer design as recommended by Zheng, Baumann and Reymond (2004); an

overhang of at least 8 bases was incorporated at the 3'-terminus of both strands, and either a G or C was placed at the 5'- and 3'-termini. Following initial polymerase denaturation (95°C for 3 min), 16 subsequent PCR cycles included template denaturation (95°C for 1 min), primer annealing (52°C for 1 min) and extension at 72°C for 4 min, except in the final cycle where extension was continued at 72°C for 40 min. Finally, the PCR cycle was terminated by reducing the temperature to 6°C.

2.2.5.4 Gel purification

PCR or digestion mixtures (30 µl) were mixed with 6x DNA loading buffer (6 µl), loaded onto a 1% agarose gel, and electrophoresed in 1x Tris-acetate EDTA buffer (40 mM Tris-acetate, 1 mM EDTA) (TAE buffer) at 100 V for 30 min. A 1 kb DNA ladder was also loaded on each gel for DNA molecular weight estimation. Following electrophoresis, gels were stained with 3x GelRed™ for 20 min and DNA fragments were visualised at 365 nm. DNA was isolated from gel slices using the ISOLATE II PCR and Gel Kit (Bioline, NSW, Australia) following the supplier's instructions.

Table 2.9 Forward and reverse primers for the cloning of wild-type CYP2C8 and site-directed mutagenesis.

Amino acid mutated	Template	Primer	Nucleotide sequence
XhoI recognition site	Wild-type	XhoI CYP2C8	5'-AACCGCCTCGAGGAGAGGTCATATGGCTCTGTTATTAGC-3'
HindIII recognition site		HindIII CYP2C8	5'-CATGTTTGACAGCTTATCATCGATAAGCTTTTCAGACAGG-3'
Asn99Ala	Wild-type	Forward	5'-GGAAGAGGCGCTTCCCAATATCTCAAAGAATTAC-3'
		Reverse	5'-GATATTGGGGAAGCGCCTCTCCAGAAAAC-3'
Ser100Ala	Wild-type	Forward	5'-GAGGCAATGCCCAATATCTCAAAGAATTACTAAAGG-3'
		Reverse	5'-GATATTGGGGCATTGCCTCTCCAGAAAAC-3'
Ser103Ala	Wild-type	Forward	5'-GGCAATTCCCAATAGCTCAAAGAATTAC-3'
		Reverse	5'-GTCCTTTAGTAATTCTTTGAGCTATTGGG-3'
Thr107Ala	Wild-type	Forward	5'-CCCAATATCTCAAAGAATTGCTAAAGGAC-3'
		Reverse	5'-GATTCCAAGTCCTTTAGCAATTCTTTGAG-3'
Thr107Val	Wild-type	Forward	5'-CCCAATATCTCAAAGAATTGTTAAAGGAC-3'
		Reverse	5'-GATTCCAAGTCCTTTAAACAATTCTTTGAG-3'
Ser114Ala	Wild-type	Forward	5'-GGAATCATTGCCAGCAATGGAAAGAGATGG-3'
		Reverse	5'-CATTGCTGGCAATGATTCCAAGTCCTTTAGTAATTCC-3'
Gln214Ala	Wild-type	Forward	5'-CCCCATGGATCGCGGTCTGCAATAATTCCC-3'
		Reverse	5'-GCAGACCGCGATCCATGGGGAGTTCAG-3'

Table 2.9 Forward and reverse primers for the cloning of wild-type CYP2C8 and site-directed mutagenesis (cont.).

Amino acid mutated	Template	Primer	Nucleotide sequence
Gln214Leu	Wild-type	Forward	5'-CCCCATGGATCCTGGTCTGCAATAATTTCCCTCTAC-3'
		Reverse	5'-GCAGACCAGGATCCATGGGGAGTTCAGAATCC-3'
Ser100Ala-Ser103Ala	Wild-type	Forward	5'-GAGGCAATGCCCAATAGCTCAAAGAATTACTAAAGGACTTGG-3'
		Reverse	5'-CTTTGAGCTATTGGGGCATTGCCTCTCCAGAAAAC-3'
Ser103Ala-Thr107Val	Wild-type	Forward	5'-CCAATAGCTCAAAGAATTGTTAAAGGACTTGGAATC-3'
		Reverse	5'-CCTTTAACAATTCTTTGAGCTATTGGGGAATTGC-3'
Ser100Ala-Ser103Ala-Thr107Val	Wild-type	Forward	5'-GAGGCAATGCCCAATAGCTCAAAGAATTGTTAAAGGACTTGGAATC-3'
		Reverse	5'-CTTTAACAATTCTTTGAGCTATTGGGGCATTGCCTCTCCAGAAAAC-3'
Ser100Ala-Ser103Ala-Thr107Val-Ser114Ala	S114A	Forward	5'-GAGGCAATGCCCAATAGCTCAAAGAATTGTTAAAGGACTTGGAATC-3'
		Reverse	5'-CTTTAACAATTCTTTGAGCTATTGGGGCATTGCCTCTCCAGAAAAC-3'

Table 2.9 Forward and reverse primers for the cloning of wild-type CYP2C8 and site-directed mutagenesis (cont.).

Amino acid mutated	Template	Primer	Nucleotide sequence
Ser100Ala-Ser103Ala-Thr107Val- Ser114Ala-Gln214Ala	Ser100Ala/Ser103Ala/ Thr107Val/Ser114Ala	Forward	5'-CCCCATGGATCGCGGTCTGCAATAATTTCCC-3'
		Reverse	5'-GCAGACCGCGATCCATGGGGAGTTCAG-3'
Ser100Ala-Ser103Ala-Thr107Val- Ser114Ala-Gln214Leu	Wild-type	Forward	5'-CCCCATGGATCCTGGTCTGCAATAATTTCCCTCTAC-3'
		Reverse	5'-GCAGACCAGGATCCATGGGGAGTTCAGAATCC-3'

2.2.5.5 Ligation of DNA fragments

As indicated previously, the wild-type CYP2C8 cDNA was ligated into pBS II SK(+) and mutant CYP2C8 cDNAs were ligated into pCW ori (+). The experimental procedures followed to generate the pBS II SK(+) - 17 α -CYP2C8 and pCW – mutant 17 α -CYP2C8 plasmids are shown in Figures 2.4 and 2.5, respectively.

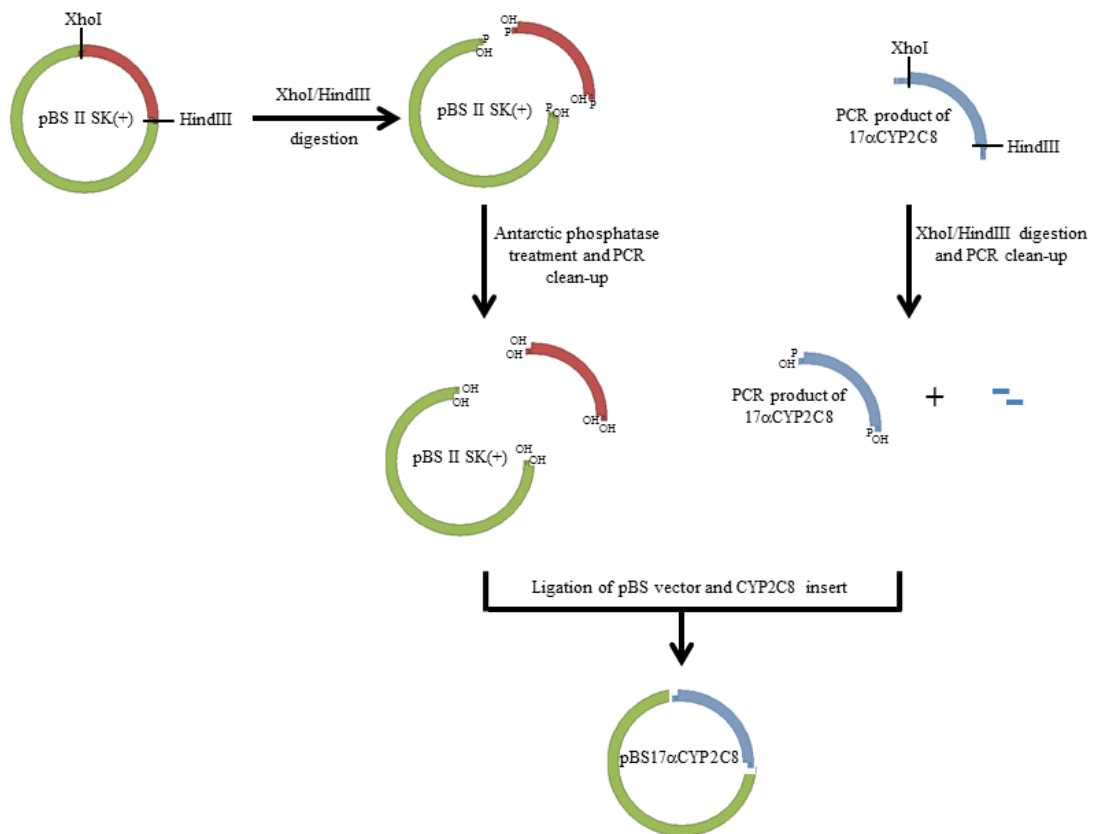


Figure 2.4 pBS II SK(+) - 17 α -CYP2C8 plasmid preparation.

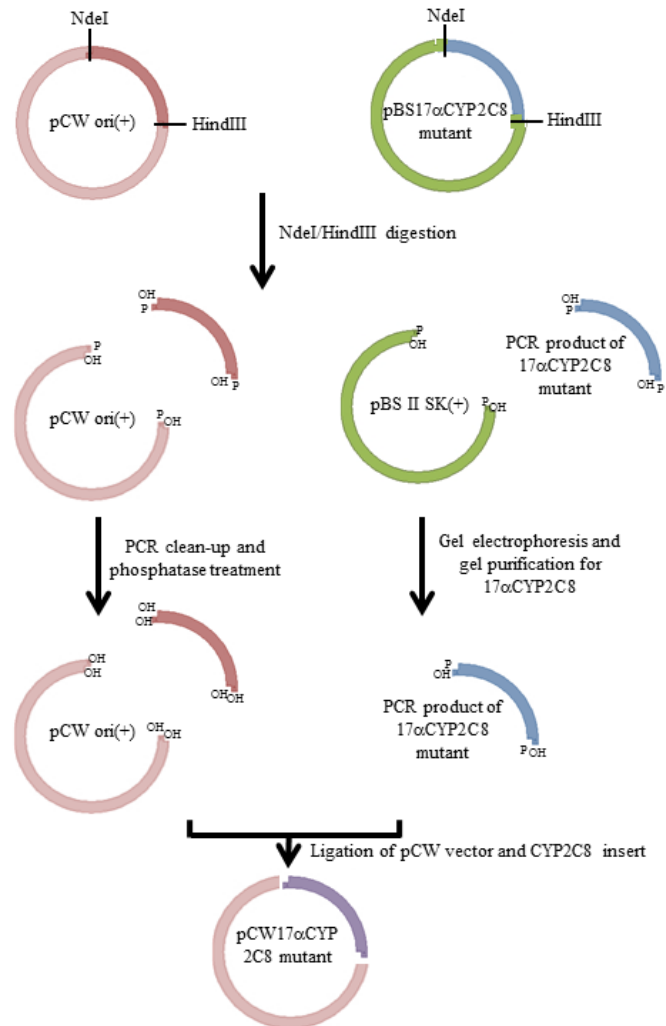


Figure 2.5 pCW – mutant 17 α -CYP2C8 plasmid preparation.

2.2.5.6 Identification of plasmid DNA

Pairs of restriction enzymes, XhoI/HindIII, NdeI/HindIII and NdeI/XbaI, were required for pBS17 α -CYP2C8, pCW17 α -CYP2C8 and pCW17 α -CYP2C8 plus pACYC-OmpA-CPR, respectively. Digestion conditions were as recommended by the Supplier (New England BioLabs). Digestion reactions contained DNA template (200 ng/ μ l), NEB buffer (1x), each pair of restriction enzymes (0.5 μ l) and nuclease-free water to a final volume of 10 μ l. Digestions were performed at 37°C for 1 hr.

2.2.5.7 Agarose gel electrophoresis

Digested plasmid DNA (10 μ l) was mixed with 2 μ l of 6x DNA loading buffer (0.25% (w/v) bromophenol blue, 0.25% (w/v) xylene cyanol, 30% (w/v) glycerol) and electrophoresed on a 1% (w/v) agarose gel in TAE buffer (1x) at 100 V for 20 min or 30 min (gel purification). Following electrophoresis, gels were stained with 3x GelRed™ for 20 min. Gels were exposed to UV light at 245 nm, and DNA fragments identified by reference to the DNA molecular weight ‘ladder’.

2.2.5.8 Bacterial transformation

DH5 α competent cells (40 μ l, from Section 2.2.5.1) were mixed with 0.5 μ l of whole plasmid or 2 μ l of PCR or ligation product in a pre-chilled Eppendorf tube. The competent cells were incubated on ice for 30 min, followed by heat shock at 42°C for 50 sec for uptake of the desired plasmid or DNA. The uptake process was terminated by placing the transformed cells on ice for 2 min. The transformation mixture was transferred to a pre-warmed 13 ml culture tube containing NZY⁺ amine broth (400 μ l). The culture tube was subsequently incubated, with shaking (220 rpm), at 37°C for 1 hr. The transformation mixtures (50 – 200 μ l) were then plated onto LB agar in the presence of the desired antibiotic(s), either 100 μ g/ml ampicillin (for pBS II SK(+)) and

the pCW ori(+) plasmid) or 50 µg/ml chloramphenicol (for the pACYC-OmpA-rCPR plasmid) and incubated at 37°C for 16 hr.

2.2.5.9 Enzyme expression

Single colonies of pCW17 α -CYP2C8 (wild-type or mutants) and pACYC-OmpA-rCPR were co-transformed according to Boye et al. (2004). Cells were subcultured in LB broth (5 ml) containing the desired antibiotic (see above) at 37°C for 16 hr. One ml of the cultures was used to inoculate 50 ml of Terrific broth (TB) (Table 2.10) containing 100 µg/ml ampicillin and 10 µg/ml chloramphenicol. Cells were cultured with shaking (200 rpm) at 37°C until obtaining an optical density of 0.7 – 0.9 AU at 600 nm. After cooling to 30°C, the culture was supplemented with 100 µl of 1 M δ -aminolevulinic acid (δ -ALA; 1 mM at final concentration) and 1 M isopropyl β -D-1-thiogalactopyranoside (IPTG; 1 mM at final concentration) and then incubated at 30°C for 24 hr with shaking (160 rpm). The bacterial cells were chilled on ice for 10 min and harvested by centrifugation (1,912 g) for 10 min at 4°C (K15 centrifuge). The cell pellet was suspended in TES buffer (15 ml/g wet-weight of cells) (Table 2.10). One hundred µl of lysozyme (3 mg/ml) per gram wet-weight of cells was employed to digest the outer bacterial membrane to yield spheroplasts. The suspension was diluted (1:1) with pre-chilled sterile water, and the spheroplast preparation was then incubated on ice with gentle shaking for 30 min. Spheroplasts were sedimented by centrifugation at 9,780 g for 10 min at 4°C (JA20 rotor, Beckman J2-21M/E centrifuge). The spheroplasts were subsequently resuspended in Spheroplast resuspension buffer (SRB) (Table 2.10), and then supplemented with protease inhibitors (200 µl of 30 mg/ml per 5 ml of SRB) and PMSF (50 µl of a 100 mM solution). Suspensions were sonicated on a salt-ice bath. Sonication involved 10 cycles, each separated by 1 min, of 8 ‘bursts’,

at 45% duty cycle. Membrane fractions were separated by centrifugation (9,780 *g*) for 20 min at 4°C (JA20 rotor, Beckman J2-21M/E centrifuge). The supernatant fraction was carefully transferred to clean centrifuge tubes and then centrifuged at 203,539 *g* for 1.5 hr at 4°C (60Ti rotor, Beckman L8-70M centrifuge). The membrane fractions containing CYP2C8 and rCPR were resuspended in 600 µl of TES-water (1:1). The protein concentration of membrane fractions was determined according to Lowry et al. (1951) (see Table 2.11 for reagents). The membrane fractions were stored at -80°C until use.

Table 2.10 Modified Terrific Broth, TES buffer and Spheroplast Resuspension Buffer preparation for enzyme expression.

Chemical/amount (or concentration)
<p>Modified Terrific Broth (TB) (per litre)</p> <p>Bacto-tryptone (12 g), yeast extract (24 g) and bacto-peptone (2 g) were dissolved in 896 ml of distilled water containing 4 ml of glycerol. After autoclaving, the solution was supplemented with a 100 ml sterile solution containing 170 mM KH_2PO_4 and 720 mM K_2HPO_4.</p>
<p>TES buffer (per litre)</p> <p>A 1 litre solution in distilled water contained Tris-base (or Tris-acetate; 100 mM), sucrose (500 mM) and EDTA (0.5 mM). HCl or glacial acetic acid was added dropwise to adjust the pH to 7.6. The solution was sterilised by autoclaving.</p>
<p>Spheroplast Resuspension Buffer (SRB) (per litre)</p> <p>One hundred ml of a solution of 170 mM KH_2PO_4 and 720 mM K_2HPO_4 solution (pH 7.6) was mixed with glycerol (200 ml) and autoclaved. The solution was allowed to cool overnight and then supplemented with sterilised 1 M magnesium acetate (6 ml) and 0.1 M DTT (100 ml).</p>

Table 2.11 Preparation of Lowry-Folin reagents for protein quantification.

Chemical/amount (g)
<p>Lowry reagent</p>
<p>Lowry A: 0.4 % sodium hydroxide (4 g) and 3 % sodium carbonate (30 g) in 100 ml water</p>
<p>Lowry B: 4 % sodium tartrate (8 g) in 200 ml water</p>
<p>Lowry C: 2 % copper sulphate (4 g) in 200 ml water</p>
<p><i>The Lowry reagent was prepared by mixing 100 parts of Lowry A with 1 part Lowry B and 1 part Lowry C.</i></p>
<p>Folin's reagent</p>
<p><i>Folin's Reagent was prepared by mixing 1 part Folin – Ciocalteu's Phenol Reagent with 1 part of water.</i></p>

2.2.5.10 Cytochrome P450 (CYP) and cytochrome P450 oxidoreductase (CPR)

quantification

- **Determination of CYP content.** The total CYP content of membrane fractions was quantified according to Omura and Sato (1964). Samples contained *E. coli* membrane fraction (1 mg/ml), phosphate buffer (0.1 M, pH 7.4) containing 20% glycerol, and 60 μ l of 10% Emulgen in a total volume of 2 ml. Sodium dithionite (~ 20 mg) was added and mixed by inversion of the sample tube until completely dissolved. One ml aliquots of the mixture were transferred into two quartz cuvettes, which were separately placed in the sample and reference positions of a Cary 300 scanning spectrophotometer (Varian Inc, Melbourne Vic, Australia). Background absorbance was zeroed and then spectra were recorded between 520 and 400 nm at a scan rate of 600 nm/min, with a spectral bandwidth of 1 nm. Carbon monoxide, at a flow rate of ~1.5 bubbles/sec, was bubbled through the sample cuvette for 1 min and then the difference spectrum was recorded. The CYP content and concentration of membrane fractions were calculated using equations 2.1 and 2.2.

Equation 2.1,

$$\text{CYP content (nmol/ml)} = \left(\frac{(\text{Abs}_{450} - \text{Abs}_{490}) \times \text{dilution factor} \times 1000}{91 \text{ mM}^{-1} \cdot \text{cm}^{-1}} \right)$$

Equation 2.2,

$$\text{CYP concentration (nmol/mg)} = \left(\frac{\text{P450 content (nmol/ml)}}{\text{protein concentration (mg/ml)}} \right)$$

- **Determination of CPR content.** The CPR activity of membrane fractions was determined using the procedure of Yasukochi and Masters (1976) with cytochrome c as the substrate. Reactions, in a volume of 2 ml, contained KCN (1 mM in potassium phosphate buffer (0.1 M, pH 7.4)), cytochrome c (52.5 μ M), and membrane fraction (100 μ g) in potassium phosphate buffer (0.3 M, pH 7.7). After 5 min at room temperature, 1 ml aliquots were transferred into two 1 ml quartz cuvettes, which were separately placed into the sample and reference positions of a Cary 300 scanning spectrophotometer. The reaction was initiated by the addition of NADPH (25 μ l of a 12 mM solution in potassium phosphate buffer (0.3 M, pH 7.7)) to the sample cuvette. The reduction of cytochrome c was measured over 1 min at 550 nm. The linear section of the curve was used to calculate CPR activity using equations 2.3 and 2.4.

Equation 2.3,

$$\text{nmol/min/mg protein} = \left(\frac{\text{OD}_{500}/\text{min} \times 1000 \times \text{total volume (ml)}}{19.1 \text{ mM}^{-1}\text{cm}^{-1} \times 1 \text{ cm} \times \text{protein conc (mg/ml)}} \right)$$

where $\text{OD}_{500}/\text{min}$ is the change in optical density at 500 nm per minute.

Equation 2.4,

$$\text{CPR concentration (nmol/mg)} = \left(\frac{\text{nmol cytochrome c reduced/min/mg}}{3000} \right)$$

2.2.5.11 Assessment of recombinant CYP2C8 protein expression by western immunoblotting

- Polyacrylamide gel electrophoresis (PAGE)

SDS-PAGE was performed using a BIORAD mini-PROTEAN[®] Electrophoresis Cell with a running buffer comprised of 25 mM Tris-base, 192 mM glycine and 3.5 mM SDS. Samples, in a total volume of 20 μ l, contained protein (25 μ g: HLM, positive

control; recombinant rCPR, negative control; and recombinant CYP2C8 enzymes), 4x SDS buffer (5 µl: 250 mM Tris-base, pH 6.8; 50% (v/v) glycerol; 5% (w/v) SDS; 0.2% (w/v) bromophenol blue; and 250 mM DTT) in sterile water. Samples were denatured at 98°C for 5 min and then loaded onto a 4% stacking gel and electrophoresed at 100 V (150 W/150 mA) until samples passed through the stacking gel (*ca.* 25-30 min). Samples were subsequently separated at 170 V (150 W/150 mA) on 10% polyacrylamide running gels until the dye eluted from the base of the gel (*ca.* 50-60 min). A western blotting marker (BIORAD®) (4 µl) was also run for molecular weight estimation.

- ***Protein transfer***

Separated proteins were rectilinearly transferred to a Trans-Blot® Transfer Medium pure nitrocellulose membrane (0.45 µm) at 100 V (150 W/150 mA) over 1 hr in pre-chilled transfer buffer (25 mM Tris-base, 192 mM glycine and 20% methanol). The nitrocellulose membrane was then washed three times with 60 ml of TBST (50 mM Tris-base, 37.5 mM NaCl, 0.02% Tween-20), and then twice with 60 ml of TBS (50 mM Tris-base and 37.5 mM NaCl). Following the wash steps, the membrane was soaked overnight at 4°C with 4% (w/v) skim milk powder in TBS to block the non-specific binding of antibodies.

- ***Immunodetection of CYP2C8***

Membranes were subsequently incubated with polyclonal anti-rabbit CYP2C8 (primary antibody) diluted 1:3000 in 10 ml of TBST containing 2% (w/v) skim milk powder for 2 hr at room temperature with gentle shaking. Following incubation, membranes were washed three times with 60 ml of TBST for 10 min, and then twice with TBS (60 ml). Membranes were then incubated with anti-rabbit CYP2C8 IgG

(secondary antibody) conjugated with horseradish peroxidase diluted 1:4000 in TBST containing (w/v) 2% skin milk powder for 1 hr at room temperature with gentle shaking, followed by washing with TBST (60 ml, three times).

- ***Blot analysis by chemiluminescence***

The peroxidase reaction was performed over 1 min with a mixture of luminol/enhancer solution and peroxide solution (800 µl of each) (see Table 2.3 for kits and suppliers). Immunoreactivity was detected digitally using a LAS-400 Chemiluminescent Imager and Multi Gauge image viewer (both Fuji Film Life Science Corporation, Tokyo, Japan). The expression of mutant CYP2C8 proteins was determined relative to wild-type CYP2C8.

2.3 Data analysis

The fraction unbound of each compound in incubation mixtures (containing HEK293 cell lysate, Supersomes, and/or HLM, without or with BSA), $f_{u_{mic}}$, determined by equilibrium dialysis was calculated as the concentration of the compound in the buffer compartment divided by the concentration in the sample compartment, as shown in equation 2.5. The concentration of compound in the buffer and protein compartment represent unbound compound and unbound plus bound compound, respectively.

Equation 2.5, fraction unbound:

$$f_{u_{mic}} = \frac{[\text{Buffer side}]}{[\text{Protein side}]} = \frac{[\text{Unbound drug}]}{[\text{Unbound drug} + \text{Bound drug}]}$$

Several equations employed to generate kinetic constants have been given in Chapter 1. However, all equations used in this thesis are additionally given below for ease of referral. Kinetic constants are presented as the mean \pm standard deviation (SD) derived from experiments with recombinant and human liver microsomal enzymes. IC_{50} values generated from inhibition screening studies are show as the mean \pm the standard error of the parameter fit (SE). Kinetic constants and IC_{50} values determined from experiments reported in Chapters 3 and 4 were calculated by fitting equations to experimental data using Enzfitter (version 2.1, Biosoft, Cambridge, UK). IC_{50} values used to determine the IC_{50} shift in Chapter 5 were generated using GraphPad Software (version 7.01) (GraphPad Software Inc, La Jolla, CA, USA). Equations employed in this thesis to generate kinetic parameters are shown below as equations 2.6 to 2.14 below. Goodness of fit of all expressions was assessed from comparison of the parameter SE of fit, coefficient of determination (r^2), 95% confidence intervals, and F-statistic. Prediction of drug-drug interaction (DDI) *in vivo* was assessed using

equations 2.15 – 2.17, while equations 2.18 and 2.19 were used in the assessment of time-dependent inhibition.

Equation 2.6, Michaelis-Menten equation:

$$v = \frac{V_{\max} \times [S]}{K_m + [S]}$$

where v is the rate of product formation, V_{\max} is maximal velocity, $[S]$ is substrate concentration and K_m is the Michaelis constant.

Equation 2.7, substrate inhibition equation:

$$v = 1 + \left[\left(\frac{K_m}{[S]} \right) + \left(\frac{[S]}{K_{si}} \right) \right]$$

where K_{si} is the constant describing the substrate inhibition interaction.

Equation 2.8, IC_{50} :

$$v_i = v_0 \left[1 - \frac{[I]}{([I] + IC_{50})} \right]$$

where v_0 is the control activity and v_i is the activity in the presence of the inhibitor (I).

Equation 2.9, IC_{50} values used to calculate the IC_{50} shift:

$$A = 100 \times \frac{[I]^n}{(IC_{50}^n + ([I]^n))}$$

where A is the %inhibition and n is Hill coefficient.

Equation 2.10, competitive inhibition:

$$v = \frac{V_{\max} \times [S]}{K_m(1 + [I]/K_i) + [S]}$$

where $[I]$ is the inhibitor concentration and K_i is the inhibitor constant (for the EI complex).

Equation 2.11, non-competitive inhibition:

$$v = \frac{V_{\max} \times [S]}{(1 + [I]/K_i)(K_m + [S])}$$

where K_i is the inhibitor constant for the EI and ESI complexes.

Equation 2.12, mixed (competitive – non-competitive) inhibition:

$$v = \frac{V_{\max} \times [S]}{K_m(1 + [I]/K_i) + [S](1 + [I]/K_i')}$$

where K_i and K_i' are the inhibitor constants for the EI and ESI complexes, respectively.

Equation 2.13, competitive inhibition of an enzyme exhibiting sigmoidal kinetics (homotropic positive cooperativity), version 1:

$$v = \frac{V_{\max} \times S_{50}^n}{S_{50}^n \left(1 + \frac{[I]}{K_i}\right) + S^n}$$

where S_{50} is the concentration at half V_{\max} and n is the Hill coefficient.

Equation 2.14, competitive inhibition of an enzyme exhibiting sigmoidal kinetics (homotropic positive cooperativity), version 2:

$$v = \frac{V_{\max} \times S_{50}^n}{S_{50}^n \left(1 + \frac{[I]}{K_i}\right)^n + S^n}$$

Equation 2.15, ratio of the areas under the plasma concentration – time curve (AUC) of the victim drug in the absence and presence of the inhibitor:

$$\frac{AUC_i}{AUC} = \frac{1}{\frac{f_m}{1 + [I]/K_i} + (1 - f_m)}$$

where f_m is the fraction of the dose metabolised by the inhibited enzyme.

For a drug metabolised by a single enzyme along a single metabolic pathway, the extent of inhibition of the hepatic clearance by a co-administered drug (determined as the ratio of the areas under the plasma drug concentration - time curves (AUC) with and without inhibitor co-administration) simplifies to equation 2.16, which is valid for competitive and non-competitive inhibition.

Equation 2.16, Ratio of AUC of the victim drug in the absence and presence of the inhibitor when the victim drug is metabolised by a single enzyme:

$$\frac{AUC_i}{AUC} = 1 + \frac{[I]}{K_i}$$

where [I] is the inhibitor concentration. Optimally, [I] is taken the hepatic inlet concentration (Miners et al., 2010b).

Equation 2.17, hepatic inlet concentration of inhibitor:

$$[I_{\text{inlet}}] = [I_{\text{max}}] + \frac{k_a \times F_a \cdot F_g \times D}{Q_H}$$

where $[I_{\text{max}}]$, k_a , F_a , F_g , D and Q_H are the maximum drug concentration in the systemic circulation associated with a given dose, absorption rate constant, fraction of the dose absorbed from the gastrointestinal tract, fraction of the absorbed dose escaping metabolism in the intestine, inhibitor dose and liver blood flow, respectively. However, given the frequent unavailability of key pharmacokinetic parameters (particularly k_a and $F_a \cdot F_g$) for many drugs, the maximum drug plasma concentration (C_{max}) is often used as the estimate of [I] in the calculation of the AUC ratio.

Equation 2.18, rate of enzyme inactivation by a mechanism-based inhibitor:

$$k_{\text{obs}} = \frac{k_{\text{inact}} \times [I]}{K_I + [I]}$$

where k_{obs} is the rate of enzyme inactivation at inhibitor concentration [I], k_{inact} is the

maximum rate of enzyme inactivation (analogous to V_{\max} in the Michaelis-Menten equation), and K_I is the inhibitor concentration that produces half the maximum rate of enzyme inactivation (analogous to K_m in the Michaelis-Menten equation).

Equation 2.19, relationship between shifted IC_{50} and (K_I/k_{inact}) :

$$IC_{50}^t = \ln 2 \left(\frac{K_I}{k_{inact} \times t} \right) \left(1 + \frac{[S]}{K_m} \right)$$

where IC_{50}^t is the ‘shifted’ IC_{50} from time-dependent inhibition studies, t is the pre-incubation time in the presence of inhibitor and NADPH, and $[S]/K_m$ is the ratio of the concentration of the ‘probe’ substrate relative to its K_m (Parkinson et al. 2011).

Statistical comparisons of kinetic constants presented in Chapter 3 were performed using the Mann-Whitney U-test with SPSS version 22, whereas one-way ANOVA followed by post-hoc analysis was applied for comparisons of kinetic parameters in Chapter 5. Respective equal and unequal variance of data, Tukey HSD and Games-Howell test were applied for those assumptions. Levene’s test was used to determine the method of post-hoc analysis (SPSS Inc, Chicago, IL). P values < 0.05 were considered significant.

CHAPTER 3

HUMAN UDP-GLUCURONOSYLTRANSFERASE (UGT) 2B10: VALIDATION OF COTININE AS A SELECTIVE PROBE SUBSTRATE, INHIBITION BY UGT ENZYME SELECTIVE INHIBITORS AND ANTIDEPRESSANT AND ANTIPSYCHOTIC DRUGS, AND STRUCTURAL DETERMINANTS OF ENZYME INHIBITION

The majority of the contents of this Chapter have been published as: Pattanawongsa, A, Nair, PC, Rowland, A and Miners, JO (2016), 'Human UDP-glucuronosyltransferase (UGT) 2B10: Validation of cotinine as a selective probe substrate, inhibition by UGT enzyme-selective inhibitors and antidepressant and antipsychotic drugs, and structural determinants of enzyme inhibition', *Drug Metabolism and Disposition*, 44 (3): 378-388.

Reproduced with the permission of the American Society for Pharmacology and Experimental Therapeutics.

3.1 Introduction

As noted in Chapter 1, available evidence indicates that the individual UGT enzymes exhibit distinct but sometimes overlapping substrate and inhibitor selectivities. However, data are lacking for several UGTs, especially with respect to inhibitor profiles. UGT2B10 was cloned initially in this laboratory. It was observed that UGT2B10 expressed in the mammalian COS7 cell line lacked activity towards hydroxylated xenobiotics and steroids (Jin et al. 1993). Later studies similarly demonstrated that UGT2B10 expressed in HEK293 cells did not catalyse the O-glucuronidation of 4-methylumbelliferone (4MU) and 1-naphthol (1NP) (Kerdpin et al. 2009), which are used widely as substrates for the screening of activity by

recombinant UGT enzymes (Uchaipichat et al. 2004). The inability of UGT2B10 to catalyse the O-glucuronidation of these compounds was subsequently shown to arise from substitution of the near conserved His, present in the N-terminus putative substrate binding domain of all UGT family 1 and 2 enzymes except UGT1A4 and UGT2B10, with Leu (Figure 3.1) (Kerdpin et al. 2009). Substitution of Leu34 of UGT2B10 with His, which functions as the catalytic base in O-glucuronidation reactions, generated an enzyme that metabolised the phenols 4MU and 1NP.

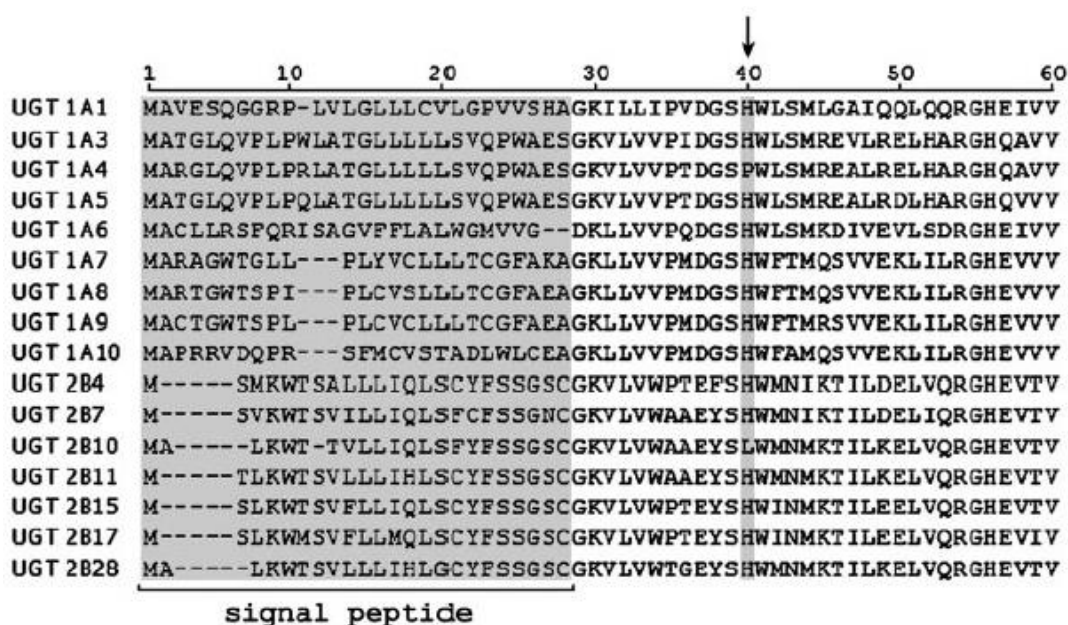


Figure 3.1 N-terminal sequence identity of UGT1A and 2B proteins.

Apart from UGT1A4 and UGT2B10, all UGT1A and UGT2B proteins have a conserved histidine at position 40 (numbering based on UGT1A1 sequence).

Reproduced with permission from Kerdpin, O, Mackenzie, PI, Bowalgaha, K, Finel, M and Miners, JO (2009), 'Influence of N-terminal domain histidine and proline residues on the substrate selectivities of human UDP-glucuronosyltransferase 1A1, 1A6, 1A9, 2B7, and 2B10', Drug Metabolism and Disposition, 37 (9): 1948-1955. Copyright (2009) the American Society for Pharmacology and Experimental Therapeutics.

Although initially considered an ‘orphan’ enzyme more recent studies have shown that UGT2B10, like UGT1A4, catalyses the N-glucuronidation of a number of xenobiotics that incorporate an aliphatic tertiary amine or aromatic N-heterocyclic group (Kaivosaaari, Finel and Koskinen 2011). Known substrates are nicotine and its oxidation product cotinine (Chen et al. 2007; Kaivosaaari et al. 2007), desloratadine (Kazmi et al. 2015a), medetomidine (Kaivosaaari et al. 2007), the tricyclic antidepressants (TCAs) amitriptyline, clomipramine, imipramine and trimipramine (Chen et al. 2007; Kato et al. 2013; Zhou et al. 2010), several tobacco-specific nitrosamines (Chen et al. 2008), RO5263397 (Fowler et al. 2015), and miscellaneous drugs that include diphenhydramine, ketoconazole, ketotifen, midazolam, olanzapine, pizotifen and tamoxifen (Erickson-Ridout, Zhu and Lazarus 2011; Kato et al. 2013). Consistent with the known selectivity of UGT1A4 for N-glucuronidation (Kubota et al. 2007), many UGT2B10 substrates are additionally glucuronidated by UGT1A4 and biphasic kinetics are frequently observed when human liver microsomes (HLM) are used as the enzyme source (Kaivosaaari, Finel and Koskinen 2011; Kato et al. 2013). However, available evidence indicates that UGT2B10 is the high affinity enzyme involved in most reactions.

Nicotine is converted to cotinine by CYP2A6, CYP2A13, and aldehyde oxidase. Cotinine is oxidised by CYP2A6 to form cotinine N-oxide and by CYP2A6 and CYP2A13 to give trans-3'-hydroxycotinine. The trans-3'-hydroxycotinine is subsequently glucuronidated by UGT2B17 to produce cotinine-3'-O-glucuronide. Cotinine itself is also glucuronidated predominantly by UGT2B10 (see Results) to form cotinine N-glucuronide, as shown in Figure 3.2.

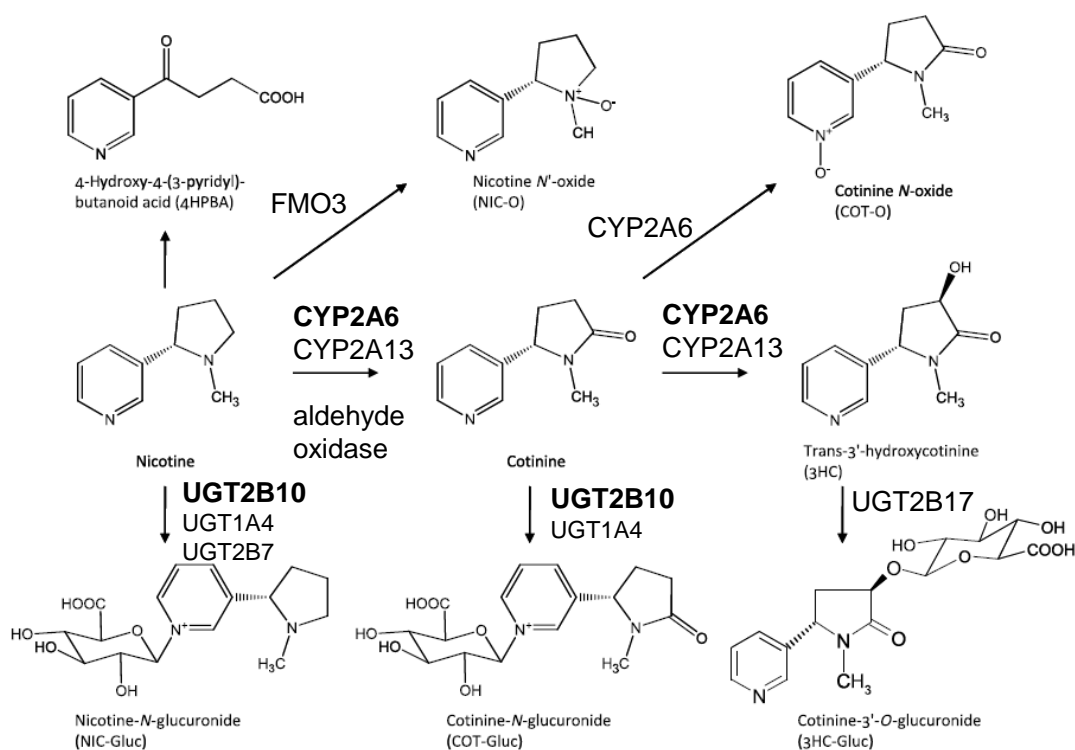


Figure 3.2 Cotinine metabolic pathway.

Adapted with permission from Chen, G, Giambone, NE, Dluzen, DF, Muscat, JE, Berg, A, Gallagher, CJ and Lazarus, P (2010), 'Glucuronidation genotypes and nicotine metabolic phenotypes: importance of functional UGT2B10 and UGT2B17 polymorphisms', *Cancer Research*, 70 (19): 7543-7552. Copyright (2010) American Association for Cancer Research. Additional data are from Benowitz et al. (1999), Chen, Giambone and Lazarus (2012), Kaivosari et al. (2007), and Murphy et al. (2014).

The UGT2B10 substrates desloratadine and nicotine further act as inhibitors of this enzyme. In particular, desloratadine has been reported to be a relatively selective and potent competitive inhibitor of UGT2B10, with a K_i of 1.3 μM (Kazmi et al. 2015b). Nicotine has also been employed as an inhibitor of UGT2B10 *in vitro*, although the UGT enzyme inhibition selectivity of this compound is incompletely characterised (Zhou et al. 2010). A large number of clinically used drugs contain an aliphatic amine or aromatic N-heterocyclic group. Notable in this regard are antidepressants (TCAs), selective serotonin reuptake inhibitors (SSRIs), serotonin and noradrenaline reuptake inhibitors (SNRIs), tetracyclic antidepressants, and monoamine oxidase inhibitors (MAOIs) and antipsychotics (both ‘typical’ and ‘atypical’) (Appendix figure 1). Indeed, the majority of drugs in these classes are either tertiary or secondary aliphatic amines. Despite their widespread clinical use, however, the potential inhibition of UGT2B10 by these compounds has not been explored in a systematic manner. Furthermore, knowledge of the effects of UGT enzyme selective inhibitors employed for reaction phenotyping *in vitro* on UGT2B10 activity is similarly lacking (Miners et al. 2010b).

The aims of the studies described in this Chapter were to: (i) confirm that UGT2B10 expressed in insect cells (*T. ni*; SupersomesTM) exhibited a similar substrate selectivity to UGT2B10 expressed in mammalian cell lines (COS7 and HEK293); (ii) confirm the UGT enzyme selectivity of cotinine as a UGT2B10 substrate and desloratadine and nicotine as UGT2B10 inhibitors; (iii) characterise the kinetics of cotinine N-glucuronidation by recombinant UGT2B10 and HLM, in the absence and presence of BSA; (iv) investigate the potential inhibition of UGT2B10 by currently used UGT enzyme selective inhibitors employed for reaction phenotyping; (v) characterise the inhibition of UGT2B10 by 34 amines (primary, secondary and tertiary) containing

antidepressants and antipsychotics from various classes (TCAs, SSRIs, SNRIs, MAOIs, and typical and atypical antipsychotics); (vi) identify the structural features of compounds required for potent inhibition of UGT2B10; and (vii) provide insights into potential drug-drug DDIs arising from inhibition of this enzyme.

3.2 Materials and Methods

3.2.1 Enzyme sources

UGT1A enzymes were expressed in HEK293 cells, as described in Section 2.2.1, while Supersomes expressing UGT2B enzymes were sourced commercially (Section 2.2.1). Pooled HLM (150 donor pool) were purchased from BD Biosciences (Section 2.2.1).

3.2.2 4-Methylumbelliferone (4MU) and 1-naphthol (1NP) glucuronidation by recombinant UGT2B10 (Supersomes)

To confirm previous findings with recombinant human UGT2B10 expressed in COS7 and HEK293 cells as the enzyme sources, 4MU and 1NP glucuronidation by Supersomes expressing UGT2B10 was investigated at three substrate concentrations (10, 100 and 1,000 μM). Incubation mixtures contained 4MU or 1NP, Supersome expressing UGT2B10 (1 mg/ml of Supersome protein), phosphate buffer (0.1 M, pH 7.4), MgCl_2 (4 mM) and UDPGA (5 mM) in a total volume of 100 μl . Reactions were initiated by the addition of UDPGA, and then continued for 120 min. Reactions were terminated with 11.6 M HClO_4 (1 μl), vortex-mixed and placed on ice for 10 min, and the precipitated protein was separated by centrifugation (5,000 g) for 10 min at 4 $^\circ\text{C}$. An aliquot of the supernatant solution was transferred into HPLC vials for analysis (see Sections 2.2.2 and 2.2.3.1).

3.2.3 Cotinine N-glucuronidation by recombinant human UGTs and HLM

Thirteen recombinant UGTs from sub-families 1A and 2B were screened for cotinine N-glucuronidation; 1A1, 1A3, 1A4, 1A6, 1A7, 1A8, 1A9, 1A10, 2B4, 2B7, 2B10, 2B15 and 2B17. Activity was assessed at cotinine concentrations of 0.25, 3 and 15 mM following the method described in Section 2.2.3.6. The kinetics of cotinine N-glucuronidation by recombinant UGT2B10 and HLM were determined (4 to 6 replicates) at nine or ten substrate concentrations spanning the range 0.25 – 15 mM.

Kinetic experiments were performed in the absence and presence of BSA (1% w/v). Incubations containing BSA were terminated by the addition of 3 μ l of 11.6 M HClO₄ (of 1 μ l for incubations without added BSA; Section 2.2.3.6).

3.2.4 Inhibition of recombinant human UGT2B10 activity by antidepressants, antipsychotics and other compounds

The inhibition of recombinant human UGT2B10 enzyme activity was determined for 43 compounds (Table 3.4). Effects on UGT2B10 activity were investigated at four inhibitor concentrations (1, 10, 100 and 500 μ M), except for fluconazole (1, 2.5, 5 and 10 mM), hecogenin (1, 10, 50 and 100 μ M), itraconazole (1, 10, 50, and 100 μ M), ketoconazole (1, 10, 100 and 200 μ M), and niflumic acid (1, 10, 100 and 200 μ M). Stock solutions of the antidepressant and antipsychotic drugs available as salts (see Section 2.1 and Table 2.1) were prepared in water. Stock solutions of all other inhibitors were prepared in DMSO, with the following exceptions; desloratadine and nicotine stock solutions were prepared in ethanol, while hecogenin was dissolved in methanol. The final concentration of solvent present in incubation mixtures was 1% (v/v). The inhibition studies were performed at a cotinine concentration of 2.8 mM, which corresponds to the apparent K_m for cotinine N-glucuronidation by recombinant UGT2B10 (Table 3.2).

3.2.5 Inhibition of recombinant human UGT enzyme activities by desloratadine and nicotine

In addition to effects on UGT2B10, desloratadine and nicotine (1, 10, 100 and 500 μ M) were screened for inhibition of the UGT1A and UGT2B subfamily enzymes UGT1A1, 1A3, 1A4, 1A6, 1A7, 1A8, 1A9, 1A10, 2B4, 2B7, 2B15 and 2B17. Effects on all enzymes except UGT1A4 and UGT2B4 were determined using the non-selective substrate 4MU. The 4MU concentration used in incubations corresponded to the published apparent K_m or S_{50} of each enzyme, while protein concentrations and

incubation time varied for each enzyme (see Section 2.2.3 and Table 2.6). 4MU glucuronide formation was quantified as described in Section 2.2.3.1. Inhibition of UGT1A4 by desloratadine and nicotine was assessed with lamotrigine (LTG) as the probe substrate (Section 2.2.3.2), while effects on UGT2B4 activity were determined with codeine (COD) as the substrate (Section 2.2.3.3). Concentrations of LTG and COD used in the UGT1A4 and UGT2B4 inhibition screening studies corresponded to the respective K_m values for each substrate/pair; 1.5 mM for lamotrigine/UGT1A4 and 2.0 mM for codeine/UGT2B4 (Table 2.6). Positive control inhibitors were used in all inhibition screening experiments: hecogenin (UGT1A4 – 10 μ M); niflumic acid (UGT1A9 – 2.5 μ M, UGT1A1 – 100 μ M); phenylbutazone (UGT 1A3, 1A6, 1A7, 1A8, 1A10 – 500 μ M); fluconazole (UGT 2B4 and 2B7 – 2.5 mM); and diclofenac (UGT 2B15 and 2B17 – 500 μ M). The magnitude of inhibition of each positive control inhibitor (data not shown) was as expected from previous studies in this and another laboratory (Kazmi et al. 2015b; Miners et al. 2011; Raungrut et al. 2010; Uchaipichat et al. 2006a; Uchaipichat et al. 2004; Uchaipichat et al. 2006b).

3.2.6 Inhibition of human liver microsomal cotinine N-glucuronidation by hecogenin and desloratadine

The relative contributions of UGT1A4 and UGT2B10 to human liver microsomal cotinine N-glucuronidation were investigated using the selective inhibitors hecogenin (UGT1A4; Uchaipichat et al. 2006a) and desloratadine (UGT2B10; Kazmi et al. 2015b). The effects of each inhibitor (10 μ M) were determined at each of 4 cotinine concentrations (0.25, 1, 3, 6 mM) following the procedure described above (Section 3.2.4). The formation of cotinine N-glucuronide in the presence of desloratadine or hecogenin or a combination of both was compared to metabolite production in the absence of the inhibitors.

3.2.7 Kinetic characterisation of amitriptyline, doxepin and mianserin inhibition of human liver microsomal cotinine N-glucuronidation

The kinetics and mechanism of inhibition of cotinine N-glucuronidation by amitriptyline, doxepin and mianserin were characterised with HLM as the enzyme source following the method described in Section 2.2.3.6. Experiments to characterise inhibitor constants (K_i) employed HLM (0.5 mg/ml) supplemented with BSA (1% w/v). Effects of four added concentrations (1, 2.5, 5 and 10 μ M) of each of amitriptyline, doxepin and mianserin were characterised at each of the three added cotinine concentrations (1, 2 and 3 mM). Concentrations of each of the inhibitors were corrected for non-specific binding to HLM and BSA.

3.2.8 Measurement of the non-specific binding of cotinine to Supersomes, HLM and BSA, and amitriptyline, doxepin and mianserin to HLM and BSA

Non-specific binding experiments were performed using rapid equilibrium dialysis (RED) devices fitted with an 8 kDa molecular weight cut-off cellulose membrane, as described in Section 2.2.4. For the assessment of cotinine binding, the sample chamber was loaded with cotinine (0.1 – 15 mM) and Supersome protein (1 mg/ml) or HLM (0.5 mg/ml) and/or BSA (1% w/v), in 0.1 M phosphate buffer (pH 7.4, total volume 100 μ l). The buffer chamber was loaded with 300 μ l of 0.1 M phosphate buffer (pH 7.4). Experiments were also performed with buffer - buffer, enzyme - enzyme and BSA - BSA controls. The RED devices were incubated at 37°C for 5 hr, by which time equilibrium was achieved. A 30 μ l aliquot was collected from each chamber and protein was precipitated with 0.3 μ l of 11.6 M HClO₄, or with 0.9 μ l of 11.6 M HClO₄ for samples containing BSA. Samples were cooled on ice for 10 min and then centrifuged (5,000 g) at 4°C for 10 min. A 10 μ l aliquot was diluted with 90 μ l of 5% acetonitrile in water. Cotinine was analysed by HPLC following the procedure described for cotinine N-glucuronide (Section 2.2.3.6), but using 83% mobile phase A

and 17% mobile phase B. Under these conditions, the retention time of cotinine was 4.6 min.

The binding of amitriptyline, doxepin and mianserin (2, 5, 10 and 25 μM) to HLM (0.5 mg/ml) plus BSA (1% w/v) was similarly measured using the RED device. Like cotinine, experiments were performed with buffer - buffer and protein - protein controls. After equilibration, a 70 μl aliquot was taken from each chamber and mixed with four volumes of 4% acetic acid in methanol, which also contained the assay internal standard (see below). Samples were cooled on ice for 10 min, and then centrifuged (5,000 g) at 4°C for 10 min. The supernatant fraction was decanted and evaporated to dryness using a miVac modular concentrator (Genevac, Suffolk, UK). The residue was reconstituted in 50 μl of the mobile phase and analysed by HPLC. HPLC conditions for the measurement of amitriptyline, doxepin and mianserin and their respective internal standards (1 μM nortriptyline, 1 μM imipramine and 2 μM amitriptyline, respectively) are given in Table 3.1.

Table 3.1 HPLC conditions for the quantification of amitriptyline, doxepin and mianserin in dialysates from equilibrium dialysis experiments.

Drug	Mobile phase composition	Detector wavelength (nm)	Retention time (min)
Amitriptyline	40% A : 60% C	240	6.0 (Amitriptyline)
			3.8 (Nortriptyline, IS)
Doxepin	48% A : 52% C	240	4.6 (Doxepin)
			6.7 (Imipramine, IS)
Mianserin	40% B : 60% C	240	4.4 (Mianserin)
			6.0 (Amitriptyline, IS)

Column: Nova-Pak[®] Waters, C-18, 3.9 x 150 mm, 4 µm particle size.

IS: internal standard

Mobile phase composition:

A: 20 mM ammonium acetate (0.002% triethylamine) containing 10% acetonitrile.

B: 4 mM 1-octanesulfonic acid (adjusted to pH 2.7 with 11.6 M HClO₄)

C: acetonitrile.

3.2.9 Molecular modelling

The three-dimensional (3D) coordinates (sdf format) of dataset molecules were obtained from the Pubchem server (<https://pubchem.ncbi.nlm.nih.gov/>). The molecules were imported into SYBYL (version X-2.1, CERTARA, Princeton, NJ, USA) and geometry optimised using the AM1 Hamiltonian (MOPAC). All molecular modelling was performed using SYBYL installed on a Macintosh workstation with an OS X 10.9.5 operating system. The structural overlay of molecules was undertaken using the Surfex-Sim program (Jain 2000 and 2004), which utilises the morphological similarity approach to generate alignments of molecules. Similarity is defined as a Gaussian function of the differences in the molecular surface distances of two

molecules at weighted observation points on a uniform grid. The computed surface represent distances to the nearest atomic surface and distances to donor and acceptor surfaces. Amitriptyline, one of the most potent UGT2B10 inhibitors (see Results), was used as the template for the overlay of dataset molecule(s). The overlay quality of the dataset molecules was evaluated by measuring the distance between key pharmacophoric features, including the centroid of either of the phenyl rings (present in the tricyclic structure of amitriptyline) and the aryl ring (closest) of the dataset molecule observed in the alignment. Moreover, the distances between the side-chain amine N atom of amitriptyline and the dataset molecules (aliphatic or alicyclic) were also estimated. The smaller the distance, the more closely the pharmacophoric features overlay between amitriptyline and the dataset molecule. In addition, for tri- and tetra-cyclic compounds, the angles between the rings of the tricyclic scaffold were measured by defining a centroid for each ring on the geometry optimised structures. The torsion angles were measured for the bridge (-CH₂-X where X= -CH₂, -O, or -N) connecting the two aromatic rings of the tricyclic scaffold. For example, in the case of amitriptyline the torsion angle was measured for the dimethylene (-CH₂-CH₂-) bridge of the central 7-membered (cycloheptene) ring.

3.2.10 Data analysis

K_m and V_{max} values were generated using Enzfitter (version 2.0, Biosoft, Cambridge, UK) by fitting the equations for empirical kinetic models to experimental data (equations 2.6 – 2.7, Section 2.3). Goodness of fit of all expressions was evaluated from comparison of standard error (SE) of the parameter of fit, r^2 , 95% confidence intervals, and F-statistic. Statistical comparisons of kinetic constants shown in Table 3.2 were performed using the Mann-Whitney U-test with SPSS version 22 (SPSS Inc, Chicago, IL, USA). P values < 0.05 were considered significant.

IC₅₀ values were generated by fitting equation 2.8 (Section 2.3) to experimental data, while the inhibitor constants ($K_{i,u}$) for amitriptyline, doxepin and mianserin based on unbound concentration of inhibitors (i.e. corrected for binding to incubation constituents) were obtained by fitting equations 2.10 – 2.12 (Section 2.3) to experimental data. Goodness of fit of the equations for competitive, non-competitive or mixed inhibition was assessed as described above.

The likelihood of a DDI arising from amitriptyline, doxepin and mianserin inhibition of UGT2B10 was evaluated using the IV-IVE approach described in Sections 1.8.2 and 2.3, which gives the predicted AUC ratio of the victim drug administered in the presence and absence of inhibitor. Where the victim drug is metabolised along a single pathway by the inhibited enzyme, the AUC ratio may be calculated using equation 2.16 (Section 2.3). Since values of the absorption rate constant and fractions absorbed from the gastrointestinal tract and escaping intestinal metabolism were not available for amitriptyline, doxepin and mianserin, the maximum total and unbound concentrations (C_{max}) of the perpetrator (see Section 1.8.2) were used as the value of [I] in equation 2.17 (Section 2.3).

C_{max} and f_u (fraction unbound in plasma) values for amitriptyline, doxepin and mianserin were taken from the following literature sources. Amitriptyline (50 mg dose): mean C_{max} 0.15 μ M (Kukes et al. 2009), f_u 0.065 (Baumann et al. 1986). Assuming linear kinetics, the C_{max} expected for a single 150 mg dose of amitriptyline is 0.45 μ M. Doxepin (50 mg dose): mean C_{max} 0.29 μ M (Virtanen, Scheinin and Iisalo 1980), f_u 0.79 (Faulkner et al. 1983). Again, assuming linear kinetics, the C_{max} expected for a single 150 mg dose of doxepin is 0.87 μ M. Mianserin (60 mg dose): mean C_{max} 0.38 μ M (Hrdina et al. 1983), f_u 0.055 (Kristensen, Gram and Kragh-Sørensen 1985).

3.3 Results

3.3.1 The glucuronidation of 4MU, 1NP and cotinine by Supersome UGT2B10

Like UGT2B10 expressed in mammalian cell lines, 120 min incubations of UGT2B10 expressed in insect cells (1 mg/ml of Supersome protein) lacked activity towards 4MU and 1NP across the concentration range 10 – 1,000 μ M. By contrast, UGT2B10 catalysed the N-glucuronidation of cotinine (see below). However, the V_{\max} for cotinine N-glucuronidation by Supersome UGT2B10 (43.7 pmol/min.mg; Table 3.2) was approximately 40-fold higher than the V_{\max} observed in this laboratory for UGT2B10 expressed in HEK293 cells (*ca.* 2 pmol/min.mg; JO Miners, unpublished data). Further, Supersome UGT2B10 activity with cotinine as the substrate was stable for at least 6 months when stored at -80°C . Thus, the commercially sourced recombinant UGT2B10 was satisfactory for ongoing kinetic and inhibition studies.

3.3.2 Kinetics of cotinine N-glucuronidation

Cotinine N-glucuronidation by recombinant UGT2B10 and HLM (\pm BSA, 1% w/v) followed Michaelis-Menten kinetics (Figure 3.3). Mean (\pm SD) kinetic constants are given in Table 3.2. The mean K_m for human liver microsomal cotinine N-glucuronidation was marginally higher ($p = 0.06$) than that for UGT2B10, while the V_{\max} with HLM as the enzyme source was 6.8-fold higher compared to UGT2B10. The activities of numerous UGTs, particularly with HLM as the enzyme source, are known to be increased in the presence of BSA (0.5 – 2% w/v) due to sequestration of inhibitory membrane long-chain unsaturated fatty acids released during the course of an incubation (Section 1.8.3). Addition of BSA (1% w/v) to incubations of HLM resulted in a 45% reduction in K_m and a small (11%) but statistically significant increase in V_{\max} . The mean Cl_{int} , calculated as V_{\max}/K_m , for human liver microsomal cotinine N-glucuronidation derived in the presence of BSA was approximately double

that determined in the absence of BSA. Cotinine was shown not to bind ($f_{u_{mic}} > 0.95$) to Supersomes (1 mg/ml), HLM (0.5 mg/ml) or BSA (1% w/v) (Table 3.5). Thus, correction of K_m and Cl_{int} values for substrate binding HLM and BSA was not required.

Table 3.2 Derived kinetic constants for cotinine N-glucuronidation by recombinant UGT2B10 and human liver microsomes (\pm BSA, 1% w/v)^a.

Kinetic parameter	Enzyme source		
	Recombinant UGT2B10	HLM	HLM + BSA
K_m (mM)	2.78 ± 0.34	3.34 ± 0.39	1.85 ± 0.07^c
V_{max} (pmol/min.mg)	43.7 ± 2.29	297 ± 14.5^b	329 ± 4.56^c
Cl_{int} (μ l/min.mg)	15.9 ± 2.48	89.7 ± 7.99^b	178 ± 4.41^c

^a Kinetic parameters expressed as mean \pm SD of 4 to 6 replicates

^b $p < 0.05$ compared to recombinant UGT2B10

^c $p < 0.05$ compared to HLM without BSA

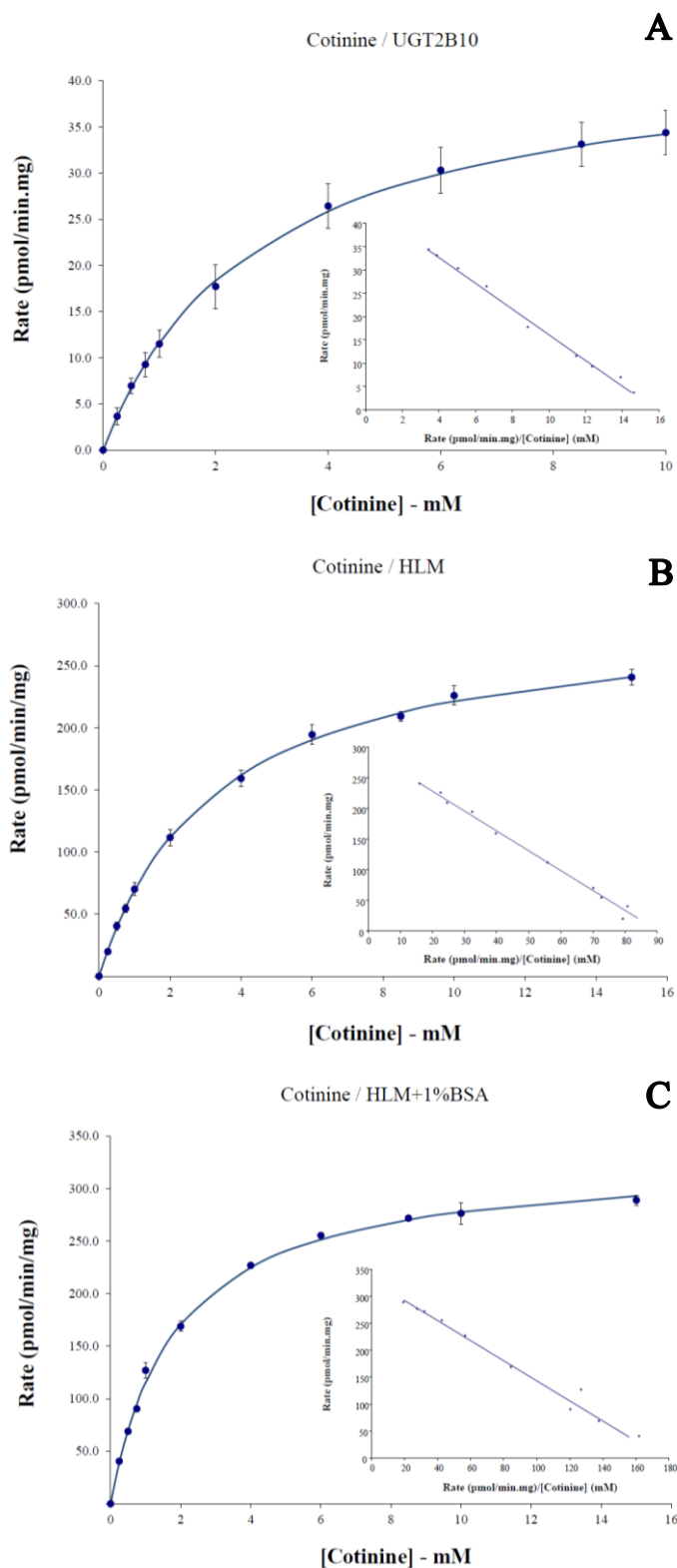


Figure 3.3 Rate vs. substrate concentration and Eadie-Hofstee (inset) plots for cotinine N-glucuronidation by recombinant UGT2B10 (Panel A), HLM (Panel B), and HLM plus BSA (Panel C).

Points with error bars represent the mean \pm SD of 4 to 6 replicates.

3.3.3 Confirmation of the UGT2B10 substrate selectivity of cotinine and the inhibitor selectivity of desloratadine and nicotine

Cotinine N-glucuronidation by UGT 1A1, 1A3, 1A4, 1A6, 1A7, 1A8, 1A9, 1A10, 2B4, 2B7, 2B10, 2B15 and 2B17 was investigated at 3 substrate concentrations (0.25, 1 and 5 mM) that spanned the K_m values reported in Table 3.2. Activity was observed only with UGT1A4 and UGT2B10. The respective mean N-glucuronidation rates by UGT2B10 at the three cotinine concentrations were 6.0, 15.4 and 38.0 pmol/min.mg. By contrast, with UGT1A4 as the enzyme source, cotinine N-glucuronidation (2.3 pmol/min.mg) was observed at just the highest substrate concentration (Figure 3.4).

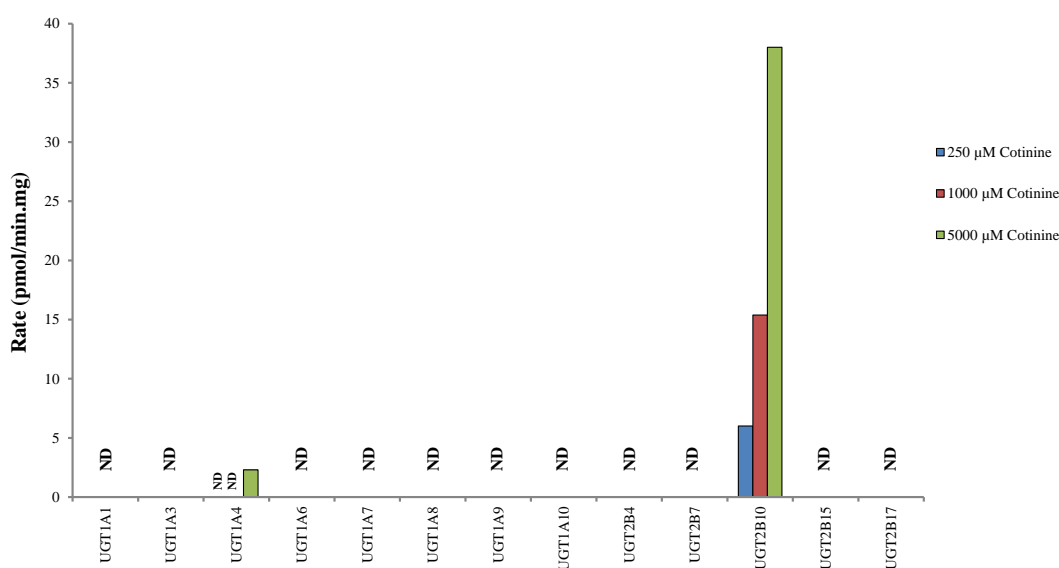


Figure 3.4 Formation of cotinine N-glucuronidation by recombinant human UGTs.

Nicotine and desloratadine (1, 10, 100 and 500 μM) were screened for inhibition of UGT 1A1, 1A3, 1A4, 1A6, 1A7, 1A8, 1A9, 1A10, 2B4, 2B7, 2B10, 2B15 and 2B17. Over the concentration range investigated, nicotine inhibited only UGT2B10 with an $\text{IC}_{50} < 500 \mu\text{M}$ (Figure 3.5); the mean (\pm SE of parameter fit) IC_{50} value was $214 \pm 2.9 \mu\text{M}$. Consistent with the recent report of Kazmi et al. (2015b), desloratadine potently inhibited UGT2B10 ($\text{IC}_{50} 3.86 \pm 0.05 \mu\text{M}$). IC_{50} values for other hepatically expressed UGT enzymes ranged from $18.9 \pm 0.10 \mu\text{M}$ for UGT2B4 to $271 \pm 7.6 \mu\text{M}$ for UGT1A6

(Figure 3.5, Panel B and Table 3.3). In general, the inhibition observed here for desloratadine (10 μ M) is in good agreement to that reported by Kazmi et al. (2015b) for hepatically expressed UGT enzymes, except UGT2B4 which was not investigated by these authors.

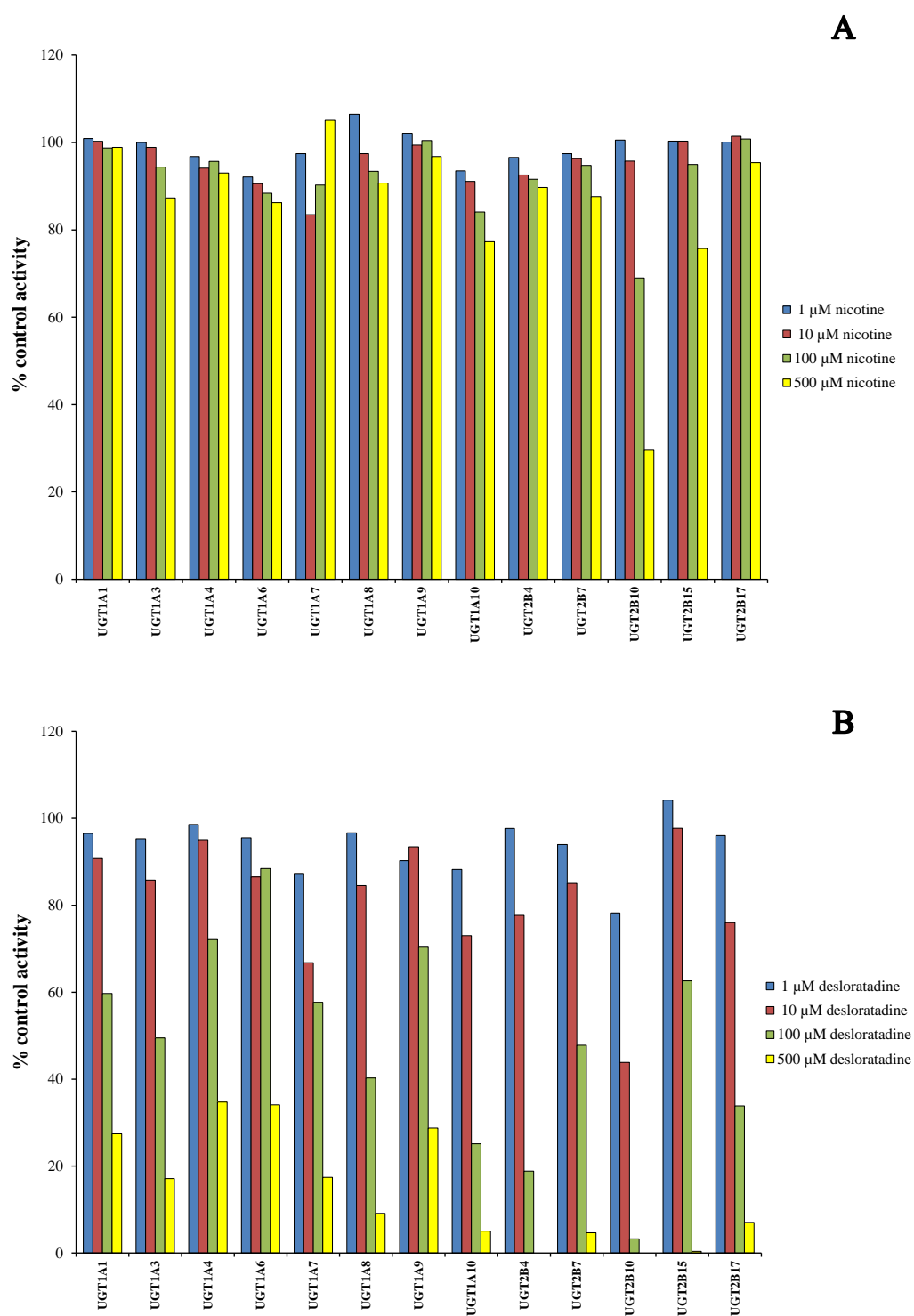


Figure 3.5 Inhibition of recombinant human UGT enzymes by nicotine (Panel A) and desloratadine (Panel B).

Each bar represents the mean of duplicate measurements (< 5% variance).

Table 3.3 IC₅₀ values for nicotine and desloratadine inhibition of recombinant UGT enzymes.

UGT enzyme	IC ₅₀ (μM) ± SE of parameter fit	
	Nicotine	Desloratadine
UGT1A1	NI	169 ± 15.2
UGT1A3	NI	104 ± 7.30
UGT1A4	NI	270 ± 3.24
UGT1A6	NI	271 ± 7.57
UGT1A7	NI	143 ± 15.0
UGT1A8	NI	65.1 ± 4.52
UGT1A9	NI	219 ± 0.26
UGT1A10	NI	30.7 ± 1.10
UGT2B4	NI	18.9 ± 0.13
UGT2B7	NI	86.1 ± 4.64
UGT2B10	214 ± 2.86	3.86 ± 0.05
UGT2B15	NI	152 ± 0.28
UGT2B17	NI	35.9 ± 0.38

NI – negligible inhibition over the concentration range investigated

3.3.4 Inhibition of recombinant UGT2B10 by UGT enzyme-selective inhibitors

Effects of putative UGT enzyme selective inhibitors on recombinant UGT2B10 activity were assessed using cotinine as the substrate probe. The UGT1A4 inhibitor hecogenin (1 – 100 μM) was without effect on UGT2B10 activity (Table 3.4), consistent with the observations of Guo, Zhou and Grimm (2011) and Kato et al. (2013). Niflumic acid, which inhibits UGT1A9 with a K_i of 0.10 μM and UGT1A1 and UGT2B15 with respective K_i's of 18 and 62 μM (Miners et al. 2011), inhibited UGT2B10 with an IC₅₀ of 168 ± 0.14 μM (Table 3.4). Fluconazole, employed as a

selective inhibitor of UGT2B4 and UGT2B7 (Raungrut et al. 2010; Uchaipichat et al. 2006b), inhibited UGT2B10 with an IC_{50} of $1,136 \pm 88.4 \mu\text{M}$ (Table 3.4), while phenylbutazone, which has been reported to be a relatively selective inhibitor of UGT1A subfamily enzyme activities (Uchaipichat et al. 2006a), inhibited UGT2B10 with an IC_{50} of $220 \pm 35.4 \mu\text{M}$. The effect of fluconazole on UGT2B10 prompted an investigation of the effects of two other azole antifungal agents, itraconazole and ketoconazole. Whereas itraconazole was without effect on UGT2B10, ketoconazole was a relatively potent inhibitor of this enzyme ($IC_{50} = 11.9 \pm 1.7 \mu\text{M}$; Table 3.4).

3.3.5 The contribution of UGT2B10 to human liver microsomal cotinine N-glucuronidation

As shown above, of the hepatically expressed enzymes in the UGT 1A and 2B subfamilies only UGT1A4 and UGT2B10 glucuronidated cotinine. Inhibition studies with hecogenin and desloratadine were performed to elucidate the relative contributions of these enzymes to human liver microsomal cotinine N-glucuronidation. Effects of desloratadine and hecogenin (both $10 \mu\text{M}$), separately and combined, were determined at four cotinine concentrations that spanned the K_m for cotinine N-glucuronidation by HLM (*viz.* 0.25, 1, 3 and 6 μM). Hecogenin had a negligible effect ($< 10\%$ inhibition) at all cotinine concentrations (Figure 3.6). By contrast, desloratadine, alone and in combination with hecogenin, inhibited human liver microsomal cotinine N-glucuronidation to a near identical extent (Figure 3.6). It should be noted that the extent of cotinine N-glucuronidation observed with $10 \mu\text{M}$ desloratadine is broadly consistent with the IC_{50} for desloratadine (*ca.* $4 \mu\text{M}$) reported in Table 3.4. Consistent with competitive inhibition by desloratadine (Kazmi et al. 2015b), greater and lesser inhibition occurred at cotinine concentrations below and above the K_m , respectively. Collectively, the data indicate that cotinine is a selective

substrate of human liver microsomal UGT2B10.

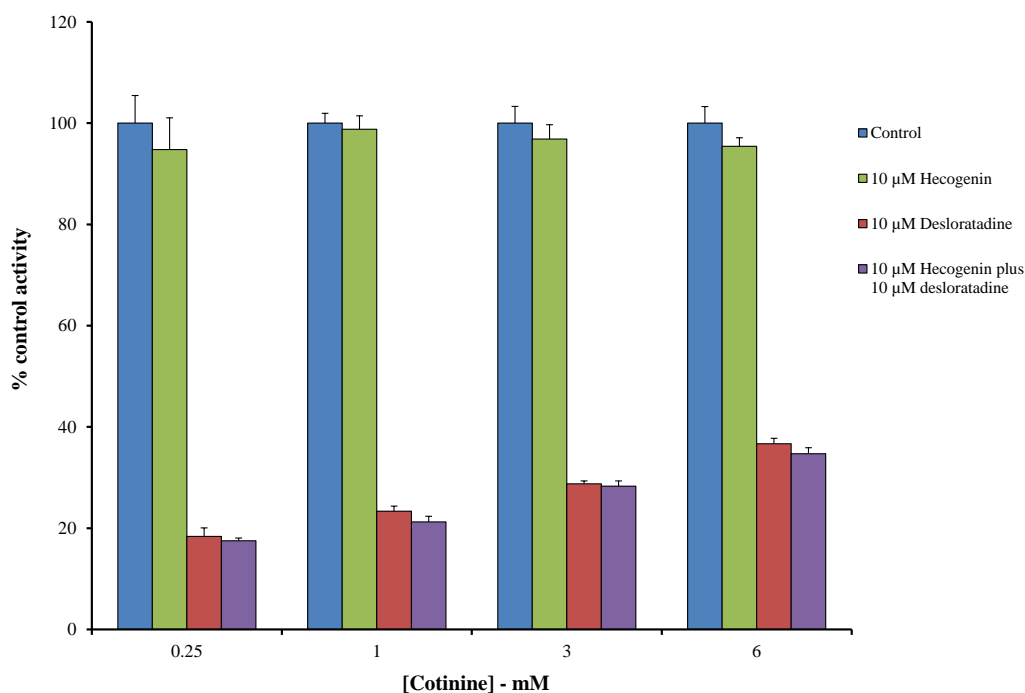


Figure 3.6 Inhibition of human liver microsomal cotinine N-glucuronidation at four substrate concentrations (0.25, 1, 3 and 6 mM) by hecogenin (10 μM), desloratadine (10 μM), and hecogenin plus desloratadine.

Each bar represents the mean ± SD of quadruplicate measurements.

3.3.6 Inhibition of recombinant UGT2B10 by antidepressant and antipsychotic drugs: modelling and structure-activity relationships

Thirty four antidepressant drugs (including didesmethylimipramine and desmethylnortriptyline, the respective demethylated metabolites of desipramine and nortriptyline) were screened as potential inhibitors of UGT2B10 (Table 3.4). Structures of these compounds are shown in Appendix Figure 1. The most potent inhibition was observed for mianserin, doxepin and amitriptyline, which have IC_{50} values in the range 2.2 - 6.5 μM. IC_{50} values for the structurally related compounds loratadine and desloratadine were also in this range (Table 3.4). Twenty five compounds additionally exhibited moderately potent inhibition (IC_{50} values 26 - 94 μM), while 6 were weak- ($IC_{50} > 200$ μM) or non- inhibitors.

Table 3.4 IC₅₀ values for the inhibition of recombinant UGT2B10 by UGT enzyme-selective inhibitors, azoles, and antidepressant and antipsychotic drugs.

Classification	Drug	IC ₅₀ (μM) ± SE of parameter fit ^a
UGT Enzyme-selective Inhibitors		
	Desloratadine	3.86 ± 0.05
	Fluconazole	1136 ± 88.4
	Hecogenin	NI
	S(-)-Nicotine	214 ± 2.86
	Niflumic acid	168 ± 0.14
	Phenylbutazone	220 ± 35.4
	Loratadine (desloratadine precursor)	2.18 ± 0.34
Azoles		
	Itraconazole	NI
	Ketoconazole	11.9 ± 1.69
Antidepressants		
TCA s		
<i>Primary amine</i> ^b	Desmethylnortriptyline	43.7 ± 2.03
	Didesmethylinipramine	36.2 ± 0.40
<i>Secondary amine</i>	Desipramine	34.1 ± 1.04
	Norclomipramine	50.8 ± 4.88
	Nortriptyline	45.3 ± 0.02
	Protriptyline	34.3 ± 0.40
<i>Tertiary amine</i>	Amitriptyline	6.45 ± 0.46
	Clomipramine	26.0 ± 0.49
	Doxepin	3.64 ± 0.16
	Imipramine	42.8 ± 1.52
	Trimipramine	32.6 ± 1.70
Tetracyclic antidepressants		
<i>Tertiary amine</i>	Mianserin	2.24 ± 0.11
	Mirtazapine	31.0 ± 0.99
SSRIs		
<i>Primary amine</i>	Fluvoxamine	224 ± 6.11
<i>Secondary amine</i>	Fluoxetine	72.4 ± 15.8
	Paroxetine	63.5 ± 4.79
	Sertraline	92.7 ± 8.99
<i>Tertiary amine</i>	Citalopram	218 ± 17.4
SNRIs		
<i>Secondary amine</i>	Duloxetine	81.2 ± 8.17
<i>Tertiary amine</i>	Desvenlafaxine	440 ± 16.5
	Venlafaxine	NI
MAOIs		
<i>Primary amine</i>	Tranlycypromine	NI
<i>Tertiary amine</i>	R(-)-Selegiline	67.2 ± 3.60
<i>Hydrazine</i>	Phenelzine	94.2 ± 1.79
Antipsychotics		
Typical antipsychotics		
<i>Tertiary amine</i>	Chlorpromazine	79.0 ± 10.7
	Fluphenazine	53.5 ± 6.54

Table 3.4 IC₅₀ values for the inhibition of recombinant UGT2B10 by UGT enzyme-selective inhibitors, azoles, and antidepressant and antipsychotic drugs (cont.).

Classification	Drug	IC ₅₀ (μM) ± SE of parameter fit ^a
	Haloperidol	NI
	Loxapine	36.0 ± 1.82
	Perphenazine	66.2 ± 0.6
	Thioridazine	71.3 ± 18.2
<i>Atypical antipsychotics</i>		
<i>Tertiary amine</i>	Aripiprazole	55.8 ± 0.80
	Clozapine	61.3 ± 1.40
	Olanzapine	276 ± 4.49

NI – negligible inhibition over the concentration range investigated

^a IC₅₀ values were calculated by fitting equation 2.8 to experimental data using Enzfitter (see Data analysis, Section 2.3). Each IC₅₀ value was derived from duplicate measurements at each of four inhibitor concentrations with cotinine as the substrate (see Inhibition of recombinant human UGT2B10 activity by antidepressants, antipsychotics and other compounds). SE is the standard error of the parameter fit from Enzfitter.

^b The designation of primary, secondary or tertiary amine or hydrazine refers to the N-containing functional group present in the side-chain (aliphatic or alicyclic) attached to the mono-, bi-, tri-, or tetra- cyclic structure (Appendix Figure 1).

Ligand-based approaches were employed to identify the structural features associated with significant inhibition (Section 3.2.9). The majority of ‘significant’ inhibitors (arbitrarily defined as having an IC₅₀ < 100 μM) are generally tri- or tetra-cyclic structures with an amine-containing side-chain (aliphatic or alicyclic), although exceptions occur. All of the tricyclic and tetracyclic compounds, except olanzapine, overlaid well on the structure of amitriptyline (Figure 3.7, Panels A - C). Olanzapine is the only compound investigated here with a 5-membered ring in the tricyclic scaffold, which results in a different geometry and poor overlay (Figure 3.8). The bis-ring structure of fluoxetine permits adoption of a conformation similar to that of amitriptyline, resulting in a reasonable overlay (Figure 3.8). Of the bicyclic compounds that exhibited significant inhibition, aripiprazole, duloxetine and

paroxetine aligned reasonably well with the structure of amitriptyline (Figure 3.8) whereas partial overlay was observed for sertraline (IC_{50} 93 μ M), presumably due to the shorter distance between the ring scaffold and side-chain amine group. Poor overlay of the SSRIs citalopram and fluvoxamine, including the side-chain amine of the latter (which aligns 3.3 Å from the side-chain N of amitriptyline) provides an explanation for the weak inhibition observed with these compounds (Figure 3.8). Overlay on the structure of amitriptyline for the remaining compounds screened for inhibition (*viz.* haloperidol, venlafaxine, desvenlafaxine and the MAOIs phenelzine, selegiline and tranylcypramine), all of which lack a fused ring scaffold, was generally consistent with the observed potency of UGT2B10 inhibition (Figure 3.8).

Compared to other TCAs, the potent UGT2B10 inhibitors amitriptyline and doxepin share in common a side-chain tertiary amine functional group linked to the central cycloheptene ring by a double bond rather than to a potentially invertible N atom (Appendix figure 1). The exocyclic double bond present in loratadine and desloratadine, and the fused piperidine ring present in mianserin similarly confer structural rigidity. Near identical geometries were observed for amitriptyline, doxepin, desloratadine and loratadine, and consequently there was near complete overlap of structural features (Figure 3.9, Panel A). By contrast, conformational differences occur around the CH_2 -X moiety of the cycloheptene ring of other TCAs (e.g. imipramine), and the ring scaffold of tricyclic compounds with a 6-membered central ring (e.g. chlorpromazine) is more planar (Figure 3.9, Panel B and C).

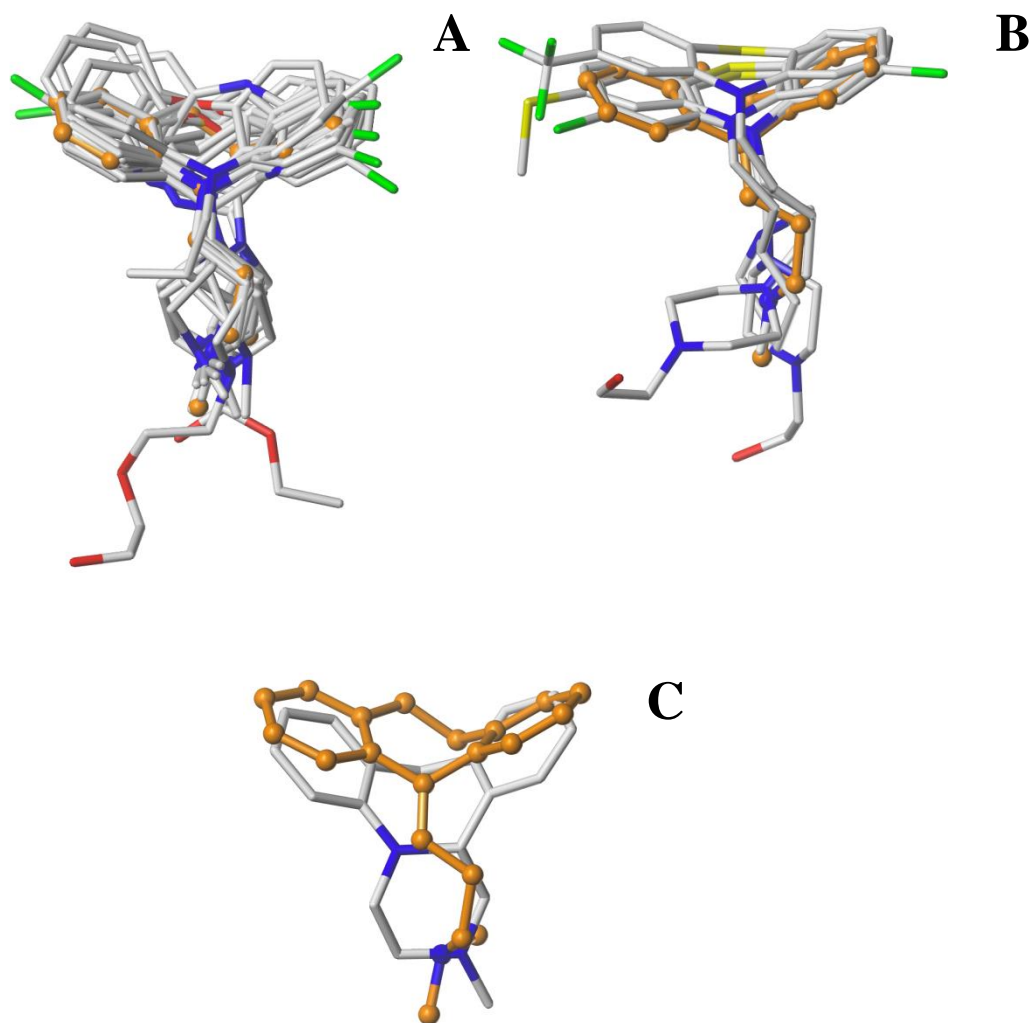


Figure 3.7 Overlay of tri- and tetra-cyclic dataset molecules on the structure of amitriptyline.

C atoms of amitriptyline and overlaid molecules are shown in orange and white, respectively, while *O*, *N*, *S* and *Cl* atoms are shown in red, blue, yellow, and green respectively. Overlay of tricyclic molecules with a central 7-membered ring scaffold (Panel A). Overlay of tricyclic molecules with central 6-membered ring scaffold (Panel B). Overlay of the tetracyclic molecule mianserin (Panel C).

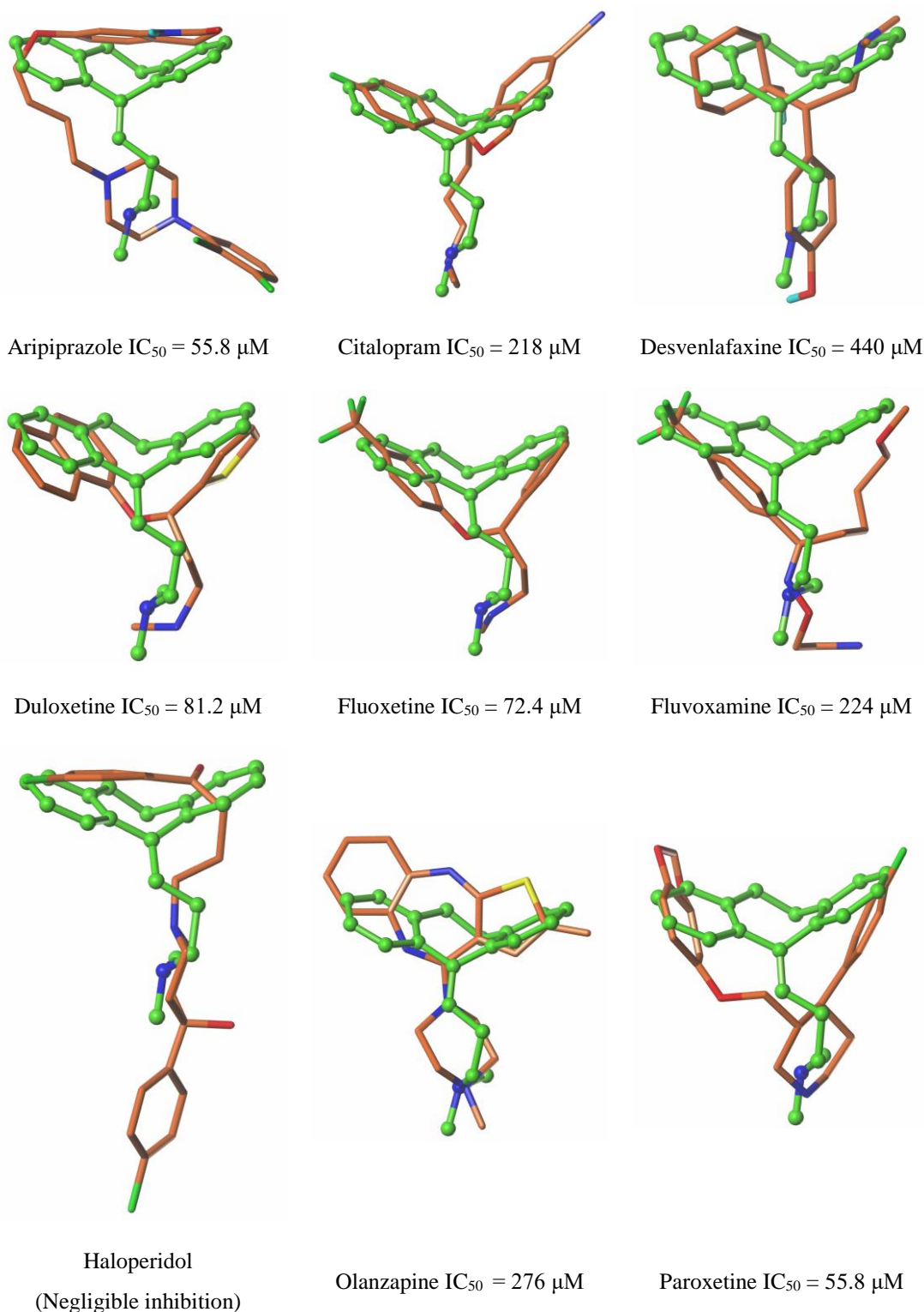


Figure 3.8 Structural overlay of dataset molecules lacking a tri- or tetra-cyclic scaffold or a scaffold without a central 6- or 7-membered ring.

The template molecule, amitriptyline used for the overlay is shown in ball and sticks (C atoms - green). The individual dataset molecules are shown in sticks (C atoms - orange). O, N, S and Cl atoms are shown in red, blue, yellow, and green respectively.

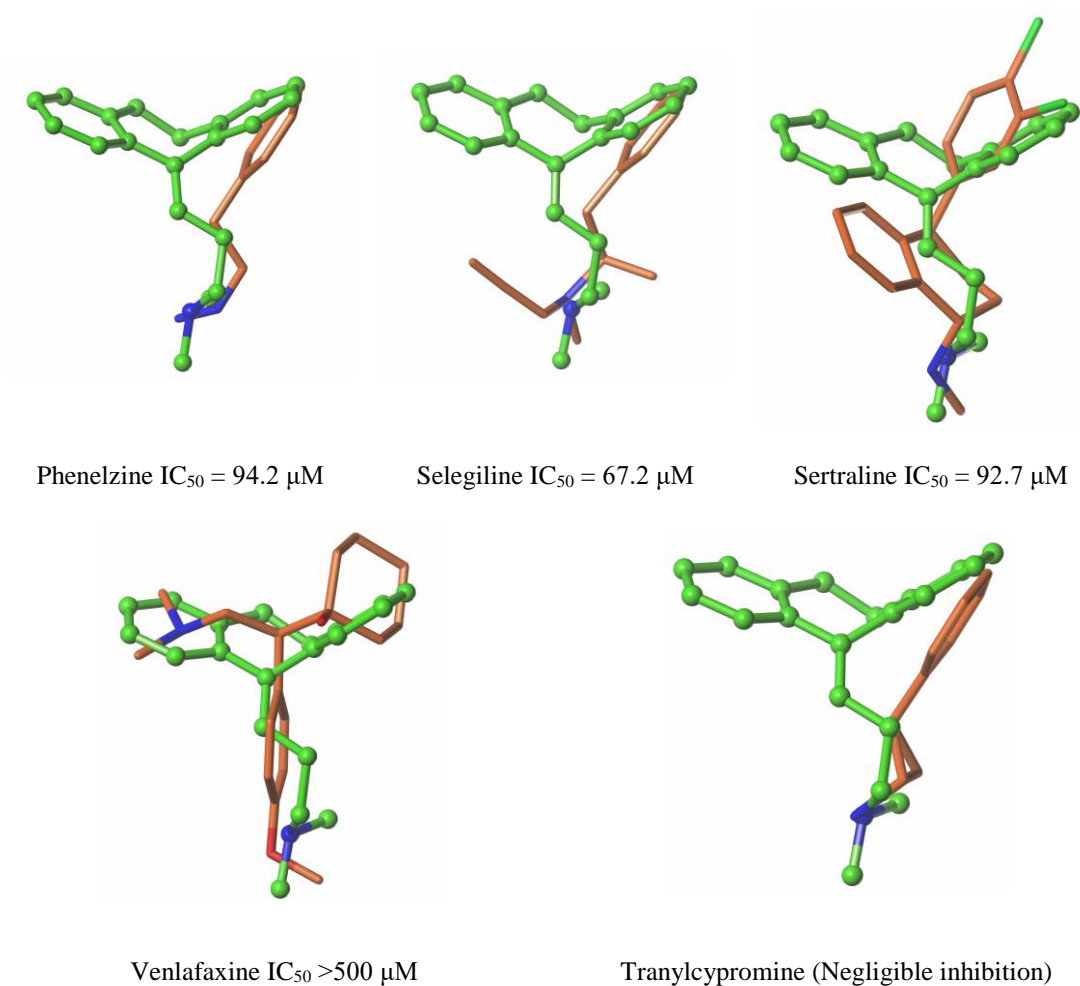


Figure 3.8 Structural overlay of dataset molecules lacking a tri- or tetra-cyclic scaffold or a scaffold without a central 6- or 7-membered ring (cont.).

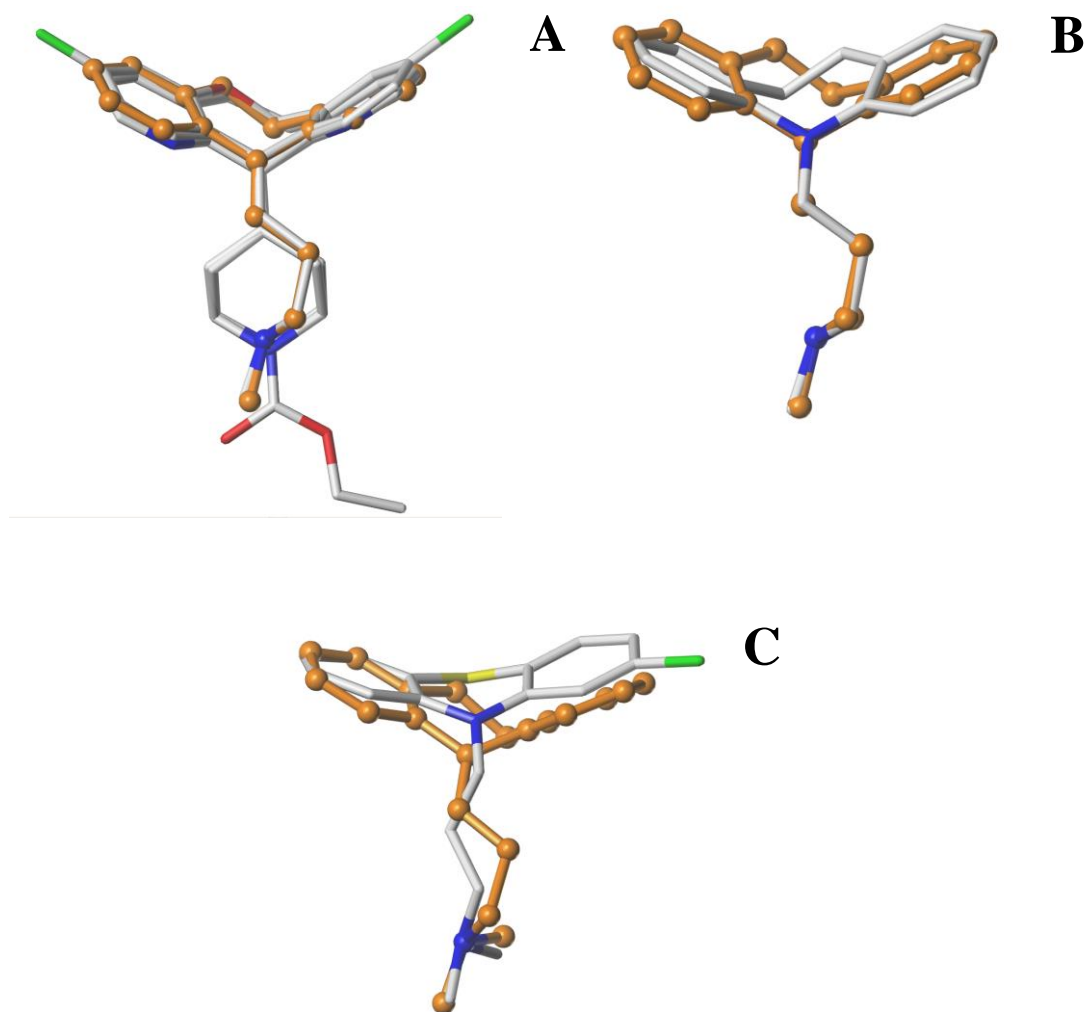


Figure 3.9 Overlay of representative molecules with a tricyclic scaffold on the structure of amitriptyline.

C atoms of amitriptyline and overlaid molecules are shown in orange and white, respectively, while *O*, *N*, *S* and *Cl* atoms are shown in red, blue, yellow, and green respectively. Overlay of doxepin, desloratadine, and loratadine (Panel A). Overlay of imipramine (Panel B). Overlay of chlorpromazine (Panel C).

3.3.7 The kinetics of amitriptyline, doxepin and mianserin inhibition of human liver microsomal UGT2B10 and *in vitro* – *in vivo* extrapolation

Given the potent inhibition of UGT2B10 observed for amitriptyline, doxepin and mianserin, kinetic studies were performed to determine the K_i values for inhibition of human liver microsomal cotinine N-glucuronidation. Incubations were supplemented with BSA (1% w/v). Concentrations of amitriptyline, doxepin and mianserin were corrected for binding to HLM and BSA, and the inhibitor constants therefore represent $K_{i,u}$ values. The binding of each compound was independent of added concentration across the range 2 to 25 μM . Mean (\pm SD) values of $f_{u_{mic}}$ for amitriptyline, doxepin and mianserin were 0.32 ± 0.03 , 0.42 ± 0.03 and 0.20 ± 0.01 , respectively (Table 3.5). As noted above, cotinine does not bind to either HLM or BSA. Amitriptyline, doxepin and mianserin competitively inhibited human liver microsomal cotinine N-glucuronidation with mean $K_{i,u}$ (\pm SD) values of 0.61 ± 0.05 , 0.95 ± 0.18 , and 0.43 ± 0.01 μM (Figure 3.10).

Table 3.5 Binding of cotinine to protein sources (Supersomes and HLM) in the absence and presence of BSA (1% w/v).

Binding is expressed as the fraction unbound in the incubation medium ($f_{u_{mic}}$).

Concentration (mM)	Protein source	$f_{u_{mic}}$
0.1, 1, 5, 10	Supersomes (1 mg/ml)	1.00 ± 0.03
0.1, 1, 5, 10, 15	HLM (0.5 mg/ml)	0.99 ± 0.02
0.1, 1, 5, 10, 15	BSA (1% w/v)	1.00 ± 0.03

Table 3.6 Binding of amitriptyline, doxepin and mianserin to HLM in the presence of BSA (1% w/v).*Binding is expressed as the fraction unbound in the incubation medium ($f_{u_{mic}}$).*

Drug (concentration, μM)	Protein source	$f_{u_{mic}}$
Amitriptyline (2, 5, 10, 25)		0.32 ± 0.03
Doxepin (2, 5, 10, 25)	HLM (0.5 mg/ml) + BSA (1% w/v)	0.42 ± 0.03
Mianserin (2, 5, 10, 25)		0.20 ± 0.01

Using the plasma concentrations for amitriptyline, doxepin and mianserin given in Section 3.2.10 (for doses at the upper end of the usual recommended dosage ranges; *viz.* 150, 150 and 60 mg/day, respectively), respective $[I]/K_{i,u}$ ratios based on total drug concentration are 0.74, 0.92 and 0.88; corresponding values of $1 + [I]/K_{i,u}$ (see equation 2.16, Section 2.3) for amitriptyline, doxepin and mianserin are 1.74, 1.92 and 1.88, respectively. When $[I]$ is taken as the unbound concentration of drug in plasma (i.e. the product of drug plasma concentration and f_u), $[I]/K_{i,u}$ values are < 0.2 .

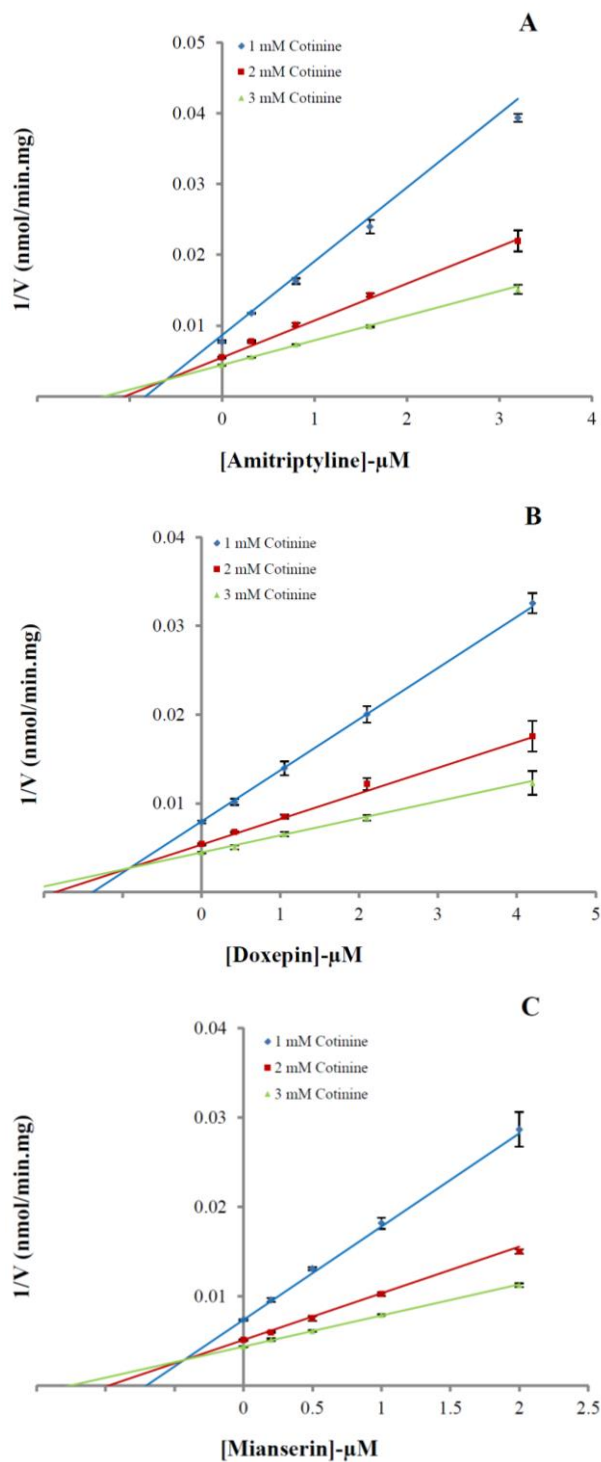


Figure 3.10 Dixon plots for the inhibition of human liver microsomal cotinine N-glucuronidation by amitriptyline (panel A), doxepin (panel B) and mianserin (panel C).

Incubations contained BSA (1% w/v). Points represent the mean \pm SD of quadruplicate measurements. Inhibitor concentrations are corrected for binding to HLM plus BSA.

3.4 Discussion

Initial studies confirmed that cotinine is a selective substrate for UGT2B10, and desloratadine and nicotine are relatively selective inhibitors of this enzyme. Cotinine N-glucuronidation by HLM followed Michaelis-Menten kinetics, consistent with the predominant involvement of a single UGT enzyme in this reaction. It has been reported previously that only UGT 1A4 and 2B10 glucuronidate cotinine (Kaivosaaari et al. 2007; Kuehl and Murphy 2003). This was confirmed here, although the cotinine N-glucuronidation activity of UGT1A4 was very low. To further elucidate the relative contributions of UGT2B10 and UGT1A4 to human liver microsomal cotinine N-glucuronidation, inhibition experiments were conducted with desloratadine and the UGT1A4 selective inhibitor hecogenin (Uchaipichat et al. 2006a). The separate and combined effects of desloratadine and hecogenin shown in Figure 3.6 demonstrate that UGT2B10 is responsible for > 90% of cotinine N-glucuronidation by HLM, making this compound a convenient, readily available UGT2B10 substrate probe. Moreover, compared to many other UGT enzyme selective substrate probes, cotinine does not bind to BSA (or HLM) and hence correction for non-specific and protein binding is not required.

Consistent with the recent report of Kazmi et al. (2015b), desloratadine was shown to be a reasonably selective inhibitor of UGT2B10 (Figure 3.5). The IC_{50} for UGT2B10 inhibition is approximately an order of magnitude lower than that for UGT2B4, the next most potently inhibited enzyme. UGT2B4 was not screened for inhibition in the study of Kazmi et al. (2015b). Thus, it may not be possible to completely differentiate the relative contributions of UGT2B10 and UGT2B4 when desloratadine (10 μ M; Kazmi et al. 2015b) is used for reaction phenotyping. Previous studies have reported

that nicotine inhibits UGT2B10 but not UGT1A4 (Zhou et al. 2010). Similar selectivity was observed here, although nicotine was observed to additionally inhibit UGT2B15, albeit less potently than UGT2B10.

Previously reported K_m and V_{max} values for cotinine N-glucuronidation by HLM range from 1.3 to 5.5 mM and 696 to 1,144 pmol/min.mg, respectively (Chen et al. 2007; Ghosheh and Hawes 2002; Kaivosaari et al. 2007), while K_m values of 3.50 and 1.0 mM have been reported for cotinine N-glucuronidation by recombinant UGT2B10 (Table 3.7). The mean K_m (3.34 mM) and V_{max} (297 pmol/mg.min) values for human liver microsomal cotinine N-glucuronidation determined here tended to be higher and lower, respectively, than previously reported values. The reasons for this are unclear, although 89-fold variability in the rates of nicotine N-glucuronidation has been observed in a panel of microsomes from 14 livers (Nakajima and Yokoi 2005). The commercially-sourced HLM employed here is a pool from 150 donors (equal numbers of males and females), whereas most reports have generally used microsomes from fewer donors (Ghosheh and Hawes 2002; Kaivosaari et al. 2007; Nakajima et al. 2002). Similarly, previous studies with UGT2B10 have used different expression systems to the Supersomes studied here. Nevertheless, the differences in reported K_m values are surprising. Of note, we have found that the UGT2B10 activity of Supersomes remains stable for at least 6 months. By contrast, recombinant UGT2B10 expressed in *Spodoptera frugiperda* 9 (Sf9) cells exhibits only short term stability (M. Finel, personal communication to JO Miners).

The addition of BSA (0.5 – 2% w/v) to incubations has been reported to decrease the K_m values (with occasional effects on V_{max}) for substrates of several hepatically expressed UGT enzymes, particularly UGT 1A9, 2B4, 2B7 and 2B15 (see Section 1.8.3). Addition of BSA (1% w/v) was found here to reduce the K_m for human liver

microsomal cotinine N-glucuronidation by approximately 50%, with a small (11%) but statistically significant increase in V_{\max} . Thus, subsequent inhibition kinetic studies included BSA in order to determine K_i values accurately. Further, HLM were preferred to UGT2B10 in these studies due to the considerably lower cost of HLM compared to the recombinant enzyme.

Table 3.7 Published kinetic parameters for cotinine N-glucuronidation by UGT2B10 and human liver microsomes.

Enzyme source	K_m (mM)	V_{\max} (pmol/min.mg)	Reference
UGT2B10	3.50 ± 0.19	25.0 ± 1.10	Chen et al. (2007)
	1.00 ± 0.01	-	Kaivosaaari et al. (2007)
HLM	5.43 ± 0.32	696 ± 18.9	Ghosheh and Hawes (2002)
	5.50 ± 1.10	$1,144 \pm 852$	Chen et al. (2007)
	1.30 ± 0.20	-	Kaivosaaari et al. (2007)

UGT enzyme-selective inhibitors are a valuable experimental tool for the reaction phenotyping of human liver microsomal drug and chemical glucuronidation (Section 1.8.1). However, previous studies that have characterised UGT enzyme inhibition selectivity have generally excluded UGT2B10. Niflumic acid at a concentration of 2.5 μM is considered a highly selective inhibitor of UGT1A9 (Miners et al. 2011), whereas at 100 μM it additionally inhibits UGT1A1 and UGT2B15. The IC_{50} for niflumic acid inhibition of UGT2B10 observed here (168 μM) confirms the UGT1A9 inhibition selectivity of niflumic acid at a low concentration, but indicates that this compound will significantly inhibit UGT2B10 as well as UGT1A1 and UGT2B15 at a

concentration of 100 μM . As noted above, hecogenin does not inhibit UGT2B10 consistent with the reported inhibition selectivity for UGT1A4 (Uchaipichat et al. 2006b). By contrast, fluconazole (2.5 mM), which is considered a selective inhibitor of UGT2B4 and UGT2B7, inhibited UGT2B10 to a similar extent to that reported for UGT2B4/7 (Raungrut et al. 2010; Uchaipichat et al. 2006a). The latter observation prompted an investigation of the potential UGT2B10 inhibition of UGT2B10 by two additional azole antifungals; itraconazole and ketoconazole. While the triazole itraconazole was without effect on UGT2B10, the imidazole ketoconazole was a relatively potent inhibitor of this enzyme ($\text{IC}_{50} = 11.9 \pm 1.7 \mu\text{M}$). Similar to the inhibition selectivity of fluconazole, ketoconazole has previously been reported to be a relatively potent inhibitor of UGT2B4 (Raungrut et al. 2010) and an inhibitor of UGT2B7 (Takeda et al. 2006).

Previous studies have shown that the TCAs amitriptyline, clomipramine, imipramine and trimipramine, and the atypical antipsychotic olanzapine are substrates and/or inhibitors of UGT2B10 (Chen et al. 2007; Guo, Zhou and Grimm 2011; Kato et al. 2013; Zhou et al. 2010). As noted in Section 3.1, antidepressant and antipsychotic drugs typically contain an amine functional group (see structures in Appendix Figure 1). Thus, nine TCAs (plus the respective N-demethylated metabolites of desipramine and nortriptyline), 5 SSRIs, 3 SNRIs, 3 MAOIs, the tetracyclic antidepressants mianserin and mirtazapine, and 6 ‘typical’ and 4 ‘atypical’ antipsychotic drugs were screened for inhibition of UGT2B10. Although the majority of the compounds investigated inhibited UGT2B10 with IC_{50} values $< 100 \mu\text{M}$, most potent inhibition was observed for the TCAs amitriptyline and doxepin, and the tetracyclic mianserin. Desloratadine and loratadine were also potent inhibitors of UGT2B10. Structural interrogation of these data suggests that potent and moderate inhibition of UGT2B10

requires a hydrophobic domain (particularly a tetra- or tri-cyclic scaffold containing an aromatic ring(s)) and an amine (or hydrazine) functional group, which is most commonly located 3 bond lengths (C-C and/or C-N) from the hydrophobic domain. All but one of the potent inhibitors identified here, namely desloratadine, are tertiary amines. However, the presence of a tertiary amine is not an obligatory requirement for inhibition; moderate inhibition also occurred with primary and secondary amines. Since the amines will be largely charged at physiological pH, the data suggest that hydrophobic and charge interactions (e.g. with aspartic or glutamic acid) are involved in inhibitor binding.

The data also suggest that spatial features influence the potency of UGT2B10 inhibition. TCAs with a dihydrodibenzazepine moiety (e.g. clomipramine, desipramine and imipramine) are inherently more flexible with more degrees of conformational freedom than dibenzocycloheptenes such as amitriptyline and doxepin. It has been proposed that such conformational differences, particularly in the tricyclic ring scaffold, may be associated with differences in the receptor binding selectivity and affinity of TCAs (Casarotto and Craik 2001; Munro, Craik and Andrews 1987). As noted above and shown in Figure 3.9, Panels A - C, the relatively subtle conformational differences noted between amitriptyline, doxepin, desloratadine and loratadine compared to other TCAs (e.g. imipramine) and tricyclic compounds with a 6-membered central ring (e.g. antipsychotics such as chlorpromazine) may similarly account for differences in binding affinity to UGT2B10.

Given the potent inhibition ($K_{i,u} < 1 \mu\text{M}$) of human liver microsomal UGT2B10 by amitriptyline, doxepin and mianserin, the potential of these drugs to inhibit UGT2B10 catalysed drug glucuronidation was explored. Estimates of $1 + [I]/K_{i,u}$ based on total maximum drug concentration ranged from 1.74 to 1.92 for inhibitor doses near the

upper end of the usual therapeutic dosage ranges, although doses double these may be used if required (Australian Medicines Handbook 2015). However, no clinically significant interactions were predicted when [I] was taken as the unbound maximum drug concentration in plasma. As discussed in Chapter 1 (Section 1.8.2), up to late 2017 the FDA recommended use of total inhibitor concentration whereas the EMA recommended use of the unbound inhibitor concentration for prediction of DDI potential from *in vitro* data (see Chapter 6 for further discussion). Based on the reported K_i for desloratadine (*ca.* 1 μM), Kazmi et al. (2015b) predicted a 2.2-fold increase in the AUC ratio for UGT2B10 substrates (based on total inhibitor concentration in plasma), which is similar to that proposed here for amitriptyline, doxepin and mianserin.

Few compounds appear to be solely metabolised by UGT2B10, although the clearance of the experimental antipsychotic agent RO5263397 appears to be mediated largely by UGT2B10 (Fowler et al. 2015). Thus, the inhibition of UGT2B10 by amitriptyline, doxepin and mianserin observed here is currently of minor clinical significance. However, the physicochemical properties of drug molecules have changed substantially in recent years (Walters et al. 2011). New synthetic drugs tend to be larger (higher molecular mass) than in the past, with more hydrogen bond donors and acceptors (particularly N). The changing properties of drug molecules favour an increasing contribution of non-CYP enzymes in drug elimination, including UGT (Cerny 2016). Further, the trend for newer drugs to contain aliphatic and heterocyclic nitrogens may favour an increasing rate of UGT2B10 (and UGT1A4) in drug glucuronidation.

CHAPTER 4

INHIBITION OF HUMAN UDP- GLUCURONOSYLTRANSFERASE (UGT) ENZYMES BY SGLT2 INHIBITORS

The contents of this chapter have been published in part as: (i) Pattanawongsa, A, Chau, N, Rowland, A and Miners, JO (2015), 'Inhibition of human UDP-glucuronosyltransferase enzymes by canagliflozin and dapagliflozin: Implications for drug-drug interactions', *Drug Metabolism and Disposition*, 43 (10): 1468-1476; and (ii) Miners, JO, Pattanawongsa, A and Rowland, A (2018), 'Response to *in vitro* and physiologically-based pharmacokinetic assessment of the drug–drug interaction potential of canagliflozin', *British Journal of Clinical Pharmacology*, 84 (2): 392-393.

Reproduced with the permission of the American Society for Pharmacology and Experimental Therapeutics.

4.1 Introduction

Diabetic mellitus is characterised by a fasting plasma glucose > 7.0 mmol/l or plasma glucose > 11.1 mmol/l 2 hr after a meal (Deshmukh et al. 2013), and glycosylated haemoglobin A1C (HbA1C) $\geq 6.5\%$ (WHO 2011). Type 2 diabetes, which accounts for more than 90% of all cases of diabetes, is a chronic disease characterised by hyperglycaemia due to a progressive insulin secretory defect on a background of insulin resistance (American Diabetes Association 2012). The microvascular and macrovascular changes that occur in patients with diabetes may cause cardiovascular disease, retinopathy, neuropathy and chronic kidney disease (Basile 2013; Deshmukh et al. 2013). Further, type 2 diabetes associates with comorbidities such as hyperlipidaemia, hypertension and stroke. Consequently, type 2 diabetes results in

significant morbidity and mortality, which in turn have important social and economic consequences. Indeed, it has been estimated that diabetes accounts for more than 10% of total worldwide healthcare costs for adults, and this is likely to increase into the future given the number of people with diabetes is increasing in all countries and has been projected to total almost 600 million by 2035 (International Diabetes Foundation 2014).

Although metformin is the first-line drug for the treatment of type 2 diabetes, combination therapy with another agent is generally required to achieve and maintain recommended levels of glycaemic control (American Diabetes Association 2012 and 2015; Australian Medicines Handbook 2014) . While most antidiabetic drugs target insulin secretion or insulin action, modulation of glucose homeostasis provides an alternative approach to glycaemic control. The kidney plays a critical role in glucose homeostasis through the absorption of filtered glucose (Figure 4.1). Sodium-glucose co-transporters (SGLT) 1 and 2, located in the proximal convoluted tubule, are together responsible for almost all glucose reabsorption. Of these, the low-affinity, high-capacity SGLT2 accounts for approximately 90% of glucose reabsorption under normal circumstances.

Based on the early observation that phlorizin, a β -glucoside, inhibits SGLT1 and SGLT2 (Kinne and Castaneda 2011) a number of phlorizin analogues that specifically inhibit SGLT2 and hence enhance urinary glucose excretion have been developed as antidiabetic agents. Currently, there are two subclasses of SGLT2 inhibitors, which contain either a C- and O-linked glucoside moiety (Dardi, Kouvatso and Jabbour 2016; Grempler et al. 2012) (Figure 4.2). Since all SGLT2 inhibitors are named with the suffix 'flozin', drugs in this class are generally referred to as 'flozins'. The selectivity of flozins for SGLT2 (over SGLT1) is shown in Table 4.1. The higher the

SGLT1 to SGLT2 IC₅₀ ratio, the greater is the selectivity for the latter.

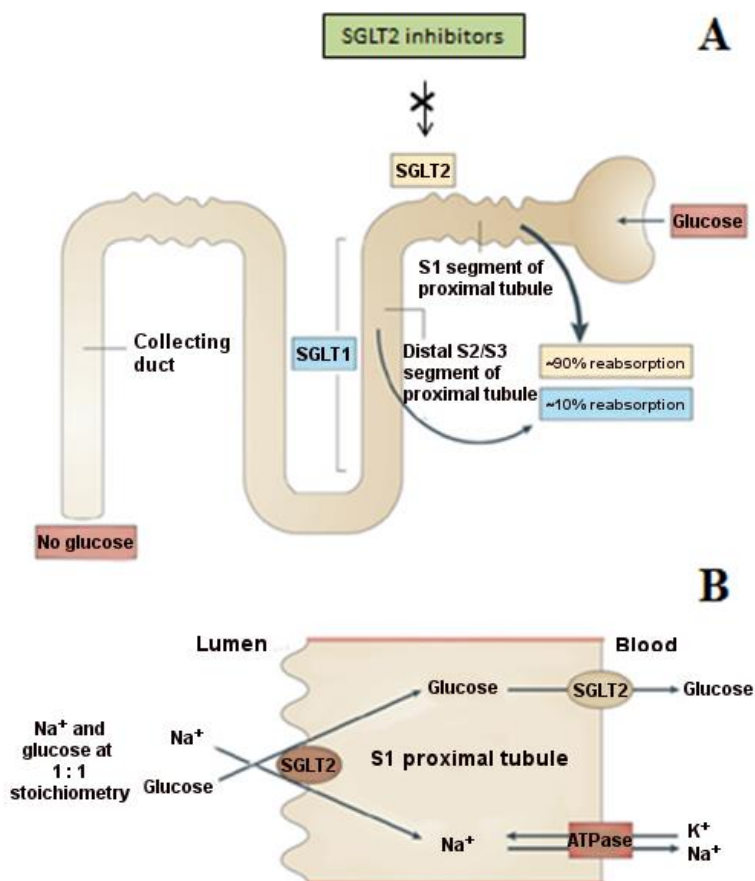


Figure 4.1 Mechanism of action of SGLT2 inhibitors.

Flozins inhibit SGLT2 at the S1 segment of the proximal tubule (Panel A). SGLT2 transports glucose from the tubular lumen into S1 proximal cells, from where glucose is transferred into the circulation by glucose transporter 2 (GLUT2) (Panel B).

Reproduced with permission from Nigro, SC, Riche, DM, Pheng, M and Baker, WL (2013), 'Canagliflozin, a novel SGLT2 inhibitor for treatment of type 2 diabetes', *Annals of Pharmacotherapy*, 47 (10): 1301-1311. Copyright (2013) SAGE Publications.

Table 4.1 Selectivity of SGLT2 inhibitors.

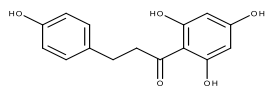
Modified from Grempler *et al.* (2012) and Scheen (2014b).

Adapted with permission from Grempler, R, Thomas, L, Eckhardt, M, Himmelsbach, F, Sauer, A, Sharp, DE, Bakker, RA, Mark, M, Klein, T and Eickelmann, P (2012), 'Empagliflozin, a novel selective sodium glucose cotransporter-2 (SGLT-2) inhibitor: Characterisation and comparison with other SGLT-2 inhibitors', *Diabetes, Obesity and Metabolism*, 14 (1): 83-90 and Scheen, AJ (2014b), 'Pharmacokinetic and pharmacodynamic profile of empagliflozin, a sodium glucose co-transporter 2 inhibitor', *Clinical Pharmacokinetics*, 53 (3): 213-225. Copyright (2012) John Wiley and Sons, and copyright (2014) Springer Nature.

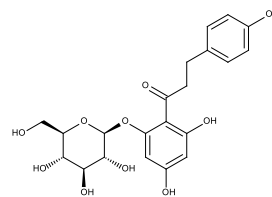
Flozin	Mean IC ₅₀ (nM)		Ratio ^a
	SGLT1	SGLT2	
C-glucosides			
Canagliflozin	710	2.7	263
Dapagliflozin	1400	1.2	1167
Empagliflozin	8300	3.1	2677
Ipragliflozin	3000	5.3	566
Tofogliflozin	12000	6.4	1875
O-glucosides			
Phlorizin	290	21	14
Remogliflozin	6500	12	542
Sergliflozin	2100	7.5	280
T-1095A	260	4.4	59

^a Ratio refers to mean IC₅₀(SGLT1)/mean IC₅₀(SGLT2) and represents SGLT selectivity.

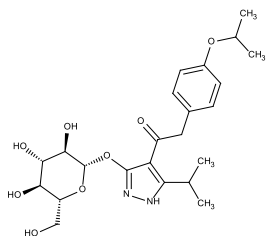
O-glucosides



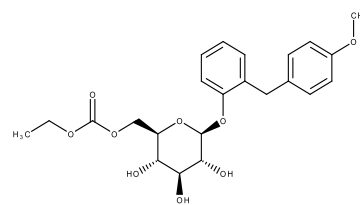
Phloretin



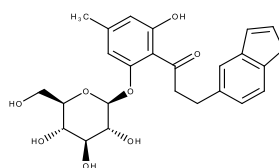
Phlorizin



Remogliflozin

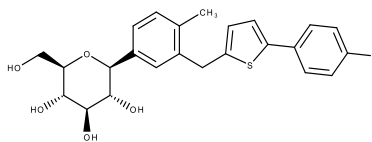


Sergliflozin

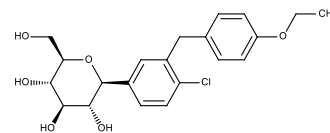


T-1095A

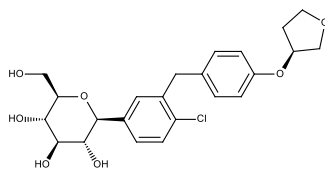
C-glucosides



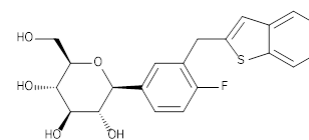
Canagliflozin



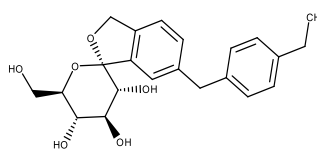
Dapagliflozin



Empagliflozin



Ipragliflozin



Tofogliflozin

Figure 4.2 Chemical structures of SGLT inhibitors.

Canagliflozin (CNF), dapaliflozin (DPF) and empagliflozin (EPF) are the first three SGLT2 inhibitors approved for clinical use. Although they have been used alone, more commonly SGLT2 inhibitors are combined with another antidiabetic drug such as metformin. All three drugs have been demonstrated to improve short-term outcomes in adults with type 2 diabetes (Brand et al. 2012; Devineni et al. 2015b; Ferrannini et al. 2013; Friedrich et al. 2013; Häring et al. 2014; Häring et al. 2013; Heise et al. 2013; Jabbour et al. 2014; Kovacs et al. 2014; Plosker 2012; Rosenstock et al. 2012b). CNF, DPF and EPF are C-glucosides (Figure 4.2), and available evidence indicates that glucuronidation of the glucoside moiety is the major metabolic pathway of these compounds in humans. CNF is glucuronidated at the 2- and 3-hydroxyl groups of the glucoside rings; the respective glucuronides are referred to as M5 and M7 (Mamidi et al. 2014) (Figure 4.3, Panel A). The urinary excretion of M5 and M7 in patients with type 2 diabetes ranges from 7-10% and 21-32% of the administered dose, respectively (Devineni et al. 2013). It has been reported that CNF glucuronidation is catalysed by UGT1A9 and UGT2B4 (Scheen 2014a), but actual data appear not to have been published.

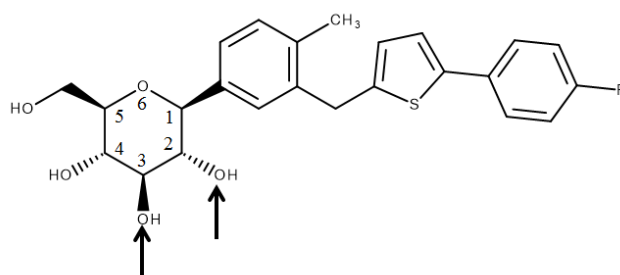
Several glucuronides were observed following incubation of DPF with hepatocytes from various species (Obermeier et al. 2010). One of these, termed M15, was the major metabolite from human hepatocytes. Following administration of radiolabelled DPF to healthy volunteers, DPF plus M15 accounted for > 72% of total plasma radioactivity (Obermeier et al. 2010). A later report confirmed that M15, now identified as DPF 3-O-glucuronide (Figure 4.3, Panel B), was formed by incubations of human liver, kidney and intestinal microsomes with UDP-glucuronic acid (UDPGA) (Kasichayanula et al. 2013b). Rates of DPF 2-O-glucuronidation by human liver microsomes (HLM) and kidney microsomes were < 5% those of DPF 3-O-

glucuronide. Peak plasma concentrations of DPF 3-O-glucuronide measured following a single oral 50 mg dose of DPF ranged from approximately 1 µg/l in healthy subjects to 2 µg/l in type 2 diabetes patients with moderate to severe renal impairment (Kasichayanula et al. 2013b). It has been reported that DPF 3-O-glucuronidation is catalysed by UGT1A9 (Kasichayanula et al. 2014; Kasichayanula et al. 2013b; Plosker 2012; Scheen 2014a). As with CNF, however, actual data relating to the involvement of UGT1A9 in DPF glucuronidation appear not to have been published.

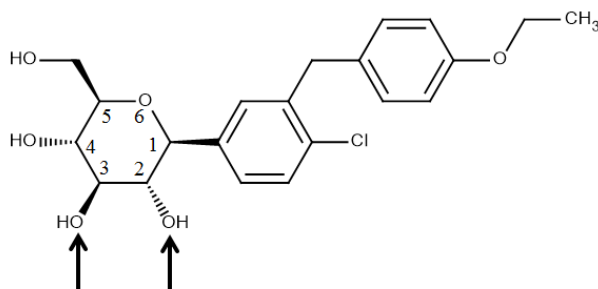
EPF metabolism has been investigated in healthy volunteers, who were administered a single 50 mg oral dose of EPF containing ~100 µCi [¹⁴C]-EPF (Chen et al. 2015). Three glucuronides were identified, namely the 2-O, 3-O and 6-O glucuronides (Figure 4.3, Panel C). Respective area under the plasma concentration – time curves (AUC) from time of administration to 12 hr post-dose for the 2-, 3- and 6- glucuronides were 596, 708 and 472 nM/1.hr, representing 5.9, 7.1 and 4.7% of total radioactivity. The glucuronides were excreted in urine, but not bile. It has been reported that EPF is glucuronidated by UGT 1A3, 1A8, 1A9 and 2B7 (Jardiance Product Information 2015) but, like CNF and DPF, actual data appear not to have been published in the scientific literature.

DDIs are an important consideration in type 2 diabetes since patients frequently receive multiple drugs, both for the treatment of diabetes itself and for comorbidities. There have been a number of DDI studies in humans *in vivo* performed with CNF, DPF and EPF, primarily assessing these drugs as perpetrators of DDIs. In general, the three drugs had no or only a minor effect on the pharmacokinetics of drugs cleared by OCT2 (*viz.* metformin), CYP2C8 (pioglitazone), CYP2C9 (e.g. glyburide, warfarin),

A



B



C

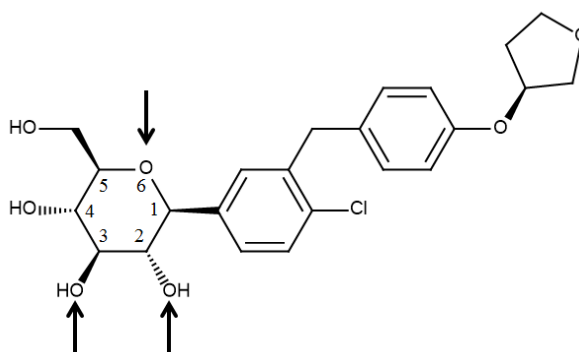


Figure 4.3 Sites (shown by arrows) of glucuronidation of canagliflozin (A), dapagliflozin (B) and empagliflozin (C).

CYP3A4 (e.g. simvastatin, which is also an OATP1B1 substrate), and digoxin (a P-glycoprotein substrate) (Devineni et al. 2015b; Kasichayanula et al. 2012; Kasichayanula et al. 2011a; Macha et al. 2014a; Macha et al. 2013; Yamashiro et al. 2006). There have also been a number of reports of *in vitro* inhibition studies with CNF, DPF and EPF. IC₅₀ values for DPF inhibition of the major drug metabolising human liver microsomal cytochromes P450 exceed 45 µM (Obermeier et al. 2010), and it is claimed that CNF and EPF also appears not to inhibit CYP and UGT enzyme activities to a clinically significant extent (Invokana Product Information 2013; Jardiance Product Information 2015).

However, no systematic investigations of the effects of CNF, DPF and EPF on human UGT enzymes have been reported. As indicated earlier, CNF, DPF and EPF all contain a C-glucoside moiety and are substrates for UGT enzymes. This suggests the possibility of an interaction between these drugs and other glucuronidated compounds. Thus, studies were undertaken here to characterise the inhibition of human recombinant UGTs and, based on the results of these screening studies, the inhibition kinetics of human liver microsomal UGT1A1 and UGT1A9. Whereas DPF and EPF were weak to ‘modest’ inhibitors of these enzymes, CNF was shown to be a potent inhibitor of UGT1A1 and UGT1A9, raising the possibility that this drug may potentially act as a perpetrator of metabolic inhibitory DDIs.

4.2 Methods

4.2.1 Inhibition of recombinant and human liver microsomal UGT activities

CNF, DPF and EPF at concentrations of 1, 10 and 100 μM were screened for inhibition of thirteen recombinant human UGTs; 1A1, 1A3, 1A4, 1A6, 1A7, 1A8, 1A9, 1A10, 2B4, 2B7, 2B10, 2B15 and 2B17. The concentrations of protein and probe substrate present in incubations along with other incubation conditions are detailed in Section 2.2.3, Table 2.6). The final concentration of DMSO (used to dissolve CNF, DPF and EPF) present in incubations was 0.5% v/v. This concentration of DMSO has been reported previously to have only a minor effect on UGT activities (Uchaipichat et al. 2004). Positive control inhibitors were used in all inhibition screening experiments as previously presented in Chapter 3, Section 3.2.4. Quantification of the metabolites of probe substrates was as described in Chapter 2, Section 2.2.3.

4.2.2 Kinetic characterisation of canagliflozin, dapagliflozin and empagliflozin inhibition of recombinant and human liver microsomal UGT 1A1 and 1A9 activities

The kinetics and mechanisms of CNF, DPF and EPF inhibition of recombinant and human liver microsomal UGT1A1 and UGT1A9 were determined using β -EST and PRO as the respective probe substrates. Incubation conditions and analytical procedures used to quantify β -EST and PRO glucuronidation were as described in Sections 2.2.3.4 and 2.2.3.5 below, and are essentially as published in Miners et al. (2011), Rowland et al. (2008b) and Zhou, Tracy and Remmel (2011). As with the inhibition screening studies, CNF, DPF and EPF were added to incubations in DMSO such that the final concentration was 0.5% v/v.

UGT1A1. Experiments to determine the inhibitor constants with UGT1A1 (0.25 mg/ml HEK293 cell lysate) as the enzyme source included four added CNF (3, 6, 9 and 12 μM), DPF (30, 60, 90 and 120 μM) or EPF (40, 80, 120 and 160 μM)

concentrations at each of three added β -EST (3, 6 and 15 μ M) concentrations. Similarly, studies with pooled HLM (0.25 mg/ml) employed four added concentrations of CNF (15, 30, 45 and 90 μ M), DPF (30, 60, 90 and 120 μ M) or EPF (40, 80, 120 and 160 μ M) at each of the three added β -EST concentrations specified above.

UGT1A9. The effects of four added CNF (30, 60, 90 and 120 μ M), DPF (45, 90, 135 and 180 μ M) or EPF (60, 120, 180 and 240 μ M) concentrations were investigated at each of three PRO concentrations; 2, 4 and 8 μ M with CNF as the inhibitor, and 10, 15 and 20 μ M with DPF and EPF as the inhibitors. Studies with HLM as the enzyme source used a protein concentration of 0.5 mg/ml. Experiments employed four added CNF (30, 60, 90 and 120 μ M), DPF (80, 150, 220 and 300 μ M) or EPF (60, 120, 180 and 240 μ M) concentrations at each of three added PRO concentrations (10, 25 and 50 μ M). In addition, incubations contained BSA, either 0.5% (CNF) or 1% (DPF and EPF) w/v, since measurement of optimal UGT1A9 activity (recombinant and human liver microsomal enzyme) requires the presence of BSA to sequester inhibitory long-chain unsaturated fatty acids (see Chapter 1, Section 1.8.3). Binding of CNF, DPF, EPF, β -EST and PRO to enzyme sources and, where relevant, to BSA was corrected for in the calculation of inhibitor constants.

4.2.3 Binding of canagliflozin, dapagliflozin, empagliflozin, β -estradiol, and propofol to HEK293 cell lysates, HLM and BSA

The binding of DPF and EPF to HEK293 cell lysate (0.25 mg/ml) and HLM (0.25 and 0.5 mg/ml), in the absence and presence of BSA where indicated, was performed over the concentration ranges shown in Results (Tables 4.5 and 4.6) using a commercial rapid equilibrium dialysis (RED) device (Section 2.2.4). The sample chamber contained the enzyme source (\pm BSA, 1% w/v) and DPF or EPF (in DMSO, final concentration 0.5% v/v) in phosphate buffer (0.1 M, pH 7.4) while the buffer chamber

side contained only phosphate buffer. Respective volumes of the sample and buffer chambers were 400 and 600 μ l. Dialysis experiments were performed for 8 hr. Attainment of equilibrium was demonstrated using enzyme – enzyme (HEK293 cell lysate or HLM) and buffer – buffer controls at the lowest and highest DPF concentrations investigated in each experiment.

In contrast to DPF and EPF, equilibrium was not achieved with CNF in enzyme – enzyme and buffer – buffer controls over 8 hr using the commercial RED device. However, equilibrium was achieved over this time using conventional equilibrium dialysis (employing dialysis cells). Thus, the binding of CNF to HEK293 cell lysate (0.025 and 0.25 mg/ml) and HLM (0.25 and 0.5 mg/ml), in the absence and presence of BSA where indicated, was performed over the concentration range shown in Table 4.4 according to the procedure of McLure, Miners and Birkett (2000) using Dianorm equilibrium dialysis cells (Dianorm, Munich, Germany) of 1.2 ml capacity per side, separated by Spectrapor number 4 dialysis membrane (molecular mass cut-off 12 – 14 kDa; Spectrum Medical Industries Inc, Los Angeles, CA, USA). One cell contained the enzyme source (\pm BSA, 0.5% w/v) and CNF (in DMSO, final concentration 0.5% v/v) in phosphate buffer (0.1 M, pH 7.4), and the other phosphate buffer alone. The dialysis cell assembly was immersed in a water bath at 37° C and rotated at 12 rpm for 8 hr.

The potential effects of CNF, DPF and EPF on the binding of β -EST and PRO to enzyme sources (HEK293 cell lysate and HLM), in the absence and presence of BSA as appropriate, was assessed over the concentration ranges shown in Results (Tables 4.7 and 4.8). β -EST binding was measured using the commercial RED device and conditions described for DPF (above). Like CNF, equilibrium was not established in enzyme – enzyme and buffer – buffer controls over 8 hr for PRO using the RED device.

However, equilibrium was attained within 8 hr using conventional equilibrium dialysis. Thus, the binding of PRO to incubation constituents was determined as described for CNF.

4.2.4 Quantification of fraction unbound in dialysate media

Samples (100 μ l) from each side of the dialysis apparatus were treated with ice-cold 4% acetic acid in methanol. The concentration of each drug in the dialysate medium was determined by HPLC using a Waters Nova-Pak[®] C-18 (3.9 x 150 mm, 4 μ m particle size) column. Mobile phase compositions and other chromatography parameters are shown in Table 4.2.

4.2.5 Data analysis

Inhibition screening experiments (with recombinant UGT enzymes) and inhibition kinetic studies were performed in duplicate. IC₅₀ values were calculated by fitting equation 2.8 (Section 2.3) to these data and are presented as the parameter \pm standard error (SE) of the parameter fit (Table 4.3). Inhibition data from kinetic experiments are corrected for binding to the enzyme source (plus BSA, where appropriate) and thus inhibitor constants represent $K_{i,u}$. $K_{i,u}$ values were determined by fitting equations 2.10, 2.11 and 2.12 (Section 2.3) to experimental data using Enzfitter. Goodness of fit of each equation was evaluated statistically from the SE of the parameter fit, coefficient of determination (r^2), 95% confidence intervals and F-statistic. The predicted magnitude of a DDI arising from inhibition of the UGT enzyme of interest was assessed as $1 + [I]/K_{i,u}$, where [I] is the concentration of the flozin in blood (equation 2.15 – 2.17, Section 2.3).

Table 4.2 HPLC conditions for the quantification of drug binding in dialysates from equilibrium dialysis experiments.

Drug	Mobile phase composition	Gradient elution time (min)	Detector wavelength (nm)	Retention time (min)
Isocratic elution				
Canagliflozin	60%A : 40%D	-	291	3.9
Dapagliflozin	65%A : 35%D	-	236	3.2
Empagliflozin	70%A : 30%D	-	230	3.3
β -Estradiol	60%B : 40%D	-	220	2.9
Propofol	30%C : 70%D	-	214	2.3
Gradient elution				
Canagliflozin (in the presence of β -estradiol)	70%A : 30%D	0	291	5.9 (CNF)
	50%A : 50%D	5		5.4 (β -EST)
	50%A : 50%D	5.5		
	70%A : 30%D	6.5		
β -Estradiol (in the presence of canagliflozin)	80%B : 20%D	0	220	7.9 (β -EST)
	60%B : 40%D	7		8.9 (CNF)
	60%B : 40%D	7.5		
	80%B : 20%D	8.5		

A: 5% acetonitrile in water.

B: 10 mM triethylamine (adjusted to pH 2.5 with 11.6 M HClO₄) containing 10% acetonitrile.

C: 5 mM ammonium acetate (adjusted to pH 4.6 with glacial acetic acid) containing 5% acetonitrile.

D: acetonitrile.

4.3 Results

4.3.1 Canagliflozin, dapagliflozin and empagliflozin inhibition of recombinant human UGT enzymes

Inhibition of individual UGT enzymes by CNF, DPF and EPF are shown in Figure 4.4 and derived IC₅₀ values in Table 4.3. CNF inhibited all UGT1A subfamily enzymes with IC₅₀ values < 50 µM (Figure 4.4, Panel A). Greatest inhibition was observed with UGT 1A1, 1A9 and 1A10, with respective mean IC₅₀ values of 9.5, 6.9 and 7.0 µM. Inhibition of UGT 2B7, 2B10 and 2B15 was ‘moderate’ (IC₅₀ mean values approximately 50 – 80 µM), whereas CNF had a negligible effect on UGT 2B4 and 2B17 activities (IC₅₀ > 100 µM). Like CNF, DPF most potently inhibited UGT 1A1, 1A9 and 1A10 (Figure 4.4, Panel B). However, mean IC₅₀ values (39 – 66 µM) were approximately 6-fold higher than those for CNF inhibition of these enzymes. Inhibition of UGT 1A3, 1A4, 1A6 and 1A7, and all UGT2B enzymes UGT, 1A4, 1A6 and 1A8 and all UGT2B enzymes was negligible. EPF exhibited least inhibition of the three flozins. Mean IC₅₀ values were < 100 µM only for UGT 1A1, 1A3 and 1A9 (Figure 4.4, Panel C).

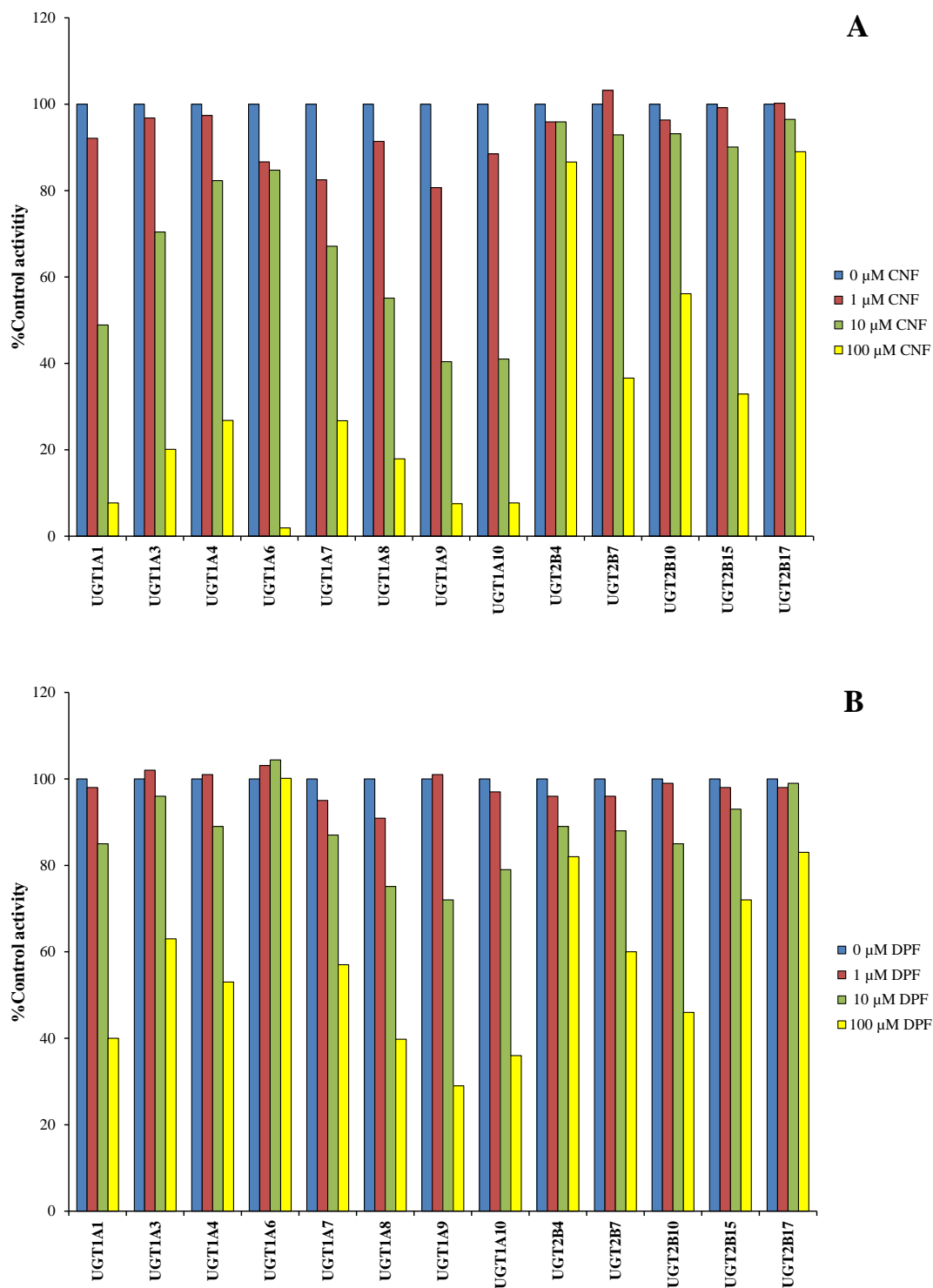


Figure 4.4 Inhibition of recombinant human UGT enzymes by canagliflozin (Panel A), dapagliflozin (Panel B) and empagliflozin (Panel C).

Concentrations of each flozin were 1, 10 and 100 μ M. Bars represent the mean of duplicate estimates (< 5% variance).

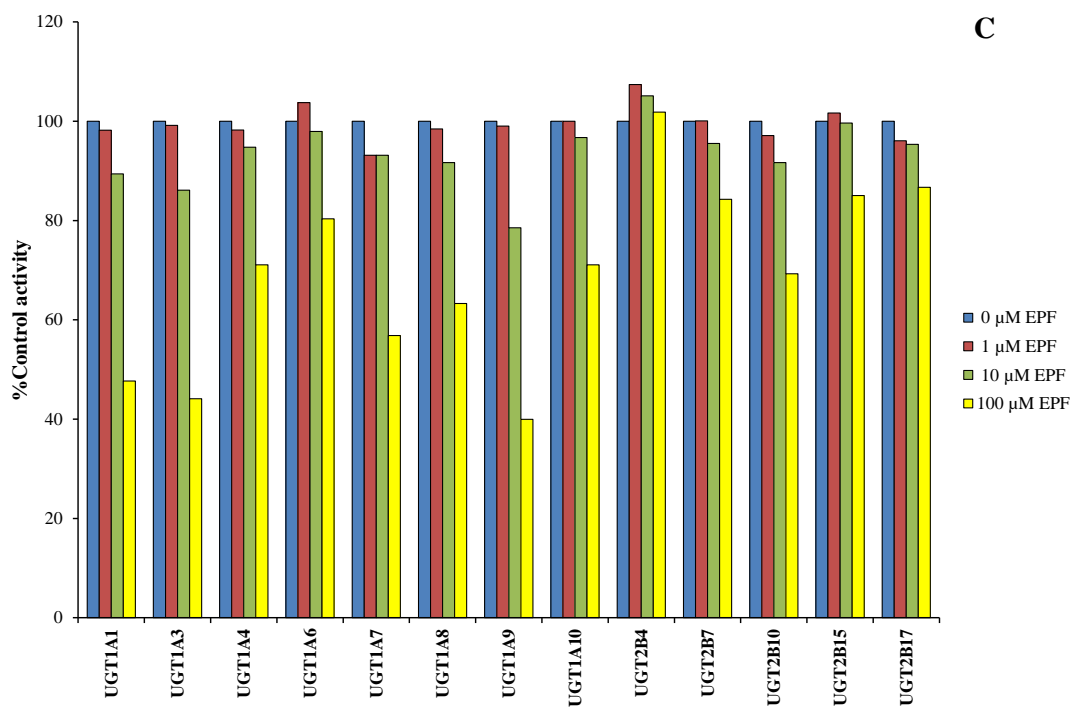


Figure 4.4 Inhibition of recombinant human UGT enzymes by canagliflozin (Panel A), dapagliflozin (Panel B) and empagliflozin (Panel C) (cont.).

Table 4.3 IC₅₀ values for CNF, DPF and EPF inhibition of recombinant UGT enzymes.

UGT enzyme	IC ₅₀ (μM) ± SE parameter fit		
	CNF	DPF	EPF
UGT1A1	9.5 ± 0.41	66 ± 2.4	92 ± 1.5
UGT1A3	24 ± 0.19	> 100	78 ± 0.98
UGT1A4	48 ± 0.45	> 100	> 100
UGT1A6	22 ± 0.82	> 100	> 100
UGT1A7	42 ± 1.04	> 100	> 100
UGT1A8	13 ± 1.59	75 ± 7.9	> 100
UGT1A9	6.9 ± 0.01	39 ± 1.7	64 ± 2.5
UGT1A10	7.0 ± 0.07	55 ± 0.72	> 100
UGT2B4	> 100	> 100	> 100
UGT2B7	59 ± 2.55	> 100	> 100
UGT2B10	85 ± 0.36	> 100	> 100
UGT2B15	49 ± 0.55	> 100	> 100
UGT2B17	> 100	> 100	> 100

4.3.2 Binding of canagliflozin, dapagliflozin and empagliflozin to HEK293 cell lysate and HLM, with and without BSA

It is known that recombinant and human liver microsomal UGT1A9, but not UGT1A1, activities are under-estimated in the absence of BSA (see Section 1.8.3). Thus, experiments undertaken to characterise the inhibition kinetics of recombinant and human liver microsomal UGT1A9 included BSA in the incubation medium. The binding of CNF to albumin is extensive and, due to limitations of assay sensitivity, the concentration of BSA added to incubations containing CNF was 0.5% w/v. It is

acknowledged that this BSA concentration may produce a less than optimal decrease in the K_i values for inhibitors of UGT1A9. The somewhat less extensive binding of DPF and EPF to albumin permitted kinetic experiments to be performed in the presence of 1% w/v BSA. Experience in this laboratory indicates that the optimal effect of BSA on UGT activities occurs for concentrations in the range 1 to 2% w/v (for example Rowland et al., 2007 and 2008). The binding of CNF, DPF and EPF to HEK293 cell lysate and to HLM was determined in the absence and presence of BSA. Data are shown in Tables 4.4, 4.5 and 4.6. The binding of CNF, DPF and EPF to each enzyme source (\pm BSA) was concentration-independent over the ranges studied. The mean $f_{u_{mic}}$ values for CNF binding to HLM and HEK293 cell lysate (both 0.25 mg/ml) in the absence of BSA (UGT1A1 inhibition studies) were 0.38 and 0.96, respectively (Table 4.4). When BSA (0.5% w/v) was added to suspensions of HEK293 cell lysate (0.025 and 0.25 mg/ml) and HLM (0.5 mg/ml) (UGT1A9 inhibition studies), CNF binding increased substantially; mean $f_{u_{mic}}$ values were 0.08 to 0.12. Addition of β -EST and PRO at concentrations at the upper end of the ranges used in inhibition experiments did not affect CNF binding.

Similar trends were observed with DPF binding, although binding of DPF to enzyme sources and BSA (1% w/v) was lower than for CNF (Table 4.5). The mean $f_{u_{mic}}$ values for DPF binding to HEK293 cell lysate and HLM (both 0.25 mg/ml) in the absence of BSA (UGT1A1 inhibition studies) were 0.94 and 0.86, respectively.

Mean $f_{u_{mic}}$ values for DPF binding to HEK293 cell lysate and HLM in the presence of BSA (1% w/v) ranged from 0.27 to 0.30. As with CNF, addition of concentrations of β -EST and PRO at the upper end of the ranges used in inhibition experiments did not affect DPF binding. The binding of EPF to HEK293 cell lysate and HLM (both 0.25 mg/ml) in the absence of BSA was negligible ($< 5\%$) (Table 4.6). Mean $f_{u_{mic}}$ values

for EPF binding to HEK293 cell lysate and HLM in the presence of BSA (1% w/v) ranged from 0.33 to 0.35. As with CNF and DPF, addition of PRO at the upper end of the concentration range used in inhibition experiments did not affect DPF binding. Since binding of EPF to enzyme sources was negligible, measurement of the effects of β -EST on EPF binding was not required.

Binding data for the probe substrates PRO and β -EST is shown in Tables 4.7 and 4.8, respectively. PRO bound extensively to HEK293 cell lysate (0.25 mg/ml) and HLM (0.5 mg/ml) in the presence of BSA (0.5 and 1% w/v) with mean $f_{u_{mic}}$ values in the range 0.21 to 0.34. The mean $f_{u_{mic}}$ for β -EST binding to HLM (0.25 mg/ml) was 0.79. β -EST did not bind to HEK293 cell lysate (0.25 mg/ml).

It was further demonstrated that concentrations of CNF, DPF and EPF at the upper end of the ranges used in inhibition experiments did not affect PRO binding to HEK293 cell lysate and HLM plus BSA (UGT1A9 inhibition experiments) (Table 4.7). Similarly, concentrations of CNF and DPF at the upper end of the ranges used in inhibition experiments did not affect the binding of β -EST to HEK293 cell lysate and HLM (UGT1A1 inhibition experiments) (Table 4.8). The potential influence of EPF on the binding of β -EST to enzyme sources was not assessed given the negligible binding of EPF (see above).

As indicated previously, binding of CNF, DPF, EPF, β -EST and PRO to enzyme sources and, where relevant, to BSA was corrected for in the calculation of $K_{i,u}$ values for inhibition of UGT1A1 and UGT1A9.

Table 4.4 Binding of CNF to protein sources (HEK cell lysate and HLM) in the absence and presence of BSA (0.5% w/v).*Binding is expressed as the fraction unbound in the incubation medium ($f_{u_{mic}}$).*

Concentration (μM)	Protein source	$f_{u_{mic}}$
2.5, 10, 25, 50, 100	HEK (0.25 mg/ml)	0.96 ± 0.09
2.5, 10, 50, 100, 200	HLM (0.25 mg/ml)	0.38 ± 0.02
2.5, 10, 25, 50, 100	HEK (0.025 mg/ml) + 0.5%BSA	0.10 ± 0.01
2.5, 10, 25, 50, 100	HEK (0.25 mg/ml) + 0.5%BSA	0.10 ± 0.01
2.5, 10, 25, 50, 100, 200	HLM (0.5 mg/ml) + 0.5%BSA	0.08 ± 0.01
10 and 100 μM (20 μM β -EST added)	HLM (0.25 mg/ml)	0.40 ± 0.03
10 and 100 μM (10 μM PRO added)	HEK (0.25 mg/ml) + 0.5%BSA	0.12 ± 0.01
10 and 100 μM (50 μM PRO added)	HLM (0.5 mg/ml) + 0.5%BSA	0.08 ± 0.02

Table 4.5 Binding of DPF to protein sources (HEK cell lysate and HLM) in the absence and presence of BSA (1% w/v).*Binding is expressed as the fraction unbound in the incubation medium ($f_{u_{mic}}$).*

Concentration (μM)	Protein source	$f_{u_{mic}}$
10, 50, 100, 200	HEK (0.25 mg/ml)	0.94 ± 0.02
10, 50, 100, 200, 500, 1000	HLM (0.25 mg/ml)	0.86 ± 0.03
10, 50, 100, 200	HEK (0.025 mg/ml) + 1%BSA	0.27 ± 0.03
10, 50, 100, 200	HEK (0.25 mg/ml) + 1%BSA	0.30 ± 0.01
10, 50, 100, 200, 500, 1000	HLM (0.5 mg/ml) + 1%BSA	0.29 ± 0.02
10 and 200 (20 μM β -EST added)	HLM (0.25 mg/ml)	0.85 ± 0.01
10 and 200 μM (50 μM PRO added)	HEK (0.25 mg/ml) + 1%BSA	0.29 ± 0.02
10 and 400 μM (50 μM PRO added)	HLM (0.5 mg/ml) + 1%BSA	0.30 ± 0.04

Table 4.6 Binding of EPF to protein sources (HEK cell lysate and HLM) in the absence and presence of BSA (1% w/v).*Binding is expressed as the fraction unbound in the incubation medium ($f_{u_{mic}}$).*

Concentration (μM)	Protein source	$f_{u_{mic}}$
10, 50, 100, 250	HEK (0.25 mg/ml)	0.97 ± 0.03
10, 50, 100, 250	HLM (0.25 mg/ml)	0.96 ± 0.01
10, 50, 100, 250	HEK (0.025 mg/ml) + 1%BSA	0.33 ± 0.02
10, 50, 100, 250	HEK (0.25 mg/ml) + 1%BSA	0.33 ± 0.03
10, 50, 100, 250	HLM (0.5 mg/ml) + 1%BSA	0.33 ± 0.03
10 and 250 μM (20 μM β -EST added)	HLM (0.25 mg/ml)	- ^a
10 and 250 μM (50 μM PRO added)	HEK (0.25 mg/ml) + 1%BSA	0.34 ± 0.03
10 and 250 μM (50 μM PRO added)	HLM (0.5 mg/ml) + 1%BSA	0.35 ± 0.04

^a *Binding of EPF to 0.25 mg/ml HLM was negligible (with < 5%).*

Table 4.7 Binding of propofol to protein sources (HEK cell lysate and HLM) in the presence of BSA (0.5 and 1% w/v).*Binding is expressed as the fraction unbound in the incubation medium ($f_{u_{mic}}$).*

Concentration (μM)	Protein source	$f_{u_{mic}}$
2, 4, 8, 10	HEK (0.25 mg/ml) + 0.5%BSA	0.34 ± 0.03
10, 50, 100, 200	HEK (0.25 mg/ml) + 1%BSA	0.24 ± 0.02
5, 10, 50, 100	HLM (0.5 mg/ml) + 0.5%BSA	0.32 ± 0.05
5, 10, 50, 100	HLM (0.5 mg/ml) + 1%BSA	0.21 ± 0.02
2 and 10 (100 μM CNF added)	HEK (0.25 mg/ml) + 0.5%BSA	0.36 ± 0.01
5 and 50 (200 μM CNF added)	HLM (0.5 mg/ml) + 0.5%BSA	0.34 ± 0.01
5 and 50 (200 μM DPF added)	HEK (0.25 mg/ml) + 1%BSA	0.25 ± 0.03
5 and 50 (400 μM DPF added)	HLM (0.5 mg/ml) + 1%BSA	0.23 ± 0.03
5 and 50 (250 μM EPF added)	HEK (0.25 mg/ml) + 1%BSA	0.23 ± 0.02
5 and 50 (250 μM EPF added)	HLM (0.5 mg/ml) + 1%BSA	0.24 ± 0.02

Table 4.8 Binding of β -estradiol to HEK cell lysate and HLM.*Binding is expressed as the fraction unbound in the incubation medium ($f_{u_{mic}}$).*

Concentration (μM)	Protein source	$f_{u_{mic}}$
2, 5, 10, 20	HEK (0.25 mg/ml)	1.01 ± 0.07
2, 5, 10, 20	HLM (0.25 mg/ml)	0.79 ± 0.05
2 and 20 (100 μM CNF added)	HLM (0.25 mg/ml)	0.80 ± 0.03
2 and 20 (200 μM DPF added)	HLM (0.25 mg/ml)	0.82 ± 0.03
2 and 20 (250 μM EPF added)	HLM (0.25 mg/ml)	- ^a

^a Binding of EPF to 0.25 mg/ml HLM was negligible (< 5%).

4.3.3 Kinetics of canagliflozin, dapagliflozin and empagliflozin inhibition of recombinant and human liver microsomal UGT1A1 and UGT1A9

β -EST was used as the UGT1A1 probe substrate, both for the recombinant enzyme and HLM. β -EST 3-glucuronidation by recombinant UGT1A1 exhibits sigmoidal kinetics, with an S_{50} of 10 μ M (Udomuksorn et al. 2007). It was confirmed here that β -EST 3-glucuronidation by HLM also exhibits sigmoidal kinetics, with a mean S_{50} of 14 μ M (data not shown). Experimental data for inhibition of β -EST 3-glucuronidation by CNF, DPF and EPF were poorly fit by the expressions for competitive, non-competitive and mixed inhibition (equations 2.10 – 2.12, Section 2.3), presumably because the concentrations of β -EST employed in the inhibition experiments (3, 6 and 15 μ M) spanned the S_{50} and therefore included the early curved and pseudo-linear sections of the sigmoidal substrate concentration versus velocity plots. As a result, Eadie-Hostee plots were curvi-linear rather than linear. Thus, the Hill equation, which describes sigmoidicity, was modified to include an inhibition term analogous to the equation for competitive inhibition of an enzyme exhibiting Michaelis-Menten kinetics (equations 2.13 and 2.14, Section 2.3). Both expressions derived from the Hill equation described CNF, DPF and EPF inhibition of UGT1A1 well, both visually and statistically. However, equation 2.14 (Section 2.3) gave marginally improved fits statistically (Figures 4.5 – 4.7, Panel A and B); F-statistic > 4,980, $r^2 = 0.999$, and standard error of parameter fits < 5%. By contrast, experimental data for CNF, DPF and EPF inhibition of recombinant UGT1A9 (PRO as substrate) and human liver microsomal UGT1A9 (PRO as substrate) were well described by the equation for competitive inhibition of an enzyme exhibiting Michaelis-Menten kinetics (equation 2.10, Section 2.3).

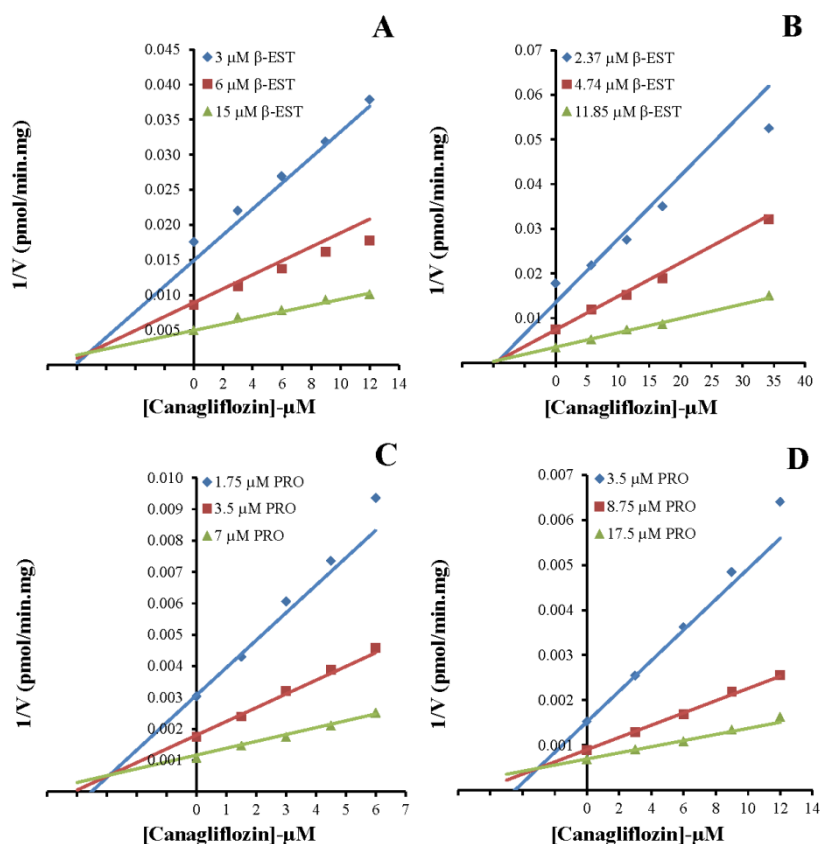


Figure 4.5 Dixon plots for canagliflozin inhibition of UGT activities.

Enzyme/substrate pairs: UGT1A1/β-EST (Panel A); HLM/β-EST (Panel B); UGT1A9+BSA/PRO (Panel C); HLM+BSA/PRO (Panel D). Concentrations of canagliflozin and substrate are corrected for binding to the respective enzyme sources and BSA (0.5 % w/v). Points are experimentally derived values (mean of duplicate estimates; < 5% variance), while lines are from fitting with equation 2.10 (UGT1A9) or 2.14 (UGT1A1).

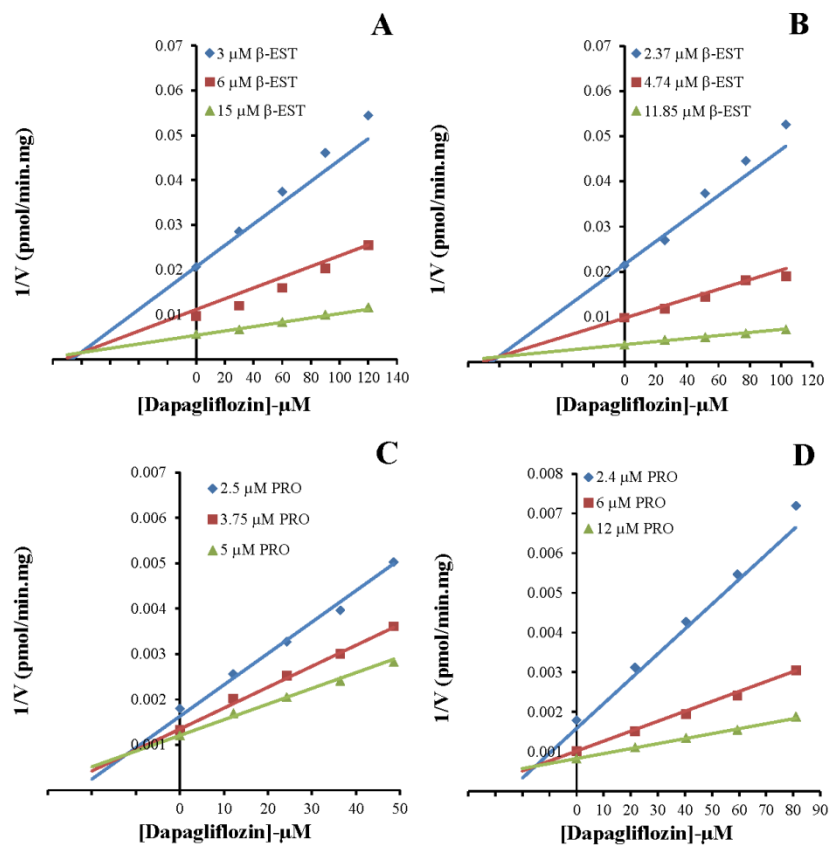


Figure 4.6 Dixon plots for dapagliflozin inhibition of UGT activities.

Enzyme/substrate pairs: UGT1A1/β-EST (Panel A); HLM/β-EST (Panel B); UGT1A9+BSA/PRO (Panel C); HLM+BSA/PRO (Panel D). Concentrations of dapagliflozin and substrate are corrected for binding to the respective enzyme sources and BSA (1 % w/v). Points are experimentally derived values (mean of duplicate estimates; < 5% variance), while lines are from fitting with equation 2.10 (UGT1A9) or 2.14 (UGT1A1).

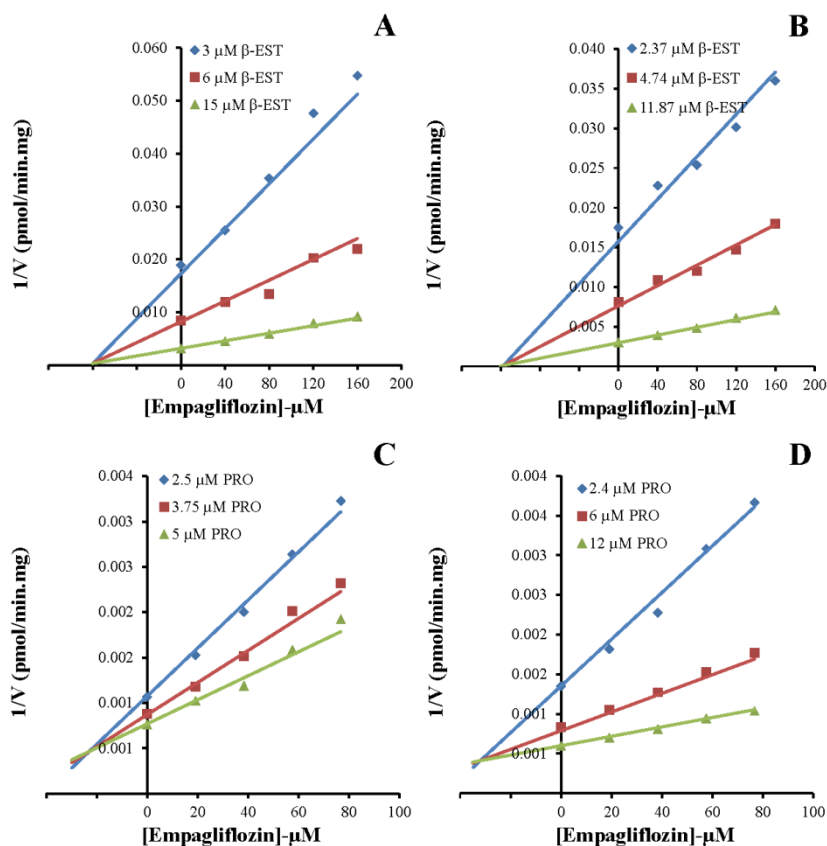


Figure 4.7 Dixon plots for empagliflozin inhibition of UGT activities.

Enzyme/substrate pairs: *UGT1A1/β-EST* (Panel A); *HLM/β-EST* (Panel B); *UGT1A9+BSA/PRO* (Panel C); *HLM+BSA/PRO* (Panel D). Concentrations of empagliflozin and substrates are corrected for binding to the respective enzyme sources and BSA (1 % w/v). Points are experimentally derived values (mean of duplicate estimates; < 5% variance), while lines are from fitting with equations 2.10 (*UGT1A9*) or 2.14 (*UGT1A1*).

Kinetic plots for CNF, DPF and EPF inhibition of UGT activities are shown in Figures 4.5, 4.6 and 4.7, respectively, and derived $K_{i,u}$ values are given in Table 4.9. CNF was a potent inhibitor of recombinant and human liver microsomal UGT1A9, with $K_{i,u}$ values around 3.0 μM . $K_{i,u}$ values for CNF inhibition of UGT1A1 were approximately 3-fold higher. Consistent with the activity screening data, DPF was a less potent inhibitor of UGT1A1 and UGT1A9. The $K_{i,u}$ for DPF inhibition of recombinant and human liver microsomal UGT1A1 was 81 μM , while $K_{i,u}$ values for inhibition of UGT1A9 ranged from 12 to 15 μM . EPF was the weakest inhibitor of the three flozins investigated here. The $K_{i,u}$ value for EPF inhibition of human liver microsomal UGT1A1 was approximately 13- and 1.5-fold higher than the respective values for CNF and DPF, although the $K_{i,u}$ value for recombinant UGT1A1 was similar to that of DPF. $K_{i,u}$ values for EPF inhibition of recombinant and human liver microsomal UGT1A9 were approximately double those of DPF and 10-fold higher than those of CNF.

Table 4.9 Derived $K_{i,u}$ values for CNF, DPF and EPF inhibition of recombinant and human liver microsomal UGT1A1 and UGT1A9.

Enzyme source / substrate	$K_{i,u}$ (μM) ^a		
	CNF	DPF	EPF
UGT1A1 / β -estradiol	7.2 \pm 1.4	81 \pm 1.4	80 \pm 0.9
HLM / β -estradiol	9.1 \pm 0.2	81 \pm 3.8	117 \pm 1.3
UGT1A9 / propofol	2.9 \pm 0.1	12 \pm 0.6	23 \pm 1.0
HLM / propofol	3.0 \pm 0.1	15 \pm 0.6	32 \pm 1.2

^a \pm SE of the parameter fit

4.4 Discussion

CNF, DPF and EPF are the first SGLT2 inhibitors to be approved for clinical use. They are generally prescribed in combination with other antidiabetic drugs (particularly metformin) to improve glycemic control (Bailey et al. 2013; Häring et al. 2014; Häring et al. 2013; Matthaai et al. 2015; Rosenstock et al. 2012a; Schernthaner et al. 2013). Additionally, antidiabetic drugs are frequently co-administered with antihypertensive and/or hypolipidemic drugs to improve cardiovascular risk (Basile 2013; Foote, Perkovic and Neal 2012; Scheen 2014a; Zinman et al. 2015). Since many patients with type 2 diabetes present with multiple co-morbidities, polypharmacy is common highlighting the need to carefully evaluate potential DDIs. As indicated in Chapter 1, FDA and EMA guidelines now recommend that new drugs are evaluated for their potential to inhibit the major human drug metabolising CYP and UGT enzymes *in vitro* in order to assess their potential role as perpetrators of inhibitory DDIs (European Medicines Agency (EMA) 2012; Food and Drug Administration (FDA) 2012; 2017). The Product Information for CNF indicates a low propensity for inhibition of CYP enzyme activities (Invokana Prescribing Information 2013). Similarly, it has been reported that IC₅₀ values for DPF inhibition of the major drug metabolising human liver microsomal CYP enzymes exceed 45 µM (Obermeier et al. 2010). Although EPF has been reported not inhibit CYP enzymes and UGT1A1, actual data appear not to have been published (Jardiance Product Information 2015). No systematic investigations of the effects of CNF and DPF on human UGT enzymes have been reported and, as indicated above, effects of EPF have apparently only been studied with UGT1A1. Results presented in this chapter demonstrate that CNF is a relatively potent inhibitor of UGT 1A1 and 1A9 *in vitro*, whereas DPF and EPF inhibition of

these enzymes is 'moderate to weak'. UGT 1A1 and 1A9 are both expressed in the liver, while UGT1A9 is additionally expressed in the kidney (Knights et al. 2016a). Hence, inhibition of UGT 1A1 and 1A9 may potentially result in the reduced clearance of drugs, non-drug xenobiotics, and endogenous compounds that are eliminated by these enzymes.

As discussed in Chapter 1 (Section 1.8.3), long-chain unsaturated fatty acids released from the microsomal membrane during the course of an incubation are known to inhibit UGT1A9, but not UGT1A1, activity resulting in over-estimation of the K_m and K_i values of substrates and inhibitors of this enzyme, respectively. Thus, experiments to determine $K_{i,u}$ values for CNF, DPF and EPF glucuronidation by recombinant and human liver microsomal UGT1A9 were undertaken in the presence of BSA, which sequesters the inhibitory fatty acids thereby providing a more accurate value of the inhibitor constant. $K_{i,u}$ values for inhibition of human liver microsomal and recombinant UGT1A9 of the three flozins were determined with PRO, which is a selective substrate for this enzyme (Chapter 1, Section 1.8.3). $K_{i,u}$ values for CNF inhibition of recombinant and human liver microsomal UGT1A9 were essentially identical (3.0 μM), while the respective $K_{i,u}$ values for DPF and EPF inhibition were similarly close in value (12 and 15 μM , and 23 and 32 μM) (Table 4.9). There was also close agreement in the $K_{i,u}$ values for CNF (7.2 and 9.1 μM), DPF (both 81 μM) and EPF (80 and 117 μM) inhibition of recombinant and human liver microsomal UGT1A1, which were determined using the selective substrate β -EST (see Chapter 1). The propensity of a compound to act as a perpetrator of inhibitory DDIs may be assessed using equation 2.15 (Section 2.3), where the key term is the $[I]/K_i$ ratio. For a victim drug completely metabolised along a single metabolic pathway by a single enzyme, $f_m = 1$ and equation 2.16 simplifies to the expression $\text{AUC ratio} = (1 + [I]/K_i)$,

(Section 2.3). In the absence of data which allows calculation of the hepatic input concentration (i.e. k_a and/or $F_a.F_g$), the inhibitor concentration may be taken as the maximum plasma concentration of the putative perpetrator (European Medicines Agency (EMA) 2012; Food and Drug Administration (FDA) 2012; 2017).

The reported mean maximum plasma concentrations of CNF at steady-state for doses of 100 mg/day and 300 mg/day (the highest recommended dose) are 1,227 $\mu\text{g/l}$ (2.8 μM) and 4,678 $\mu\text{g/l}$ (10.7 μM), respectively (Devineni et al. 2013). These concentrations are similar to or exceed the $K_{i,u}$ values observed for CNF inhibition of UGT1A9 (3.0 μM) and UGT1A1 (7.2 – 9.1 μM). Based on these CNF plasma concentrations and the experimentally determined $K_{i,u}$ values, approximate 131 - 139% and 118 - 249% increases in the AUC ratio for exclusive UGT1A1 substrates are predicted for the 100 and 300 mg/day doses, respectively, using the simplified equation given above. For exclusive UGT1A9 substrates, predicted AUC ratio increases range from 193% and 457% for the 100 and 300 mg/day CNF doses, respectively. Assuming a fraction unbound in plasma of 0.01 (Devineni et al. 2015a; Devineni et al. 2013), the corresponding maximum unbound concentrations of CNF in plasma are 0.02 and 0.07 μM , respectively, both of which are lower than the range of $K_{i,u}$ values observed for CNF inhibition of UGT1A1 and UGT1A9. Although it is expected that the unbound concentration of the inhibitor in blood better reflects the drug concentration in hepatocytes, up to late 2017 FDA guidelines recommended the use of total perpetrator concentration and several studies have reported that optimal prediction of DDI potential arising from inhibition of UGT and CYP enzymes is obtained using total perpetrator drug concentration (Brown et al. 2005; Ito, Brown and Houston 2004; Raungrut et al. 2010; Rowland et al. 2006a). Thus, inhibition of UGT1A1 and UGT1A9 by CNF *in vivo* cannot be discounted. (Note: this issue is discussed further

in Chapter 6.) Since the C_{\max} values of CNF in patients with severe renal dysfunction and mild hepatic impairment have been reported to be similar to C_{\max} values in subjects with normal organ function (Devineni et al. 2015a; Invokana Product Information 2013), the predicted increase in AUC due to CNF would not be expected to be higher in these patients. (It should be noted that CNF pharmacokinetics appear not to have been studied in patients with severe hepatic impairment.). The mean maximum plasma concentration of DPF (10 mg/day) at steady-state is reported as 169 $\mu\text{g/l}$ (0.41 μM) and the unbound fraction in plasma as 0.09 (Kasichayanula et al. 2014; Plosker 2012), providing a maximum unbound concentration of 0.04 μM . Thus, both the maximum total and unbound DPF concentrations are low compared to the $K_{i,u}$ values for inhibition of UGT1A1 and UGT1A9. Although the C_{\max} of DPF increases in patients with severe hepatic impairment (by 40%) compared to subjects with normal hepatic function (Kasichayanula et al. 2011b), the higher observed total and unbound C_{\max} values are still low compared to $K_{i,u}$. Similarly, the increase in the C_{\max} of DPF reported for patients with renal dysfunction (9 – 27%) (Kasichayanula et al. 2013b) provides $[I]/K_{i,u}$ values inconsistent with clinically significant inhibition of UGT1A1 and UGT1A9 *in vivo*. Interestingly, co-administration of the known UGT1A9 inhibitor mefenamic acid (Gaganis, Miners and Knights 2007) increased the area under the plasma concentration – time curve of DPF in healthy subjects by 51% (Kasichayanula et al. 2013a).

Reported mean maximum plasma concentrations of EPF for doses of 10 mg/day (the recommended starting dose) and 25 mg/day (the highest recommended dose) at steady-state are reported as 259 nmol/l (0.26 μM) and 687 nmol/l (0.69 μM), respectively (Heise et al. 2013) and the unbound fraction in plasma as 0.14 (Chen et al. 2015). Thus, the respective maximum unbound concentrations in plasma for the 10 and 25 mg/day

doses are 0.04 μM and 0.09 μM . Clearly, the $K_{i,u}$ values for inhibition of UGT1A1 and UGT1A9 (23 - 117 μM ; Table 4.9) substantially exceed the maximum unbound concentrations at steady-state. Like DPF, the C_{max} of EPF has been reported to be higher (by 44%) in patients with severe hepatic impairment and in patients with severe renal dysfunction (by 23%) compared to subjects with normal hepatic and renal function (Macha et al. 2014b; Macha et al. 2014c). However, the total and unbound plasma concentrations of EPF in these patients still remain low compared to $K_{i,u}$.

CNF has been reported not to alter the clearance of co-administered paracetamol (Invokana Product Information 2013), a drug cleared predominantly by UGT1A6 (with lesser contributions of UGT 1A1, 1A9 and 2B15) (Miners et al. 2011). As discussed above, DPF and EPF are not predicted to inhibit UGT1A9, but a potential effect of CNF on UGT1A1 and UGT1A9-catalysed drug glucuronidation cannot be discounted. Moreover, it is conceivable that CNF may inhibit renal UGT1A9 activity *in vivo* to a greater extent than predicted from the $[I]/K_{i,u}$ ratio. It has been demonstrated in this laboratory that basolateral uptake of 4MU in the isolated rat perfused kidney is high, resulting in extensive renal 4MU glucuronidation (Wang et al. 2011). Thus, the intra-renal concentration of drugs such as CNF (and DPF, and EPF) may be higher than in plasma, resulting in a larger than expected $[I]/K_{i,u}$ ratio. Importantly, UGT1A9 is the predominant UGT protein expressed in the kidney (Knights et al. 2016a; Margailan et al. 2015), consistent with the observation that numerous UGT1A9 substrates are glucuronidated by this organ (*in vitro* and/or *in vivo*) (Knights and Miners 2010). Indeed, available data suggests that renal glucuronidation contributes significantly to DPF metabolic clearance (Kasichayanula et al. 2013b). As noted above, it is possible that CNF in particular may inhibit UGT1A9 catalysed glucuronidation in the kidney, thereby increasing the intra-renal concentration and

response of the victim drug. By way of example, UGT1A9-catalysed glucuronidation of the diuretic frusemide, which appears to occur solely in the kidney, is the major metabolic pathway of this drug in humans (Kerdpin et al. 2008; Smith and Benet 1983).

Although it has been reported that UGT2B4 contributes to CNF glucuronidation (see Section 4.1), CNF inhibition of this enzyme was negligible. Apart from UGT1A1 and UGT1A9, CNF inhibited UGT1A10 with similar potency to UGT1A9. Available evidence indicates that UGT1A10 is expressed exclusively in the gastrointestinal tract (Rowland, Miners and Mackenzie 2013). However, the contribution of UGT1A10 to the intestinal metabolism of drugs *in vivo* is currently unknown.

During the writing of this thesis, Mamidi and colleagues (2017) published a paper entitled, ‘*In vitro* and physiologically-based pharmacokinetic assessment of drug-drug interaction potential of canagliflozin’. Mamidi et al. determined IC₅₀ values for CNF inhibition of drug metabolising cytochrome P450 enzymes and UGT 1A1, 1A4, 1A6, 1A9 and 2B7 using HLM as the enzyme source. IC₅₀ values for the inhibition of the UGT and CYP enzymes ranged from 50 to > 100 µM and 16 to > 100 µM, respectively. Based on the assumption that inhibition was competitive, K_i values for CNF were calculated as IC₅₀/2. These values were then employed for IV – IVE using Simcyp. Mamidi et al. concluded that CNF is neither a perpetrator nor victim of DDIs.

As we highlighted in a subsequent Letter to the Editor (Miners, Pattanawongsa and Rowland 2018), there are large discrepancies between the data described in this thesis (and published as Pattanawongsa et al. (2015)) and the results of Mamidi et al. In addition, Mamidi et al. failed to consider their data in the context of our previously published data. Whereas Mamidi et al. reported weak inhibition of human liver

microsomal UGT 1A1 and 1A9, results presented here demonstrate that CNF is a potent inhibitor of both recombinant and human liver microsomal UGT1A9 and UGT1A1. Such a large discrepancy is surprising and, at least in the case of UGT1A9, unanticipated since, as stated earlier, CNF is glucuronidated predominantly by UGT1A9. It is likely that the differences between the studies arise from the experimental approaches adopted. Whereas K_i values were determined here from carefully conducted kinetic studies, Mamidi et al. estimated K_i values from the experimentally determined IC_{50} (as $IC_{50}/2$), where IC_{50} values were generated from an unspecified number of data points. Notably, there is large variability in some of the data reported by Mamidi et al. For example, the mean (\pm SE) IC_{50} for UGT1A1 was reported as $91 \pm 53 \mu\text{M}$.

The single point IV-IVE data reported here based on total plasma CNF concentrations indicate potential inhibitory DDIs with UGT1A1 and UGT1A9 substrates, but no interaction based on unbound plasma CNF concentrations. Based on total plasma CNF concentration, Mamidi et al. predicted CNF may inhibit UGT1A1 and UGT1A6 *in vivo* but, similar to this work, concluded CNF has a low potential to precipitate DDIs arising from inhibition of UGT enzymes when calculations were performed with unbound plasma concentrations. However, as stated by Miners, Pattanawongsa and Rowland (2018), any concordant conclusions are fortuitous given the differences in the UGT inhibition data reported by Mamidi et al. and in this thesis.

In summary, data presented here showed that CNF is a potent inhibitor of UGT1A1 and UGT1A9 *in vitro*, whereas DPF and EPF cause 'lesser' inhibition of these enzymes. *In vitro* – *in vivo* extrapolation based on the $[I]/K_{i,u}$ ratios excludes DPF and EPF as perpetrators of DDIs arising from inhibition of UGT enzymes, but inhibition of UGT1A1 and UGT1A9 by CNF *in vivo* cannot be discounted. Like CNF, DPF and

EPF, other SGLT2 inhibitors in clinical development (e.g. ertugliflozin, remogliflozin and sotogliflozin) contain a glycoside moiety, which is presumably an important structural feature for CNF, DPF and EPF binding to UGT enzymes. Thus, the screening of SGLT2 inhibitors for effects on UGT enzymes is warranted in order to identify or exclude potential DDIs.

CHAPTER 5

MOLECULAR BASIS OF THE INHIBITION OF CYTOCHROME P450 2C8 (CYP2C8) BY GLUCURONIDE CONJUGATES

5.1 Introduction

As described in Section 1.3.2, accumulating evidence from *in vitro* and *in vivo* studies demonstrates that CYP2C8 has the capacity to catalyse the oxidative metabolism of a large number of drugs, non-drug xenobiotics and endogenous compounds (Backman et al. 2016). These include numerous drug glucuronide conjugates, for example clopidogrel acyl glucuronide (referred to subsequently as clopidogrel glucuronide), deleobuvir acyl glucuronide, desloratadine glucuronide, diclofenac acyl glucuronide (referred to subsequently as diclofenac glucuronide), estradiol 17- β -D glucuronide (referred to subsequently as estradiol glucuronide), gemfibrozil acyl glucuronide (referred to subsequently as gemfibrozil glucuronide), Lu AA34893 carbamoyl glucuronide, and sipoglitazar acyl glucuronide. In addition, and as discussed in Chapter 1 (Section 1.6.2), several drug glucuronide conjugates act as competitive or irreversible inhibitors of CYP2C8.

Gemfibrozil and clopidogrel are converted to their respective acyl glucuronides *in vivo* and it is the glucuronide conjugates that act as perpetrators of DDIs rather than the aglycones. In particular, the acyl glucuronides of gemfibrozil and clopidogrel are potent mechanism based inhibitors (MBIs) of CYP2C8 that cause long-lasting inhibition of the oxidative metabolism of CYP2C8 substrates (Ogilvie et al. 2006; Tornio et al. 2014). For example, co-administration of clopidogrel and repaglinide increases the area under the plasma concentration – time curve (AUC) of repaglinide approximately 5-fold (Tornio et al. 2014), while co-administration of gemfibrozil with

cerivastatin, dasabuvir, montelukast, pioglitazone or repaglinide results in 4- to 8-fold increases in the AUCs of the ‘victim’ drugs (Backman et al. 2016; Backman et al. 2002; Jaakkola et al. 2005; Karonen et al. 2010; Menon et al. 2015; Niemi et al. 2003; Tornio et al. 2014; Tornio et al. 2017). There is also evidence indicating that several other drugs (e.g. deleobuvir and Lu AA34893) are MBIs of CYP2C8 (Kazmi et al. 2010; Sane et al. 2016). The molecular basis of the MBI of CYP2C8 by gemfibrozil glucuronide has been characterised by Baer et al. (2009). Experimental and molecular modelling evidence suggests that the gemfibrozil moiety of the glucuronide conjugate aligns above the heme, leading to formation of a benzyl radical (from proton abstraction) which subsequently covalently binds at the γ -meso position of the heme (Figure 5.1). Radical formation appears to occur preferentially at the *ortho* (5') -methyl of gemfibrozil (Jenkins et al. 2011). The mechanism by which clopidogrel glucuronide irreversibly inhibits CYP2C8 has not been elucidated, but presumably arises from metabolic activation of the thiophene group of clopidogrel. Docking of clopidogrel glucuronide in the CYP2C8 X-ray crystal structure found the thiophene group binds approximately 5 Å from the heme iron (Tornio et al. 2014). As indicated above, it is noteworthy that, while the clopidogrel- and gemfibrozil-glucuronides are potent MBIs of CYP2C8, gemfibrozil and clopidogrel appear to be weak non-time dependent inhibitors (Jenkins et al. 2011; Tornio et al. 2014).

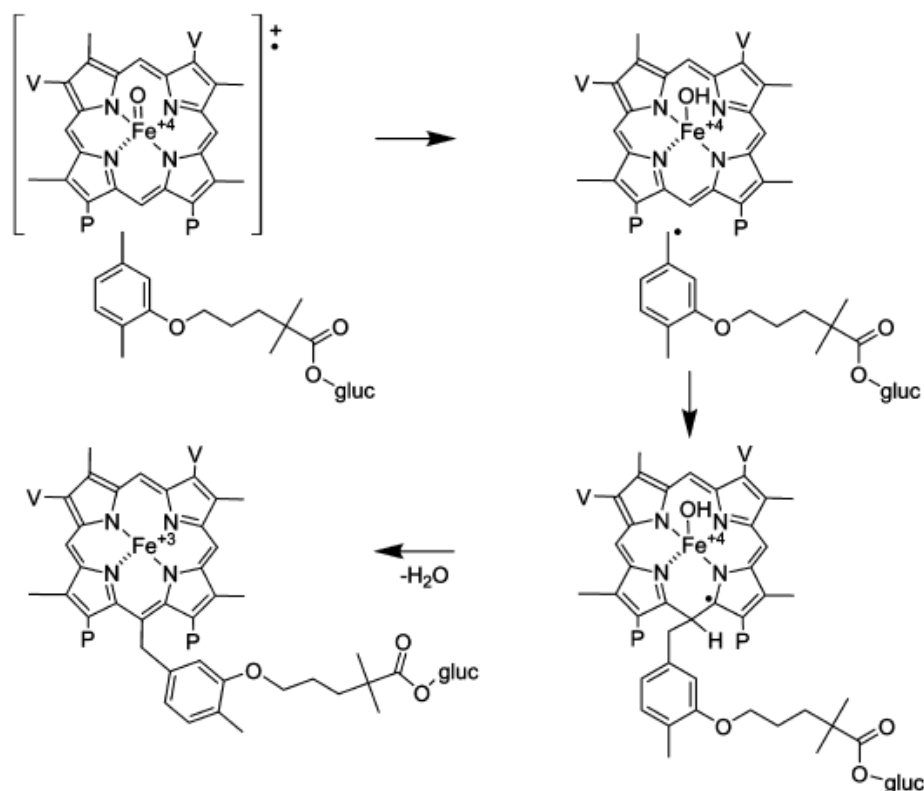


Figure 5.1 Proposed mechanism for the irreversible inhibition of CYP2C8 by gemfibrozil glucuronide.

Adapted with permission from Baer, BR, DeLisle, RK and Allen, A (2009), 'Benzylic oxidation of gemfibrozil-1-O-β-glucuronide by P450 2C8 leads to heme alkylation and irreversible inhibition', Chemical Research in Toxicology, 22 (7): 1298-1309. Copyright (2009) American Chemical Society.

The published X-ray crystal structures of CYP2C8 show a large, flexible active site (volume ~1,400 Å³) that is capable of binding large molecules (Schoch et al. 2008; Schoch et al. 2004). The active site cavity contains both hydrophobic and hydrophilic domains. In particular, there is a cluster of polar residues near the N-terminus of helix B', including Ser100, Ser103, Thr107 and Ser114 (all within SRS1), and Asn217 which is located just outside SRS2 in a sub-helix between helices F and G (Schoch et al. 2008). Molecular modelling suggests a role for this region in the binding of drug glucuronide conjugates. Docking of gemfibrozil glucuronide in the CYP2C8 active site identified potential hydrogen bonding interactions between the glucuronic acid

moiety and Ser103, Gln214 and Asn217 (Baer, DeLisle and Allen 2009; Jenkins et al. 2011). Asn99 and Ser100 were additionally identified as potential hydrogen bonding residues by Baer et al. and Jenkins et al., respectively. In a subsequent study, Tornio et al. (2014) reported docking of the gemfibrozil- and clopidogrel- glucuronides in the CYP2C8 active site. Potential hydrogen bonding interactions were observed between the glucuronic acid moiety of gemfibrozil glucuronide and Ser103, Ser114 and Asn204, and between the glucuronic acid moiety of clopidogrel glucuronide and Ser100 and Ser103 (Tornio et al. 2014).

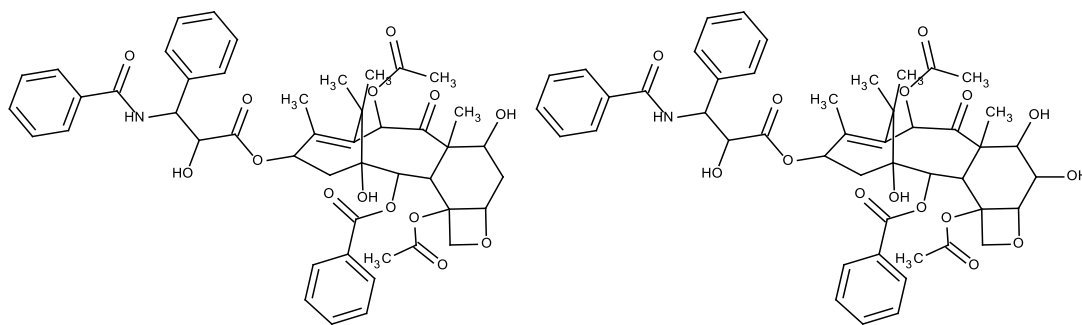
X-ray crystal structures of CYP2C8 have been published with bound montelukast and retinoic acid, which like glucuronic acid, both contain a carboxylic acid group (Schoch et al. 2008). Hydrogen bonding interactions were identified with Ser100 and Ser103. A second molecule of retinoic acid co-crystallised in the CYP2C8 active site also exhibited hydrogen bonding interactions with Gly98, Asn204 and Arg241. The X-ray crystallography and molecular modelling data further highlight the role of hydrophobic interactions in the binding of lipophilic compounds and the lipophilic aglycone of glucuronide conjugates. Although the importance of specific active site amino acids on the binding of glucuronide conjugates has not been confirmed by site-directed mutagenesis, a combination of kinetic, mutagenesis, and pharmacophore modelling approaches was used to assess the structural features of CYP2C8 that contribute to the binding of non-glucuronide containing substrates (Melet et al. 2004). A pharmacophore generated from eight substrates contained an anionic/polar group located ~13 Å from the site of oxidation. Consistent with the X-ray crystal structures and computational analyses discussed above, Ser100 and possibly Ser114 were identified as important residues for substrate binding.

Based on the data summarised above the hypothesis underpinning the studies outlined

in this Chapter is that hydrogen bonding interactions play a pivotal role in the binding and alignment of glucuronide conjugates in the CYP2C8 active site, thereby facilitating metabolism (e.g. hydroxylation) and/or metabolic activation (e.g. radical formation) of the aglycone. To test this hypothesis, specific amino acids that interact with the glucuronic acid moiety of three model glucuronide conjugates (*viz.* diclofenac-, gemfibrozil- and estradiol- glucuronide) were confirmed by molecular modelling and then mutated (by site-directed mutagenesis). The ability of each model glucuronide conjugate to inhibit paclitaxel (PAC) 6 α -hydroxylation by wild-type CYP2C8 and each mutant was then assessed under conditions that favour MBI, which manifests as non-time dependent inhibition.

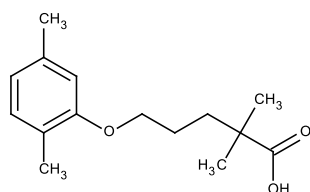
As indicated above, the three model glucuronides selected for investigation were diclofenac-, gemfibrozil-, and estradiol- glucuronide. The structures of the three glucuronide conjugates and their respective aglycones are shown in Figure 5.2, along with the structures of the CYP2C8 probe substrate PAC and its 6-hydroxy metabolite. Gemfibrozil glucuronide is considered the prototypic MBI of CYP2C8, and MBI has been characterised both *in vitro* and *in vivo* (Backman et al. 2016; Ogilvie et al. 2006). Diclofenac glucuronide was the first glucuronide conjugate shown to be metabolised by CYP2C8, forming 4'-hydroxydiclofenac acyl glucuronide (Kumar et al. 2002). This contrasts to the preferential formation of 4'-hydroxydiclofenac by CYP2C9, and CYP2C8-catalysed formation of the minor metabolite 5'-hydroxydiclofenac (Bort et al. 1999; Daly et al. 2007). Similarly, estradiol glucuronide is hydroxylated at the aromatic C-2 position by CYP2C8, forming 2-hydroxy-estradiol 17- β -D-glucuronide (Delaforge et al. 2005). In contrast to gemfibrozil glucuronide, diclofenac glucuronide has been reported to be a non-time dependent inhibitor of human liver microsomal CYP2C8 with an IC₅₀ of 14 μ M (Jenkins et al. 2011), while estradiol glucuronide

appears not to have been investigated as an inhibitor. Importantly, docking studies with all three glucuronide conjugates support the overall hypothesis and all are available commercially.

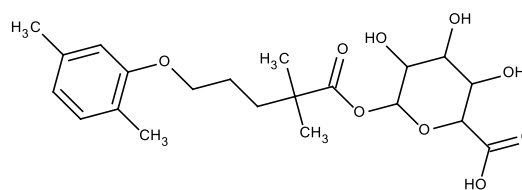


Paclitaxel

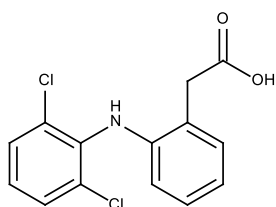
6 α -Hydroxy paclitaxel



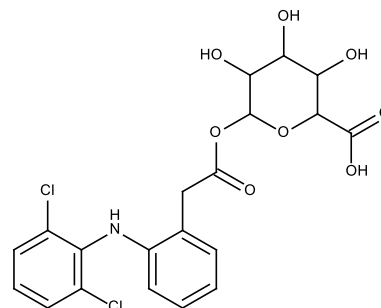
Gemfibrozil



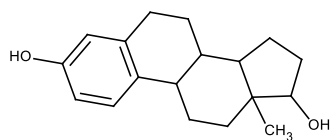
Gemfibrozil acyl glucuronide



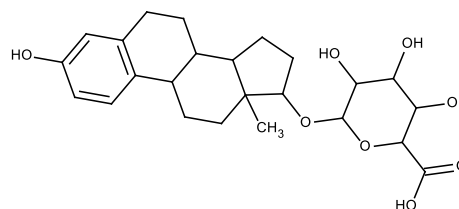
Diclofenac



Diclofenac acyl glucuronide



β -Estradiol



Estradiol 17- β -D-glucuronide

Figure 5.2 Chemical structures of paclitaxel (PAC), 6 α -hydroxy PAC, gemfibrozil, diclofenac, β -estradiol, gemfibrozil acyl glucuronide, diclofenac acyl glucuronide and estradiol 17- β -D-glucuronide.

5.2 Materials and Methods

5.2.1 Enzyme expression

Wild-type CYP2C8 and CYP2C8 mutants were co-expressed with CPR as described in Section 2.2.5. CYP2C8 mutants were generated by PCR according to the procedure given in Section 2.2.5.3. Fourteen mutants were generated based on *in silico* docking experiments (Section 5.3.1); 8 single, 2 double, 1 triple, 1 quadruple and 2 quintuple mutants. The wild-type CYP2C8 cDNA was used as the template for the single mutants whereas the multiple mutants were generated by sequential modification (i.e. single → double → triple, etc.). CYP and CPR contents were measured as described in Section 2.2.5.10. In addition, expression of CYP2C8 proteins was confirmed by western blotting (Section 2.2.5.11).

5.2.2 Kinetics of paclitaxel (PAC) 6 α -hydroxylation and time-dependent inhibition of CYP2C8 by glucuronides and aglycones

PAC 6 α -hydroxylation kinetic constants (K_m , V_{max} and Cl_{int}) were determined for wild-type CYP2C8 and each mutant according to the method given in Section 2.2.3.8. Incubations contained recombinant CYP2C8 protein (2 or 4 pmol CYP/200 μ l) and were performed for 15 min at 37°C. All incubations were conducted in triplicate and included at least 8 PAC concentrations that spanned the K_m for each CYP2C8 enzyme. IC_{50} values from experiments where the CYP2C8 enzyme was pre-incubated for 30 min at 37°C with and without NADPH prior to measuring inhibition of PAC 6 α -hydroxylation were determined for the gemfibrozil-, diclofenac- and estradiol glucuronides, and for gemfibrozil and diclofenac (Figure 5.2). It was not possible to determine an IC_{50} for 17 β -estradiol given the limited solubility of this compound.

Co-incubation inhibition experiments (i.e. without pre-incubation step) were additionally performed to provide insights into non-time dependent inhibition (Section

2.2.2.8).

It has been recommended by some authors that the so-called dilution method is preferable for MBI studies (Obach, Walsky and Venkatakrishnan 2007; Sekiguchi et al. 2009). In this approach, a high concentration of the enzyme source is pre-incubated with the inhibitor (\pm NADPH), and then samples are aliquoted from the pre-incubation mixture into separate incubation tubes for the measurement of residual enzyme activity using the probe substrate (PAC in the case of CYP2C8). With the alternative non-dilution method, each inhibition measurement is performed in a discrete incubation tube containing the exact amount of protein required for measurement of enzyme activity. The latter (non-dilution approach) was adopted here based on the recommendation of Parkinson et al. (2011). As indicated by these authors, the non-dilution method offers several advantages over the dilution method: it is technically easier; data processing is unambiguous; and inhibitor non-specific binding and depletion are minimised.

Gemfibrozil- and diclofenac- glucuronide stock solutions were prepared in acetonitrile containing dilute formic acid (0.1% v/v) to minimise hydrolysis on storage. All other inhibitors were prepared in DMSO. The final concentration of organic solvent in incubations did not exceed 0.5% (for DMSO) or 1% (for acetonitrile/0.1% formic acid). IC₅₀ values were determined using 6 inhibitor concentrations that spanned the following ranges: 1 – 1,000 μ M for gemfibrozil; 0.03 – 90 μ M for gemfibrozil glucuronide; 1 – 500 μ M for diclofenac; 0.3 – 100 μ M for diclofenac glucuronide; and 1 – 250 μ M for estradiol glucuronide. These ranges were optimised to provide 20 – 80% inhibition, wherever feasible. Montelukast (10 μ M), a known reversible inhibitor of CYP2C8, was used as a positive control in the inhibition studies.

5.2.3 Molecular docking

Docking conditions were essentially as described for a previous study from this laboratory (Lewis et al. 2016). Briefly, isomeric SMILES strings for diclofenac, diclofenac glucuronide, β -estradiol, estradiol glucuronide, gemfibrozil, gemfibrozil glucuronide and PAC were obtained from PubChem (<https://pubchem.ncbi.nlm.nih.gov>). Three dimensional structures were generated using OMEGA version 2.5.1.4 (Openeye Scientific Software, Inc), and ‘-maxconfs 1’, ‘buildff’ and ‘strictstereo’ parameters were input to SYBYL.mol2 files. Each structure was assessed for the correct atom typing and stereochemistry prior to the assignment of partial atomic charges for energy minimisation using the Tripos Force Field. A termination gradient of less than 0.05 kcal/(mol)(Å) was utilised to ensure that structures converged to a favourable energy.

The coordinates of the X-ray crystal structure of unliganded CYP2C8 (PDB code 1PQ2) were retrieved from the RCSB Protein Data Bank. Automated docking was performed using the Surflex-Dock GeomX docking suite of SYBYL-X (version 2.1.1). Automated docking of ligands was performed using a protomol generation threshold of 0.30 and bloat of 2 Å. A maximum of 40 conformations per fragment and 100 rotatable bonds was allowed for each ligand. Three hundred binding poses were generated for each ligand, with a RMSD between final poses of 0.50 Å. Poses were ranked based on their energy consensus scores (CScore; SYBYL-X 2.1.1). Residues within a 4 Å radius of each of the top 20 ranked poses were used to identify potential ligand binding interactions within the CYP2C8 active site.

5.2.4 Data analysis

K_m and V_{max} values for PAC 6 α -hydroxylation were generated with Enzfitter (version 2.0, Biosoft, Cambridge, UK) and expressed as the mean \pm SD of three replicates. All

kinetic data were well described by the Michaelis-Menten equation (equation 2.6, Section 2.3) and kinetic parameters are expressed as the mean \pm SD. Intrinsic clearance (Cl_{int}) was calculated as V_{max}/K_m . IC_{50} values were generated by fitting equation 2.9 (Section 2.3) to experimental data using GraphPad Software (version 7.01) (GraphPad Software, Inc, La Jolla, CA, USA). Experiments to determine IC_{50} values were performed in triplicate and data are expressed as the mean \pm SD. The statistical significance for the difference between the IC_{50} values for the wild-type and each mutant CYP2C8 enzyme was determined for each inhibitor (glucuronide conjugates and the respective aglycones) as described in Section 2.3. Values of k_{inact}/K_I for each inhibitor/enzyme pair were determined using equation 2.19 (Section 2.3), with $t = 30$ min (the pre-incubation time) and $K_m = [S]$ (Section 5.3.4). Here, k_{inact} is the maximal rate of enzyme inactivation and K_I is the inhibitor concentration that produces half k_{inact} .

5.3 RESULTS

5.3.1 *In silico* docking experiments: rationale for CYP2C8 mutant design

Diclofenac, diclofenac glucuronide, gemfibrozil, gemfibrozil glucuronide, β -estradiol, estradiol glucuronide and PAC were docked in the active site of CYP2C8 as described in Section 5.2.3. Amino acids located within 4 Å of the aglycone and glucuronic acid moieties are shown in Table 5.1. Consensus residues involved in binding of the glucuronide and aglycone (including PAC) moieties are highlighted in blue and red, respectively. Gly98, Asn99, Ser100, Ser103 and Ser114 are located within 4 Å of the glucuronide moieties of the diclofenac-, gemfibrozil- and β -estradiol- glucuronides, and potentially stabilise the binding of all three glucuronide conjugates by hydrogen bonding via the side-chain hydroxyl of Ser or nitrogen of Asn. Gly98 is additionally located within 4 Å of each glucuronide, but hydrogen bonding occurs between the Gly backbone nitrogen and an –OH group of the glucuronide moiety. Gln214 and Asn217 are both within 4 Å of the glucuronide moieties of diclofenac and estradiol, but not that of gemfibrozil. Conversely, Thr107 is located within 4 Å of the glucuronide moieties of diclofenac and gemfibrozil, but not that of estradiol. A limited number of non-polar amino acids (e.g. Ile) are additionally located within 4 Å of the glucuronide moiety. While these will clearly not be involved in hydrogen bonding interactions, they may contribute to orientating the glucuronide conjugate in a catalytically favourable orientation via steric effects. As would be expected, most amino acids located within 4 Å of the lipophilic aglycones (*viz.* diclofenac, gemfibrozil and β -estradiol) are hydrophobic. The distance of the site of oxidation on the aglycone moiety to the heme iron of each docked glucuronide conjugate ranged from 3.88 to 5.26 Å, which is within the optimal range for efficient metabolism.

Not surprisingly, many amino acids are located within 4 Å of the docked structure of

PAC, which is a large compound (Figure 5.2). While PAC overall is a lipophilic molecule, it also contains 13 hetero-atoms (N or O). The amino acids identified as being within 4 Å of PAC include both non-polar and polar residues that potentially contribute to binding by hydrophobic and hydrogen bonding interactions. The distance from the 6-position to the heme iron in the docked PAC structure is 6.79 Å which, while still favourable for metabolism, may explain the relatively low V_{\max} for PAC 6 α -hydroxylation (see Section 5.3.3). Notably, residues identified as being important for glucuronide binding (Gly98, Asn99, Ser100, Ser103, Thr107, Ser114, Gln214 and Asn217) are also located within 4 Å of PAC (Table 5.1).

Table 5.1 CYP2C8 residues within 4Å of the glucuronic acid and aglycone moieties of docked diclofenac acyl glucuronide, gemfibrozil acyl glucuronide, and estradiol 17- β -D-glucuronide.

Docked ligand	Residues within 4 Å	Distance from the heme iron to the site of metabolism (Å)
<i>Diclofenac acyl glucuronide:</i>		
Glucuronide moiety	Gly98, Asn99, Ser100, Ser103, Thr107, Ile113, Ser114, Ile213, Gln214, Asn217, Val366, Pro367	N/A
Diclofenac moiety	Phe205, Leu208, Asn209, Val296, Ala297, Glu300, Thr301, Leu361, Val362, Ile476, Val477	4.97 (4' position)
<i>Gemfibrozil acyl glucuronide:</i>		
Glucuronide moiety	Arg97, Gly98, Asn99, Ser100, Ile102, Ser103, Ile106, Thr107, Ile113, Ser114, Leu208, Asp293, Val296	N/A

Table 5.1 CYP2C8 residues within 4Å of the glucuronic acid and aglycone moieties of docked diclofenac acyl glucuronide, gemfibrozil acyl glucuronide, and estradiol 17-β-D-glucuronide (cont.).

Docked ligand	Residues within 4 Å	Distance from the heme iron to the site of metabolism (Å)
Gemfibrozil moiety	Ile113, Phe205 , Asp293, Val296 , Ala297 , Thr301, Leu361, Val362 , Val366, Val477	5.26 (5' position)
<i>Estradiol 17-β-D-glucuronide:</i>		
Glucuronide moiety	Gly98, Asn99 , Ser100 , Ser103 , Ser114 , Ile213, Gln214, Asn217, Phe367	N/A
Estradiol moiety	Ile113, Phe205 , Leu208, Val296 , Ala297 , Thr301, Val362 , Val366, Ile467, Val477	3.88 (2 position)
<i>Paclitaxel:</i>		
	Arg97, Gly98, Asn99 , Ser100 , Ile102, Ser103 , Ile106, Thr107, Ile113, Ser114 , Pro201, Asn204, Phe205 , Leu208, Asn209, Ile213, Gln214, Asn217, Asn218, Val237, Val296 , Ala297 , Val362 , Thr364, Gly365, Val366, Pro367, Thr386, Met388, Ile476, Val477	6.79 (6α position)

Blue: consensus residues involved in glucuronide binding.

Red: consensus residues involved in aglycone binding.

N/A: not applicable.

Six residues were identified for mutagenesis based on the results of the *in silico* docking experiments; Asn99, Ser100, Ser103, Thr107, Ser114 and Gln214. Potential hydrogen bonding interactions between the side-chains of each of these amino acids were variably observed with the diclofenac-, estradiol- and gemfibrozil glucuronides and it is hypothesised that these residues play a role in binding the glucuronide conjugates within the CYP2C8 active site in an orientation that is suitable for oxidation of the aglycone moiety. Asn99, Ser100, Ser103 and Ser114 were identified as potentially hydrogen bonding with all three glucuronides, whereas Thr107 was identified as a potential hydrogen bonding residue for diclofenac- and gemfibrozil-glucuronide. Since gemfibrozil glucuronide is a potent TDI of CYP2C8, mutagenesis of Thr107 was considered to be of interest. Docking experiments identified Gln214 and Asn217 as potential binding residues for the diclofenac- and estradiol glucuronides, but not gemfibrozil glucuronide. One of these, Gln214, was selected (pragmatically) for mutagenesis. Although Gly98 was identified to be within 4 Å of all three glucuronides, hydrogen bonding occurred with the backbone oxygen (as opposed to a side-chain) and hence this residue was not selected for mutagenesis. Figures 5.3 to 5.6 show the positions of Asn99, Ser100, Ser103, Thr107, Ser114 and Gln214 relative to the docked structures of diclofenac glucuronide, gemfibrozil glucuronide, estradiol glucuronide and PAC.

All six amino acids were individually substituted with Ala, which has a small non-polar (methyl group) side-chain (Figure 5.7). However, since Thr is a β -branched amino acid which impacts on secondary and tertiary protein structure this residue was also substituted with Val, which is a β -branched amino acid with a hydrophobic side-chain. Similarly, Gln (at position 214), which has a relatively large, polar side-chain, was also substituted with Leu (a non-polar amino acid with a similar volume to Gln).

In addition to the eight single mutants, two double (Ser100Ala-Ser103Ala and Ser103Ala-Thr107Val), one triple (Ser100Ala-Ser103Ala-Thr107Val), one quadruple (Ser100Ala-Ser103Ala-Thr107Val-Ser114Ala), and two quintuple (Ser100Ala-Ser103Ala-Thr107Val-Ser114Ala-Gln214Ala and Ser100Ala-Ser103Ala-Thr107Val-Ser114Ala-Gln214Leu) mutants were generated to ascertain the extent to which interactions with Ser100, Ser103, Thr107, Ser114 and Gln214 might have an additive effect on glucuronide conjugate binding.

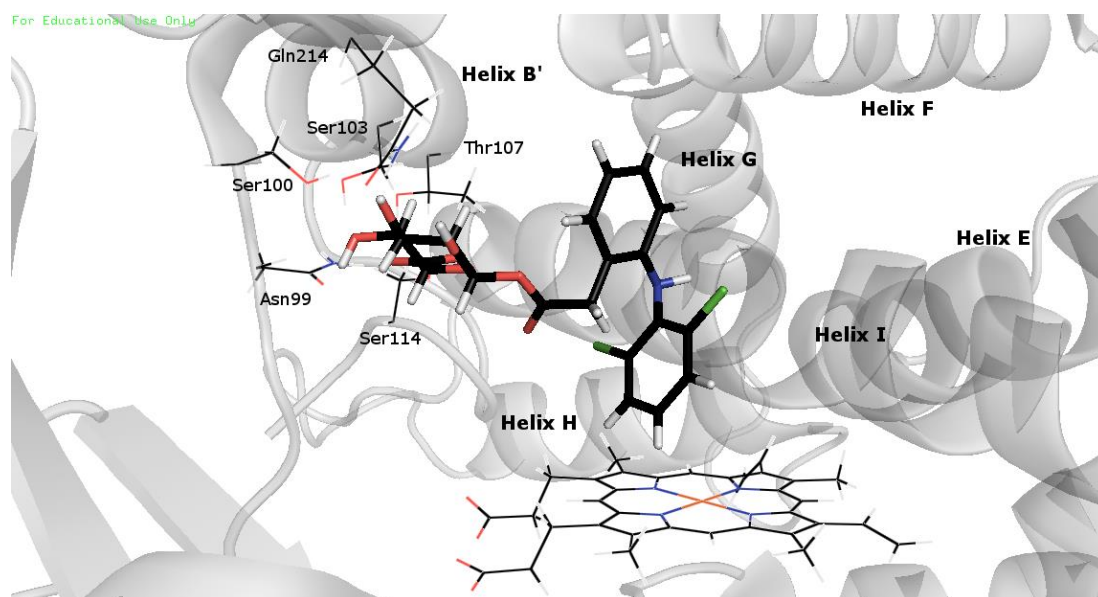


Figure 5.3 Diclofenac acyl glucuronide docked in the active site of CYP2C8.

Orthogonal image of diclofenac glucuronide docked in the active site of CYP2C8, showing the relative positions of the side-chains of the amino acids selected for site-directed mutagenesis. The heme moiety is positioned bottom right of centre. C, N and O atoms are coloured black, blue and red, respectively.

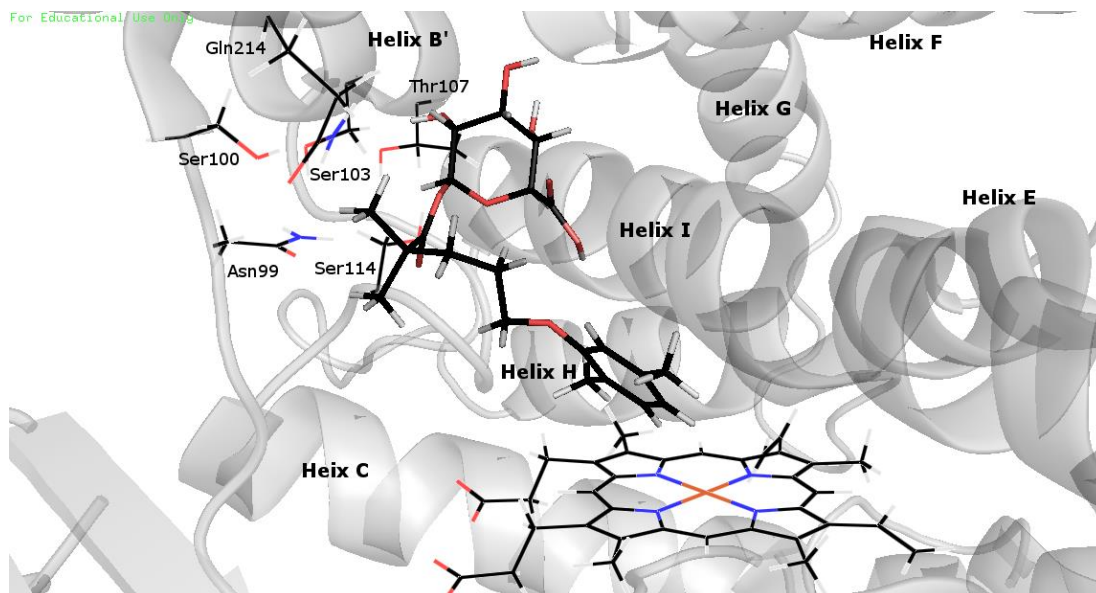


Figure 5.4 Gemfibrozil acyl glucuronide docked in the active site of CYP2C8.

Orthogonal image of gemfibrozil glucuronide docked in the active site of CYP2C8, showing the relative positions of the side-chains of the amino acids selected for site-directed mutagenesis. The heme moiety is positioned bottom right of centre. C, N and O atoms are coloured black, blue and red, respectively.

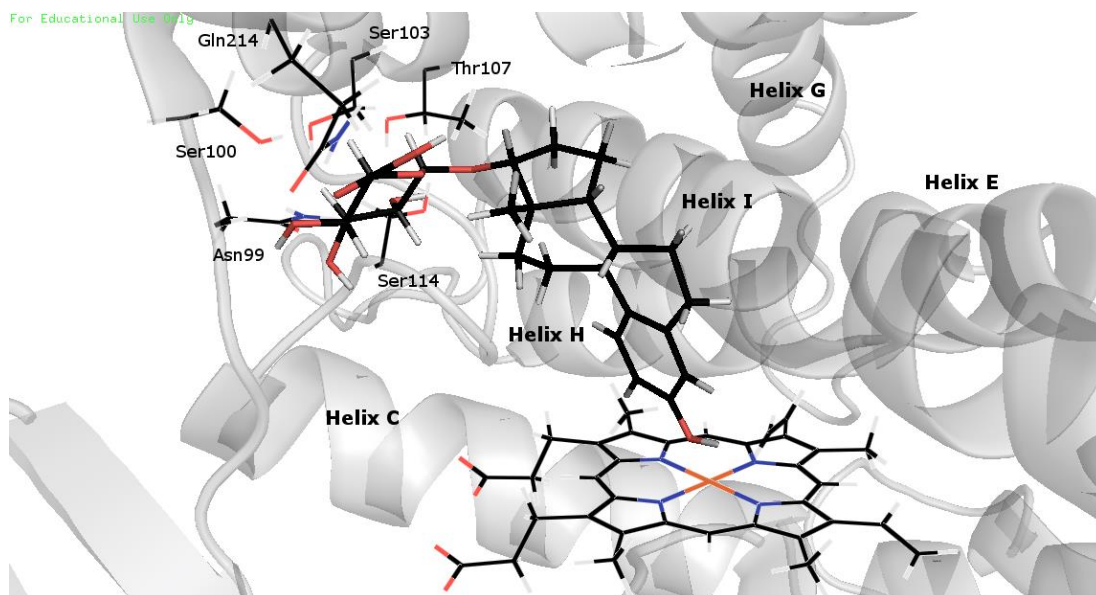


Figure 5.5 Estradiol 17-β-D-glucuronide docked in the active site of CYP2C8.

Orthogonal image of estradiol glucuronide docked in the active site of CYP2C8, showing the relative positions of the side-chains of the amino acids selected for site-directed mutagenesis. The heme moiety is positioned bottom right of centre. C, N and O atoms are coloured black, blue and red, respectively.

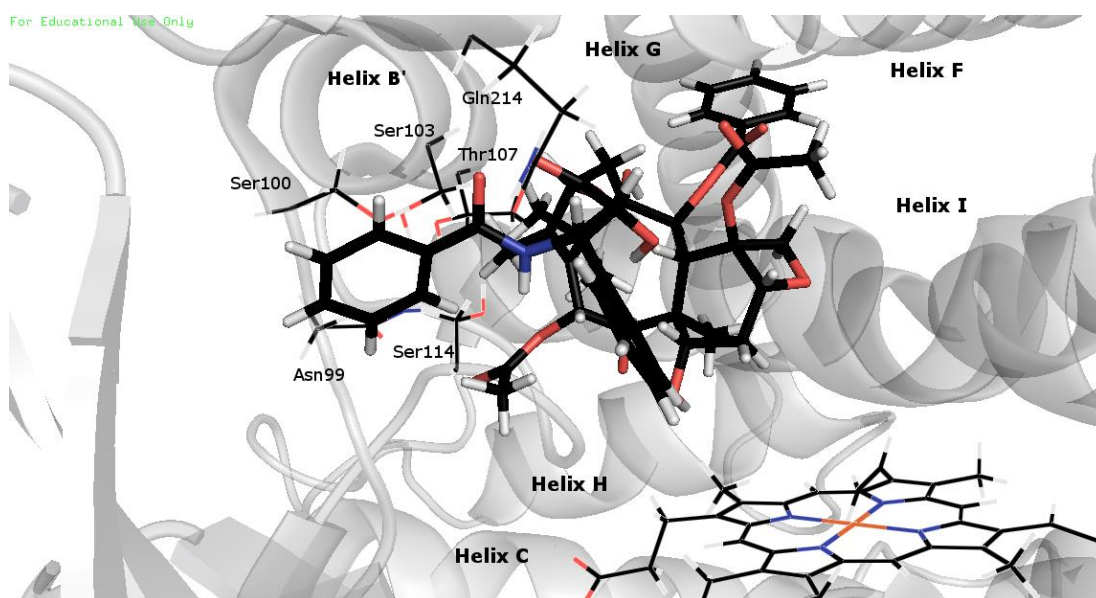
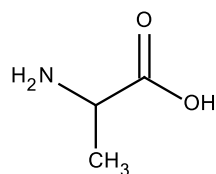
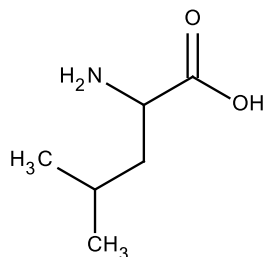


Figure 5.6 Paclitaxel docked in the active site of CYP2C8.

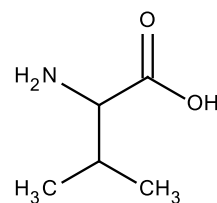
Orthogonal image of paclitaxel docked in the active site of CYP2C8, showing the relative positions of the side-chains of the amino acids selected for site-directed mutagenesis. The heme moiety is positioned bottom right of centre. C, N and O atoms are coloured black, blue and red, respectively.



Alanine

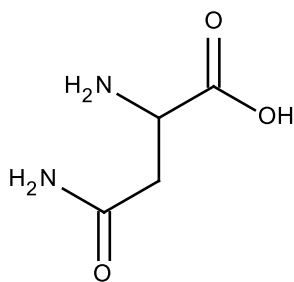


Leucine

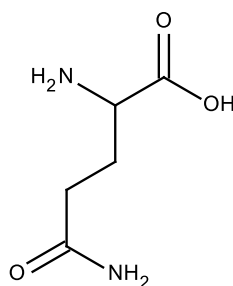


Valine

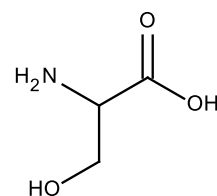
Hydrophobic side chain



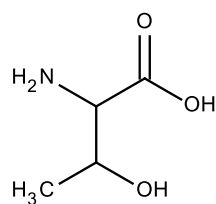
Asparagine



Glutamine



Serine



Threonine

Polar, uncharged side chain

Figure 5.7 Chemical structures of amino acids relevant to site-directed mutagenesis.

5.3.2 Expression of cytochrome P450 (CYP) 2C8 and cytochrome P450 oxidoreductase (CPR) in *E. coli* DH5 α cells.

Functional CYP and CPR contents of *E. coli* membrane fractions expressing the wild-type and mutant CYP2C8 proteins are shown in Table 5.2. Western blots and relative protein expression levels of CYP2C8 mutants are presented in Figure 5.8 and Table 5.2, respectively. Based on spectral P450 content, most of the single and double mutants expressed well (Table 5.2). CYP contents of the single and double mutants, determined as nmol P450/l of culture, ranged from 23% to 77% of the wild-type content. Of the single and double mutants, lowest P450 content was observed for the mutants generated at position 107. CYP contents of the triple, quadruple and quintuple mutants were lower still; 5% to 13% of wild-type. The presence of non-functional CYP protein, assessed visually from absorption at 420 nm in the CO absorbance spectra, was observable for Thr107Ala, Thr107Val (both minor) and the multiple mutants. The intensity of the peak at 420 nm observed with the multiple mutants tended to increase as the intensity of the peak at 450 nm decreased. However, the detection software did not quantify absorbance at 420 nm, and quantitative data are not available. Variation in CPR expression was lower than for CYP content (Table 5.2). CPR contents ranged from 296 to 599 nmol/l of culture, although most were in the range 513 to 599 nmol/l of culture. Despite the variability, CYP to CPR ratios for wild-type CYP2C8 and most single and double mutants were approximately 1:1, which is consistent with previous studies in this laboratory involving CYP2C8 and CYP2C9 expression in *E. coli* (Boye et al. 2004; Kerdpin et al. 2004; Polasek et al. 2004). Given the lower CYP expression levels of the Thr107Ala and Thr107Val mutants, CYP:CPR ratios were similarly lower; approximately 1:2 and 1:3, respectively. Since the mutants with more than two substitutions expressed with even lower CYP levels, but 'normal' CPR contents (510 to 555 nmol/l of culture), the CYP:CPR ratios for these mutants were higher, ranging

from 1:5.26 to 1:13.5.

Generally consistent with expression data based on CYP (spectral P450) content, the mean relative expression of immunoreactive CYP2C8 protein was lower for all of the single mutants compared to the wild-type protein (Figure 5.8 and Table 5.3), although there was not a direct relationship between spectral P450 content and relative protein expression. Interestingly, protein expression of all of the multiple mutants except Ser100Ala-Ser103Ala was similar to or higher than that of wild-type CYP2C8. Taken together, the expression data and subsequent activity results indicate instability of the triple, quadruple and quintuple mutants.

Table 5.2 Cytochrome P450 and NADPH cytochrome P450 oxidoreductase (CPR) contents of CYP2C8 proteins co-expressed with CPR in *E. coli*.

CYP2C8 protein	CYP (nmol/l of culture)	CPR (nmol/l of culture)	CYP : CPR ratio
Wild-type	791 ± 5.2	599 ± 9.8	1 : 0.76
N99A	308 ± 3.0	368 ± 6.5	1 : 1.20
S100A	470 ± 7.2	519 ± 3.6	1 : 1.10
S103A	525 ± 6.2	517 ± 11.3	1 : 0.99
T107A	285 ± 0.57	567 ± 17.1	1 : 1.99
T107V	179 ± 2.3	578 ± 16.8	1 : 3.22
S114A	607 ± 0.49	513 ± 8.8	1 : 0.85
Q214A	491 ± 15.4	406 ± 2.0	1 : 0.83
Q214L	301 ± 8.8	539 ± 19.6	1 : 1.79
S100A-S103A	454 ± 21.1	425 ± 9.5	1 : 0.93
S103A-T107V	385 ± 21.1	296 ± 8.3	1 : 0.77
S100A-S103A-T107V	105 ± 3.2	555 ± 41.4	1 : 5.26
S100A-S103A-T107V-S114A	91 ± 0.99	516 ± 6.8	1 : 5.70
S100A-S103A-T107V-S114A-Q214A	51 ± 0.42	510 ± 30.6	1 : 9.93
S100A-S103A-T107V-S114A-Q214L	38 ± 3.8	520 ± 50.9	1 : 13.5
Average	-	495 ± 84.3	-

Abbreviations: A, Ala; L, Leu; N, Asn; Q, Gln; S, Ser; T, Thr; V, Val.

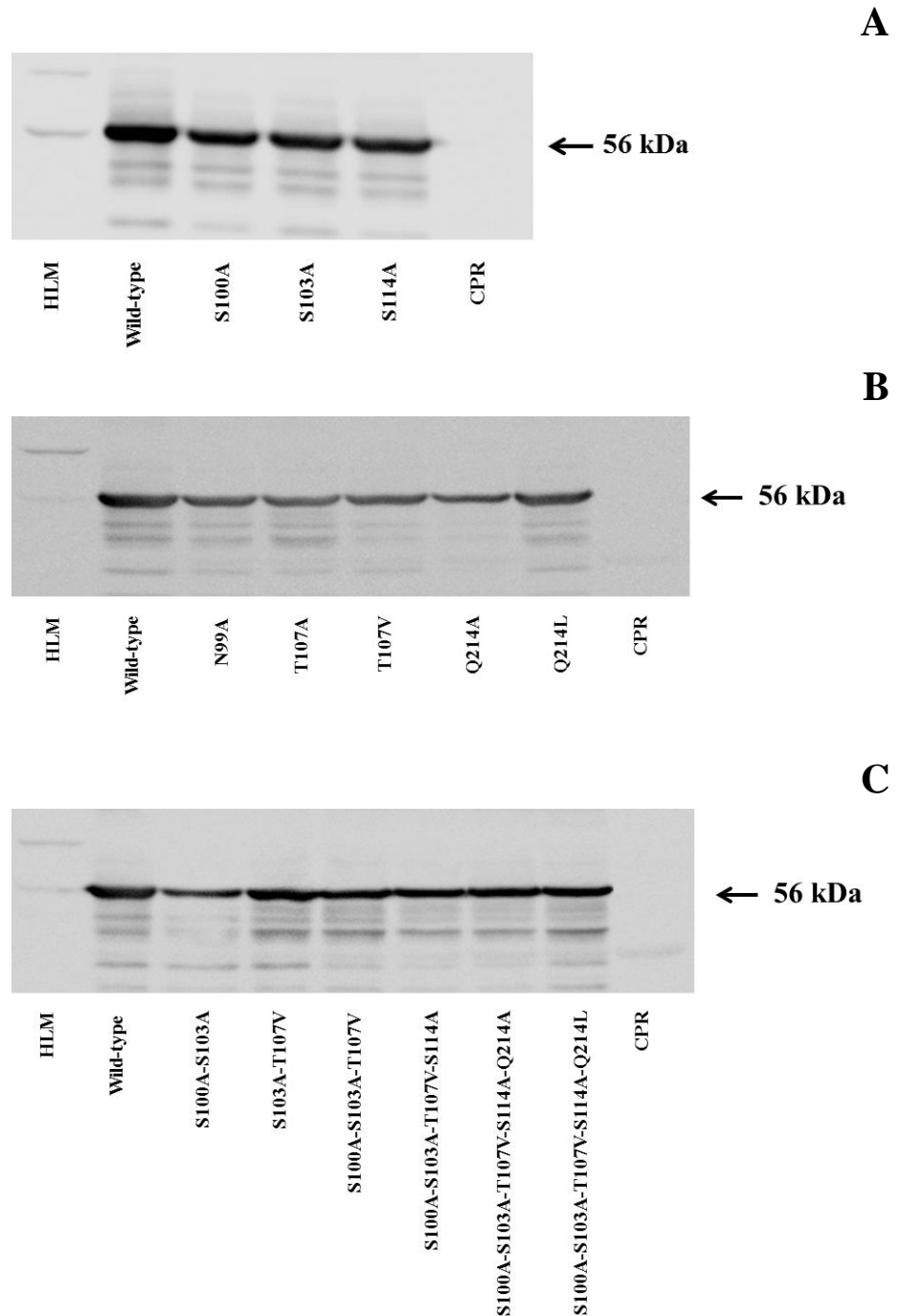


Figure 5.8 Western blots for wild-type and mutant CYP2C8 proteins.

HLM (positive control), wild-type, *S100A*, *S103A*, *S114A*, *CPR* (negative control) (Panel A), *HLM* (positive control), *N99A*, *T107A*, *T107V*, *Q214A*, *Q214L*, *CPR* (negative control) (Panel B) and *HLM* (positive control), *S100A-S103A*, *S103A-T107V*, *S100A-S103A-T107V*, *S100A-S103A-T107V-S114A*, *S100A-S103A-T107V-S114A-Q214A*, *S100A-S103A-T107V-S114A-Q214L*, *CPR* (negative control) (Panel C).

Abbreviations: A, Ala; L, Leu; N, Asn; Q, Gln; S, Ser; T, Thr; V, Val.

Table 5.3 Expression levels of wild-type cytochrome P450 2C8 and mutants from western blotting.

CYP2C8 protein	Mean relative intensity (compared to wild-type CYP2C8)
N99A	0.53
S100A	0.65
S103A	0.67
T107A	0.60
T107V	0.63
S114A	0.55
Q214A	0.57
Q214L	0.81
S100A-S103A	0.70
S103A-T107V	1.39
S100A-S103A-T107V	1.20
S100A-S103A-T107V-S114A	1.01
S100A-S103A-T107V-S114A-Q214A	1.11
S100A-S103A-T107V-S114A-Q214L	1.21

Abbreviations: A, Ala; L, Leu; N, Asn; Q, Gln; S, Ser; T, Thr; V, Val.

5.3.3 Kinetics of paclitaxel 6 α -hydroxylation

As indicated in Chapter 1 (Section 1.3.2), PAC 6 α -hydroxylation is catalysed predominantly by CYP2C8 and PAC is used widely as the ‘probe’ substrate for measurement of CYP2C8 activity *in vitro*. In order to optimise the reaction conditions for subsequent inhibition experiments (which utilised PAC as the probe substrate), PAC 6 α -hydroxylation kinetics were characterised for wild-type CYP2C8 and each mutant. Derived kinetic parameters are presented in Table 5.4, and velocity vs. substrate concentration and Eadie-Hofstee plots in Figure 5.9. It should be noted that activities (and hence V_{\max} and Cl_{int} values) are normalised for CYP expression (i.e. pmol/min.pmol CYP). V_{\max} is therefore equivalent to k_{cat} (i.e. turnover).

K_m , V_{\max} and Cl_{int} values for PAC 6 α -hydroxylation by wild-type CYP2C8 are similar to those reported previously by this laboratory (Kerdpin et al. 2004; Polasek et al. 2004). All mutants had readily measurable PAC 6 α -hydroxylation activities. K_m values for the Asn99Ala, Ser103Ala and Gln214Leu mutants did not differ significantly from that of the wild-type enzyme. With the exception of the Ser114Ala and Gln214Ala mutants (respective K_m values approximately 65% and 40% that of wild-type), K_m values for the remaining mutants were 1.7- to 4.3-fold higher than the K_m for wild-type CYP2C8. A relatively wide range (6-fold) of V_{\max} values was also evident. When considered as catalytic efficiencies, all mutants except Asn99Ala had significantly lower Cl_{int} values than wild-type CYP2C8 (Figure 5.10). However, with the exception of Thr107Ala, Cl_{int} values for the single mutants were generally no more than 50% lower than that of wild-type. Ser103Ala-Thr107Val and the triple, quadruple and quintuple mutants exhibited the lowest catalytic efficiencies.

Table 5.4 Derived kinetic constants for PAC 6 α -hydroxylation by recombinant wild-type CYP2C8 and CYP2C8 mutants.

CYP2C8	Kinetic parameters		
	K_m (μ M)	V_{max} (pmol/min.pmol CYP)	Cl_{int} (μ l/min.pmol CYP)
Wild-type	1.55 \pm 0.05	2.70 \pm 0.06	1.74 \pm 0.06
N99A	1.55 \pm 0.11	2.66 \pm 0.12	1.72 \pm 0.14
S100A	4.18 \pm 0.41*	3.38 \pm 0.24	0.81 \pm 0.02*
S103A	1.76 \pm 0.09	1.94 \pm 0.10*	1.10 \pm 0.01*
T107A	6.10 \pm 0.62*	3.80 \pm 0.24*	0.62 \pm 0.03*
T107V	3.40 \pm 0.17*	4.47 \pm 0.15*	1.31 \pm 0.03*
S114A	1.00 \pm 0.04*	1.31 \pm 0.03*	1.31 \pm 0.03*
Q214A	0.66 \pm 0.02*	0.92 \pm 0.02*	1.39 \pm 0.05*
Q214L	1.55 \pm 0.07	1.42 \pm 0.08*	0.91 \pm 0.02*
S100A-S103A	2.70 \pm 0.09*	2.09 \pm 0.02*	0.77 \pm 0.02*
S103A-T107V	4.78 \pm 0.24*	1.04 \pm 0.05*	0.22 \pm 0.01*
S100A-S103A-T107V	6.69 \pm 0.08*	2.69 \pm 0.06	0.40 \pm 0.01*
S100A-S103A-T107V- S114A	5.82 \pm 0.12*	2.68 \pm 0.14	0.46 \pm 0.01*
S100A-S103A-T107V- S114A-Q214A	2.68 \pm 0.03*	0.75 \pm 0.02*	0.28 \pm 0.01*
S100A-S103A-T107V- S114A-Q214L	5.72 \pm 0.58*	1.78 \pm 0.15*	0.31 \pm 0.01*

Abbreviations: A, Ala; L, Leu; N, Asn; Q, Gln; S, Ser; T, Thr; V, Val.

Experiments were performed in triplicate and data are shown as the mean \pm SD.

*Statistically significantly different ($p < 0.05$) compared to corresponding parameter for wild-type CYP2C8.

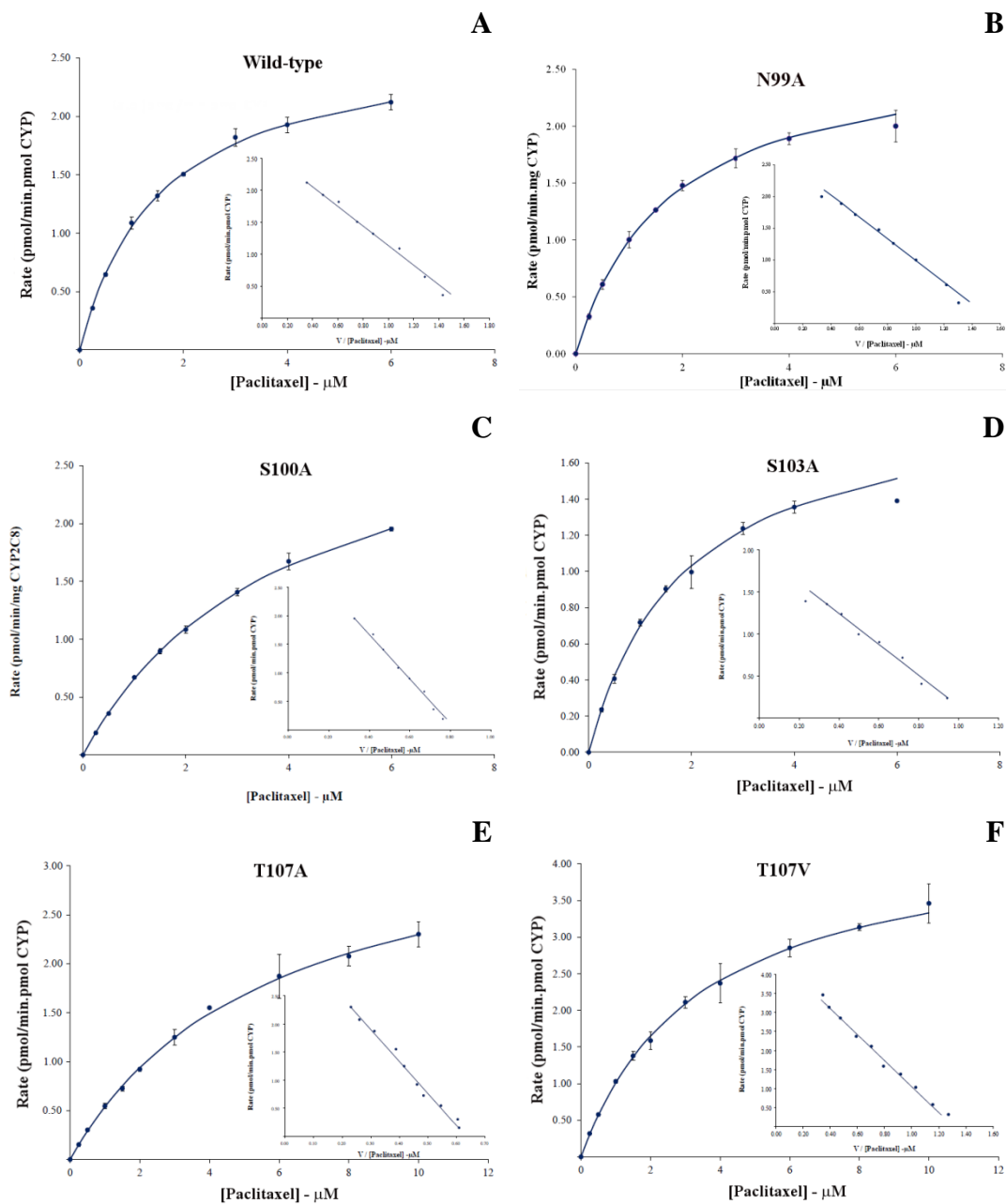


Figure 5.9 Rate vs. substrate concentration plots and Eadie-Hofstee (inset) plots for paclitaxel 6 α -hydroxylation formation by recombinant wild-type and mutant CYP2C8 enzymes.

Points and error bars represent the mean \pm SD of triplicate measurements at each substrate concentration.

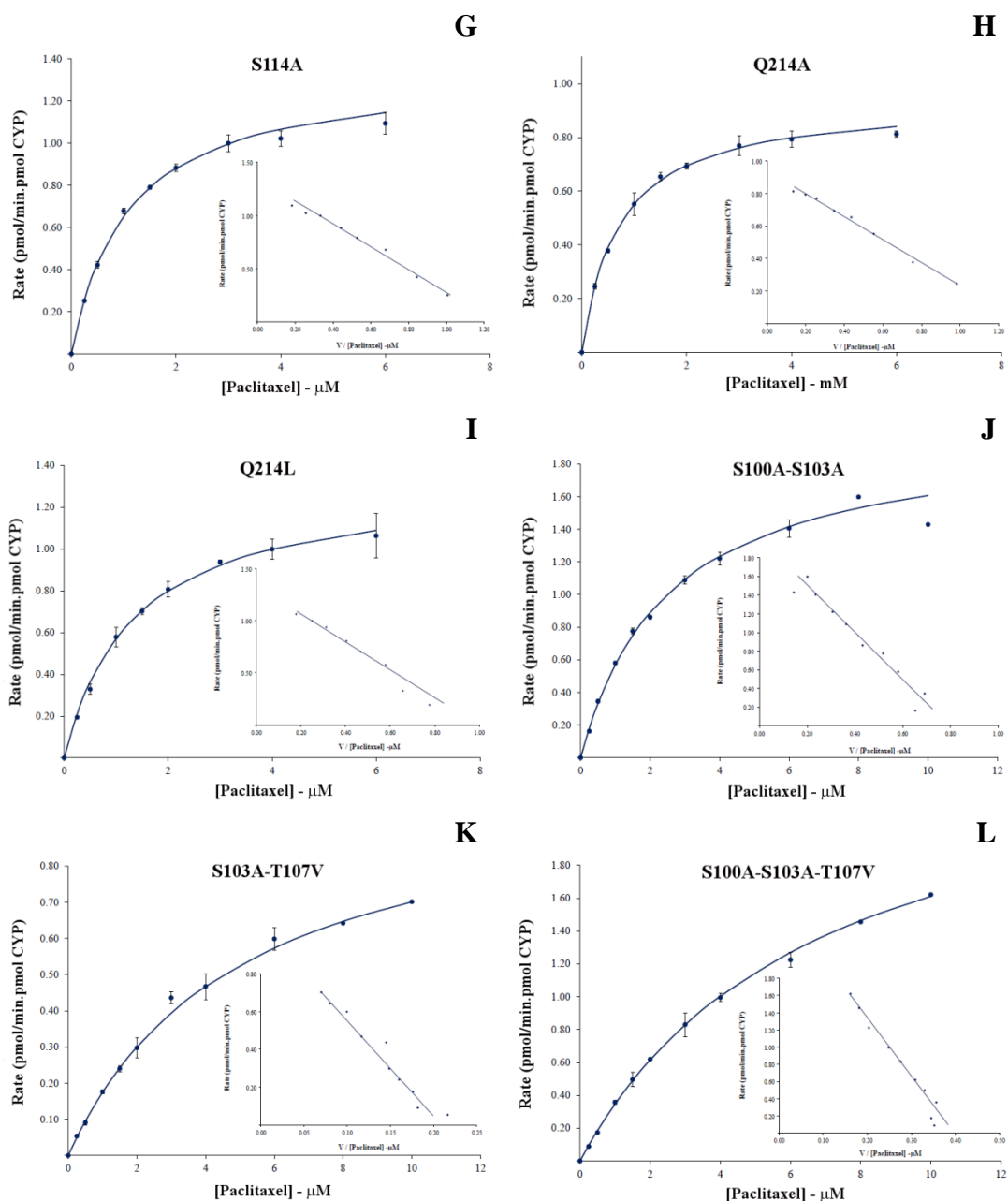


Figure 5.9 Rate vs. substrate concentration plots and Eadie-Hofstee (inset) plots for paclitaxel 6 α -hydroxylation formation by recombinant wild-type and mutant CYP2C8 enzymes (cont.).

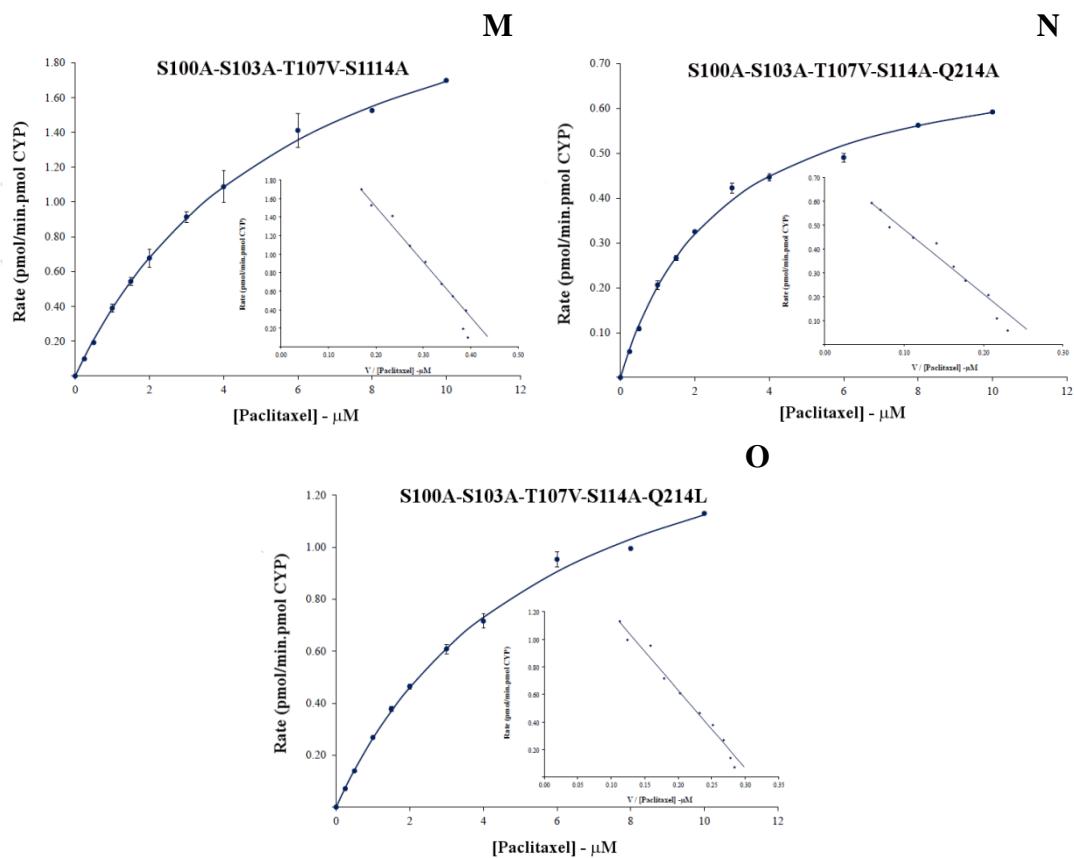


Figure 5.9 Rate vs. substrate concentration plots and Eadie-Hofstee (inset) plots for paclitaxel 6 α -hydroxylation formation by recombinant wild-type and mutant CYP2C8 enzymes (cont.).

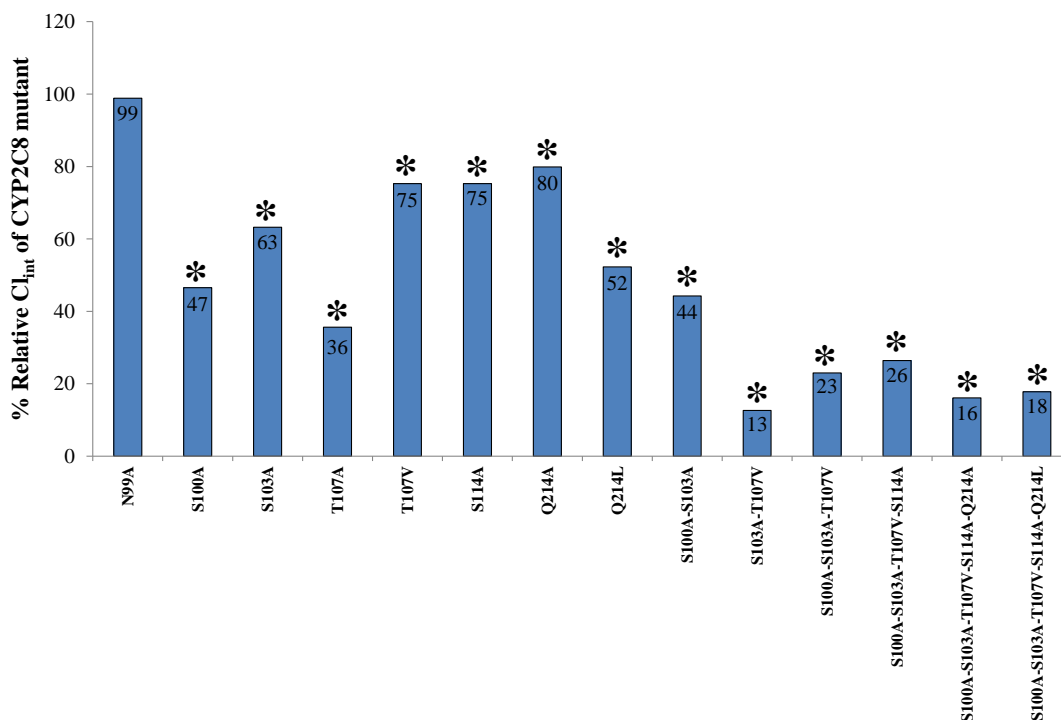


Figure 5.10 Mean relative Cl_{int} values of the CYP2C8 mutants (normalised to wild-type CYP2C8).

Abbreviations: A, Ala; L, Leu; N, Asn; Q, Gln; S, Ser; T, Thr; V, Val.

5.3.4 Inhibition of wild-type and mutant CYP2C8 enzyme activities by gemfibrozil, gemfibrozil acyl glucuronide, diclofenac, diclofenac acyl glucuronide and estradiol 17- β -D-glucuronide.

Inhibition of wild-type CYP2C8 and each mutant by gemfibrozil, gemfibrozil glucuronide, diclofenac, diclofenac glucuronide and estradiol glucuronide was characterised with PAC as the probe substrate. Inhibition was measured as the IC_{50} . As noted previously, the limited solubility of β -estradiol precluded measurement of an IC_{50} value. Co-incubation experiments, where the inhibitor and PAC are incubated without prior incubation of the enzyme source and inhibitor, were performed to assess non-time dependent inhibition (presumably competitive), although there will undoubtedly be a contribution of time-dependent inhibition (TDI) (where this occurs) during the 15 min co-incubation period. To measure TDI, each recombinant CYP2C8 enzyme was pre-incubated for 30 min with an inhibitor in the absence and presence of

NADPH (1 mM final concentration) prior to addition of PAC. TDI will result in loss of enzyme activity when a mechanism-based inhibitor is pre-incubated in the presence of NADPH, but not in the absence of NADPH. Inhibition is time-dependent because loss of enzyme activity is a function of pre-incubation time. Where MBI occurs, there will be a shift in the IC_{50} curve (the 'shifted' IC_{50}) to the left producing an increase in the IC_{50} ratio. Six inhibitor concentrations were employed to produce at least 20 to 80% inhibition, wherever possible. Inhibition experiments were performed at a PAC concentration corresponding to its K_m for each individual enzyme, as recommended in the literature (Obach, Walsky and Venkatakrishnan 2007; Parkinson et al. 2011; Perloff et al. 2009). The cut-off value for TDI was arbitrarily taken as an IC_{50} ratio greater than 2 (see Discussion section). The k_{inact}/K_I ratio was calculated from the shifted IC_{50} for each inhibitor/CYP2C8 enzyme pair using equation 2.19. This TDI metric is analogous to the Cl_{int} (V_{max}/K_m) as a measure of catalytic efficiency. A higher value of k_{inact}/K_I indicates greater enzyme inactivation, due to a higher k_{inact} and/or lower K_I . As described subsequently in the Discussion section, the k_{inact}/K_I ratio (determined from the shifted IC_{50}) provides a better measure of inactivation efficiency than the IC_{50} ratio.

Initial experiments were performed to assess the stability of wild-type CYP2C8 and each mutant when pre-incubated for 30 min at 37°C in either phosphate buffer (0.1 M, pH 7.4) alone or phosphate buffer containing NADPH (1 mM final concentration). As observed in previous studies in this laboratory (Polasek et al. 2004), the activity of wild-type CYP2C8 declined by approximately 50% when pre-incubated in the presence of NADPH. Similar loss of activity was observed for all of the single mutants, except Asn99Ala and Thr107Ala which lost approximately 80 - 90% of PAC 6 α -hydroxylation activity after pre-incubation in the presence of NADPH. Pre-incubation

in the presence of NADPH also resulted in > 80% loss of enzyme activity for all multiple mutants. Somewhat surprisingly, there was also some loss of activity (up to 30%) when the wild-type and mutant CYP2C8 enzymes were pre-incubated in phosphate buffer alone. As a result of these observations, IC₅₀ shift experiments were performed only with wild-type CYP2C8 and the Ser100Ala, Ser103Ala, Thr107Val, Ser114Ala, Gln214Ala and Gln214Leu mutants.

Gemfibrozil glucuronide. Significant changes in the co-incubation IC₅₀ compared to wild-type CYP2C8 were observed for all single mutants except Ser100Ala, Ser103Ala and Gln214Ala, and for all multiple mutants except Ser100Ala-Ser103Ala (Table 5.5). However, among the single mutants co-incubation IC₅₀ values differed by more than 50% (relative to wild-type CYP2C8) only for Asn99Ala and Thr107Val. The IC₅₀ values for the Asn99Ala and Thr107Val mutants were 2.2-fold higher and 82% lower, respectively, compared to the IC₅₀ for wild-type CYP2C8. Co-incubation IC₅₀ values tended to increase with increasing number of mutations, especially the quadruple and quintuple mutants. The IC₅₀ ratios, determined from pre-incubation experiments, were consistent with TDI (i.e. IC₅₀ ratio > 2). The IC₅₀ ratio for inhibition of wild-type CYP2C8 by gemfibrozil glucuronide was 15, which is similar to the IC₅₀ ratio (*ca.* 13) reported for inhibition of human liver microsomal CYP2C8 (Jenkins et al. 2011; Ogilvie et al. 2006) (Table 5.5). The IC₅₀ ratios for gemfibrozil glucuronide inhibition of the Ser100Ala, Thr107Val and Ser114Ala mutants were significantly lower than the IC₅₀ ratio of the wild-type enzyme, but still consistent with TDI. Interestingly, except for the Thr107Val mutant, variability in the IC₅₀ ratio was associated more with variability in the IC₅₀ values generated from experiments where pre-incubations were performed without added NADPH (Table 5.5). As shown in Table 5.5, except for Thr107Val, IC₅₀ values from experiments where pre-incubations were performed in

the presence of NADPH spanned a narrow range (0.25 to 0.33 μM). As a result, the $k_{\text{inact}}/K_{\text{I}}$ ratios for wild-type CYP2C8 and the Ser100Ala, Ser103Ala, Ser114Ala, Gln214Ala and Gln214Leu mutants similarly spanned a narrow range (141 – 189 $\text{ml}/\mu\text{mol}\cdot\text{min}$), whereas that for the Thr107Val mutant was significantly higher (773 $\text{ml}/\mu\text{mol}\cdot\text{min}$). The latter result arose from a large effect of the Thr107Val mutation on the pre-incubation ($\pm\text{NADPH}$) IC_{50} values (Table 5.5). It should be noted that the lower IC_{50} observed for the pre-incubation experiment in the absence of NADPH is consistent with lower IC_{50} measured in the co-incubation experiment (Table 5.5).

Gemfibrozil. In contrast to gemfibrozil glucuronide, gemfibrozil itself was a relatively weak inhibitor of wild-type and the CYP2C8 mutants (Table 5.6). IC_{50} values from co-incubation experiments were an order of magnitude higher than those for gemfibrozil glucuronide. The co-incubation IC_{50} values for the Ser100Ala, Ser103Ala, Thr107Ala, Gln214Ala, Gln214Leu and all multiple mutants were significantly higher than those for wild-type CYP2C8. Although the highest co-incubation IC_{50} was observed for the Ser100Ala-Ser103Ala-Thr107Val-Ser114Ala-Gln214Leu mutant, IC_{50} values tended not to increase with increasing number of mutations. IC_{50} ratios from pre-incubation experiments with all enzymes were < 2 , inconsistent with TDI. This result is in agreement with previous reports of the effect of gemfibrozil on human liver microsomal CYP2C8 activity (Jenkins et al. 2011; Ogilvie et al. 2006). While $k_{\text{inact}}/K_{\text{I}}$ ratios are shown in Table 5.6 for completeness, these values are of little meaning given the absence of TDI. Of note, the IC_{50} values for the co-incubation and pre-incubation ($-\text{NADPH}$) inhibition experiments for each enzyme were generally close in value for both gemfibrozil glucuronide and gemfibrozil, suggesting both approaches reflect non-TDI but almost certainly with an added element of irreversible inhibition occurring during the course of the incubation in the case of gemfibrozil glucuronide.

Diclofenac glucuronide. The co-incubation IC_{50} for diclofenac glucuronide inhibition of wild-type CYP2C8 (4.32 μ M) was similar to that for gemfibrozil glucuronide (3.50 μ M) (Table 5.7, cf. Table 5.5). All single mutations except Ser100Ala and Thr107Val significantly affected the co-incubation IC_{50} . However, except for Thr107Ala and Gln214Leu, co-incubation IC_{50} values were within $\pm 50\%$ of the wild-type value. As observed for gemfibrozil glucuronide, the IC_{50} tended to increase with increasing number of mutations (Table 5.7). Trends in the effects of the mutations at position 107 warrant comment. Whereas the Thr107Ala mutation had no significant effect on co-incubation IC_{50} of gemfibrozil glucuronide (Table 5.5), this mutation resulted in an almost 7-fold increase in the co-incubation IC_{50} of diclofenac glucuronide (Table 5.7). Conversely, while the Thr107Val mutation caused an 81% reduction in the co-incubation IC_{50} of gemfibrozil glucuronide, it had no significant effect on the co-incubation IC_{50} of diclofenac glucuronide. Based on an IC_{50} ratio cut-off value of 2 for TDI, diclofenac glucuronide is classified as a weak TDI of wild-type CYP2C8. All single mutations significantly reduced the IC_{50} ratios for diclofenac acyl glucuronide inhibition (Table 5.7). When data are considered as k_{inact}/K_I , a reduction was apparent with all mutants.

Diclofenac. As with gemfibrozil, diclofenac was a less potent inhibitor of the CYP2C8 enzymes investigated here compared to its glucuronide conjugate (Table 5.8, cf. Table 5.7). Diclofenac IC_{50} values from co-incubation experiments were an order of magnitude higher than those for diclofenac glucuronide. Of the single mutations, only the Thr107 mutants significantly altered the co-incubation IC_{50} (compared to wild-type CYP2C8). Even so, all co-incubation IC_{50} values spanned an approximate 2-fold range. Like gemfibrozil, the highest co-incubation IC_{50} was observed for the quintuple Ser100Ala-Ser103Ala-Thr107Val-Ser114Ala-Gln214Leu mutant, but IC_{50} values

tended not to increase with increasing number of mutations. IC₅₀ ratios from pre-incubation experiments with all enzymes were < 2 and k_{inact}/K_I ratios were low. Both of these observations are inconsistent with TDI. k_{inact}/K_I ratios are reported for completeness even though they have little meaning apart from providing a comparison to the ratios for demonstrated TDIs (e.g. gemfibrozil glucuronide).

Estradiol glucuronide. Estradiol glucuronide IC₅₀ values from co-incubation experiments were an order of magnitude higher than those for the gemfibrozil and diclofenac glucuronides, more comparable to those of the aglycones gemfibrozil and diclofenac (Table 5.9, cf. Tables 5.5 to 5.8). The single mutations had a variable effect on the co-incubation IC₅₀ values of estradiol glucuronide, causing either a reduction (Ser103Ala, Thr107Val, Ser114Ala), an increase (Asn99Ala, Thr107Ala, Gln214Ala, Gln214Leu), or having no significant effect (Ser100Ala) compared to wild-type CYP2C8 (Table 5.9). Except for Ser100Ala-Ser103Ala, all multiple mutants caused a similar (2.6- to 3.9-fold) increase in the co-incubation IC₅₀ compared to wild-type CYP2C8. According to the IC₅₀ > 2 criterion, estradiol glucuronide is a TDI of wild-type CYP2C8. However, TDI is very weak; the k_{inact}/K_I ratio is one- and two-orders of magnitude lower than those of diclofenac glucuronide and gemfibrozil glucuronide, respectively (Table 5.9, cf. Tables 5.5 and 5.7). Based on the IC₅₀ ratio and/or k_{inact}/K_I values, the Ser100Ala, Thr107Val, Gln214Ala and Gln214Leu mutations decreased the extent of TDI, the Ser103Ala mutation increased TDI, while the Ser114Ala mutation had a marginal effect. However, care should be taken not to over-interpret these data given the very weak TDI.

Table 5.5 IC₅₀ and k_{inact}/K_I values for gemfibrozil acyl glucuronide inhibition of recombinant wild type CYP2C8 and CYP2C8 mutants.

Enzyme	IC ₅₀ (μM)			IC ₅₀ ratio ^a	k _{inact} /K _I (ml/μmol.min)
	Co-incubation	Pre-incubation (-NADPH)	Pre-incubation (+NADPH)		
Wild type	3.51 ± 0.32	3.96 ± 0.13	0.26 ± 0.04	15.4	183 ± 30.9
N99A	7.74 ± 0.21*	ND	ND	ND	ND
S100A	3.24 ± 0.33	2.77 ± 0.23*	0.25 ± 0.04	11.2*	189 ± 26.0
S103A	3.74 ± 0.19	4.46 ± 0.19	0.25 ± 0.01	18.1	188 ± 8.48
T107A	2.66 ± 0.17*	ND	ND	ND	ND
T107V	0.66 ± 0.01*	0.49 ± 0.01*	0.06 ± 0.01*	8.12*	773 ± 104*
S114A	2.72 ± 0.08*	2.88 ± 0.13*	0.27 ± 0.02	10.5*	169 ± 10.8
Q214A	4.33 ± 0.45	4.88 ± 0.46*	0.33 ± 0.03*	14.8	141 ± 12.4
Q214L	4.53 ± 0.12*	3.67 ± 0.20	0.26 ± 0.01	14.1	178 ± 7.86
S100A-S103A	3.69 ± 0.39	ND	ND	ND	ND
S103A-T107V	5.65 ± 0.56*	ND	ND	ND	ND
S100A-S103A-T107V	5.99 ± 0.56*	ND	ND	ND	ND
S100A-S103A-T107V-S114A	16.4 ± 1.98*	ND	ND	ND	ND
S100A-S103A-T107V-S114A-Q214A	20.7 ± 0.76*	ND	ND	ND	ND
S100A-S103A-T107V-S114A-Q214L	26.8 ± 1.33*	ND	ND	ND	ND

^a IC₅₀ ratio = IC₅₀ (-NADPH) / IC₅₀ (+NADPH).

Experiments were performed in triplicate and results for each parameter are shown as the mean ± SD.

*Statistically significantly different ($p < 0.05$) compared to corresponding parameter for wild-type CYP2C8.

ND, Not determined.

Abbreviations: A, Ala; L, Leu; N, Asn; Q, Gln; S, Ser; T, Thr; V, Val.

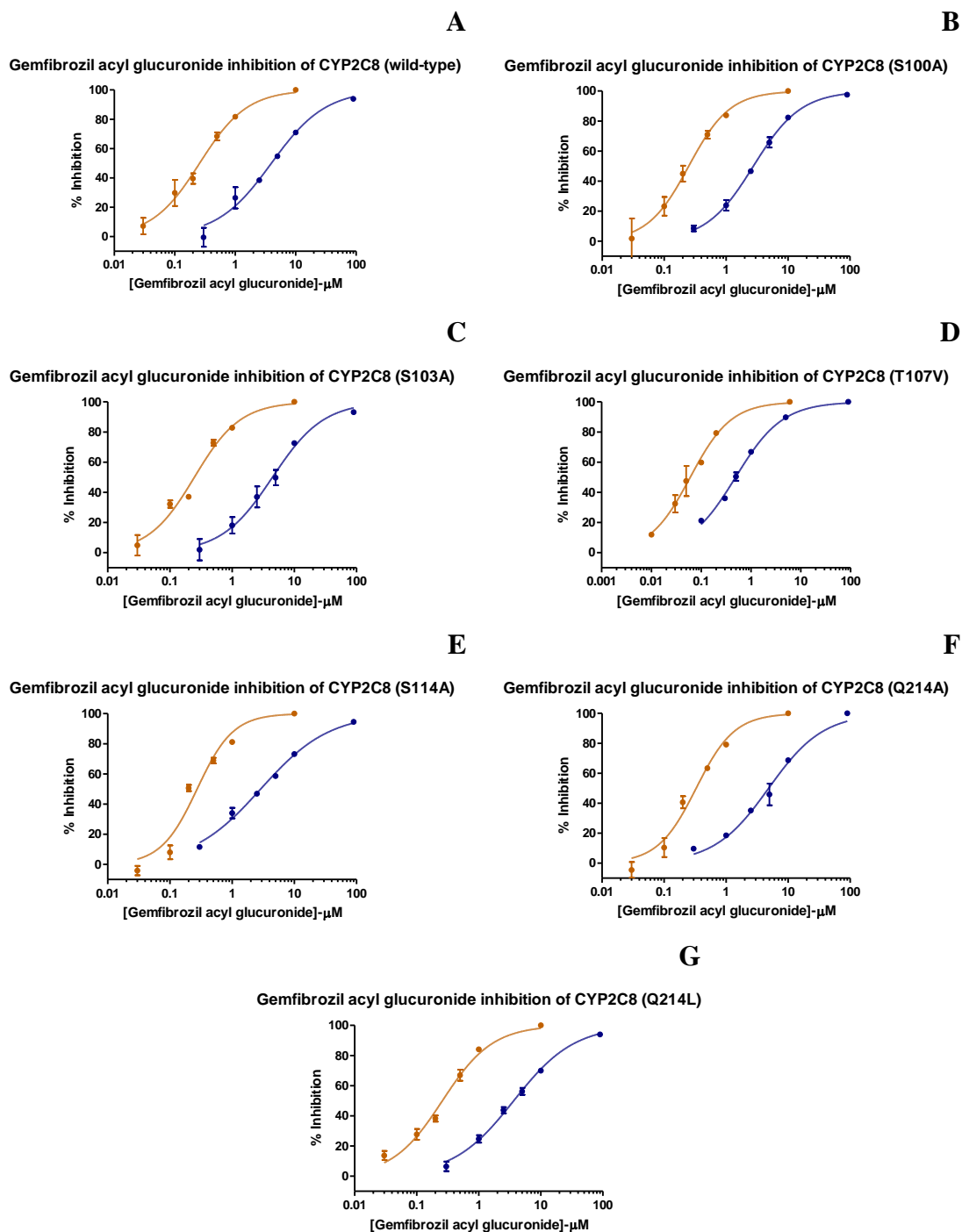


Figure 5.11 Inhibition of CYP2C8 activity by gemfibrozil acyl glucuronide following a 30 min pre-incubation in the absence (blue line) and presence (red line) of NADPH.

Error bars show the standard deviation.

Table 5.6 IC₅₀ and k_{inact}/K_I values for gemfibrozil inhibition of recombinant wild type CYP2C8 and CYP2C8 mutants.

Enzyme	IC ₅₀ (μM)			IC ₅₀ ratio ^a	k _{inact} /K _I (ml/μmol.min)
	Co-incubation	Pre-incubation (-NADPH)	Pre-incubation (+NADPH)		
Wild type	54.3 ± 4.60	65.7 ± 3.48	35.5 ± 2.59	1.85	1.31 ± 0.09
N99A	50.6 ± 4.72	ND	ND	ND	ND
S100A	96.1 ± 2.46*	81.1 ± 6.72*	47.0 ± 4.36*	1.73	0.99 ± 0.09*
S103A	70.0 ± 6.46*	85.6 ± 11.3*	51.2 ± 4.03	1.67	0.91 ± 0.07*
T107A	100 ± 10.3*	ND	ND	ND	ND
T107V	61.4 ± 1.70	56.3 ± 5.18*	48.0 ± 4.80*	1.17*	0.97 ± 0.09*
S114A	51.2 ± 2.67	46.6 ± 1.32*	41.2 ± 0.87*	1.13*	1.12 ± 0.02*
Q214A	78.4 ± 1.97*	77.3 ± 6.62*	55.9 ± 5.84*	1.38*	0.83 ± 0.09*
Q214L	102 ± 9.05*	101 ± 12.1*	78.8 ± 8.97*	1.29*	0.59 ± 0.07*
S100A-S103A	122 ± 3.39*	ND	ND	ND	ND
S103A-T107V	158 ± 4.80*	ND	ND	ND	ND
S100A-S103A-T107V	95.2 ± 2.17*	ND	ND	ND	ND
S100A-S103A-T107V-S114A	81.7 ± 8.60*	ND	ND	ND	ND
S100A-S103A-T107V-S114A-Q214A	108 ± 5.66*	ND	ND	ND	ND
S100A-S103A-T107V-S114A-Q214L	198 ± 3.45*	ND	ND	ND	ND

^a IC₅₀ ratio = IC₅₀ (-NADPH) / IC₅₀ (+NADPH).

Experiments were performed in triplicate and results for each parameter are shown as the mean ± SD.

*Statistically significantly different ($p < 0.05$) compared to corresponding parameter for wild-type CYP2C8.

ND, Not determined.

Abbreviations: A, Ala; L, Leu; N, Asn; Q, Gln; S, Ser; T, Thr; V, Val.

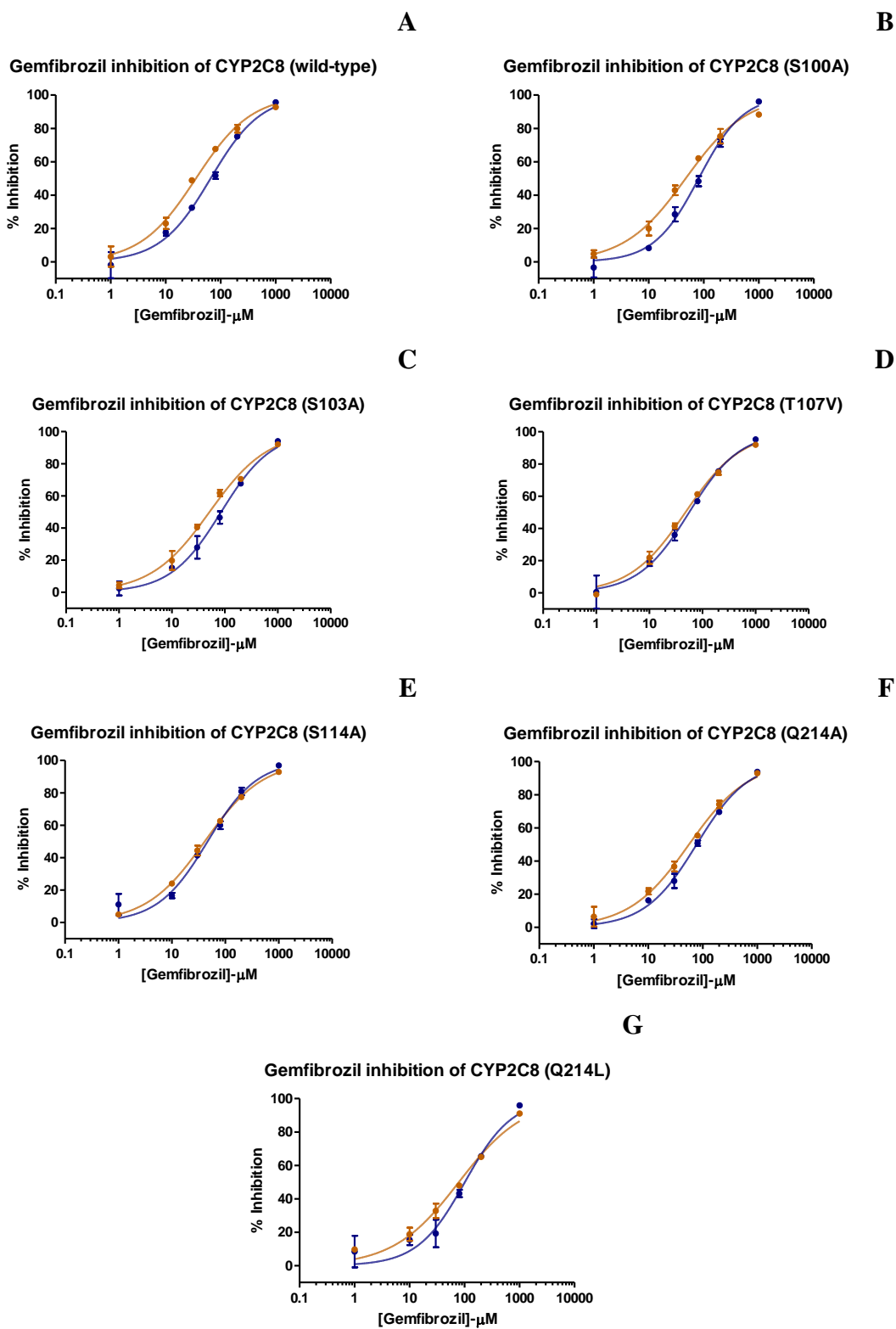


Figure 5.12 Inhibition of CYP2C8 activity by gemfibrozil following a 30 min pre-incubation in the absence (blue line) and presence (red line) of NADPH.

Error bars show the standard deviation.

Table 5.7 IC₅₀ and k_{inact}/K_I values for diclofenac acyl glucuronide inhibition of recombinant wild type CYP2C8 and CYP2C8 mutants.

Enzyme	IC ₅₀ (μM)			IC ₅₀ ratio ^a	k _{inact} /K _I (ml/μmol.min)
	Co-incubation	Pre-incubation (-NADPH)	Pre-incubation (+NADPH)		
Wild type	4.33 ± 0.48	7.32 ± 0.32	2.68 ± 0.34	2.73	17.5 ± 2.37
N99A	6.43 ± 0.05*	ND	ND	ND	ND
S100A	5.39 ± 0.47	4.44 ± 0.93*	5.77 ± 0.51*	0.77*	8.05 ± 0.75*
S103A	2.86 ± 0.04*	6.69 ± 0.19*	4.50 ± 0.31*	1.49*	10.3 ± 0.71*
T107A	28.6 ± 1.58*	ND	ND	ND	ND
T107V	3.87 ± 0.35	5.50 ± 0.75*	7.74 ± 0.29*	0.71*	5.97 ± 0.22*
S114A	2.48 ± 0.23*	8.24 ± 0.32*	4.09 ± 0.63*	2.01*	11.5 ± 1.72*
Q214A	5.84 ± 0.48*	10.2 ± 1.02*	5.78 ± 1.07*	1.77*	8.16 ± 1.35*
Q214L	10.6 ± 0.41*	17.6 ± 0.66*	8.18 ± 0.81*	2.16*	5.68 ± 0.54*
S100A-S103A	13.2 ± 0.43*	ND	ND	ND	ND
S103A-T107V	28.3 ± 1.33*	ND	ND	ND	ND
S100A-S103A-T107V	45.1 ± 0.79*	ND	ND	ND	ND
S100A-S103A-T107V-S114A	49.5 ± 0.60*	ND	ND	ND	ND
S100A-S103A-T107V-S114A-Q214A	74.0 ± 8.31*	ND	ND	ND	ND
S100A-S103A-T107V-S114A-Q214L	111 ± 22.6*	ND	ND	ND	ND

^a IC₅₀ ratio = IC₅₀ (-NADPH) / IC₅₀ (+NADPH).

Experiments were performed in triplicate and results for each parameter are shown as the mean ± SD.

*Statistically significantly different ($p < 0.05$) compared to corresponding parameter for wild-type CYP2C8.

ND, Not determined.

Abbreviations: A, Ala; L, Leu; N, Asn; Q, Gln; S, Ser; T, Thr; V, Val.

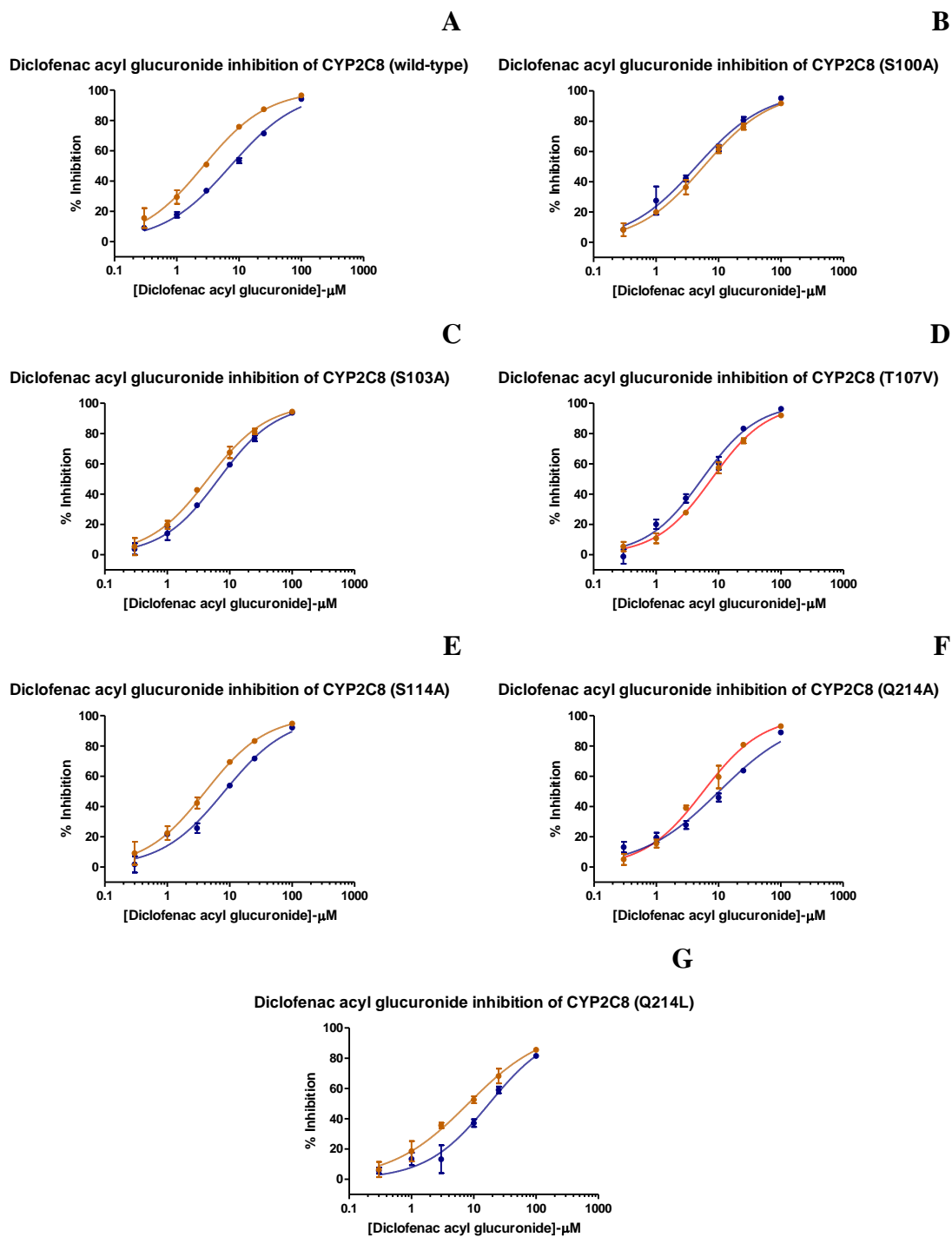


Figure 5.13 Inhibition of CYP2C8 activity by diclofenac acyl glucuronide following a 30 min pre-incubation in the presence (red line) and absence (blue line) of NADPH.

Error bars show the standard deviation.

Table 5.8 IC₅₀ and k_{inact}/K_I values for diclofenac inhibition of recombinant wild type CYP2C8 and CYP2C8 mutants.

Enzyme	IC ₅₀ (μM)			IC ₅₀ ratio ^a	k _{inact} /K _I (ml/μmol.min)
	Co-incubation	Pre-incubation (-NADPH)	Pre-incubation (+NADPH)		
Wild type	31.1 ± 1.31	37.2 ± 1.65	25.9 ± 1.41	1.44	1.79 ± 0.10
N99A	33.7 ± 3.88	ND	ND	ND	ND
S100A	27.4 ± 3.98	21.0 ± 3.57*	47.7 ± 1.37*	0.44*	0.97 ± 0.03*
S103A	43.1 ± 1.63	46.5 ± 2.47*	30.2 ± 3.16	1.54	1.54 ± 0.16*
T107A	55.4 ± 6.62*	ND	ND	ND	ND
T107V	51.9 ± 5.00*	18.3 ± 1.61*	33.0 ± 0.76*	0.55*	1.40 ± 0.03*
S114A	41.6 ± 2.04	41.0 ± 2.61	28.7 ± 2.59	1.43	1.62 ± 0.14*
Q214A	44.7 ± 2.27	42.8 ± 4.32	47.6 ± 3.47*	0.90*	0.97 ± 0.07*
Q214L	41.7 ± 4.59	40.9 ± 4.83	47.2 ± 2.71*	0.87*	0.98 ± 0.05*
S100A-S103A	51.2 ± 1.45*	ND	ND	ND	ND
S103A-T107V	81.2 ± 2.41*	ND	ND	ND	ND
S100A-S103A-T107V	159 ± 18.2*	ND	ND	ND	ND
S100A-S103A-T107V-S114A	130 ± 18.0*	ND	ND	ND	ND
S100A-S103A-T107V-S114A-Q214A	141 ± 3.91*	ND	ND	ND	ND
S100A-S103A-T107V-S114A-Q214L	779 ± 23.5*	ND	ND	ND	ND

^a IC₅₀ ratio = IC₅₀ (-NADPH) / IC₅₀ (+NADPH).

Experiments were performed in triplicate and IC₅₀ values and results for each parameter are shown as the mean ± SD.

*Statistically significantly different ($p < 0.05$) compared to corresponding parameter for wild-type CYP2C8.

ND, Not determined.

Abbreviations: A, Ala; L, Leu; N, Asn; Q, Gln; S, Ser; T, Thr; V, Val.

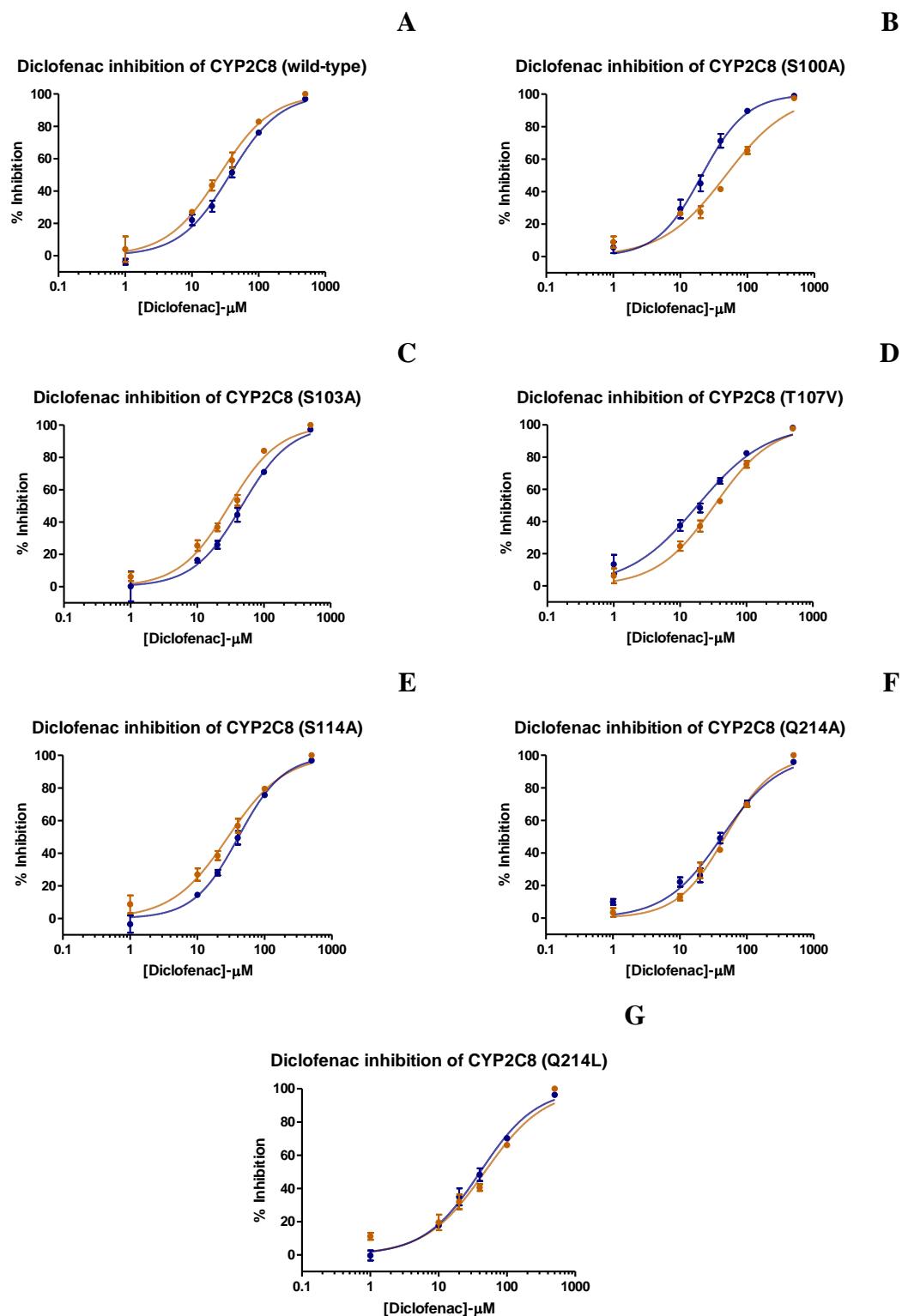


Figure 5.14 Inhibition plots of CYP2C8 activity by diclofenac (30 min pre-incubation in the absence (blue line) and presence (red line) of NADPH).

Error bars show the standard deviation.

Table 5.9 IC₅₀ and k_{inact}/K_I values for estradiol 17-β-D-glucuronide inhibition of recombinant wild type CYP2C8 and CYP2C8 mutants.

Enzyme	IC ₅₀ (μM)			IC ₅₀ ratio ^a	k _{inact} /K _I (ml/μmol.min)
	Co-incubation	Pre-incubation (-NADPH)	Pre-incubation (+NADPH)		
Wild type	79.1 ± 2.62	86.8 ± 5.77	36.3 ± 3.42	2.39	1.28 ± 0.11
N99A	113 ± 9.72*	ND	ND	ND	ND
S100A	91.6 ± 7.69	87.3 ± 15.0	58.2 ± 7.66*	1.50*	0.80 ± 0.11*
S103A	45.2 ± 2.15*	54.9 ± 6.32*	20.8 ± 3.91*	2.63*	2.27 ± 0.39*
T107A	234 ± 11.8*	ND	ND	ND	ND
T107V	30.1 ± 1.17*	33.2 ± 2.20*	49.2 ± 2.53*	0.68*	0.94 ± 0.05*
S114A	43.2 ± 1.36*	67.7 ± 3.45*	27.2 ± 3.16*	2.49	1.71 ± 0.19*
Q214A	103 ± 7.83	157 ± 22.2*	73.8 ± 7.89*	2.11*	0.63 ± 0.07*
Q214L	213 ± 22.1*	197 ± 7.01*	147 ± 8.84*	1.34*	0.31 ± 0.02*
S100A-S103A	104 ± 13.1	ND	ND	ND	ND
S103A-T107V	283 ± 48.9*	ND	ND	ND	ND
S100A-S103A-T107V	253 ± 3.03*	ND	ND	ND	ND
S100A-S103A-T107V-S114A	204 ± 16.7*	ND	ND	ND	ND
S100A-S103A-T107V-S114A-Q214A	256 ± 10.8*	ND	ND	ND	ND
S100A-S103A-T107V-S114A-Q214L	314 ± 54.9*	ND	ND	ND	ND

^a IC₅₀ ratio = IC₅₀ (-NADPH) / IC₅₀ (+NADPH).

Experiments were performed in triplicate and IC₅₀ values and results for each parameter are shown as the mean ± SD.

*Statistically significantly different ($p < 0.05$) compared to corresponding parameter for wild-type CYP2C8.

ND, Not determined.

Abbreviations: A, Ala; L, Leu; N, Asn; Q, Gln; S, Ser; T, Thr; V, Val.

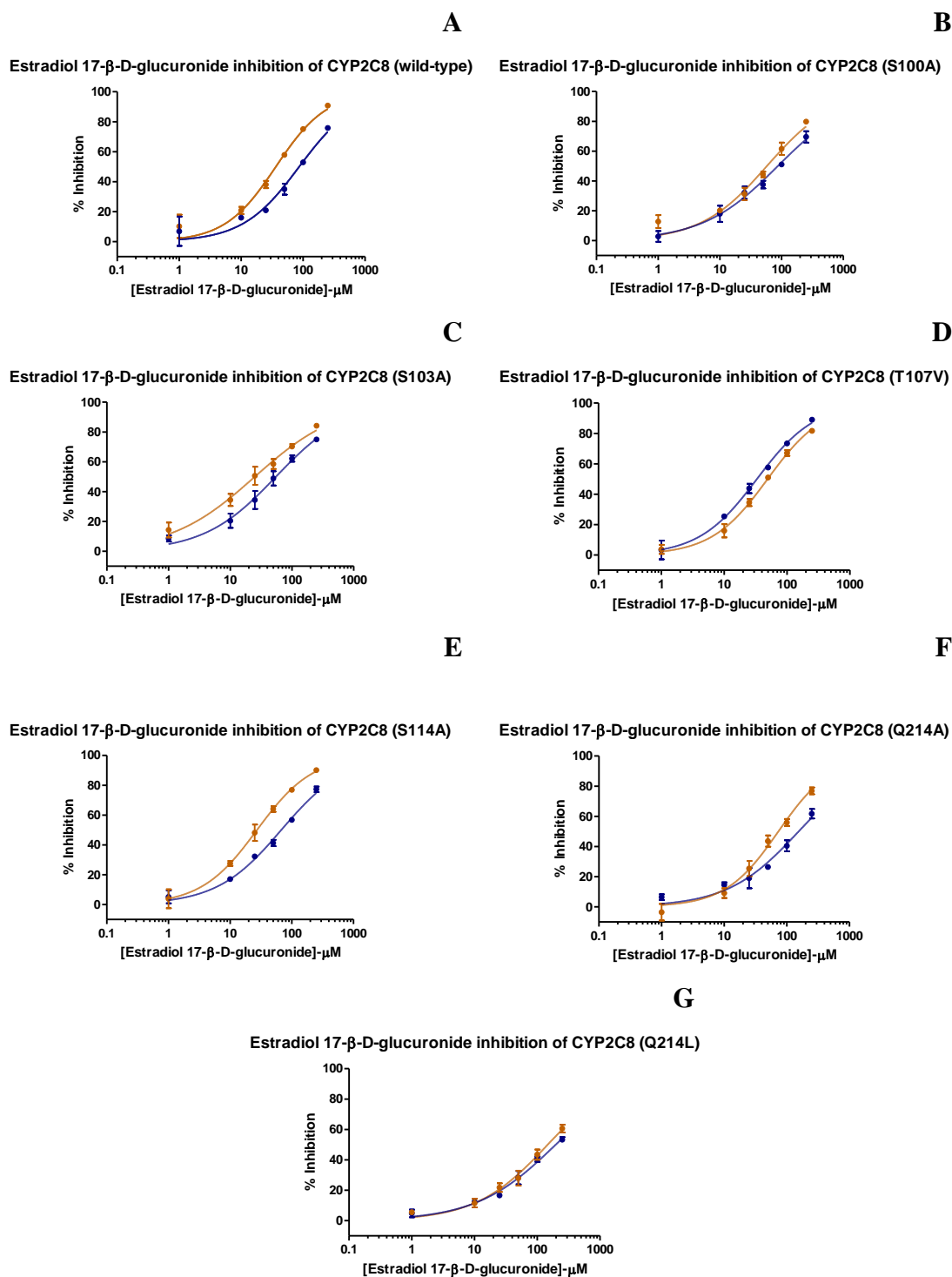


Figure 5.15 Inhibition of CYP2C8 activity by estradiol 17- β -D-glucuronide following a 30 min pre-incubation in the absence (blue line) and presence (red line) of NADPH.

Error bars show the standard deviation.

5.4 Discussion

Molecular docking of diclofenac, diclofenac acyl glucuronide, gemfibrozil, gemfibrozil acyl glucuronide, β -estradiol and estradiol 17- β -D-glucuronide in the active site of CYP2C8 was performed to identify amino acids that potentially contribute to the binding and alignment of each glucuronide conjugate. Gly98, Asn99, Ser100, Ser103 and Ser114 were located within 4 Å of the glucuronide moieties of diclofenac, gemfibrozil and estradiol, but did not contribute to the binding of the respective aglycones. In addition, Thr107, Gln214 and Asn217 were variably located within 4 Å of the three glucuronides. As described in Section 5.3.1, Asn99, Ser100, Ser103, Thr107, Ser114 and Gln214 were therefore selected for subsequent mutagenesis and MBI studies.

The results of the gemfibrozil glucuronide docking experiments are generally similar to previously published data. Consistent with data reported by Baer, DeLisle and Allen (2009), Jenkins et al. (2011) and Tornio et al. (2014), docking positioned the glucuronic acid moiety of gemfibrozil glucuronide in SRS1 towards the N-terminus of helix B', with the benzylic methyl group of the aglycone located above the γ -meso position of the heme (Figure 5.3). Published docking data variably implicate hydrogen bonding interactions between Asn99, Ser100, Ser103, Ser114, Asn204, Gln214 and Asn217 with the glucuronic acid moiety (see Section 5.1). Notably, Asn99 and Ser103 are the only common contact residues identified in the present study and in all three published studies. Even then, Jenkins et al. (2011) reported the hydrogen bonding interaction with Ser103 involved the backbone NH group rather than the side-chain hydroxyl (see Figure 5.7 for the structure of serine). This is the first study that implicates Thr107 in gemfibrozil glucuronide binding, a not unsurprising finding

given the proximity of this residue to Ser103 and Ser114 (see Figure 5.3 and subsequent discussion). In contrast to Baer et al. (2009) and Jenkins et al. (2011), this study did not locate Gln214 and Asn217 within 4 Å of docked gemfibrozil glucuronide, although both were found to potentially contribute to the binding of the diclofenac- and estradiol glucuronides. This finding may relate to the different CYP2C8 X-ray crystal templates and docking programs used in the various studies (see below). Nevertheless, mutagenesis and MBI studies were performed with Gln214. Delaforge and colleagues employed docking and Molecular Dynamics Simulations (MDS) to identify residues potentially involved in the binding of estradiol glucuronide within the CYP2C8 active site, although the simulation time (1 fs) was extremely short (Delaforge et al. 2005). Asn204 and Asp293 were suggested to form hydrogen bonds with the glucuronic acid carboxyl group, and Ser100 and Ser114 were also found in close proximity to hydroxyl groups of the glucuronide moiety. As alluded to above, however, the results of this study should be interpreted with caution given the very short simulation time (Nair, McKinnon and Miners 2016a).

It should be noted that different docking programs were used in this study (SYBYL) and by Baer et al. and Jenkins et al. (both Glide), and by Tornio et al. (Gold). In addition, there were differences in the CYP2C8 X-ray crystal structure template used for docking. This study used the unliganded structure (PDB - 1PQ2) rather than a crystal structure generated with a bound substrate to avoid a 'biased' active site. In contrast, Jenkins et al. employed the structure generated with bound montelukast (PDB - 2NNI), Tornio et al. the structure with bound felodipine (PDB - 2NNJ) while Baer et al. performed docking studies with three X-ray crystal templates, PDB - 1PQ2, 2NNI and 2NNH, the latter solved with bound retinoic acid). Importantly, however, Baer et al. (2009) reported that, despite differences in the active site geometry of the three

templates employed for docking, poses were consistent in the positioning of gemfibrozil glucuronide. Like the present study, the unliganded structure (PDB - 1PQ2) was used by Delaforge et al. (2005) for the docking of estradiol glucuronide.

Since it was necessary to perform TDI (IC_{50} shift) experiments at a PAC concentration that corresponded to the K_m for wild-type CYP2C8 and each mutant, the kinetics of PAC 6 α -hydroxylation were characterised for each enzyme. From data presented in Table 5.4, it is evident that the mutations variably affected the K_m and V_{max} values for PAC 6 α -hydroxylation. Apart from the Asn99Ala, Ser103Ala and Gln214Leu mutants, K_m values for most other mutants were significantly higher (1.7- to 4.3- fold) than the K_m for wild-type CYP2C8. Ser114Ala and Gln214Ala were the only enzymes with a lower K_m . Turnover (i.e. V_{max} , which is equivalent here to k_{cat}) was altered for all mutants except Ser100Ala, Ser100Ala-Ser103Ala-Thr107Val, and Ser100Ala-Ser103Ala-Thr107Val-Ser114Ala. In most cases turnover was lower than for wild-type CYP2C8, although the two Thr107 single mutants exhibited a higher V_{max} . Notably, all mutations except Asn99Ala were associated with a significantly lower Cl_{int} . The observation that almost all mutations altered at least one PAC 6 α -hydroxylation kinetic parameter (K_m , V_{max} and/or Cl_{int}) is not unsurprising given the molecular modelling data presented in Section 5.3.1. PAC is a large molecule (molecular mass 854 Da), that contains both hydrophobic domains and heteroatoms capable of hydrogen bonding. Thirty one residues were found to be located within 4 Å of bound PAC, including those mutated in this study; Asn99, Ser100, Ser103, Thr107, Ser114 and Gln214.

Consistent with the data presented here, a previous site-directed mutagenesis study, using yeast-expressed CYP2C8 enzymes, reported that the K_m values for PAC 6 α -hydroxylation by the Ser100Ala mutant was approximately 4-fold higher than for

wild-type CYP2C8, while the Ser103Ala and Ser114Ala mutations had relatively minor effects on K_m (Melet et al. 2004). Based on activity data for multiple CYP2C8 substrates, Melet et al. concluded that Ser100 appears to be involved in hydrogen bonding interactions with a polar site on CYP2C8 substrates. Interestingly, a previous study from this laboratory Kerdpin et al. (2004) and Melet et al. (2004) found that the Ser114Phe mutation abolished PAC 6 α -hydroxylation, presumably due to steric hindrance.

Notably, the K_m value for PAC 6 α -hydroxylation by yeast-expressed wild-type CYP2C8 was approximately 5- to 6-fold higher than the K_m observed in this and previous studies in this laboratory using CYP2C8 protein expressed in *E. coli* (Kerdpin et al. 2004; Polasek et al. 2004; Wattanachai et al. 2011). The difference between expression systems presumably reflects the effects of differences in the spectrum of inhibitory long-chain unsaturated fatty acids released by yeast and *E. coli* membranes during the course of an incubation (Wattanachai et al. 2011). It is also noteworthy that the PAC 6 α -hydroxylation kinetic data generated here for the CYP2C8 mutants (using an incubation time of 15 min) are not excessively dissimilar to the kinetic parameters for the wild-type enzyme, despite the apparent instability of the multiple mutants when incubated in the presence of NADPH for 30 min. This suggests that sufficient enzyme remained throughout the co-incubation experiments to generate meaningful IC_{50} values. It should also be noted that, in contrast to HLM, PAC does not bind to *E. coli* membranes (Wattanachai et al. 2011). Hence correction for non-specific binding of PAC (and inhibitors, which are all acids) to the enzyme source is not required. This is an important consideration since the protein content of incubations varied between mutant CYP2C8 enzymes. (Variation in protein content was necessary to obtain the desired P450 concentration required for incubations.)

Effects of gemfibrozil glucuronide, gemfibrozil, diclofenac glucuronide, diclofenac and estradiol glucuronide on PAC 6 α -hydroxylation by wild-type CYP2C8 and each mutant was investigated using co- and pre-incubation approaches. As described earlier, co-incubation experiments, where the inhibitor and PAC are incubated without prior incubation of the enzyme source and inhibitor, were performed to assess non-time dependent inhibition. Inhibition measured in these experiments is presumably competitive or non-competitive, together with a contribution of TDI (where this occurs) during the 15 min co-incubation period. The IC₅₀ values measured in co-incubation experiments and in pre-incubation experiments in the absence of NADPH should be close in value, because exclusion of NADPH in the pre-incubation step precludes TDI; MBI can only occur in the presence of NADPH. As indicated in Section 5.3.4, IC₅₀ values measured in the co-incubation and pre-incubation (-NADPH) inhibition experiments for each CYP2C8 enzyme were generally close in value for both gemfibrozil glucuronide and gemfibrozil (Tables 5.5 and 5.6). Agreement was also reasonable with diclofenac glucuronide (Table 5.7), diclofenac (Table 5.8) and estradiol glucuronide (Table 5.9) as the inhibitors, although there were some outliers. Where observed, differences in the stability of individual mutants (see below) may contribute to this variability, although it is unclear why it should differ between inhibitors.

To identify TDI, each recombinant CYP2C8 enzyme was pre-incubated for 30 min with each inhibitor in the absence and presence of NADPH (1 mM final concentration) prior to addition of PAC. TDI will result in loss of enzyme activity when a MBI is pre-incubated with the CYP enzyme in the presence of NADPH, but not in the absence of NADPH. Where TDI occurs, there will be a shift in the IC₅₀ curve (the 'shifted' IC₅₀) to the left producing an increase in the IC₅₀ ratio. The non-dilution method was used

here to measure the shifted IC_{50} . As described in Section 5.2.2, this approach has advantages over the so-called dilution method because it is technically simpler, data processing is less complex and is unambiguous, and inhibitor non-specific binding and depletion are minimised (Parkinson et al. 2011). Although TDI is normally identified by an IC_{50} ratio > 1.5 when HLM are used as the enzyme source (Grimm et al. 2009), the cut-off for TDI was arbitrarily taken as an IC_{50} ratio > 2 in this study. Recombinant CYP2C8 appears to be more sensitive to MBI and more unstable in incubation media (see below) than is human liver microsomal CYP2C8. It should be noted that studies investigating MBI of CYP2C8 have most commonly employed HLM as the enzyme source (Bertelsen et al. 2003; Grime et al. 2009; Li et al. 2011; Mayhew, Jones and Hall 2000; Obach, Walsky and Venkatakrishnan 2007; Parkinson et al. 2011; Perloff et al. 2009). Clearly, however, HLM do not allow site-directed mutagenesis based investigations of the molecular basis of protein function.

In addition to the IC_{50} ratio, the k_{inact}/K_I ratio was calculated to assess potential TDI for each inhibitor/CYP2C8 enzyme pair. A higher value of k_{inact}/K_I indicates greater enzyme inactivation, due to a higher k_{inact} and/or lower K_I (Obach, Walsky and Venkatakrishnan 2007; Parkinson et al. 2011). The k_{inact}/K_I ratio may be calculated from the shifted IC_{50} using equation 2.19. Obach, Walsky and Venkatakrishnan (2007) validated the use of the shifted IC_{50} to calculate k_{inact}/K_I by demonstrating that experimentally determined k_{inact}/K_I ratios (from measurement of the individual parameters) for 33 drugs were highly correlated with the corresponding independently measured shifted IC_{50} . By contrast, the correlation between IC_{50} ratio and k_{inact}/K_I was relatively poor, indicating that the IC_{50} ratio itself is not the most important predictor of inactivation efficiency.

A previous study from this laboratory found that there was greater spontaneous loss of

recombinant CYP2C8 activity compared to human liver microsomal CYP2C8 activity when the respective enzyme sources were pre-incubated with NADPH according the TDI protocol (Polasek et al. 2004). Approximately 50% loss of activity of recombinant wild-type CYP2C8 occurred over the 30 min pre-incubation period. Although not widely reported, it appears that other recombinant human CYP enzymes, for example CYP2D6, similarly exhibit spontaneous loss of activity under these conditions (RS Obach, Pharmacokinetics, Dynamics, and Drug Metabolism, Pfizer Inc; personal communication to JO Miners). Surprisingly, most of the recombinant CYP2C8 proteins exhibited loss of activity (up to 30%) when incubated for 30 min at 37°C in phosphate buffer alone (i.e. without NADPH). Thus, the proteins are inherently unstable at 37°C, at least when expressed in *E. coli*.

The mechanism responsible for the higher loss of activity of the CYP2C8 proteins when pre-incubated with NADPH is unclear, but probably relates to the formation of reactive oxygen species (ROS) and uncoupling of the CYP catalytic cycle (Zangar, Davydov and Verma 2004) (see Chapter 1, Section 1.2.1). This may relate to the ‘unnatural’ CYP:CPR ratios observed in recombinant CYP enzyme expression systems along with a reduced ability of *E. coli* membranes (compared to HLM and hepatocytes) to ‘scavenge’ ROS. In this regard, it has been reported that loss of activity of rat liver microsomal CYP enzymes over prolonged incubation periods is greater than loss of rat hepatocyte CYP enzyme activity (Jones and Houston 2004). It is noteworthy that the CYP:CPR ratio tended to decline with increasing number of mutations in this study (Table 5.2), and the ratio was also low for the Thr107 mutants (although not for Asn99Ala). Of further interest, Jones and Houston (2004) reported that spontaneous loss of rat liver microsomal CYP enzyme activity tended to increase with increasing concentrations of microsomal protein in the incubation medium. In

this study, increased *E. coli* membrane protein concentrations in incubations was necessary to maintain the desired CYP protein content (as pmol CYP/ml) for those mutants with lower expression levels, including Asn99Ala, Thr107Ala, Thr107Val, and the triple, quadruple and quintuple mutants (Table 5.2). Moreover, as indicated in Section 5.3.2, the triple, quadruple and quintuple mutants appear to be inherently unstable.

Despite the foregoing discussion, the high spontaneous loss of activity of the Asn99Ala, Thr107Ala, and double, triple, quadruple and quintuple mutants when pre-incubated with NADPH for 30 min (according to the TDI protocol) was unanticipated. Although it was possible to measure IC₅₀ values for inhibition of PAC 6 α -hydroxylation activity for all mutants using the co-incubation protocol, which employed a 15 min incubation time, the loss of activity observed for the Asn99Ala, Thr107Ala, and double, triple, quadruple and quintuple mutants during the 30 min pre-incubation step (in the presence of NADPH) of the TDI protocol precluded measurement of IC₅₀ ratios (and hence k_{inact}/K_I values).

Gemfibrozil glucuronide is the prototypic TDI of CYP2C8 (Backman et al. 2016; Ogilvie et al. 2006). The reported IC₅₀ ratio for TDI of human liver microsomal CYP2C8 with PAC and amodiaquine as the substrate ‘probes’ is approximately 13 (Jenkins et al. 2011; Ogilvie et al. 2006), while the experimentally determined k_{inact}/K_I value with PAC as the probe substrate was 105 ml/ μ mol.min (Ogilvie et al. 2006). This is of a comparable order to the k_{inact}/K_I values for other potent TDIs, for example furafylline TDI of CYP1A2 (120 ml/ μ mol.min) and tienilic TDI of CYP2C9 (280 ml/ μ mol.min) (Obach, Walsky and Venkatakrishnan 2007). The IC₅₀ ratio and k_{inact}/K_I value for gemfibrozil glucuronide TDI of recombinant wild-type CYP2C8 obtained here were 15.3 and 183 ml/ μ mol.min, respectively (Table 5.5).

Apart from Asn99Ala (2.2-fold increase) and Thr107Val (82% decrease), the single mutations had a statistically and/or mechanistically non-significant effect on the co-incubation IC_{50} values for gemfibrozil glucuronide (Table 5.5). This indicates that the Ser103Ala, Ser114Ala, Gln214Ala and Gln214Ala mutations had little effect on gemfibrozil glucuronide binding in the CYP2C8 active site. Assuming that the co-incubation IC_{50} largely reflects competitive or non-competitive inhibition (although, as indicated previously, there will also be a contribution from TDI), the data suggest that the Asn99Ala mutation modestly decreases gemfibrozil glucuronide binding affinity (since $IC_{50} = 2 \times K_i$ for competitive and non-competitive inhibition). By contrast, it would appear that the Thr107Val, but not the Thr107Ala, mutation enhances binding. Intriguingly, the same phenomenon was not observed for the multiple mutants containing the Thr107Val mutation, presumably due to more global changes in the architecture of the active sites of the multiple mutants. Co-incubation IC_{50} values for most multiple mutants were higher than those for all single mutants, except Asn99Ala. In particular, co-incubation IC_{50} values for the quintuple mutants were 6- to 7.5-fold higher than the IC_{50} for wild-type CYP2C8 (Table 5.5). Overall, the data suggest that no single amino acid (i.e. Asn99, Ser100, Ser103, Thr107, Ser114 or Gln214) dominates gemfibrozil glucuronide binding. Rather, binding in the active site is stabilised by hydrogen bonding with all six residues, and additionally by hydrophobic interactions with the gemfibrozil moiety (Table 5.1). As discussed below, the effect of the Thr107Val mutation may arise from an altered binding orientation of gemfibrozil glucuronide in the active site.

The IC_{50} ratios and k_{inact}/K_i values from the TDI studies are broadly consistent with the above conclusions relating to the single mutants. IC_{50} ratios for the Ser100Ala, Ser103Ala, Thr107Val, Ser114Ala, Gln214Ala and Gln214Leu mutants were all

consistent with TDI (Table 5.5). Consideration of data as the $k_{\text{inact}}/K_{\text{I}}$ ratio indicated that all single mutations except Thr107Val had no significant effect on TDI efficiency. In agreement with the co-incubation data, the Thr107Val mutation increased $k_{\text{inact}}/K_{\text{I}}$ 4.2-fold relative to wild-type CYP2C8. In order to gain insights into the role of the Thr107 mutations on inhibitor binding, Ala and Val were separately substituted for Thr in the computational CYP2C8 model. Effects are complex, but primarily relate to disruption of intra-molecular hydrogen bonding between Thr107 and Ser114, affecting rotation of the Ser114 side-chain. Thus, the mutations not only disrupt hydrogen bonding between Thr107 and the ligand, but also between Ser114 and the ligand. In particular, the Thr107Val mutation shifts the side-chain -OH of Ser114 approximately 3 Å closer to the heme, whereas the Thr107Ala mutation moves the side-chain -OH marginally (1.2 Å) away from the heme. Docking of the gemfibrozil glucuronide in the active site of the Thr107 mutant proteins gave a surprising result. The most energetically favoured pose for the Thr107Val mutant had the orientation of gemfibrozil glucuronide inverted relative to wild-type CYP2C8 that is the glucuronide moiety was orientated above the heme. Time did not allow further investigation of this observation and the structural analysis of other ligand/mutant enzyme pairs.

Interestingly, the IC_{50} values for the Ser100Ala, Ser103Ala, Thr107Ala, Gln214Ala, Gln214Leu mutants and all multiple mutants with gemfibrozil as the inhibitor were significantly higher than those for wild-type CYP2C8, despite none of the mutated positions being within 4 Å of docked gemfibrozil in wild-type CYP2C8. However, inhibition was relatively weak (IC_{50} values > 50 μM), especially compared to gemfibrozil glucuronide. The data suggest that all of the above mutations influence gemfibrozil binding within the active site, although a more than doubling in the co-incubation IC_{50} (compared to wild-type CYP2C8) was observed only for the double

mutants (Ser100Ala-Ser103Ala and Ser103Ala-Thr107Val) and Ser100Ala-Ser103Ala-Thr107Val-Sr14Ala-Gln214Leu. In agreement with previous reports (Jenkins et al. 2011; Ogilvie et al. 2006), gemfibrozil was not a TDI of CYP2C8 or of the mutants investigated here (i.e. IC_{50} ratio < 2).

Comparison of co-incubation IC_{50} data in Tables 5.4 and 5.6 demonstrate that diclofenac glucuronide and gemfibrozil glucuronide are equipotent competitive (or possibly non-competitive) inhibitors of CYP2C8. A similar observation has been reported by Jenkins et al. (2011). Competitive inhibition is consistent with the fact that diclofenac glucuronide is a substrate of CYP2C8 (Kumar et al. 2002). All of the single mutants except Ser100Ala and Thr107Val had a small or non-significant effect on diclofenac glucuronide co-incubation IC_{50} values, and all reduced the IC_{50} ratio and k_{inact}/K_I (Table 5.7). However, when taken together the co- and pre-incubation data indicate that none of the positions mutated dominate diclofenac glucuronide binding in the CYP2C8 active site. Similar to gemfibrozil glucuronide, the co-incubation IC_{50} increased with increasing number of mutations further suggesting that binding in the active site is stabilised by hydrogen bonding with all six residues. Effects of the Thr107 mutants were dramatically different to those obtained with gemfibrozil glucuronide as the inhibitor (cf. Tables 5.4 and 5.6). Whereas the Thr107Ala mutation was without effect on the gemfibrozil glucuronide co-incubation IC_{50} , it resulted in an approximate 7-fold increase in the co-incubation IC_{50} for diclofenac glucuronide. In contrast, the Thr107Val mutation had no effect on diclofenac glucuronide inhibition but reduced the co-incubation IC_{50} for gemfibrozil glucuronide by more than 80%. The differing effects of Thr107 mutations almost certainly arises from the different orientations of the gemfibrozil-, diclofenac- and estradiol glucuronides adopted in the CYP2C8 active site (see Figures 5.3 to 5.5). This conclusion is supported by the observation that there

is no consistent effect of all single mutations on gemfibrozil glucuronide and diclofenac glucuronide co-incubation IC₅₀ values, although similar trends are observed for some mutations (Asn99Ala, Ser100Ala, Ser114Ala and Gln214Leu) (Tables 5.4 and 5.6).

Based on the IC₅₀ ratio cut-off of 2, diclofenac glucuronide is classified as a TDI of wild-type CYP2C8 (Table 5.7). However, based on k_{inact}/K_I , the efficiency of diclofenac glucuronide as a TDI is an order of magnitude lower than that of gemfibrozil glucuronide. Classification of diclofenac glucuronide as a weak or 'borderline' TDI is consistent with the IC₅₀ ratio of 1.4 reported for inhibition of human liver microsomal CYP2C8 (Jenkins et al. 2011). As noted above, in contrast to gemfibrozil glucuronide all single mutations reduced the k_{inact}/K_I values for diclofenac glucuronide, although the meaning of these data is unclear where the criterion for TDI (i.e. IC₅₀ ratio > 2) is not met. Although it is known that diclofenac glucuronide is hydroxylated at the 4'-position by CYP2C8 (Kumar et al. 2002), the putative site of metabolic activation that results in TDI is unknown.

Like gemfibrozil, diclofenac is a relatively weak inhibitor of CYP2C8 with co-incubation IC₅₀ values an order of magnitude higher than those of diclofenac glucuronide (Table 5.8). Of the single mutations, only the Thr107 mutants had a significant, albeit modest, effect on co-incubation IC₅₀. However, this parameter was significantly increased by all multiple mutations. As with gemfibrozil, diclofenac was not a TDI of CYP2C8.

Estradiol glucuronide was a weak competitive (or non-competitive) inhibitor of CYP2C8, with co-incubation IC₅₀ values an order of magnitude higher than those of the gemfibrozil- and diclofenac- glucuronides (Table 5.9). The single mutations had a

variable effect on co-incubation IC_{50} , with some exhibiting no significant effect (Ser100Ala) or an increase (Asn99Ala, Thr107Ala, Gln214Ala, Gln214Leu) or decrease (Ser103Ala, Thr107Val, Ser114Ala). As for diclofenac glucuronide, the largest change occurred with the Thr107Ala mutant where a 3.2-fold increase in co-incubation IC_{50} was observed. By contrast, there was an approximate 60% reduction in the co-incubation IC_{50} determined for the Thr107Val mutant. The differences between the two mutants presumably arise from the changes in CYP2C8 tertiary structure caused by the Val and Ala mutations (see previous discussion). All multiple mutations except Ser100Ala-Ser103Ala caused a similar increase (2.6- to 3.9-fold) in the pre-incubation (co-incubation) IC_{50} . Based on the IC_{50} ratio cut-off of 2 for TDI, estradiol glucuronide was a TDI of CYP2C8. However, the k_{inact}/K_I value (1.28 ml/ μ mol.min) was very low, one- and two-orders of magnitude lower than those for diclofenac glucuronide and gemfibrozil glucuronide, respectively. Although the mutations variably caused significant changes in the IC_{50} ratio and in k_{inact}/K_I , these should not be over-interpreted given the very weak TDI.

In summary, the data indicate that neither Ser100, Ser103, Ser114 nor Gln214 alone are critical for gemfibrozil glucuronide, diclofenac glucuronide and estradiol glucuronide binding to CYP2C8. Mutation of each of these amino acids generally had a modest or no effect on the ability of each glucuronide to inhibit CYP2C8-catalysed PAC 6 α -hydroxylation, either competitively/non-competitively or in a time-dependent manner. However, various combinations of the mutations (which also included Thr107Val) caused a reduction in inhibition efficiency, indicating that hydrogen bonding interactions with all of the amino acids contribute to the binding of each glucuronide within the CYP2C8 active site. Co-incubation inhibition data for the Asn99Ala mutant similarly suggest Asn99 alone is not critical for glucuronide binding.

Interpretation of the data for the Thr107 mutants is more problematic given the changes in tertiary structure that appear to occur upon substitution of this residue with Ala or Val, although the results suggest that Thr107 is similarly not critical for glucuronide binding (e.g. data for gemfibrozil glucuronide inhibition of Thr107Ala and diclofenac glucuronide inhibition of Thr107Val). Clearly, other binding modes (e.g. hydrophobic interactions with the aglycone) will contribute to glucuronide conjugate binding. In this regard, it was somewhat surprising to observe that a number of single mutations and various combination mutations of Ser100, Ser103, Thr107, Ser114 and Gln214 reduced gemfibrozil and diclofenac binding (as evidenced by a higher co-incubation IC₅₀ compared to the single mutants), although none of these residues were located within 4 Å of the bound ligand. This observation presumably reflects changes to the architecture of the active site that occur with multiple mutations. Nevertheless, binding of the aglycones, measured as co-incubation IC₅₀, was weaker than for the corresponding glucuronides.

A number of limitations are acknowledged. The first is the instability of the recombinant CYP2C8 enzymes, especially Asn99Ala, Thr107Ala and the multiple mutants, upon prolonged incubation with NADPH. This precluded TDI studies with these mutants, although available data indicated that lesser spontaneous loss of activity occurred with the shorter incubation times employed for the co-incubation experiments. Docking of ligands was performed using the ‘static’ CYP2C8 X-ray crystal structure when it is now known that CYP proteins are dynamic structures. The use of MDS may provide further insights into the binding of glucuronide conjugates within the wild-type CYP2C8 (and mutants) active site (Nair, McKinnon and Miners 2016a), although MDS is a time-consuming and computationally demanding procedure. Finally, binding of gemfibrozil glucuronide, gemfibrozil, diclofenac

glucuronide, diclofenac and estradiol glucuronide was measured indirectly from inhibition of PAC 6 α -hydroxylase activity, with binding efficiency assessed from the measurement of IC₅₀ and calculated $k_{\text{inact}}/K_{\text{I}}$ values, rather than from direct measurement of K_{i} and $k_{\text{inact}}/K_{\text{I}}$. However, measurement of individual kinetic constants for multiple mutants would have been immensely time consuming, and outside of the scope of this thesis. Further, and as discussed earlier, the IC₅₀ ratio and calculation of $k_{\text{inact}}/K_{\text{I}}$ from the shifted IC₅₀ are now considered a valid approach for assessment of TDI potential and efficiency, respectively.

CHAPTER 6

GENERAL DISCUSSION AND CONCLUSIONS

As described in Chapter 1 (Section 1.8.2), the overarching theme of the studies described in this thesis is the *in vitro* characterisation of DDIs. Two studies characterised potential DDIs arising from the inhibition of UGT enzymes while the third investigated the molecular basis of the inhibition of cytochrome P450, specifically CYP2C8, by glucuronide conjugates. DDIs arising from inhibition of drug metabolising enzymes are considered to be a significant cause of drug-related toxicity, and it has been suggested that the incidence of inhibitory DDIs may be under-estimated since only the most obvious are recorded (Rowland-Yeo and Tucker 2016). Furthermore, inhibitory DDIs are often difficult to identify as they are not defined by the pharmacological actions of the drug. As indicated in Section 1.6.1, DDIs also represent a potential economic loss and marketing disadvantage to the pharmaceutical industry. Several drugs (e.g. astemizole, cerivastatin, cisapride, mibefradil, nefazodone, and terfenadine) have been withdrawn from the market due to DDIs (Rowland-Yeo and Tucker 2016; Wienkers and Heath 2005). Assessment of the DDI potential of new drugs is now mandated by the U.S. Food and Drug Administration and the European Medicines Agency (European Medicines Agency (EMA) 2012; Food and Drug Administration (FDA) 2012; 2017).

The studies detailed in Chapter 3 primarily sought to characterise the inhibition of UGT2B10 by 34 amine-containing antidepressant and antipsychotic drugs and identify potential perpetrators of DDIs. UGT2B10 was first cloned in this laboratory in 1993 (Jin et al. 1993), and was thought to be an ‘orphan’ enzyme because it lacked activity towards prototypic UGT substrates containing a hydroxyl or carboxylic acid functional group. Later studies demonstrated that the inability of UGT2B10 to catalyse O-

glucuronidation reactions arose from the lack of an N-terminal domain histidine residue that functions as the catalytic base (Kerdpin et al. 2009). UGT1A4 is the only other enzyme in UGT families 1 and 2 that lacks the near-conserved N-terminal domain His. As described in Section 3.1, UGT2B10, like UGT1A4, was subsequently shown to catalyse the N-glucuronidation of amine-containing substrates, especially those containing an aliphatic tertiary amine or aromatic N-heterocyclic group. Although many clinically-used drugs contain an aliphatic amine or N-heterocyclic group, the inhibition selectivity of UGT2B10 has not been explored in a systematic manner.

Prior to screening for the inhibition of UGT2B10 by amine-containing drugs, it was necessary to confirm the selectivity of putative substrate and inhibitor ‘probes’ for UGT2B10. As emphasised in Section 1.8.1, the availability of enzyme selective substrates and inhibitors is essential for reaction phenotyping and for characterising enzyme inhibition when HLM (and hepatocytes) are used as the enzyme source. Thus, initial experiments confirmed that cotinine is a selective substrate of UGT2B10, and desloratadine is a selective inhibitor. The IC_{50} for desloratadine inhibition of UGT2B10 was 3.9 μ M, which is approximately 80% lower than the IC_{50} (18.9 μ M) for the next most potently inhibited enzyme (UGT2B4). The availability of UGT enzyme selective inhibitors for reaction phenotyping has lagged behind the identification of CYP enzyme selective inhibitors. Based on current data (Section 1.8.1 and Chapter 3), there is reasonable evidence to suggest that atazanavir/sorafenib, hecogenin, niflumic acid (2.5 μ M)/digoxin, and desloratadine are selective inhibitors of UGT1A1, UGT1A4, UGT1A9 and UGT2B10, respectively, whereas data for selective inhibition of other enzymes is less convincing. In this regard, results presented in Chapter 3 demonstrated that fluconazole, which was thought to be a

selective inhibitor of UGT2B7/2B4 (Raungrut et al. 2010; Uchaipichat et al. 2006a), inhibited UGT2B10 with an IC_{50} comparable to those for UGT2B7 and UGT2B4. Thus, caution should be exercised when fluconazole is used for reaction phenotyping. The identification of UGT enzyme selective inhibitors suitable for reaction phenotyping represents an ongoing challenge, especially for UGT2B7 which is considered one of the most important drug metabolising UGTs (Miners, Mackenzie and Knights 2010a).

Initial experiments conducted in Chapter 3 additionally sought to determine whether addition of BSA to incubations enhanced human liver microsomal UGT2B10 activity. As described in Section 1.8.3, addition of BSA (1 – 2%, w/v) to incubations of HLM reduces the K_m values of substrates for numerous UGT and CYP enzymes, with the largest reductions (as much as 90%) observed for substrates of UGT1A9, UGT2B7 and CYP2C9. In turn, this increases the *in vitro* Cl_{int} by about an order of magnitude and improves *in vivo* clearance prediction. Of relevance to the studies performed here, addition of BSA to incubations also results in a reduction in the measured K_i values of inhibitors of enzymes for which the ‘albumin effect’ is observed. This was first demonstrated for the fluconazole – zidovudine interaction (Uchaipichat et al. 2006b). The mean K_i values for inhibition of human liver microsomal zidovudine glucuronidation (a reaction catalysed primarily by UGT2B7) measured in the absence and presence of BSA were 1,133 μ M and 145 μ M, respectively. Use of the latter value for IV-IVE provided a predicted increase (~ 2-fold) in the zidovudine AUC-ratio that was in excellent agreement with the increase reported in patients.

Addition of BSA (1% w/v) to incubations of HLM resulted in a 45% reduction in the K_m for cotinine glucuronidation, and a small (11%) but statistically significant increase in V_{max} , resulting in an approximate 50% increase in Cl_{int} . The magnitude of the

decrease in K_m is smaller than changes observed for most other human liver microsomal UGTs (e.g. UGT 1A9, 2B4, 2B7) studied in this laboratory. An increase in V_{max} that is generally substantially smaller than the change in K_m has also been reported by some authors for substrates of other UGT enzymes, for example UGT1A9 (Manevski et al. 2011). Based on the results reported in Chapter 3, subsequent inhibition studies performed to generate K_i values included BSA in the incubation medium.

Twenty two antidepressant drugs from different therapeutic classes along with the dimethylated metabolites of amitriptyline and imipramine, and 10 antipsychotic drugs were screened for inhibition of recombinant UGT2B10. Of these compounds, the side-chains of four contained a primary amine, 7 contained a secondary amine, 21 a tertiary amine, and one (phenelzine) a hydrazine. All but 6 drugs (citalopram, desvenlafaxine, fluvoxamine, haloperidol, tranlycypromine, and olanzapine) had IC_{50} values $< 100 \mu M$; the structures of these compounds overlaid poorly on the structure of amitriptyline, one of the most potent inhibitors identified. By contrast, moderate (IC_{50} 20 – 100 μM) to potent ($IC_{50} < 10 \mu M$) inhibitors all overlaid well on the structure of amitriptyline. The moderate to potent inhibitors all contained a hydrophobic domain (comprising a tetra-, tri- or bi-cyclic ring structure or a single aromatic ring as the central ‘scaffold’) and an amine (or hydrazine) functional group that was most commonly located 3 C-C or C-N bond lengths from the central scaffold.

Overall, the data indicate that specific chemical and stereochemical features are required for inhibition of UGT2B10. Since the side-chain amine functional group will be charged at physiological pH, both charge and hydrophobic interactions appear to be important for inhibitor binding. It is possible that the side-chain amine interacts electrostatically with the side-chain of an acidic amino acid (aspartic or glutamic acid).

For example, it is known that glutamate-216 and aspartate-301 are key binding residues for the typically basic nitrogen containing substrates of CYP2D6 (Paine et al. 2003; Rowland et al. 2006b). The N-terminal domain of UGT2B10 contains 12 aspartic acid and 16 glutamic acid residues. Although amino acids that interact with the side-chain amine could potentially be identified by site-directed mutagenesis, selection of putative binding residues is not feasible in the absence of a protein homology model.

The five most potent inhibitors of UGT2B10 were amitriptyline, desloratadine, doxepin, loratadine, and mianserin; the side-chains of all but desloratadine contain a tertiary amine. While this might suggest that potent inhibition normally requires the presence of a tertiary amine containing side-chain, most tertiary amines studied were moderate or even weak inhibitors of UGT2B10 (Table 3.4). By contrast, spatial features were important for potent inhibition. Compared to other tricyclic antidepressants, amitriptyline and doxepin contain a dibenzocycloheptene (rather than a dihydrobenzazepine) central scaffold, which is inherently more rigid with fewer degrees of freedom. Similarly, desloratadine, loratadine and mianserin contain a rigid central scaffold, due either to the presence of a ‘fused’ tetracycle (mianserin) or a tricyclic group bound to a fourth ring by an exocyclic double bond. As noted in Chapter 3, the conformational rigidity of tricyclic antidepressants has also been proposed as being of importance for receptor binding affinity. There have been few systematic studies of the inhibitor selectivity of UGT enzymes. This work shows that a combination of *in vitro* inhibition and computational modelling approaches can provide important insights into the structural basis UGT enzyme inhibition selectivity, even in the absence of a protein X-ray crystal structure.

Given the potent inhibition of recombinant UGT2B10 observed for amitriptyline,

doxepin and mianserin, K_i values were generated with HLM (+ BSA) as the enzyme source to assess DDI potential. K_i values ranged from 0.43 to 0.95 μM . IV-IVE based on the maximum total inhibitor (i.e. amitriptyline, doxepin or mianserin) concentration in plasma suggested an approximate doubling in the AUC-ratio for a victim drug eliminated solely by UGT2B10 catalysed glucuronidation. However, a minor increase in the AUC-ratio is predicted when unbound concentration of the inhibitor is used for IV-IVE. This aspect of IV-IVE will be discussed subsequently. Nortriptyline, which forms as an active metabolite of amitriptyline, was also found to inhibit UGT2B10. Enhanced inhibition following amitriptyline administration is unlikely, however, since the IC_{50} for nortriptyline inhibition of UGT2B10 is an order of magnitude higher than that of amitriptyline.

At present, inhibition of UGT2B10 would appear to be of minor relevance since few drugs appear to be cleared to a major extent by this enzyme. There has been a recent report, however, that UGT2B10 is the main enzyme involved in the metabolism of RO5263397, an antipsychotic drug in clinical development (Fowler et al. 2015). As described in Section 3.1, the commonly used antihistamine desloratadine (marketed in Australia as Aeries) is a substrate of UGT2B10, and additionally forms as the active metabolite of loratadine (Claratyne). UGT2B10 catalysed N-glucuronidation followed by CYP2C8-catalysed 3-hydroxylation and deconjugation is the major metabolic pathway of desloratadine (Kazmi et al. 2015a; Kazmi et al. 2015b). Thus, inhibition of UGT2B10 may impair the elimination of desloratadine. Conversely, co-administration of desloratadine or loratadine with amitriptyline, doxepin or mianserin could result in augmented inhibition of UGT2B10 given their comparable IC_{50} 's. Given the past lack of selective substrate and inhibitor probes for UGT2B10, it is possible that the contribution of UGT2B10 to drug N-glucuronidation may be under-estimated in

favour of UGT1A4 (see Section 3.1). Also in this regard it should be noted that, although Supersome-expressed UGT2B10 has good activity (as described in Chapter 3), UGT2B10 expressed in some laboratories may be less reliable for activity screening studies. For example, UGT2B10 expressed in this laboratory in HEK293 cells has very low activity and the UGT2B10 expressed in insect cells by Finel and colleagues is relatively unstable (M Finel, personal communication to JO Miners).

Studies described in Chapter 4 continued the theme of the *in vitro* characterisation of human UGT inhibition. As described in Section 4.1, SGLT2 inhibitors are a new class of drugs (referred to as ‘flozins’) used to treat type 2 diabetes. Early evidence indicates that flozin treatment is associated with improved morbidity and mortality. Flozins contain a C- or O-glucoside moiety, which is essential for SGLT2 inhibition. The first three flozins introduced into clinical practice, canagliflozin (CNF), dapagliflozin (DPF) and empagliflozin (EPF), are C-glucosides (Figure 4.3) and all are metabolised by glucuronidation, typically at the 2- and 3-hydroxy groups of the glucoside ring. UGT1A9 is involved in the glucuronidation of all three drugs (Section 4.1). Given CNF, DPF and EPF all contain a glycoside ring and are metabolised via glucuronidation, it was postulated they may potentially inhibit human UGT enzymes.

As predicted, the three flozins inhibited UGT enzyme activity to some extent. CNF and DPF inhibited UGT1A1, UGT1A9 and the extrahepatic UGT1A10 to the greatest extent. However, there were differences in the potencies of inhibition. IC₅₀ values for CNF inhibition of these enzymes ranged from 6.9 to 9.5 µM, whereas the IC₅₀ range for DPF was 39 to 66 µM. EPF also inhibited UGT1A1 and UGT1A9, but IC₅₀ values were higher still (92 and 64 µM, respectively). Since the three flozins share in common a C-glucoside, the data indicate that the aglycone moiety has a major influence on the potency of inhibition. Too few compounds were studied here to meaningfully assess

the structural features that affect potency of inhibition, although it is noteworthy that CNF contains an S-containing thiophene ring. As indicated previously, CNF, DPF and EPF are glucuronidated by UGT1A9, and this was the enzyme most potently inhibited. UGT1A1 was the other common enzyme inhibited by CNF, DPF and EPF. Studies in his laboratory suggest that UGT1A9 substrates not uncommonly inhibit UGT1A1, and *vice versa*. For example, the protein kinase inhibitors regorafenib and sorafenib are glucuronidated by UGT1A9 but are remarkably potent inhibitors of UGT1A1, with K_i values < 50 nM (Miners et al. 2017a). The K_i 's for inhibition of UGT1A1 are an order of magnitude lower than for UGT1A9. Conversely, niflumic acid is glucuronidated by UGT1A1 but is a much more potent inhibitor of UGT1A9 (Miners et al. 2011).

IV-IVE based on the total C_{max} of CNF predicted increases in the AUC-ratio for a victim drug glucuronidated solely by UGT1A1 or UGT1A9 ranging from 118 – 249% and 193 – 457%, respectively. CNF is highly bound to plasma protein and, not unexpectantly, use of the unbound CNF C_{max} for IV-IVE predicted clinically insignificant inhibition *in vivo*. As for the inhibition of UGT2B10 by amitriptyline, doxepin and mianserin, it was not possible to determine the hepatic input concentration of the perpetrator since values of k_a and the fraction of the dose absorbed (and escaping gut wall metabolism) are unknown. As discussed earlier, the FDA have proposed default values of 0.1 min^{-1} and 1 for k_a and $F_a \cdot F_g$, respectively. However, adoption of these values is likely to over-estimate the concentration of inhibitor ([I]) in many cases. Alternatively, [I] can be estimated as the unbound concentration of inhibitor in plasma (European Medicines Agency (EMA) 2012; Food and Drug Administration (FDA) 2012; 2017). As noted in Chapter 1, the EMA Guidance recommends the use of maximal unbound plasma concentration of inhibitor whereas the 2012 FDA Guidance recommends the use of total (bound plus unbound) inhibitor concentration. Of note,

the FDA Guidance was updated in late 2017 (after the studies described in Chapters 3 and 4 had been published) and, like the EMA Guidance, recommends the use of maximal unbound concentration of the perpetrator for IV-IVE.

There are mixed results from studies that have investigated whether the use of total or unbound C_{\max} /hepatic input concentration best predicts the magnitude of a DDI arising from inhibition of UGT, even when f_m (the fraction of victim drug clearance mediated by the inhibited enzyme) is taken into account. The fluconazole – zidovudine and regorafenib/sorafenib – bilirubin interactions were well predicted using the unbound hepatic input and the unbound plasma maximum inhibitor concentration, respectively (Miners et al. 2017a; Uchaipichat et al. 2006b). By contrast, the magnitude of the valproic acid – lamotrigine and methadone – codeine interactions were well predicted using total maximum inhibitor hepatic input concentration (Raungrut et al. 2010; Rowland et al. 2006a). While it would be expected that the unbound inhibitor concentration in blood reflects the concentration in hepatocytes, Houston and colleagues have also reported that the use of total drug hepatic input concentration provides reasonable prediction of DDI magnitude for victim drugs metabolised by CYP enzymes (Brown et al. 2005; Ito et al. 2005).

Irrespective of which approach is adopted, it is presumed that the use of total drug C_{\max} , as recommended initially by the FDA, provides a ‘worst case’ scenario. That said, while inhibition of UGT1A1 and UGT1A9 by CNF *in vivo* cannot be discounted, there is currently no evidence to suggest that CNF acts as a perpetrator of DDIs, including the development of jaundice due to inhibition of UGT1A1-catalysed bilirubin glucuronidation. Nevertheless, given the relatively potent inhibition of UGT1A1 and UGT1A9 by CNF, the screening of other SGLT2 inhibitors in clinical development (e.g. ertugliflozin, remogliflozin and sotogliflozin) is recommended.

As indicated in Section 4.1, all SGLT2 inhibitors are structurally related, sharing a glucoside ring as the structural ‘scaffold’. Similar considerations to those discussed above apply to the screening of a new drug metabolised primarily by UGT2B10 for inhibition by amitriptyline, desloratadine, doxepin, loratadine and mianserin. Taken together with the recent demonstration that regorafenib and sorafenib are extremely potent inhibitors of UGT1A1, and to a lesser extent UGT1A9 (Miners et al. 2017a), the data presented in Chapters 3 and 4 show that numerous drugs are able to inhibit UGT enzymes with K_i values in the low micromolar to nanomolar range and hence the potential for DDIs arising from impairment of UGT enzyme activity should not be ignored.

In Chapter 5, the focus changed from inhibition of glucuronide formation to inhibition of CYP2C8 by glucuronide conjugates. CYP2C8 is unique in the ability to oxidise glucuronides, due in part to its large active site. Numerous glucuronides are known to be metabolised by CYP2C8, and several of these act as inhibitors of CYP2C8 *in vitro* and *in vivo*. Amongst these, gemfibrozil and clopidogrel glucuronides are potent MBIs of CYP2C8 and are known to precipitate clinically important DDIs in patients. Docking of glucuronides in the X-ray crystal structure of CYP2C8 has implicated a number of polar amino acids, particularly in SRS1, in the binding of the glucuronide moiety. However, the role of these residues in glucuronide binding has not been verified by site-directed mutagenesis.

Molecular docking of the mechanism-based inhibitor gemfibrozil glucuronide and the diclofenac and estradiol glucuronides, both known to be glucuronidated by CYP2C8, in the CYP2C8 X-ray crystal structure confirmed that the side-chains of Asn99, Ser100, Ser103, Thr107, Ser114 and Gln214 were within hydrogen bonding distance to the polar groups of the glucuronide moiety. Based on these observations, eight

single mutants were generated by site-directed mutagenesis: Asn99Ala, Ser100Ala, Ser103Ala, Thr107Ala, Thr107Val, Ser114Ala, Gln214Ala and Gln214Leu. In addition, two double (Ser100Ala-Ser103Ala and Ser103Ala-Thr107Val), one triple (Ser100Ala-Ser103Ala-Thr107Val), one quadruple (Ser100Ala-Ser103Ala-Thr107Val-Ser114Ala), and two quintuple (Ser100Ala-Ser103Ala-Thr107Val-Ser114Ala-Gln214Ala and Ser100Ala-Ser103Ala-Thr107Val-Ser114Ala-Gln214Leu) mutants were generated to ascertain the extent to which interactions with Ser100, Ser103, Thr107, Ser114 and Gln214 might have an additive effect on glucuronide conjugate binding. The kinetics of PAC 6 α -hydroxylation, were characterised for each mutant. Non-TDI and TDI for the three glucuronides was assessed for wild-type CYP2C8 and each mutant as the IC₅₀ values from co-incubation and pre-incubation (in the presence of NADPH) experiments, respectively.

Previous work in this laboratory showed an approximate 50% loss of wild-type CYP2C8 activity when the recombinant enzyme was pre-incubated with NADPH (Polasek et al. 2004), and a similar finding was observed here. However, sufficient enzyme remained following pre-incubation for the characterisation of PAC 6 α -hydroxylation kinetics, suggesting enzyme was still in excess. While it was possible to measure the IC₅₀ from co-incubation experiments for each inhibitor with all mutants studied here, very high spontaneous loss of activity occurred when Asn99Ala, Thr107Ala and all multiple mutants were pre-incubated for 30 min in the presence of NADPH according to the TDI protocol. This was an unexpected result. Previous studies of MBI of CYP2C8 have generally employed HLM as the enzyme source, but site-directed mutagenesis requires the use of recombinant enzymes. There appear to be no studies that have formally investigated the stability of recombinant wild-type and mutant CYP2C8, or indeed other human CYP enzymes, when pre-incubated in the

presence of NADPH. Thus, it is unknown whether the instability relates to the expression system (e.g. *E. coli*, yeast, or baculoviral mediated expression in insect cells) used or some other factor(s). The low or absent activity of the mutant enzymes remaining after pre-incubation was a disappointing result given the amount of work involved in their generation, and prompts the need for a detailed investigation of recombinant CYP enzyme stability when used in TDI protocols.

Consistent with previous reports using HLM as the enzyme source, gemfibrozil glucuronide, but not gemfibrozil, was shown to be a potent MBI of wild-type CYP2C8. Results from the co-incubation experiments (assessed as IC_{50}) with all mutants and the pre-incubation experiments (assessed as IC_{50} ratio and k_{inact}/K_I) with the single mutants were generally consistent with the conclusion that no single amino acid (Asn99, Ser100, Ser103, Thr107, Ser114, Gln214) dominates gemfibrozil glucuronide binding. Rather, all six residues appear to contribute to the binding of the glucuronic acid moiety to a significant extent.

Both the diclofenac and estradiol glucuronides were weak to borderline TDIs of CYP2C8, with k_{inact}/K_I ratios that were 1- and 2- orders of magnitude lower than that of gemfibrozil glucuronide, respectively. Whereas the CYP2C8-catalysed metabolism of the diclofenac and estradiol glucuronides is hydroxylation of the aglycone, gemfibrozil glucuronide forms a reactive benzyl radical (Section 5.1). It would therefore appear that where hydroxylation of the aglycone occurs as the primary metabolic pathway, TDI is weak or absent. However, further studies are required to confirm this hypothesis.

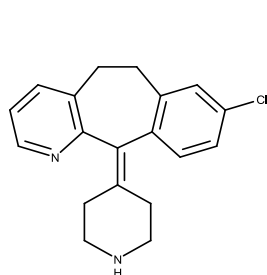
Interestingly, co-incubation IC_{50} values for the gemfibrozil and diclofenac glucuronides were similar, for wild-type CYP2C8 and most of the single mutants,

suggestive of similar binding affinities for competitive inhibition. By contrast, the co-incubation IC_{50} values for estradiol glucuronide with wild-type CYP2C8 and most single mutants were generally an order of magnitude higher. Although the single mutations had a variable effect on the co-incubation IC_{50} 's for diclofenac and (especially) estradiol glucuronide inhibition of the single mutants, when considered together with the results obtained for the multiple mutants it is evident that neither Asn99, Ser100, Ser103, Thr107, Ser114 nor Gln214 alone are 'critical' for glucuronide conjugate binding.

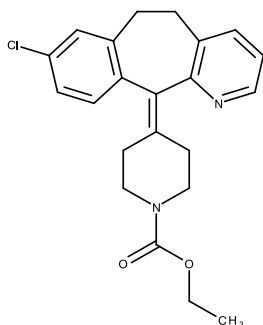
The rationale for substituting Asn99, Ser100, Ser103, Thr107, Ser114 and Gln214 with Ala was to replace the polar side-chains of these residues with an amino acid that was incapable of hydrogen bonding to the carboxylic acid and hydroxyl groups of glucuronic acid. Given Thr is a β -branched amino acid, Thr107 was also substituted with another β -branched amino acid, Val, in order to avoid potential changes in secondary and tertiary structure. Similarly, Gln214, which has a relatively large side-chain, was also substituted with Leu, a non-polar amino acid which has a similar volume to Gln. The high spontaneous loss of activity of Asn99Ala and Thr107Ala when pre-incubated with NADPH suggests the mutations resulted in an unstable protein, presumably due to secondary/tertiary structural changes. Similar considerations apply to the multiple mutants. However, unexpected changes were also observed with the Thr107Val mutation. Whereas most single mutations had an insignificant effect on the TDI efficiency (i.e. k_{inact}/K_I) of gemfibrozil glucuronide, the Thr107Val mutation increased k_{inact}/K_I by approximately 4-fold relative to wild-type CYP2C8. Molecular modelling of the Thr107 mutants indicated that the mutations not only abolish hydrogen bonding to the glucuronide moiety, but also disrupt the tertiary structure of the protein. Thus, interpretation of site-directed mutagenesis data in

isolation can be misleading. However, even when used in conjunction with ligand docking into the protein X-ray crystal structure, data interpretation is not straightforward. In the case of the Thr107Val mutation, the most energetically favoured pose unexpectedly had the orientation of gemfibrozil glucuronide inverted relative to wild-type CYP2C8. The application of molecular dynamics simulations may provide further insights into the effects of mutations on ligand docking (Nair, McKinnon and Miners 2016a), but this is a technically complex and computationally demanding technique.

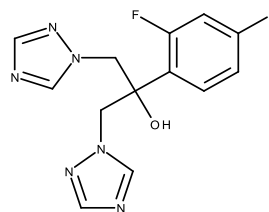
UGT Enzyme-Selective Inhibitors



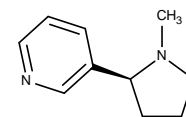
Desloratadine



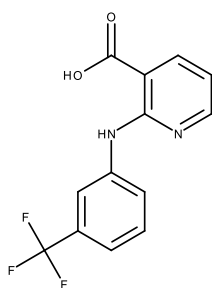
Loratadine
(desloratadine
precursor)



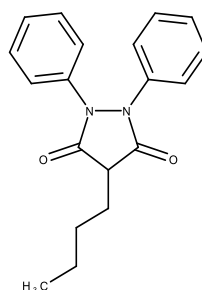
Fluconazole



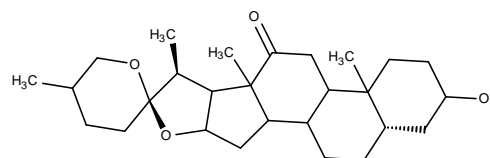
S-(-)-Nicotine



Niflumic acid

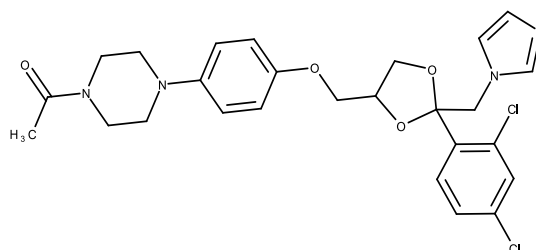


Phenylbutazone



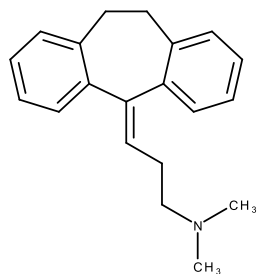
Hecogenin

Azoles

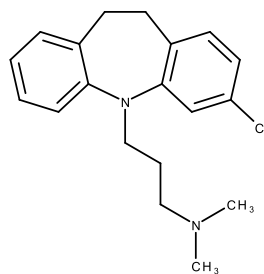


Ketoconazole

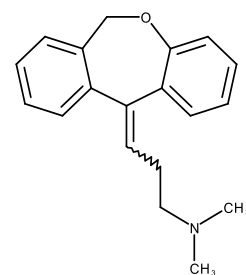
Appendix figure 1. Chemical structures of compounds screened as inhibitors of UGT2B10.

Tertiary amine

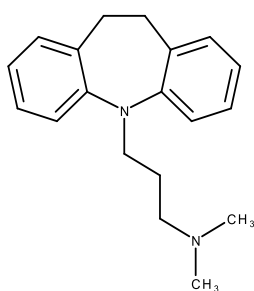
Amitriptyline



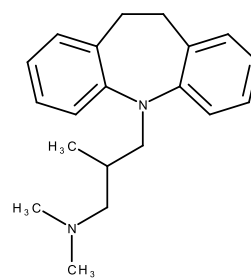
Clomipramine



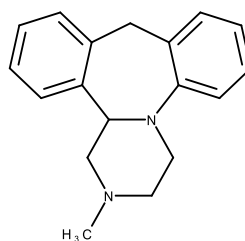
Doxepin



Imipramine

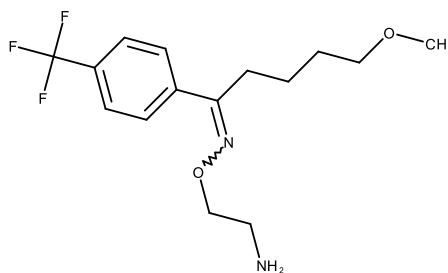


Trimipramine

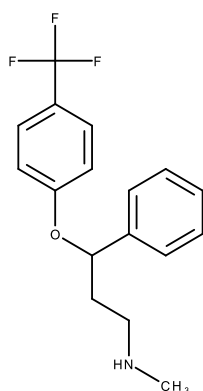
Tetracyclic-tertiary amine

Mianserin

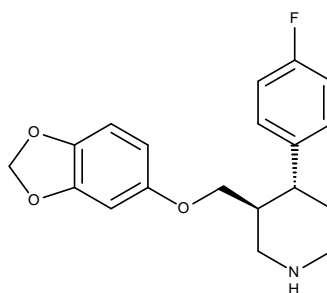
Appendix figure 1. Chemical structures of compounds screened as inhibitors of UGT2B10 (cont.).

Selective serotonin reuptake inhibitors (SSRIs)**Primary amine**

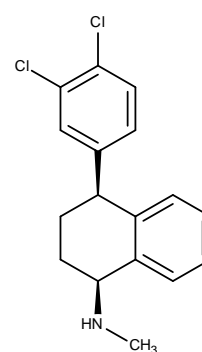
Fluvoxamine

Secondary amine

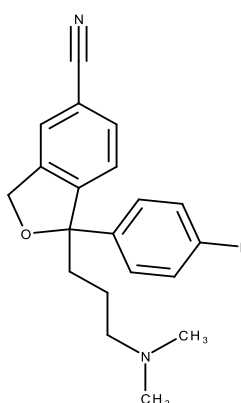
Fluoxetine



Paroxetine

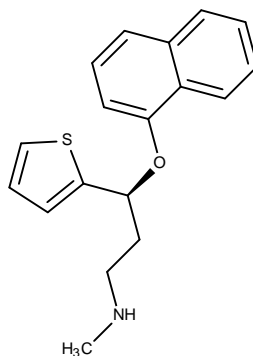


Sertraline

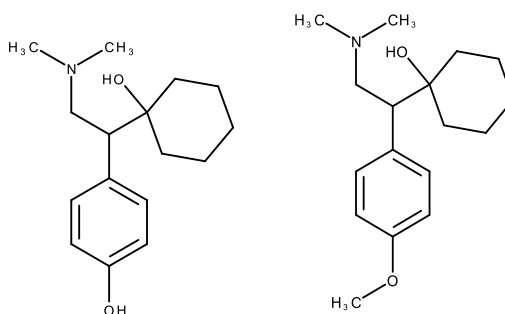
Tertiary amine

Citalopram

Appendix figure 1. Chemical structures of compounds screened as inhibitors of UGT2B10 (cont.).

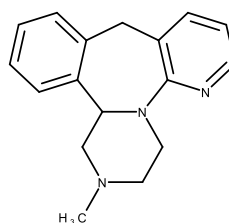
Serotonin norepinephrine reuptake inhibitors (SNRIs)**Secondary amine**

Duloxetine

Tertiary amine

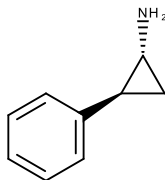
Desvenlafaxine

Venlafaxine

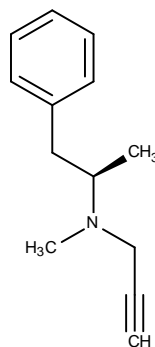
Serotonin receptor modulator (SRM)**Tertiary amine**

Mirtazapine

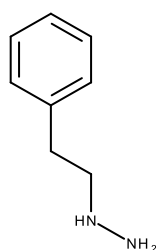
Appendix figure 1. Chemical structures of compounds screened as inhibitors of UGT2B10 (cont.).

Monoamine oxidase inhibitors (MAOIs)**Primary amine**

Tranylcypromine

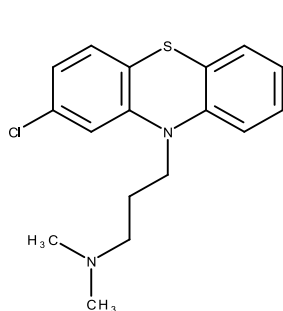
Tertiary amine

R-(-)-Selegiline

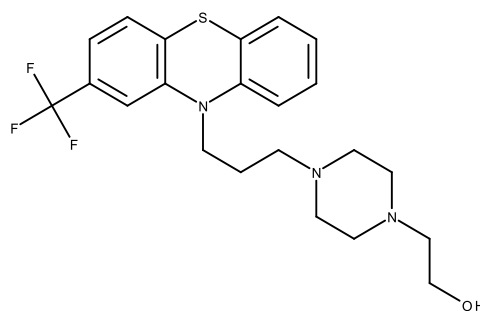
Hydrazine

Phenelzine

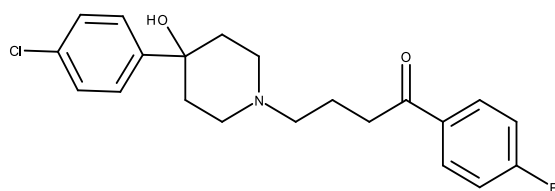
Appendix figure 1. Chemical structures of compounds screened as inhibitors of UGT2B10 (cont.).

Antipsychotics**Typical antipsychotics****Tertiary amine**

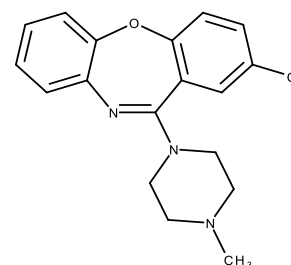
Chlorpromazine



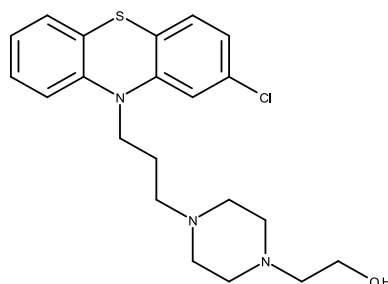
Fluphenazine



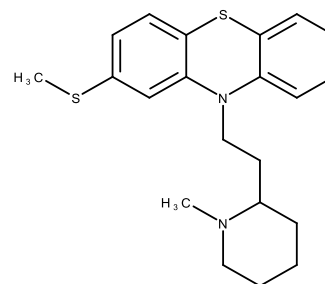
Haloperidol



Loxapine

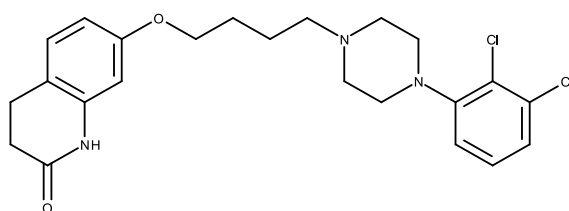


Perphenazine

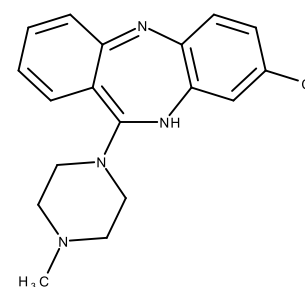


Thioridazine

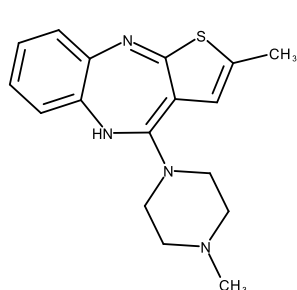
Appendix figure 1. Chemical structures of compounds screened as inhibitors of UGT2B10 (cont.).

*Atypical antipsychotics**Tertiary amine*

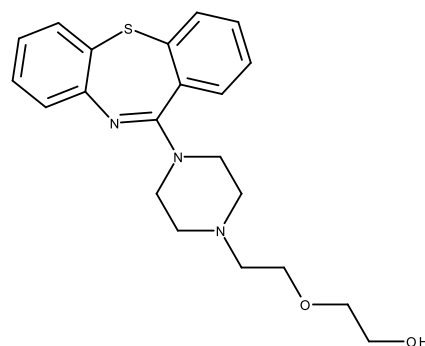
Aripiprazole



Clozapine



Olanzapine



Quetiapine

Appendix figure 1. Chemical structures of compounds screened as inhibitors of UGT2B10 (cont.).

REFERENCES

- Achour, B, Dantonio, A, Niosi, M, Novak, JJ, Fallon, JK, Barber, J, Smith, PC, Rostami-Hodjegan, A and Goosen, TC (2017), 'Quantitative characterization of major hepatic UDP-glucuronosyltransferase enzymes in human liver microsomes: Comparison of two proteomic methods and correlation with catalytic activity', *Drug Metabolism and Disposition*, 45 (10): 1102-1112.
- Albrecht, W, Unger, A, Nussler, AK and Laufer, S (2008), 'In vitro metabolism of 2-[6-(4-chlorophenyl)-2, 2-dimethyl-7-phenyl-2, 3-dihydro-1H-pyrrolizin-5-yl] acetic acid (licofelone, ML3000), an inhibitor of cyclooxygenase-1 and-2 and 5-lipoxygenase', *Drug Metabolism and Disposition*, 36 (5): 894-903.
- American Diabetes Association (2012), 'Standards of medical care in diabetes—2012', *Diabetes Care*, 35 (Suppl 1): S11-S63.
- American Diabetes Association (2015), 'Standards of medical care in diabetes—2015: Summary of revisions', *Diabetes Care*, 38 (Suppl 1): S4.
- Austin, RP, Barton, P, Cockroft, SL, Wenlock, MC and Riley, RJ (2002), 'The influence of nonspecific microsomal binding on apparent intrinsic clearance, and its prediction from physicochemical properties', *Drug Metabolism and Disposition*, 30 (12): 1497-1503.
- Australian Medicines Handbook (2014), 'Drugs for diabetes', *Australian Medicines Handbook Pty Ltd*, 408-422.
- Australian Medicines Handbook (2015), *Psychotropic drugs, in Australian Medicines Handbook*.
- Backman, JT, Filppula, AM, Niemi, M and Neuvonen, PJ (2016), 'Role of cytochrome P450 2C8 in drug metabolism and interactions', *Pharmacological Reviews*, 68 (1): 168-241.
- Backman, JT, Kyrklund, C, Neuvonen, M and Neuvonen, PJ (2002), 'Gemfibrozil greatly increases plasma concentrations of cerivastatin', *Clinical Pharmacology and Therapeutics*, 72 (6): 685-691.
- Baer, BR, DeLisle, RK and Allen, A (2009), 'Benzylic oxidation of gemfibrozil-1-O- β -glucuronide by P450 2C8 leads to heme alkylation and irreversible inhibition', *Chemical Research in Toxicology*, 22 (7): 1298-1309.
- Bailey, CJ, Gross, JL, Hennicken, D, Iqbal, N, Mansfield, TA and List, JF (2013), 'Dapagliflozin add-on to metformin in type 2 diabetes inadequately controlled with metformin: A randomized, double-blind, placebo-controlled 102-week trial', *BMC Medicine*, 11 (1): 43.
- Baraka, O, Truman, C, Ford, J and Roberts, C (1990), 'The effect of propranolol on paracetamol metabolism in man', *British Journal of Clinical Pharmacology*, 29 (2): 261-264.

- Barre, L, Fournel-Gigleux, S, Finel, M, Netter, P, Magdalou, J and Ouzzine, M (2007), 'Substrate specificity of the human UDP-glucuronosyltransferase UGT2B4 and UGT2B7', *The FEBS Journal*, 274 (5): 1256-1264.
- Barter, ZE, Bayliss, MK, Beaune, PH, Boobis, AR, Carlile, DJ, Edwards, RJ, Houston, JB, Lake, BG, Lipscomb, JC, Pelkonen, OR, Tucker, GT and Rostami-Hodjegan, A (2007), 'Scaling factors for the extrapolation of *in vivo* metabolic drug clearance from *in vitro* data: Reaching a consensus on values of human microsomal protein and hepatocellularity per gram of liver', *Current Drug Metabolism*, 8 (1): 33-45.
- Basile, JN (2013), 'The potential of sodium glucose cotransporter 2 (SGLT2) inhibitors to reduce cardiovascular risk in patients with type 2 diabetes (T2DM)', *Journal of Diabetes and Its Complications*, 27 (3): 280-286.
- Baumann, P, Jonzier-Perey, M, Koeb, L, K pfer, A, Tinguely, D and Sch pf, J (1986), 'Amitriptyline pharmacokinetics and clinical response: II. Metabolic polymorphism assessed by hydroxylation of debrisoquine and mephenytoin', *International Clinical Psychopharmacology*, 1 (2): 102-112.
- Benet, L (2009), *The drug transporter-metabolism alliance: Uncovering and defining the interplay in Molecular Pharmaceutics*, Vol. 6,
- Benowitz, NL, Perez-Stable, EJ, Fong, I, Modin, G, Herrera, B and Jacob, P (1999), 'Ethnic differences in N-glucuronidation of nicotine and cotinine', *Journal of Pharmacology and Experimental Therapeutics*, 291 (3): 1196-1203.
- Berry, LM and Zhao, Z (2008), 'An examination of IC₅₀ and IC₅₀-shift experiments in assessing time-dependent inhibition of CYP3A4, CYP2D6 and CYP2C9 in human liver microsomes', *Drug Metabolism Letters*, 2 (1): 51-59.
- Bertelsen, KM, Venkatakrisnan, K, Von Moltke, LL, Obach, RS and Greenblatt, DJ (2003), 'Apparent mechanism-based inhibition of human CYP2D6 *in vitro* by paroxetine: Comparison with fluoxetine and quinidine', *Drug Metabolism and Disposition*, 31 (3): 289-293.
- Bichlmaier, I, Finel, M, Sippl, W and Yli-Kauhaluoma, J (2007), 'Stereochemical and steric control of the UDP-glucuronosyltransferase-catalyzed conjugation reaction: A rational approach for the design of inhibitors for the human UGT2B7', *ChemMedChem*, 2 (12): 1730.
- Bj rkman, IK, Fastbom, J, Schmidt, IK, Bernsten, CB, Caramona, M, Crealey, G, Fr kj r, B, Gr nberger, E, Gustafsson, T, Henman, M, Herborg, H, Hughes, C, McElnay, JC, Magner, M, van Mil, F, Schaeffer, M, Silva, S, S ndergaard, B, Sturgess, I, Tromp, D, Vivero, L and Winterstein, A (2002), 'Drug—Drug Interactions in the elderly', *Annals of Pharmacotherapy*, 36 (11): 1675-1681.
- Boase, S and Miners, JO (2002), '*In vitro*—*in vivo* correlations for drugs eliminated by glucuronidation: Investigations with the model substrate zidovudine', *British Journal of Clinical Pharmacology*, 54 (5): 493-503.

- Bort, R, Ponsoda, X, Jover, R, Gómez-Lechón, MJ and Castell, JV (1999), 'Diclofenac toxicity to hepatocytes: a role for drug metabolism in cell toxicity', *Journal of Pharmacology and Experimental Therapeutics*, 288 (1): 65-72.
- Boyd, MA, Srasuebkul, P, Ruxrungtham, K, Mackenzie, PI, Uchaipichat, V, Stek Jr, M, Lange, JM, Phanuphak, P, Cooper, DA and Udomuksorn, W (2006), 'Relationship between hyperbilirubinaemia and UDP-glucuronosyltransferase 1A1 (UGT1A1) polymorphism in adult HIV-infected Thai patients treated with indinavir', *Pharmacogenetics and Genomics*, 16 (5): 321-329.
- Boye, S, Kerdpin, O, Elliot, D, Miners, JO, Kelly, L, McKinnon, R, Bhasker, C, Yoovathaworn, K and Birkett, D (2004), 'Optimizing bacterial expression of catalytically active human cytochromes P450: Comparison of CYP2C8 and CYP2C9', *Xenobiotica*, 34 (1): 49-60.
- Brand, T, Macha, S, Mattheus, M, Pinnetti, S and Woerle, HJ (2012), 'Pharmacokinetics of empagliflozin, a sodium glucose cotransporter-2 (SGLT-2) inhibitor, coadministered with sitagliptin in healthy volunteers', *Advances in Therapy*, 29 (10): 889-899.
- Brown, HS, Ito, K, Galetin, A and Houston, JB (2005), 'Prediction of *in vivo* drug–drug interactions from *in vitro* data: Impact of incorporating parallel pathways of drug elimination and inhibitor absorption rate constant', *British Journal of Clinical Pharmacology*, 60 (5): 508-518.
- Brown, HS, Wilby, AJ, Alder, J and Houston, JB (2010), 'Comparative use of isolated hepatocytes and hepatic microsomes for cytochrome P450 inhibition studies: Transporter-enzyme interplay', *Drug Metabolism and Disposition*, 38 (12): 2139-2146.
- Busby, WF, Ackermann, JM and Crespi, CL (1999), 'Effect of methanol, ethanol, dimethyl sulfoxide, and acetonitrile on *in vitro* activities of cDNA-expressed human cytochromes P-450', *Drug Metabolism and Disposition*, 27 (2): 246-249.
- Buxton, ILO and Benet, LZ (2011), 'Pharmacokinetics: The dynamics of drug absorption, distribution, metabolism, and elimination', In *Goodman & Gilman's: The Pharmacological Basis of Therapeutics, 12 edition*, eds LL Brunton, BA Chabner and BC Knollmann, Chapter 2: 19-39, McGraw-Hill, New York.
- Casarotto, MG and Craik, DJ (2001), 'Ring flexibility within tricyclic antidepressant drugs', *Journal of Pharmaceutical Sciences*, 90 (6): 713-721.
- Cerny, MA (2016), 'Prevalence of non-cytochrome P450-mediated metabolism in food and drug administration-approved oral and intravenous drugs: 2006-2015', *Drug Metabolism and Disposition*, 44 (8): 1246-1252.
- Chau, N, Elliot, DJ, Lewis, BC, Burns, K, Johnston, MR, Mackenzie, PI and Miners, JO (2014), 'Morphine glucuronidation and glucosidation represent complementary metabolic pathways that are both catalyzed by UDP-glucuronosyltransferase 2B7: Kinetic, inhibition, and molecular modeling studies', *Journal of Pharmacology and Experimental Therapeutics*, 349 (1): 126-137.

- Chen, G, Blevins-Primeau, AS, Dellinger, RW, Muscat, JE and Lazarus, P (2007), 'Glucuronidation of nicotine and cotinine by UGT2B10: Loss of function by the UGT2B10 Codon 67 (Asp> Tyr) polymorphism', *Cancer Research*, 67 (19): 9024-9029.
- Chen, G, Dellinger, RW, Sun, D, Spratt, TE and Lazarus, P (2008), 'Glucuronidation of tobacco-specific nitrosamines by UGT2B10', *Drug Metabolism and Disposition*, 36 (5): 824-830.
- Chen, G, Giambone, NE, Dluzen, DF, Muscat, JE, Berg, A, Gallagher, CJ and Lazarus, P (2010), 'Glucuronidation genotypes and nicotine metabolic phenotypes: Importance of functional UGT2B10 and UGT2B17 polymorphisms', *Cancer Research*, 70 (19): 7543-7552.
- Chen, G, Giambone, NE and Lazarus, P (2012), 'Glucuronidation of trans-3'-hydroxycotinine by UGT2B17 and UGT2B10', *Pharmacogenetics and Genomics*, 22 (3): 183.
- Chen, L-Z, Jungnik, A, Mao, Y, Philip, E, Sharp, D, Unsel, A, Seman, L, Woerle, H-J and Macha, S (2015), 'Biotransformation and mass balance of the SGLT2 inhibitor empagliflozin in healthy volunteers', *Xenobiotica*, 45 (6): 520-529.
- Cheng, Y-C and Prusoff, WH (1973), 'Relationship between the inhibition constant (K_i) and the concentration of inhibitor which causes 50 per cent inhibition (I_{50}) of an enzymatic reaction', *Biochemical Pharmacology*, 22 (23): 3099-3108.
- Correia, MA (2012), 'Drug biotransformation', In *Basic and Clinical Pharmacology, 12 edition*, eds BG Katzung and AJ Trevor, Chapter 4: 53-68, McGraw-Hill, New York.
- Court, MH, Zhang, X, Ding, X, Yee, KK, Hesse, LM and Finel, M (2012), 'Quantitative distribution of mRNAs encoding the 19 human UDP-glucuronosyltransferase enzymes in 26 adult and 3 fetal tissues', *Xenobiotica*, 42 (3): 266-277.
- Daly, AC, Rettie, AE and Miners, JO (2018), 'The pharmacogenetics of cytochrome P450 2C9: Functional and clinical implications', *Personalized Medicine*, In press.
- Daly, AK, Aithal, GP, Leathart, JB, Swainsbury, RA, Dang, TS and Day, CP (2007), 'Genetic susceptibility to diclofenac-induced hepatotoxicity: Contribution of UGT2B7, CYP2C8, and ABCC2 genotypes', *Gastroenterology*, 132 (1): 272-281.
- Dardi, I, Kouvatsos, T and Jabbour, SA (2016), 'SGLT2 inhibitors', *Biochemical Pharmacology*, 101: 27-39.
- Delaforge, M, Pruvost, A, Perrin, L and Andre, F (2005), 'Cytochrome P450-mediated oxidation of glucuronide derivatives: Example of estradiol-17 β -glucuronide oxidation to 2-hydroxy-estradiol-17 β -glucuronide by CYP 2C8', *Drug Metabolism and Disposition*, 33 (3): 466-473.

- Deshmukh, VS, Motghare, VM, Padwal, SL, Jaykare, S, Patil, J and Pise, H (2013), 'Newer drugs in the management of diabetes mellitus', *International Journal of Basic and Clinical Pharmacology*, 2 (1): 4-11.
- Devineni, D, Curtin, CR, Marbury, TC, Smith, W, Vaccaro, N, Wexler, D, Vandebosch, A, Rusch, S, Stieltjes, H and Wajs, E (2015a), 'Effect of hepatic or renal impairment on the pharmacokinetics of canagliflozin, a sodium glucose co-transporter 2 inhibitor', *Clinical Therapeutics*, 37 (3): 610-628.
- Devineni, D, Curtin, CR, Polidori, D, Gutierrez, MJ, Murphy, J, Rusch, S and Rothenberg, PL (2013), 'Pharmacokinetics and pharmacodynamics of canagliflozin, a sodium glucose co-transporter 2 inhibitor, in subjects with type 2 diabetes mellitus', *The Journal of Clinical Pharmacology*, 53 (6): 601-610.
- Devineni, D, Manitpisitkul, P, Murphy, J, Skee, D, Wajs, E, Mamidi, RNVS, Tian, H, Vandebosch, A, Wang, SS, Verhaeghe, T, Stieltjes, H and Usiskin, K (2015b), 'Effect of canagliflozin on the pharmacokinetics of glyburide, metformin, and simvastatin in healthy participants', *Clinical Pharmacology in Drug Development*, 4 (3): 226-236.
- Dubois, SG, Beaulieu, M, Lévesque, É, Hum, DW and Bélanger, A (1999), 'Alteration of human UDP-glucuronosyltransferase UGT2B17 regio-specificity by a single amino acid substitution', *Journal of Molecular Biology*, 289 (1): 29-39.
- Dutton, GJ (1980), 'Metabolic pathways immediately preceding and succeeding glucuronidation – Anabolic pathways', In *Glucuronidation of Drugs and Other Compounds*, eds GJ Dutton, Chapter 6: 83-96, CRC Press Inc, Boca Raton.
- Ekroos, M and Sjögren, T (2006), 'Structural basis for ligand promiscuity in cytochrome P450 3A4', *Proceedings of the National Academy of Sciences of the United States of America*, 103 (37): 13682-13687.
- El-Sherbeni, AA and El-Kadi, AOS (2017), 'Microsomal cytochrome P450 as a target for drug discovery and repurposing', *Drug Metabolism Reviews*, 49 (1): 1-17.
- Elliot, DJ, Suharjono, Lewis, BC, Gillam, EMJ, Birkett, DJ, Gross, AS and Miners, JO (2007), 'Identification of the human cytochromes P450 catalysing the rate-limiting pathways of gliclazide elimination', *British Journal of Clinical Pharmacology*, 64 (4): 450-457.
- Erickson-Ridout, KK, Zhu, J and Lazarus, P (2011), 'Olanzapine metabolism and the significance of UGT1A448V and UGT2B1067Y variants', *Pharmacogenetics and Genomics*, 21 (9): 539-551.
- European Medicines Agency (EMA) (2012), 'Guideline on the investigation of drug interactions'.

- Fallon, JK, Neubert, H, Goosen, TC and Smith, PC (2013), 'Targeted precise quantification of 12 human recombinant uridine-diphosphate glucuronosyl transferase 1A and 2B isoforms using nano-ultra-high-performance liquid chromatography/tandem mass spectrometry with selected reaction monitoring', *Drug Metabolism and Disposition*, 41 (12): 2076-2080.
- Faulkner, R, Pitts, W, Lee, C, Lewis, W and Fann, W (1983), 'Multiple-dose doxepin kinetics in depressed patients', *Clinical Pharmacology and Therapeutics*, 34 (4): 509-515.
- Ferrannini, E, Seman, L, Seewaldt-Becker, E, Hantel, S, Pinnetti, S and Woerle, H (2013), 'A Phase IIb, randomized, placebo-controlled study of the SGLT2 inhibitor empagliflozin in patients with type 2 diabetes', *Diabetes, Obesity and Metabolism*, 15 (8): 721-728.
- Fisher, MB, Campanale, K, Ackermann, BL, Vandenbranden, M and Wrighton, SA (2000), 'In vitro glucuronidation using human liver microsomes and the pore-forming peptide alamethicin', *Drug Metabolism and Disposition*, 28 (5): 560-566.
- Flockhart, DA (1995), 'Drug interactions and the cytochrome P450 system: The role of cytochrome P450 2C19', *Clinical Pharmacokinetics*, 29 (1): 45-52.
- Food and Drug Administration (FDA) (2012), 'Guidance for industry: Drug interaction studies-study design, data analysis, implications for dosing, and labeling recommendations', *Draft Guidance*. (<http://www.fda.gov/Drugs/DevelopmentApprovalProcess/DevelopmentResources/DrugInteractionsLabeling/ucm093664.htm>)
- Food and Drug Administration (FDA) (2017), 'Guidance for industry: In vitro metabolism- and transporter-mediated drug-drug interaction studies', *Draft Guidance*.
- Foote, C, Perkovic, V and Neal, B (2012), 'Effects of SGLT2 inhibitors on cardiovascular outcomes', *Diabetes and Vascular Disease Research*, 9 (2): 117-123.
- Foti, R and Fisher, M (2003), 'Characterization of cytochrome P450 3A4 and 3A5 levels in a human liver microsome bank using midazolam and paclitaxel metabolic activity and immunoquantitation', *Drug Metabolism Reviews*, 35: 34-34.
- Foti, RS and Fisher, MB (2012), 'UDP-Glucuronosyltransferases: Pharmacogenetics, functional characterization, and clinical relevance', In *Encyclopedia of Drug Metabolism and Interactions*, eds AV Lyubimov, Chapter 15: 1-71, John Wiley & Sons Hoboken, New Jersey.
- Fowler, S, Kletzl, H, Finel, M, Manevski, N, Schmid, P, Tuerck, D, Norcross, RD, Hoener, MC, Spleiss, O and Iglesias, VA (2015), 'A UGT2B10 splicing polymorphism common in African populations may greatly increase drug exposure', *Journal of Pharmacology and Experimental Therapeutics*, 352 (2): 358-367.

Friedrich, C, Metzmann, K, Rose, P, Mattheus, M, Pinnetti, S and Woerle, HJ (2013), 'A randomized, open-label, crossover study to evaluate the pharmacokinetics of empagliflozin and linagliptin after coadministration in healthy male volunteers', *Clinical Therapeutics*, 35 (1): A33-A42.

Fuhr, U, Jetter, A and Kirchheiner, J (2007), 'Appropriate phenotyping procedures for drug metabolizing enzymes and transporters in humans and their simultaneous use in the "cocktail" approach', *Clinical Pharmacology and Therapeutics*, 81 (2): 270-283.

Fujiwara, R, Nakajima, M, Yamanaka, H and Yokoi, T (2009), 'Key amino acid residues responsible for the differences in substrate specificity of human UDP-glucuronosyltransferase (UGT) 1A9 and UGT1A8', *Drug Metabolism and Disposition*, 37 (1): 41-46.

Gaganis, P, Miners, JO and Knights, KM (2007), 'Glucuronidation of fenamates: kinetic studies using human kidney cortical microsomes and recombinant UDP-glucuronosyltransferase (UGT) 1A9 and 2B7', *Biochemical Pharmacology*, 73 (10): 1683-1691.

Galetin, A, Burt, H, Gibbons, L and Houston, JB (2006), 'Prediction of time-dependent CYP3A4 drug-drug interactions: Impact of enzyme degradation, parallel elimination pathways, and intestinal inhibition', *Drug Metabolism and Disposition*, 34 (1): 166-175.

Galetin, A, Clarke, SE and Houston, JB (2002), 'Quinidine and haloperidol as modifiers of CYP3A4 activity: Multisite kinetic model approach', *Drug Metabolism and Disposition*, 30 (12): 1512-1522.

Galetin, A, Gertz, M and Houston, JB (2008), 'Potential role of intestinal first-pass metabolism in the prediction of drug-drug interactions', *Expert Opinion on Drug Metabolism and Toxicology*, 4 (7): 909-922.

Gelston, EA, Coller, JK, Lopatko, OV, James, HM, Schmidt, H, White, JM and Somogyi, AA (2012), 'Methadone inhibits CYP2D6 and UGT2B7/2B4 *in vivo*: A study using codeine in methadone- and buprenorphine-maintained subjects', *British Journal of Clinical Pharmacology*, 73 (5): 786-794.

Ghosheh, O and Hawes, EM (2002), 'N-glucuronidation of nicotine and cotinine in human: Formation of cotinine glucuronide in liver microsomes and lack of catalysis by 10 examined UDP-glucuronosyltransferases', *Drug Metabolism and Disposition*, 30 (9): 991-996.

Giacomini, K, Huang, S-M, Tweedie, D, Benet, L, Brouwer, K, Chu, X, Dahlin, A, Evers, R, Fischer, V, Hillgren, K, Hoffmaster, K, Ishikawa, T, Keppler, D, Kim, R, Lee, C, Niemi, M, Polli, J, Sugiyama, Y, Swaan, P, Ware, J, Wright, S, Wah Yee, S, Zamek-Gliszczynski, M and Zhang, L (2010), 'Membrane transporters in drug development', *Nature Reviews Drug Discovery*, 9 (3): 215-236.

Giacomini, KM and Huang, SM (2013), 'Transporters in drug development and clinical pharmacology', *Clinical Pharmacology and Therapeutics*, 94 (1): 3.

Gibson, GG and Skett, P (2001), 'Pathways of drug metabolism', In *Introduction to Drug Metabolism, 3 edition*, eds GG Gibson and P Skett, Chapter 1: 1-36, Cengage Learning, Hampshire.

Gill, KL, Houston, JB and Galetin, A (2012), 'Characterization of *in vitro* glucuronidation clearance of a range of drugs in human kidney microsomes: Comparison with liver and intestinal glucuronidation and impact of albumin', *Drug Metabolism and Disposition*, 40 (4): 825-835.

Gonzalez, FJ, Coughtrie, M and Tukey, RH (2011), 'Drug metabolism', In *Goodman & Gilman's: The Pharmacological Basis of Therapeutics, 12 edition*, eds LL Brunton, BA Chabner and BC Knollmann, Chapter 6: 123-144, McGraw-Hill Education, New York.

Gotoh, O (1992), 'Substrate recognition sites in cytochrome P450 family 2 (CYP2) proteins inferred from comparative analyses of amino acid and coding nucleotide sequences', *Journal of Biological Chemistry*, 267 (1): 83-90.

Green, MD, King, CD, Mojarrabi, B, Mackenzie, PI and Tephly, TR (1998), 'Glucuronidation of amines and other xenobiotics catalyzed by expressed human UDP-glucuronosyltransferase 1A3', *Drug Metabolism and Disposition*, 26 (6): 507-512.

Green, MD and Tephly, TR (1998), 'Glucuronidation of amine substrates by purified and expressed UDP- glucuronosyltransferase proteins', *Drug Metabolism and Disposition*, 26 (9): 860-867.

Gregus, Z (2012), 'Mechanisms of toxicity', In *Casarett and Doull's Toxicology: The Basic Science of Poisons, 8 edition*, eds CD Klaassen, Chapter 3: 45-106, McGraw-Hill Education, New York.

Grempler, R, Thomas, L, Eckhardt, M, Himmelsbach, F, Sauer, A, Sharp, DE, Bakker, RA, Mark, M, Klein, T and Eickelmann, P (2012), 'Empagliflozin, a novel selective sodium glucose cotransporter-2 (SGLT-2) inhibitor: Characterisation and comparison with other SGLT-2 inhibitors', *Diabetes, Obesity and Metabolism*, 14 (1): 83-90.

Grime, KH, Bird, J, Ferguson, D and Riley, RJ (2009), 'Mechanism-based inhibition of cytochrome P450 enzymes: An evaluation of early decision making *in vitro* approaches and drug-drug interaction prediction methods', *European Journal of Pharmaceutical Sciences*, 36 (2): 175-191.

Grimm, SW, Einolf, HJ, Hall, SD, He, K, Lim, H-K, Ling, K-HJ, Lu, C, Nomeir, AA, Seibert, E and Skordos, KW (2009), 'The conduct of *in vitro* studies to address time-dependent inhibition of drug-metabolizing enzymes: A perspective of the pharmaceutical research and manufacturers of America', *Drug Metabolism and Disposition*, 37 (7): 1355-1370.

Guengerich, FP (2003), 'Cytochromes P450, drugs, and diseases', *Molecular Interventions*, 3 (4): 194.

Guengerich, FP (2005), 'Human cytochrome P450 enzymes', In *Cytochrome P450: Structure, Mechanism, and Biochemistry*, eds PRO de Montellano, Chapter 10: 377-530, Springer, Berlin.

Guengerich, FP (2010), 'Cytochrome P450 enzymes', In *Comprehensive toxicology*, 2 edition, eds CA McQueen, Chapter 4.04: 41-76, Elsevier Ltd, Kidlington.

Guengerich, FP (2015), 'Human cytochrome P450 enzymes', In *Cytochrome P450*, 4 edition, eds PRO de Montellano, Chapter 9: 523-785, Springer, New York.

Guengerich, FP, Waterman, MR and Egli, M (2016), 'Recent structural insights into cytochrome P450 function', *Trends in Pharmacological Sciences*, 37 (8): 625-640.

Guengerich, FP, Yun, CH and Macdonald, TL (1996), 'Evidence for a 1-electron oxidation mechanism in N-dealkylation of N,N-dialkylanilines by cytochrome P450 2B1: Kinetic hydrogen isotope effects, linear free energy relationships, comparisons with horseradish peroxidase, and studies with oxygen surrogates', *Journal of Biological Chemistry*, 271 (44): 27321-27329.

Guest, EJ, Rowland-Yeo, K, Rostami-Hodjegan, A, Tucker, GT, Houston, JB and Galetin, A (2011), 'Assessment of algorithms for predicting drug-drug interactions via inhibition mechanisms: Comparison of dynamic and static models', *British Journal of Clinical Pharmacology*, 71 (1): 72-87.

Guillemette, C, Lévesque, É and Rouleau, M (2014), 'Pharmacogenomics of human uridine diphospho-glucuronosyltransferases and clinical implications', *Clinical Pharmacology and Therapeutics*, 96 (3): 324-339.

Gundert-Remy, U, Bernauer, U, Blömeke, B, Döring, B, Fabian, E, Goebel, C, Hessel, S, Jäckh, C, Lampen, A, Oesch, F, Petzinger, E, Völkel, W and Roos, PH (2014), 'Extrahepatic metabolism at the body's internal-external interfaces', *Drug Metabolism Reviews*, 46 (3): 291-324.

Guo, J, Zhou, D and Grimm, SW (2011), 'Liquid chromatography–tandem mass spectrometry method for measurement of nicotine N-glucuronide: A marker for human UGT2B10 inhibition', *Journal of Pharmaceutical and Biomedical Analysis*, 55 (5): 964-971.

Hallifax, D, Foster, JA and Houston, JB (2010), 'Prediction of human metabolic clearance from *in vitro* systems: Retrospective analysis and prospective view', *Pharmaceutical Research*, 27 (10): 2150-2161.

Hallifax, D and Houston, JB (2009), 'Methodological uncertainty in quantitative prediction of human hepatic clearance from *in vitro* experimental systems', *Current Drug Metabolism*, 10 (3): 307-321.

Hanahan, D (1985), 'Techniques for transformation of E. coli.', In *DNA Cloning: A Practical Approach*, eds D Glover, Chapter 1: 109-135, IRL Press, Oxford.

- Häring, H-U, Merker, L, Seewaldt-Becker, E, Weimer, M, Meinicke, T, Broedl, UC and Woerle, HJ (2014), 'Empagliflozin as add-on to metformin in patients with type 2 diabetes: A 24-week, randomized, double-blind, placebo-controlled trial', *Diabetes Care*, 37 (6): 1650-1659.
- Häring, H-U, Merker, L, Seewaldt-Becker, E, Weimer, M, Meinicke, T, Woerle, HJ, Broedl, UC and Investigators, E-RMT (2013), 'Empagliflozin as add-on to metformin plus sulfonyleurea in patients with type 2 diabetes a 24-week, randomized, double-blind, placebo-controlled trial', *Diabetes Care*, 36 (11): 3396-3404.
- Heise, T, Seewaldt-Becker, E, Macha, S, Hantel, S, Pinnetti, S, Seman, L and Woerle, H (2013), 'Safety, tolerability, pharmacokinetics and pharmacodynamics following 4 weeks' treatment with empagliflozin once daily in patients with type 2 diabetes', *Diabetes, Obesity and Metabolism*, 15 (7): 613-621.
- Hollenberg, PF, Kent, UM and Bumpus, NN (2008), 'Mechanism-based inactivation of human cytochromes P450s: Experimental characterization, reactive intermediates, and clinical implications', *Chemical Research in Toxicology*, 21 (1): 189-205.
- Houston, JB (1994), 'Utility of *in vitro* drug metabolism data in predicting *in vivo* metabolic clearance', *Biochemical Pharmacology*, 47 (9): 1469-1479.
- Houston, JB and Galetin, A (2005), 'Modelling atypical CYP3A4 kinetics: Principles and pragmatism', *Archives of Biochemistry and Biophysics*, 433 (2): 351-360.
- Houston, JB and Galetin, A (2010), '*In vitro* techniques to study drug–drug interactions of drug metabolism: Cytochrome P450', In *Enzyme- and Transporter-Based Drug-Drug Interactions: Progress and Future Challenges*, eds KS Pang, AD Rodrigues and RM Peter, Chapter 7: 169-215, Springer, New York.
- Houston, JB and Kenworthy, KE (2000), '*In vitro-in vivo* scaling of CYP kinetic data not consistent with the classical Michaelis-Menten model', *Drug Metabolism and Disposition*, 28 (3): 246-254.
- Hrdina, PD, Lapierre, YD, McIntosh, B and Oyewumi, L (1983), 'Mianserin kinetics in depressed patients', *Clinical Pharmacology and Therapeutics*, 33 (6): 757-762.
- Hu, DG, Mackenzie, PI, McKinnon, RA and Meech, R (2016), 'Genetic polymorphisms of human UDP-glucuronosyltransferase (UGT) genes and cancer risk', *Drug Metabolism Reviews*, 48 (1): 47-69.
- Huang, SM and Rowland, M (2012), 'The role of physiologically based pharmacokinetic modeling in regulatory review', *Clinical Pharmacology and Therapeutics*, 91 (3): 542-549.
- Ieiri, I, Nishimura, C, Maeda, K, Sasaki, T, Kimura, M, Chiyoda, T, Hirota, T, Irie, S, Shimizu, H, Noguchi, T, Yoshida, K and Sugiyama, Y (2011), 'Pharmacokinetic and pharmacogenomic profiles of telmisartan after the oral microdose and therapeutic dose', *Pharmacogenetics and Genomics*, 21 (8): 495-505.

- International Diabetes Foundation (2014), 'IDF Diabetes Atlas', www.idf.org/diabetesatlas/update-2014.
- Invokana Prescribing Information (2013), 'Janssen Pharmaceuticals', Titusville, NJ, USA.
- Invokana Product Information (2013), 'Janssen-Cilag Pty Ltd', NSW, Australia.
- Ito, K, Brown, HS and Houston, JB (2004), 'Database analyses for the prediction of *in vivo* drug–drug interactions from *in vitro* data', *British Journal of Clinical Pharmacology*, 57 (4): 473-486.
- Ito, K, Hallifax, D, Obach, RS and Houston, JB (2005), 'Impact of parallel pathways of drug elimination and multiple cytochrome P450 involvement on drug–drug interactions: CYP2D6 paradigm', *Drug Metabolism and Disposition*, 33 (6): 837-844.
- Ito, K and Houston, J (2004), 'Comparison of the use of liver models for predicting drug clearance using *in vitro* kinetic data from hepatic microsomes and isolated hepatocytes', *An Official Journal of the American Association of Pharmaceutical Scientists*, 21 (5): 785-792.
- Ito, K, Iwatsubo, T, Kanamitsu, S, Ueda, K, Suzuki, H and Sugiyama, Y (1998), 'Prediction of pharmacokinetic alterations caused by drug–drug interactions: Metabolic interaction in the liver', *Pharmacological Reviews*, 50 (3): 387-412.
- Iwatsubo, T, Hirota, N, Ooie, T, Suzuki, H, Shimada, N, Chiba, K, Ishizaki, T, Green, CE, Tyson, CA and Sugiyama, Y (1997), 'Prediction of *in vivo* drug metabolism in the human liver from *in vitro* metabolism data', *Pharmacology and Therapeutics*, 73 (2): 147-171.
- Jaakkola, T, Backman, JT, Neuvonen, M and Neuvonen, PJ (2005), 'Effects of gemfibrozil, itraconazole, and their combination on the pharmacokinetics of pioglitazone', *Clinical Pharmacology and Therapeutics*, 77 (5): 404-414.
- Jabbour, SA, Hardy, E, Sugg, J and Parikh, S (2014), 'Dapagliflozin is effective as add-on therapy to sitagliptin with or without metformin: A 24-week, multicenter, randomized, double-blind, placebo-controlled study', *Diabetes Care*, 37 (3): 740-750.
- Jain, AN (2000), 'Morphological similarity: a 3D molecular similarity method correlated with protein-ligand recognition', *Journal of Computer-Aided Molecular Design*, 14 (2): 199-213.
- Jain, AN (2004), 'Ligand-based structural hypotheses for virtual screening', *Journal of Medicinal Chemistry*, 47 (4): 947-961.
- Jardiance Product Information (2015), 'Boehringer Ingelheim Pharmaceuticals, Inc.', Ridgefield, USA.

- Jenkins, SM, Zvyaga, T, Johnson, SR, Hurley, J, Wagner, A, Burrell, R, Turley, W, Leet, JE, Philip, T and Rodrigues, AD (2011), 'Studies to further investigate the inhibition of human liver microsomal CYP2C8 by the acyl- β -glucuronide of gemfibrozil', *Drug Metabolism and Disposition*, 39 (12): 2421-2430.
- Jeong, ES, Kim, YW, Kim, HJ, Shin, HJ, Shin, JG, Kim, KH, Chi, YH, Paik, SH and Kim, DH (2015), 'Glucuronidation of fimasartan, a new angiotensin receptor antagonist, is mainly mediated by UGT1A3', *Xenobiotica*, 45 (1): 10-18.
- Jin, C, Miners, J, Lillywhite, K and Mackenzie, P (1993), 'cDNA cloning and expression of two new members of the human liver UDP-glucuronosyltransferase 2B subfamily', *Biochemical and Biophysical Research Communications*, 194 (1): 496-503.
- Jin, CJ, Mackenzie, PI and Miners, JO (1997), 'The regio- and stereo-selectivity of C19 and C21 hydroxysteroid glucuronidation by UGT2B7 and UGT2B11', *Archives of Biochemistry and Biophysics*, 341 (2): 207-211.
- Johansson, I and Ingelman-Sundberg, M (2011), 'Genetic polymorphism and toxicology-with emphasis on cytochrome P450', *Toxicological Sciences*, 120 (1): 1-13.
- Johnson, EF (2003), 'The 2002 Bernard B. Brodie award lecture deciphering substrate recognition by drug-metabolizing cytochromes P450', *Drug Metabolism and Disposition*, 31 (12): 1532-1540.
- Johnson, EF, Connick, JP, Reed, JR, Backes, WL, Desai, MC, Xu, L, Estrada, DF, Laurence, JS and Scott, EE (2014), 'Correlating structure and function of drug-metabolizing enzymes: Progress and ongoing challenges', *Drug Metabolism and Disposition*, 42 (1): 9-22.
- Johnson, EF and Stout, CD (2005), 'Structural diversity of human xenobiotic-metabolizing cytochrome P450 monooxygenases', *Biochemical and Biophysical Research Communications*, 338 (1): 331-336.
- Johnson, EF and Stout, CD (2013), 'Structural diversity of eukaryotic membrane cytochrome P450s', *Journal of Biological Chemistry*, 288 (24): 17082-17090.
- Jones, AW (2015), 'Profiles in drug metabolism and toxicology: Richard Tecwyn Williams (1909-1979)', *Drug Metabolism Reviews*, 47 (4): 401-405.
- Jones, HM, Chen, Y, Gibson, C, Heimbach, T, Parrott, N, Peters, SA, Snoeys, J, Upreti, VV, Zheng, M and Hall, SD (2015), 'Physiologically based pharmacokinetic modeling in drug discovery and development: A pharmaceutical industry perspective', *Clinical Pharmacology and Therapeutics*, 97 (3): 247-262.
- Jones, HM and Houston, JB (2004), 'Substrate depletion approach for determining *in vitro* metabolic clearance: Time dependencies in hepatocyte and microsomal incubations', *Drug Metabolism and Disposition*, 32 (9): 973-982.

- Josephy, PD, Guengerich, FP and Miners, JO (2005), "Phase I and Phase II" drug metabolism: Terminology that we should phase out?', *Drug Metabolism Reviews*, 37 (4): 575-580.
- Kaivosaaari, S, Finel, M and Koskinen, M (2011), 'N-glucuronidation of drugs and other xenobiotics by human and animal UDP-glucuronosyltransferases', *Xenobiotica*, 41 (8): 652-669.
- Kaivosaaari, S, Toivonen, P, Hesse, LM, Koskinen, M and Finel, M (2007), 'Nicotine glucuronidation and the human UDP-glucuronosyltransferase UGT2B10', *Molecular Pharmacology*, 72 (3): 761-768.
- Kalgutkar, AS, Obach, RS and Maurer, TS (2007), 'Mechanism-based inactivation of cytochrome P450 enzymes: Chemical mechanisms, structure-activity relationships and relationship to clinical drug-drug interactions and idiosyncratic adverse drug reactions', *Current Drug Metabolism*, 8 (5): 407-447.
- Karonen, T, Filppula, A, Laitila, J, Niemi, M, Neuvonen, P and Backman, J (2010), 'Gemfibrozil markedly increases the plasma concentrations of montelukast: A previously unrecognized role for CYP2C8 in the metabolism of montelukast', *Clinical Pharmacology and Therapeutics*, 88 (2): 223-230.
- Kasichayanula, S, Chang, M, Liu, X, Shyu, W-C, Griffen, SC, LaCreta, FP and Boulton, DW (2012), 'Lack of pharmacokinetic interactions between dapagliflozin and simvastatin, valsartan, warfarin, or digoxin', *Advances in Therapy*, 29 (2): 163-177.
- Kasichayanula, S, Liu, X, Griffen, S, LaCreta, F and Boulton, D (2013a), 'Effects of rifampin and mefenamic acid on the pharmacokinetics and pharmacodynamics of dapagliflozin', *Diabetes, Obesity and Metabolism*, 15 (3): 280-283.
- Kasichayanula, S, Liu, X, LaCreta, F, Griffen, SC and Boulton, DW (2014), 'Clinical pharmacokinetics and pharmacodynamics of dapagliflozin, a selective inhibitor of sodium-glucose co-transporter type 2', *Clinical Pharmacokinetics*, 53 (1): 17-27.
- Kasichayanula, S, Liu, X, Pe Benito, M, Yao, M, Pfister, M, LaCreta, FP, Humphreys, WG and Boulton, DW (2013b), 'The influence of kidney function on dapagliflozin exposure, metabolism and pharmacodynamics in healthy subjects and in patients with type 2 diabetes mellitus', *British Journal of Clinical Pharmacology*, 76 (3): 432-444.
- Kasichayanula, S, Liu, X, Shyu, W, Zhang, W, Pfister, M, Griffen, S, Li, T, LaCreta, F and Boulton, D (2011a), 'Lack of pharmacokinetic interaction between dapagliflozin, a novel sodium-glucose transporter 2 inhibitor, and metformin, pioglitazone, glimepiride or sitagliptin in healthy subjects', *Diabetes, Obesity and Metabolism*, 13 (1): 47-54.
- Kasichayanula, S, Liu, X, Zhang, W, Pfister, M, LaCreta, FP and Boulton, DW (2011b), 'Influence of hepatic impairment on the pharmacokinetics and safety profile of dapagliflozin: An open-label, parallel-group, single-dose study', *Clinical Therapeutics*, 33 (11): 1798-1808.

- Kato, Y, Izukawa, T, Oda, S, Fukami, T, Finel, M, Yokoi, T and Nakajima, M (2013), 'Human UDP-glucuronosyltransferase (UGT) 2B10 in drug N-glucuronidation: Substrate screening and comparison with UGT1A3 and UGT1A4', *Drug Metabolism and Disposition*, 41 (7): 1389-1397.
- Kazmi, F, Barbara, JE, Yerino, P and Parkinson, A (2015a), 'A long-standing mystery solved: The formation of 3-hydroxydesloratadine is catalyzed by CYP2C8 but prior glucuronidation of desloratadine by UDP-glucuronosyltransferase 2B10 is an obligatory requirement', *Drug Metabolism and Disposition*, 43 (4): 523-533.
- Kazmi, F, Smith, B, Hvenegaard, M, Bendahl, L, Gipson, A, Buckley, D, Ogilvie, B and Parkinson, A (2010), 'Identification of a novel carbamoyl glucuronide as a metabolism-dependent inhibitor of CYP2C8', *Drug Metabolism Reviews*, 42 (S1): 143.
- Kazmi, F, Yerino, P, Barbara, JE and Parkinson, A (2015b), 'Further characterization of the metabolism of desloratadine and its cytochrome P450 and UDP-glucuronosyltransferase inhibition potential: Identification of desloratadine as a relatively selective UGT2B10 inhibitor', *Drug Metabolism and Disposition*, 43 (9): 1294-1302.
- Kenworthy, KE, Clarke, SE, Andrews, J and Houston, JB (2001), 'Multisite kinetic models for CYP3A4: Simultaneous activation and inhibition of diazepam and testosterone metabolism', *Drug Metabolism and Disposition*, 29 (12): 1644-1651.
- Kerdpin, O, Elliot, DJ, Boye, SL, Birkett, DJ, Yoovathaworn, K and Miners, JO (2004), 'Differential contribution of active site residues in substrate recognition sites 1 and 5 to cytochrome P450 2C8 substrate selectivity and regioselectivity', *Biochemistry*, 43 (24): 7834-7842.
- Kerdpin, O, Elliot, DJ, Mackenzie, PI and Miners, JO (2006), 'Sulfinpyrazone C-glucuronidation is catalyzed selectively by human UDP-glucuronosyltransferase 1A9', *Drug Metabolism and Disposition*, 34 (12): 1950-1953.
- Kerdpin, O, Knights, KM, Elliot, DJ and Miners, JO (2008), 'In vitro characterisation of human renal and hepatic frusemide glucuronidation and identification of the UDP-glucuronosyltransferase enzymes involved in this pathway', *Biochemical Pharmacology*, 76 (2): 249-257.
- Kerdpin, O, Mackenzie, PI, Bowalgaha, K, Finel, M and Miners, JO (2009), 'Influence of N-terminal domain histidine and proline residues on the substrate selectivities of human UDP-glucuronosyltransferase 1A1, 1A6, 1A9, 2B7, and 2B10', *Drug Metabolism and Disposition*, 37 (9): 1948-1955.
- Kiang, TK, Ensom, MH and Chang, TK (2005), 'UDP-glucuronosyltransferases and clinical drug-drug interactions', *Pharmacology and Therapeutics*, 106 (1): 97-132.
- Kilford, PJ, Stringer, R, Sohal, B, Houston, JB and Galetin, A (2009), 'Prediction of drug clearance by glucuronidation from *in vitro* data: use of combined cytochrome P450 and UDP-glucuronosyltransferase cofactors in alamethicin-activated human liver microsomes', *Drug Metabolism and Disposition*, 37 (1): 82-89.

- Kinne, RK and Castaneda, F (2011), 'SGLT inhibitors as new therapeutic tools in the treatment of diabetes', In *Diabetes-Perspectives in Drug Therapy*, eds M Schwanstecher, Volume 203: 105-126, Springer, Berlin.
- Kitz, R and Wilson, IB (1962), 'Esters of methanesulfonic acid as irreversible inhibitors of acetylcholinesterase', *Journal of Biological Chemistry*, 237 (10): 3245-3249.
- Knights, KM and Miners, JO (2010), 'Renal UDP-glucuronosyltransferases and the glucuronidation of xenobiotics and endogenous mediators', *Drug Metabolism Reviews*, 42 (1): 63-73.
- Knights, KM, Spencer, SM, Fallon, JK, Chau, N, Smith, PC and Miners, JO (2016a), 'Scaling factors for the *in vitro*-*in vivo* extrapolation (IV-IVE) of renal drug and xenobiotic glucuronidation clearance', *British Journal of Clinical Pharmacology*, 81 (6): 1153-1164.
- Knights, KM, Stresser, DM, Miners, JO and Crespi, CL (2016b), '*In vitro* drug metabolism using liver microsomes', *Current Protocols in Pharmacology*, 74 (1): 7.8. 1-7.8. 24.
- Korprasertthaworn, P, Rowland, A, Lewis, BC, Mackenzie, PI, Yoovathaworn, K and Miners, JO (2012), 'Effects of amino acid substitutions at positions 33 and 37 on UDP-glucuronosyltransferase 1A9 (UGT1A9) activity and substrate selectivity', *Biochemical Pharmacology*, 84 (11): 1511-1521.
- Kovacs, C, Seshiah, V, Swallow, R, Jones, R, Rattunde, H, Woerle, H and Broedl, U (2014), 'Empagliflozin improves glycaemic and weight control as add-on therapy to pioglitazone or pioglitazone plus metformin in patients with type 2 diabetes: a 24-week, randomized, placebo-controlled trial', *Diabetes, Obesity and Metabolism*, 16 (2): 147-158.
- Kristensen, CB, Gram, LF and Kragh-Sørensen, P (1985), 'Mianserin protein binding in serum and plasma from healthy subjects and patients with depression and rheumatoid arthritis', *Psychopharmacology*, 87 (2): 204-206.
- Kronbach, T, Mathys, D, Umeno, M, Gonzalez, FJ and Meyer, UA (1989), 'Oxidation of midazolam and triazolam by human liver cytochrome P450 3A4', *Molecular Pharmacology*, 36 (1): 89-96.
- Kubota, T, Lewis, BC, Elliot, DJ, Mackenzie, PI and Miners, JO (2007), 'Critical roles of residues 36 and 40 in the phenol and tertiary amine aglycone substrate selectivities of UDP-glucuronosyltransferases 1A3 and 1A4', *Molecular Pharmacology*, 72 (4): 1054-1062.
- Kuehl, GE and Murphy, SE (2003), 'N-glucuronidation of nicotine and cotinine by human liver microsomes and heterologously expressed UDP-glucuronosyltransferases', *Drug Metabolism and Disposition*, 31 (11): 1361-1368.

- Kukes, V, Kondratenko, S, Savelyeva, M, Starodubtsev, A and Gneushev, E (2009), 'Experimental and clinical pharmacokinetics of amitriptyline: Comparative analysis', *Bulletin of Experimental Biology and Medicine*, 147 (4): 434-437.
- Kumar, S, Samuel, K, Subramanian, R, Braun, MP, Stearns, RA, Chiu, S-HL, Evans, DC and Baillie, TA (2002), 'Extrapolation of diclofenac clearance from *in vitro* microsomal metabolism data: Role of acyl glucuronidation and sequential oxidative metabolism of the acyl glucuronide', *Journal of Pharmacology and Experimental Therapeutics*, 303 (3): 969-978.
- Lapham, K, Bauman, J, Walsky, R, Niosi, M, Orozco, C, Bourcier, K, Giddens, G, Obach, R and Hyland, R (2012), 'Digoxin and tranilast identified as novel isoform-selective inhibitors of human UDP-glucuronosyltransferase 1A9 (UGT1A9) activity', *Drug Metabolism Reviews*, 44 (Suppl 1): 82.
- Lapham, K, Novak, J, Niosi, M, Leung, LY and Goosen, TC (2016), 'The effect of bovine serum albumin on UDP-glucuronosyltransferase (UGT) 1A9 and 2B7 inhibitory potency', *Drug Metabolism Reviews*, 48 (Suppl 1): 88.
- Lee, BL, Täuber, MG, Sadler, B, Goldstein, D and Chambers, HF (1996), 'Atovaquone inhibits the glucuronidation and increases the plasma concentrations of zidovudine', *Clinical Pharmacology and Therapeutics*, 59 (1): 14-21.
- Leger, NP, Chirwa, MS, Nwogu, WJ, Turner, WM, Richardson, WD, Baker, WP, Leonard, WM, Erdem, WH, Olson, WL and Haas, WD (2018), 'Race/ethnicity difference in the pharmacogenetics of bilirubin-related atazanavir discontinuation', *Pharmacogenetics and Genomics*, 28 (1): 1-6.
- Lévesque, É, Turgeon, D, Carrier, J-S, Montminy, V, Beaulieu, M and Bélanger, A (2001), 'Isolation and characterization of the UGT2B28 cDNA encoding a novel human steroid conjugating UDP-glucuronosyltransferase', *Biochemistry*, 40 (13): 3869-3881.
- Lewis, BC, Mackenzie, PI, Elliot, DJ, Burchell, B, Bhasker, CR and Miners, JO (2007), 'Amino terminal domains of human UDP-glucuronosyltransferases (UGT) 2B7 and 2B15 associated with substrate selectivity and autoactivation', *Biochemical Pharmacology*, 73 (9): 1463-1473.
- Lewis, BC, Nair, PC, Heran, SS, Somogyi, AA, Bowden, JJ, Doogue, MP and Miners, JO (2016), 'Warfarin resistance associated with genetic polymorphism of VKORC1: linking clinical response to molecular mechanism using computational modeling', *Pharmacogenetics and Genomics*, 26 (1): 44-50.
- Li, P, Lu, C, Balani, SK and Gan, L-S (2011), 'A refined cytochrome P450 IC50 shift assay for reliably identifying CYP3A time-dependent inhibitors', *Drug Metabolism and Disposition*, 39 (6): 1054-1057.
- Li, P, Lu, C, Daniels, J, Labutti, J, Miwa, G and Gan, L (2005), 'A modified inhibition assay to identify CYP3A4 mechanism-based inhibitors', *Drug Metabolism Reviews*, 37 (Suppl 2): 254.

- Lin, JH and Lu, AYH (2001), 'Interindividual variability in inhibition and induction of cytochrome P450 enzymes', *Annual Review of Pharmacology and Toxicology*, 41: 535-567.
- Lowry, OH, Rosebrough, NJ, Farr, AL and Randall, RJ (1951), 'Protein measurement with the Folin phenol reagent', *Journal of Biological Chemistry*, 193 (1): 265-275.
- Ma, Y, Fu, Y, Khojasteh, SC, Dalvie, D and Zhang, D (2017), 'Glucuronides as potential anionic substrates of human cytochrome P450 2C8 (CYP2C8)', *Journal of Medicinal Chemistry*, 60 (21): 8691-8705.
- Macha, S, Lang, B, Pinnetti, S and Broedl, UC (2014a), 'Pharmacokinetics of empagliflozin, a sodium glucose cotransporter-2 inhibitor, and simvastatin following co-administration in healthy volunteers', *International Journal of Clinical Pharmacology and Therapeutics*, 52 (11): 973-980.
- Macha, S, Mattheus, M, Halabi, A, Pinnetti, S, Woerle, H and Broedl, U (2014b), 'Pharmacokinetics, pharmacodynamics and safety of empagliflozin, a sodium glucose cotransporter 2 (SGLT2) inhibitor, in subjects with renal impairment', *Diabetes, Obesity and Metabolism*, 16 (3): 215-222.
- Macha, S, Rose, P, Mattheus, M, Cinca, R, Pinnetti, S, Broedl, U and Woerle, H (2014c), 'Pharmacokinetics, safety and tolerability of empagliflozin, a sodium glucose cotransporter 2 inhibitor, in patients with hepatic impairment', *Diabetes, Obesity and Metabolism*, 16 (2): 118-123.
- Macha, S, Rose, P, Mattheus, M, Pinnetti, S and Woerle, H (2013), 'Lack of drug–drug interaction between empagliflozin, a sodium glucose cotransporter 2 inhibitor, and warfarin in healthy volunteers', *Diabetes, Obesity and Metabolism*, 15 (4): 316-323.
- Mackenzie, PI (1990), 'Expression of chimeric cDNAs in cell culture defines a region of UDP glucuronosyltransferase involved in substrate selection', *Journal of Biological Chemistry*, 265 (6): 3432-3435.
- Mackenzie, PI, Bock, KW, Burchell, B, Guillemette, C, Ikushiro, S-i, Iyanagi, T, Miners, JO, Owens, IS and Nebert, DW (2005), 'Nomenclature update for the mammalian UDP glycosyltransferase (UGT) gene superfamily', *Pharmacogenetics and Genomics*, 15 (10): 677-685.
- Mackenzie, PI, Gardner-Stephen, DA and Miners, JO (2010), 'UDP-Glucuronosyltransferases', In *Comprehensive Toxicology, 2 edition*, eds CA McQueen, Volume 4.20: 413-434, Elsevier Ltd., Kidlington.
- Mackenzie, PI and Owens, IS (1984), 'Cleavage of nascent UDP glucuronosyltransferase from rat liver by dog pancreatic microsomes', *Biochemical and Biophysical Research Communications*, 122 (3): 1441-1449.
- Mackenzie, PI, Rogers, A, Elliot, DJ, Chau, N, Hulin, J-A, Miners, JO and Meech, R (2011), 'The novel UDP glycosyltransferase 3A2: Cloning, catalytic properties, and tissue distribution', *Molecular Pharmacology*, 79 (3): 472-478.

- Mackenzie, PI, Rogers, A, Treloar, J, Jorgensen, BR, Miners, JO and Meech, R (2008), 'Identification of UDP glycosyltransferase 3A1 as a UDP N-acetylglucosaminyltransferase', *Journal of Biological Chemistry*, 283 (52): 36205-36210.
- Mamidi, RN, Cuyckens, F, Chen, J, Scheers, E, Kalamaridis, D, Lin, R, Silva, J, Sha, S, Evans, DC and Kelley, MF (2014), 'Metabolism and excretion of canagliflozin in mice, rats, dogs, and humans', *Drug Metabolism and Disposition*, 42 (5): 903-916.
- Mamidi, RNVS, Dallas, S, Sensenhauser, C, Lim, HK, Scheers, E, Verboven, P, Cuyckens, F, Leclercq, L, Evans, DC, Kelley, MF, Johnson, MD and Snoeys, J (2017), 'In vitro and physiologically-based pharmacokinetic based assessment of drug-drug interaction potential of canagliflozin', *British Journal of Clinical Pharmacology*, 83 (5): 1082-1096.
- Manevski, N, Moreolo, PS, Yli-Kauhaluoma, J and Finel, M (2011), 'Bovine serum albumin decreases K_m values of human UDP-glucuronosyltransferases 1A9 and 2B7 and increases V_{max} values of UGT1A9', *Drug Metabolism and Disposition*, 39 (11): 2117-2129.
- Manevski, N, Troberg, J, Svaluto-Moreolo, P, Dziedzic, K, Yli-Kauhaluoma, J and Finel, M (2013), 'Albumin stimulates the activity of the human UDP-glucuronosyltransferases 1A7, 1A8, 1A10, 2A1 and 2B15, but the effects are enzyme and substrate dependent', *PLOS ONE*, 8 (1): e54767.
- Margaillan, G, Rouleau, M, Fallon, JK, Caron, P, Villeneuve, L, Turcotte, V, Smith, PC, Joy, MS and Guillemette, C (2015), 'Quantitative profiling of human renal UDP-glucuronosyltransferases and glucuronidation activity: A comparison of normal and tumoral kidney tissues', *Drug Metabolism and Disposition*, 43 (4): 611-619.
- Martineau, I, Tchernof, A and Bélanger, A (2004), 'Amino acid residue ILE211 is essential for the enzymatic activity of human UDP-glucuronosyltransferase 1A10 (UGT1A10)', *Drug Metabolism and Disposition*, 32 (4): 455-459.
- Matthaei, S, Bowering, K, Rohwedder, K, Grohl, A and Parikh, S (2015), 'Dapagliflozin improves glycemic control and reduces body weight as add-on therapy to metformin plus sulfonylurea: A 24-week randomized, double-blind clinical trial', *Diabetes Care*, 38 (3): 365-372.
- Mayhew, BS, Jones, DR and Hall, SD (2000), 'An *in vitro* model for predicting *in vivo* inhibition of cytochrome P450 3A4 by metabolic intermediate complex formation', *Drug Metabolism and Disposition*, 28 (9): 1031-1037.
- McCance-Katz, EF, Sullivan, LE and Nallani, S (2010), 'Drug interactions of clinical importance among the opioids, methadone and buprenorphine, and other frequently prescribed medications: A review', *American Journal on Addictions*, 19 (1): 4-16.
- McLure, JA, Miners, JO and Birkett, DJ (2000), 'Nonspecific binding of drugs to human liver microsomes', *British Journal of Clinical Pharmacology*, 49 (5): 453-461.

- Meech, R, Miners, JO, Lewis, BC and Mackenzie, PI (2012), 'The glycosidation of xenobiotics and endogenous compounds: Versatility and redundancy in the UDP glycosyltransferase superfamily', *Pharmacology and Therapeutics*, 134 (2): 200-218.
- Melet, A, Marques-Soares, C, Schoch, GA, Macherey, A-C, Jaouen, M, Dansette, PM, Sari, M-A, Johnson, EF and Mansuy, D (2004), 'Analysis of human cytochrome P450 2C8 substrate specificity using a substrate pharmacophore and site-directed mutants', *Biochemistry*, 43 (49): 15379-15392.
- Menon, RM, Badri, PS, Wang, T, Polepally, AR, Zha, J, Khatri, A, Wang, H, Hu, B, Coakley, EP and Podsadecki, TJ (2015), 'Drug-drug interaction profile of the all-oral anti-hepatitis C virus regimen of paritaprevir/ritonavir, ombitasvir, and dasabuvir', *Journal of Hepatology*, 63 (1): 20-29.
- Miley, MJ, Zielinska, AK, Keenan, JE, Bratton, SM, Radomska-Pandya, A and Redinbo, MR (2007), 'Crystal structure of the cofactor-binding domain of the human phase II drug-metabolism enzyme UDP-glucuronosyltransferase 2B7', *Journal of Molecular Biology*, 369 (2): 498-511.
- Milne, RW, Nation, RL and Somogyi, AA (1996), 'The disposition of morphine and its 3- and 6-glucuronide metabolites in humans and animals, and the importance of the metabolites to the pharmacological effects of morphine', *Drug Metabolism Reviews*, 28 (3): 345-472.
- Miners, JO (2002), 'Evolution of drug metabolism: Hitchhiking the technology bandwagon', *Clinical and Experimental Pharmacology and Physiology*, 29 (11): 1040-1044.
- Miners, JO and Birkett, DJ (1998), 'Cytochrome P450 2C9: An enzyme of major importance in human drug metabolism', *British Journal of Clinical Pharmacology*, 45 (6): 525-538.
- Miners, JO, Bowalgaha, K, Elliot, DJ, Baranczewski, P and Knights, KM (2011), 'Characterization of niflumic acid as a selective inhibitor of human liver microsomal UDP-glucuronosyltransferase 1A9: Application to the reaction phenotyping of acetaminophen glucuronidation', *Drug Metabolism and Disposition*, 39 (4): 644-652.
- Miners, JO, Chau, N, Rowland, A, Burns, K, McKinnon, RA, Mackenzie, PI, Tucker, GT, Knights, KM and Kichenadasse, G (2017a), 'Inhibition of human UDP-glucuronosyltransferase enzymes by lapatinib, pazopanib, regorafenib and sorafenib: Implications for hyperbilirubinemia', *Biochemical Pharmacology*, 129: 85-95.
- Miners, JO, Knights, KM, Houston, JB and Mackenzie, PI (2006), 'In vitro–in vivo correlation for drugs and other compounds eliminated by glucuronidation in humans: Pitfalls and promises', *Biochemical Pharmacology*, 71 (11): 1531-1539.
- Miners, JO, Lillywhite, KJ, Yoovathaworn, K, Pongmarutai, M and Birkett, DJ (1990), 'Characterization of paracetamol UDP-glucuronosyltransferase activity in human liver microsomes', *Biochemical Pharmacology*, 40 (3): 595-600.

- Miners, JO and Mackenzie, PI (1991), 'Drug glucuronidation in humans', *Pharmacology and Therapeutics*, 51 (3): 347-369.
- Miners, JO, Mackenzie, PI and Knights, KM (2010a), 'The prediction of drug-glucuronidation parameters in humans: UDP-Glucuronosyltransferase enzyme-selective substrate and inhibitor probes for reaction phenotyping and *in vitro-in vivo* extrapolation of drug clearance and drug-drug interaction potential', *Drug Metabolism Reviews*, 42 (1): 196-208.
- Miners, JO, Pattanawongsa, A and Rowland, A (2018), 'Response to *in vitro* and physiologically-based pharmacokinetic assessment of the drug–drug interaction potential of canagliflozin', *British Journal of Clinical Pharmacology*, 84 (2): 392-393.
- Miners, JO, Polasek, TM, Mackenzie, PI and Knights, KM (2010b), 'The *in vitro* characterization of inhibitory drug–drug interactions involving UDP-glucuronosyltransferase', In *Enzyme- and Transporter-Based Drug-Drug Interactions*, eds KS Pang, AD Rodrigues and RM Peter, Chapter 8: 217-236, Springer, Berlin.
- Miners, JO, Smith, PA, Sorich, MJ, McKinnon, RA and Mackenzie, PI (2004), 'Predicting human drug glucuronidation parameters: Application of *in vitro* and *in silico* modeling approaches', *Annual Review of Pharmacology and Toxicology*, 44: 1-25.
- Miners, JO, Veronese, ME and Birkett, DJ (1994), '*In vitro* approaches for the prediction of human drug metabolism', *Annual Reports in Medicinal Chemistry*, 29 307-316.
- Miners, JO, Yang, X, Knights, KM and Zhang, L (2017b), 'The role of the kidney in drug elimination: Transport, metabolism, and the impact of kidney disease on drug clearance', *Clinical Pharmacology and Therapeutics*, 102 (3): 436-449.
- Munro, AW, Girvan, HM, Mason, AE, Dunford, AJ and McLean, KJ (2013), 'What makes a P450 tick?', *Trends in Biochemical Sciences*, 38 (3): 140-150.
- Munro, SL, Craik, DJ and Andrews, PR (1987), 'Conformational analysis of flexible antidepressant drugs', *Quantitative Structure-Activity Relationships*, 6 (3): 104-110.
- Murphy, SE, Park, S-SL, Thompson, EF, Wilkens, LR, Patel, Y, Stram, DO and Le Marchand, L (2014), 'Nicotine N-glucuronidation relative to N-oxidation and C-oxidation and UGT2B10 genotype in five ethnic/racial groups', *Carcinogenesis*, 35 (11): 2526-2533.
- Nair, PC, McKinnon, RA and Miners, JO (2016a), 'Cytochrome P450 structure–function: Insights from molecular dynamics simulations', *Drug Metabolism Reviews*, 48 (3): 434-452.
- Nair, PC, McKinnon, RA and Miners, JO (2016b), 'A fragment-based approach for the computational prediction of the nonspecific binding of drugs to hepatic microsomes', *Drug Metabolism and Disposition*, 44 (11): 1794-1798.

- Nair, PC, Meech, R, Mackenzie, PI, McKinnon, RA and Miners, JO (2015), 'Insights into the UDP-sugar selectivities of human UDP-glycosyltransferases (UGT): A molecular modeling perspective', *Drug Metabolism Reviews*, 47 (3): 335-345.
- Nakajima, M, Tanaka, E, Kwon, J-T and Yokoi, T (2002), 'Characterization of nicotine and cotinine N-glucuronidations in human liver microsomes', *Drug Metabolism and Disposition*, 30 (12): 1484-1490.
- Nakajima, M and Yokoi, T (2005), 'Interindividual variability in nicotine metabolism: C-Oxidation and glucuronidation', *Drug Metabolism and Pharmacokinetics*, 20 (4): 227-235.
- Nebert, DW, Wikvall, K and Miller, WL (2013), 'Human cytochromes P450 in health and disease', *Philosophical Transactions of the Royal Society B*, 368 (1612): 20120431.
- Nelson, DR, Koymans, L, Kamataki, T, Stegeman, JJ, Feyereisen, R, Waxman, DJ, Waterman, MR, Gotoh, O, Coon, MJ, Estabrook, RW, Gunsalus, IC and Nebert, DW (1996), 'P450 superfamily: Update on new sequences, gene mapping, accession numbers and nomenclature', *Pharmacogenetics*, 6 (1): 1-42.
- Nelson, DR, Zeldin, DC, Hoffman, SM, Maltais, LJ, Wain, HM and Nebert, DW (2004), 'Comparison of cytochrome P450 (CYP) genes from the mouse and human genomes, including nomenclature recommendations for genes, pseudogenes and alternative-splice variants', *Pharmacogenetics and Genomics*, 14 (1): 1-18.
- Niemi, M, Backman, JT, Neuvonen, M and Neuvonen, PJ (2003), 'Effects of gemfibrozil, itraconazole, and their combination on the pharmacokinetics and pharmacodynamics of repaglinide: Potentially hazardous interaction between gemfibrozil and repaglinide', *Diabetologia*, 46 (3): 347-351.
- Nigro, SC, Riche, DM, Pheng, M and Baker, WL (2013), 'Canagliflozin, a novel SGLT2 inhibitor for treatment of type 2 diabetes', *Annals of Pharmacotherapy*, 47 (10): 1301-1311.
- Nishihara, M, Sudo, M, Kawaguchi, N, Takahashi, J, Kiyota, Y, Kondo, T and Asahi, S (2012), 'An unusual metabolic pathway of sipoglitazar, a novel antidiabetic agent: Cytochrome P450-catalyzed oxidation of sipoglitazar acyl glucuronide', *Drug Metabolism and Disposition*, 40 (2): 249-258.
- Obach, RS (1999), 'Prediction of human clearance of twenty-nine drugs from hepatic microsomal intrinsic clearance data: An examination of *in vitro* half-life approach and nonspecific binding to microsomes', *Drug Metabolism and Disposition*, 27 (11): 1350-1359.
- Obach, RS, Fahmi, OA and Walsky, RL (2010), 'Inactivation of human cytochrome P450 enzymes and drug-drug interactions', In *Enzyme- and Transporter-Based Drug-Drug Interactions: Progress and Future Challenges*, eds KS Pang, AD Rodrigues and RM Peter, Chapter 19: 473-495, Springer, New York.

- Obach, RS, Walsky, RL and Venkatakrishnan, K (2007), 'Mechanism-based inactivation of human cytochrome P450 enzymes and the prediction of drug-drug interactions', *Drug Metabolism and Disposition*, 35 (2): 246-255.
- Obermeier, M, Yao, M, Khanna, A, Koplowitz, B, Zhu, M, Li, W, Komoroski, B, Kasichayanula, S, Discenza, L and Washburn, W (2010), 'In vitro characterization and pharmacokinetics of dapagliflozin (BMS-512148), a potent sodium-glucose cotransporter type II inhibitor, in animals and humans', *Drug Metabolism and Disposition*, 38 (3): 405-414.
- Ogilvie, BW, Zhang, D, Li, W, Rodrigues, AD, Gipson, AE, Holsapple, J, Toren, P and Parkinson, A (2006), 'Glucuronidation converts gemfibrozil to a potent, metabolism-dependent inhibitor of CYP2C8: Implications for drug-drug interactions', *Drug Metabolism and Disposition*, 34 (1): 191-197.
- Ohno, S and Nakajin, S (2009), 'Determination of mRNA expression of human UDP-glucuronosyltransferases and application for localization in various human tissues by real-time reverse transcriptase-polymerase chain reaction', *Drug Metabolism and Disposition*, 37 (1): 32-40.
- Omura, T and Sato, R (1964), 'The carbon monoxide-binding pigment of liver microsomes: I. Evidence for its hemoprotein nature', *Journal of Biological Chemistry*, 239 (7): 2370-2378.
- Ong, CE, Coulter, S, Birkett, DJ, Bhasker, CR and Miners, JO (2000), 'The xenobiotic inhibitor profile of cytochrome P450C8', *British Journal of Clinical Pharmacology*, 50 (6): 573-580.
- Orr, ST, Ripp, SL, Ballard, TE, Henderson, JL, Scott, DO, Obach, RS, Sun, H and Kalgutkar, AS (2012), 'Mechanism-based inactivation (MBI) of cytochrome P450 enzymes: Structure-activity relationships and discovery strategies to mitigate drug-drug interaction risks', *Journal of Medicinal Chemistry*, 55 (11): 4896-4933.
- Osborne, R, Joel, S, Trew, D and Slevin, M (1990), 'Morphine and metabolite behavior after different routes of morphine administration: Demonstration of the importance of the active metabolite morphine-6-glucuronide', *Clinical Pharmacology and Therapeutics*, 47 (1): 12-19.
- Paine, MF, Hart, HL, Ludington, SS, Haining, RL, Rettie, AE and Zeldin, DC (2006), 'The human intestinal cytochrome P450 "pie"', *Drug Metabolism and Disposition*, 34 (5): 880-886.
- Paine, MJI, McLaughlin, LA, Flanagan, JU, Kemp, CA, Sutcliffe, MJ, Roberts, GCK and Wolf, CR (2003), 'Residues glutamate 216 and aspartate 301 are key determinants of substrate specificity and product regioselectivity in cytochrome P450 2D6', *Journal of Biological Chemistry*, 278 (6): 4021-4027.
- Parkinson, A, Kazmi, F, Buckley, DB, Yerino, P, Paris, BL, Holsapple, J, Toren, P, Otradovec, SM and Ogilvie, BW (2011), 'An evaluation of the dilution method for identifying metabolism-dependent inhibitors of cytochrome P450 enzymes', *Drug Metabolism and Disposition*, 39 (8): 1370-1387.

- Patilea-Vrana, G and Unadkat, J (2016), 'Transport vs. metabolism: What determines the pharmacokinetics and pharmacodynamics of drugs? Insights from the extended clearance model', *Clinical Pharmacology and Therapeutics*, 100 (5): 413-418.
- Perloff, E, Mason, AK, Dehal, SS, Blanchard, AP, Morgan, L, Ho, T, Dandeneau, A, Crocker, RM, Chandler, CM and Boily, N (2009), 'Validation of cytochrome P450 time-dependent inhibition assays: A two-time point IC₅₀ shift approach facilitates kinact assay design', *Xenobiotica*, 39 (2): 99-112.
- Pirmohamed, M, James, S, Meakin, S, Green, C, Scott, A, Walley, T, Farrar, K, Park, B and Breckenridge, A (2004), 'Adverse drug reactions as cause of admission to hospital: Prospective analysis of 18,820 patients', *British Medical Journal*, 329 (7456): 15-19.
- Plosker, G (2012), 'Dapagliflozin: A review of its use in type 2 diabetes mellitus', *Drugs*, 72 (17): 2289-2312.
- Polasek, TM, Elliot, DJ, Lewis, BC and Miners, JO (2004), 'Mechanism-based inactivation of human cytochrome P450C8 by drugs *in vitro*', *Journal of Pharmacology and Experimental Therapeutics*, 311 (3): 996-1007.
- Polasek, TM, Elliot, DJ, Somogyi, AA, Gillam, EM, Lewis, BC and Miners, JO (2006), 'An evaluation of potential mechanism-based inactivation of human drug metabolizing cytochromes P450 by monoamine oxidase inhibitors, including isoniazid', *British Journal of Clinical Pharmacology*, 61 (5): 570-584.
- Polasek, TM, Lin, FPY, Miners, JO and Doogue, MP (2011), 'Perpetrators of pharmacokinetic drug–drug interactions arising from altered cytochrome P450 activity: A criteria-based assessment', *British Journal of Clinical Pharmacology*, 71 (5): 727-736.
- Polasek, TM and Miners, JO (2007), '*In vitro* approaches to investigate mechanism-based inactivation of CYP enzymes', *Expert Opinion on Drug Metabolism and Toxicology*, 3 (3): 321-329.
- Porubsky, PR, Battaile, KP and Scott, EE (2010), 'Human cytochrome p450 2E1 structures with fatty acid analogs reveal a previously unobserved binding mode', *Journal of Biological Chemistry*, 285 (29): 22282-22290.
- Poulos, TL, Finzel, B, Gunsalus, I, Wagner, GC and Kraut, J (1985), 'The 2.6-Å crystal structure of *Pseudomonas putida* cytochrome P-450', *Journal of Biological Chemistry*, 260 (30): 16122-16130.
- Proctor, N, Tucker, G and Rostami-Hodjegan, A (2004), 'Predicting drug clearance from recombinantly expressed CYPs: Intersystem extrapolation factors', *Xenobiotica*, 34 (2): 151-178.
- Qato, DM, Alexander, GC, Conti, RM, Johnson, M, Schumm, P and Lindau, ST (2008), 'Use of prescription and over-the-counter medications and dietary supplements among older adults in the United States', *JAMA*, 300 (24): 2867-2878.

- Radominska-Pandya, A, Czernik, PJ, Little, JM, Battaglia, E and Mackenzie, PI (1999), 'Structural and functional studies of UDP-glucuronosyltransferases', *Drug Metabolism Reviews*, 31 (4): 817-899.
- Raungrut, P, Uchaipichat, V, Elliot, DJ, Janchawee, B, Somogyi, AA and Miners, JO (2010), 'In vitro–in vivo extrapolation predicts drug–drug interactions arising from inhibition of codeine glucuronidation by dextropropoxyphene, fluconazole, ketoconazole, and methadone in humans', *Journal of Pharmacology and Experimental Therapeutics*, 334 (2): 609-618.
- Regan, SL, Maggs, JL, Hammond, TG, Lambert, C, Williams, DP and Park, BK (2010), 'Acyl glucuronides: The good, the bad and the ugly', *Biopharmaceutics and Drug Disposition*, 31 (7): 367-395.
- Rendic, S and Guengerich, FP (2015), 'Survey of human oxidoreductases and cytochrome P450 enzymes involved in the metabolism of xenobiotic and natural chemicals', *Chemical Research in Toxicology*, 28 (1): 38-42.
- Reynald, RL, Sansen, S, Stout, CD and Johnson, EF (2012), 'Structural characterization of human cytochrome P450 2C19: Active site differences between P450s 2C8, 2C9, and 2C19', *Journal of Biological Chemistry*, 287 (53): 44581-44591.
- Riley, RJ, McGinnity, DF and Austin, RP (2005), 'A unified model for predicting human hepatic, metabolic clearance from *in vitro* intrinsic clearance data in hepatocytes and microsomes', *Drug Metabolism and Disposition*, 33 (9): 1304-1311.
- Ritter, JK, Chen, F, Sheen, YY, Lubet, RA and Owens, IS (1992), 'Two human liver cDNAs encode UDP-glucuronosyltransferases with 2 log differences in activity toward parallel substrates including hyodeoxycholic acid and certain estrogen derivatives', *Biochemistry*, 31 (13): 3409-3414.
- Rodrigues, AD (1999), 'Integrated cytochrome P450 reaction phenotyping. Attempting to bridge the gap between cDNA-expressed cytochromes P450 and native human liver microsomes', *Biochemical Pharmacology*, 57 (5): 465-480.
- Ronaldson, P, Bauer, B, El-Kattan, A, Shen, H, Salphati, L and Louie, S (2016), 'Highlights from the American Association of Pharmaceutical Scientists/ International transporter consortium joint workshop on drug transporters in absorption, distribution, metabolism, and excretion: From the bench to the bedside – Clinical Pharmacology Considerations', *Clinical Pharmacology and Therapeutics*, 100 (5): 419-422.
- Rosenstock, J, Aggarwal, N, Polidori, D, Zhao, Y, Arbit, D, Usiskin, K, Capuano, G, Canovatchel, W and Group, CDS (2012a), 'Dose-ranging effects of canagliflozin, a sodium-glucose cotransporter 2 inhibitor, as add-on to metformin in subjects with type 2 diabetes', *Diabetes care*, 35 (6): 1232-1238.

- Rosenstock, J, Vico, M, Wei, L, Salsali, A and List, JF (2012b), 'Effects of dapagliflozin, an SGLT2 inhibitor, on HbA1c, body weight, and hypoglycemia risk in patients with type 2 diabetes inadequately controlled on pioglitazone monotherapy', *Diabetes Care*, 35 (7): 1473-1478.
- Rostami-Hodjegan, A and Tucker, GT (2007), 'Simulation and prediction of *in vivo* drug metabolism in human populations from *in vitro* data', *Nature Reviews Drug Discovery*, 6 (2): 140-148.
- Rowland-Yeo, K and Tucker, GT (2016), 'Drug–drug interactions: Computational approaches', In *New Horizons in Predictive Drug Metabolism and Pharmacokinetics*, eds AGE Wilson, Chapter 13: 283-308, The Royal Society of Chemistry, London.
- Rowland, A, Elliot, DJ, Knights, KM, Mackenzie, PI and Miners, JO (2008a), 'The "albumin effect" and *in vitro-in vivo* extrapolation: Sequestration of long-chain unsaturated fatty acids enhances phenytoin hydroxylation by human liver microsomal and recombinant cytochrome P450 2C9', *Drug Metabolism and Disposition*, 36 (5): 870-877.
- Rowland, A, Elliot, DJ, Williams, JA, Mackenzie, PI, Dickinson, RG and Miners, JO (2006a), '*In vitro* characterization of lamotrigine N2-glucuronidation and the lamotrigine-valproic acid interaction', *Drug Metabolism and Disposition*, 34 (6): 1055-1062.
- Rowland, A, Gaganis, P, Elliot, DJ, Mackenzie, PI, Knights, KM and Miners, JO (2007), 'Binding of inhibitory fatty acids is responsible for the enhancement of UDP-glucuronosyltransferase 2B7 activity by albumin: Implications for *in vitro-in vivo* extrapolation', *Journal of Pharmacology and Experimental Therapeutics*, 321 (1): 137-147.
- Rowland, A, Knights, KM, Mackenzie, PI and Miners, JO (2008b), 'The “albumin effect” and drug glucuronidation: Bovine serum albumin and fatty acid-free human serum albumin enhance the glucuronidation of UDP-glucuronosyltransferase (UGT) 1A9 substrates but not UGT1A1 and UGT1A6 activities', *Drug Metabolism and Disposition*, 36 (6): 1056-1062.
- Rowland, A, Knights, KM, Mackenzie, PI and Miners, JO (2009), 'Characterization of the binding of drugs to human intestinal fatty acid binding protein (IFABP): Potential role of IFABP as an alternative to albumin for *in vitro-in vivo* extrapolation of drug kinetic parameters', *Drug Metabolism and Disposition*, 37 (7): 1395-1403.
- Rowland, A, Mackenzie, PI and Miners, JO (2015), 'Transporter-mediated uptake of UDP–glucuronic acid by human liver microsomes: Assay conditions, kinetics, and inhibition', *Drug Metabolism and Disposition*, 43 (1): 147-153.
- Rowland, A, Miners, JO and Mackenzie, PI (2013), 'The UDP-glucuronosyltransferases: Their role in drug metabolism and detoxification', *The International Journal of Biochemistry and Cell Biology*, 45 (6): 1121-1132.

- Rowland, M, Peck, C and Tucker, G (2011), 'Physiologically-based pharmacokinetics in drug development and regulatory science', *Annual Review of Pharmacology and Toxicology*, 51: 45-73.
- Rowland, P, Blaney, FE, Smyth, MG, Jones, JJ, Leydon, VR, Oxbrow, AK, Lewis, CJ, Tennant, MG, Modi, S, Eggleston, DS, Chenery, RJ and Bridges, AM (2006b), 'Crystal structure of human cytochrome P450 2D6', *Journal of Biological Chemistry*, 281 (11): 7614-7622.
- Sane, RS, Ramsden, D, Sabo, JP, Cooper, C, Rowland, L, Ting, N, Whitcher-Johnstone, A and Tweedie, DJ (2016), 'Contribution of major metabolites toward complex drug-drug interactions of deleobuvir: *In vitro* predictions and *in vivo* outcomes', *Drug Metabolism and Disposition*, 44 (3): 466-475.
- Sansen, S, Yano, JK, Reynald, RL, Schoch, GA, Griffin, KJ, Stout, CD and Johnson, EF (2007), 'Adaptations for the oxidation of polycyclic aromatic hydrocarbons exhibited by the structure of human P450 1A2', *Journal of Biological Chemistry*, 282 (19): 14348-14355.
- Scheen, AJ (2014a), 'Evaluating SGLT2 inhibitors for type 2 diabetes: Pharmacokinetic and toxicological considerations', *Expert Opinion on Drug Metabolism and Toxicology*, 10 (5): 647-663.
- Scheen, AJ (2014b), 'Pharmacokinetic and pharmacodynamic profile of empagliflozin, a sodium glucose co-transporter 2 inhibitor', *Clinical Pharmacokinetics*, 53 (3): 213-225.
- Schernthaner, G, Gross, JL, Rosenstock, J, Guarisco, M, Fu, M, Yee, J, Kawaguchi, M, Canovatchel, W and Meininger, G (2013), 'Canagliflozin compared with sitagliptin for patients with type 2 diabetes who do not have adequate glycemic control with metformin plus sulfonylurea a 52-week randomized trial', *Diabetes Care*, 36 (9): 2508-2515.
- Schoch, GA, Yano, JK, Sansen, S, Dansette, PM, Stout, CD and Johnson, EF (2008), 'Determinants of cytochrome P450 2C8 substrate binding structures of complexes with montelukast, troglitazone, felodipine, and 9-cis-retinoic acid', *Journal of Biological Chemistry*, 283 (25): 17227-17237.
- Schoch, GA, Yano, JK, Wester, MR, Griffin, KJ, Stout, CD and Johnson, EF (2004), 'Structure of human microsomal cytochrome P450 2C8: Evidence for a peripheral fatty acid binding site', *Journal of Biological Chemistry*, 279 (10): 9497-9503.
- Scotcher, D, Billington, S, Brown, J, Jones, CR, Brown, CDA, Rostami-Hodjegan, A and Galetin, A (2017), 'Microsomal and cytosolic scaling factors in dog and human kidney cortex and application for *in vitro-in vivo* extrapolation of renal metabolic clearance', *Drug metabolism and disposition: the biological fate of chemicals*, 45 (5): 556-568.
- Segel, I (1993), *Enzyme kinetics*, John Wiley & Sons, New York.

- Sekiguchi, N, Higashida, A, Kato, M, Nabuchi, Y, Mitsui, T, Takanashi, K, Aso, Y and Ishigai, M (2009), 'Prediction of drug-drug interactions based on time-dependent inhibition from high throughput screening of cytochrome P450 3A4 inhibition', *Drug Metabolism and Pharmacokinetics*, 24 (6): 500-510.
- Shi, S and Li, Y (2014), 'Interplay of drug-metabolizing enzymes and transporters in drug absorption and disposition', *Current Drug Metabolism*, 15 (10): 915-941.
- Silverman, RB (1988), *Mechanism-Based Enzyme Inactivation: Chemistry and Enzymology*, CRC Press Inc, Boca Raton.
- Sim, SC and Ingelman-Sundberg, M (2010), 'The human cytochrome P450 (CYP) allele nomenclature website: A peer-reviewed database of CYP variants and their associated effects', *Human Genomics*, 4 (4): 278.
- Smith, DE and Benet, LZ (1983), 'Biotransformation of furosemide in kidney transplant patients', *European Journal of Clinical Pharmacology*, 24 (6): 787-790.
- Snyder, BD, Polasek, TM and Doogue, MP (2012), 'Drug interactions: Principles and practice', *Australian Prescriber*, 35 (3): 85-88.
- Sorich, MJ, Miners, JO, McKinnon, RA and Smith, PA (2004), 'Multiple pharmacophores for the investigation of human UDP-glucuronosyltransferase isoform substrate selectivity', *Molecular Pharmacology*, 65 (2): 301-308.
- Stingl, J, Bartels, H, Viviani, R, Lehmann, M and Brockmöller, J (2014), 'Relevance of UDP-glucuronosyltransferase polymorphisms for drug dosing: A quantitative systematic review', *Pharmacology and Therapeutics*, 141 (1): 92-116.
- Stone, AN, Mackenzie, PI, Galetin, A, Houston, JB and Miners, JO (2003), 'Isoform selectivity and kinetics of morphine 3-and 6-glucuronidation by human UDP-glucuronosyltransferases: Evidence for atypical glucuronidation kinetics by UGT2B7', *Drug Metabolism and Disposition*, 31 (9): 1086-1089.
- Takeda, S, Kitajima, Y, Ishii, Y, Nishimura, Y, Mackenzie, PI, Oguri, K and Yamada, H (2006), 'Inhibition of UDP-glucuronosyltransferase 2b7-catalyzed morphine glucuronidation by ketoconazole: Dual mechanisms involving a novel noncompetitive mode', *Drug Metabolism and Disposition*, 34 (8): 1277-1282.
- Tassaneeyakul, W, Birkett, DJ, McManus, ME, Tassaneeyakul, W, Veronese, ME, Andersson, T, Tukey, RH and Miners, JO (1994), 'Caffeine metabolism by human hepatic cytochromes p450: Contributions of 1A2, 2E1 and 3A isoforms', *Biochemical Pharmacology*, 47 (10): 1767-1776.
- Tassaneeyakul, W, Birkett, DJ, Veronese, ME, McManus, ME, Tukey, RH, Quattrochi, LC, Gelboin, HV and Miners, JO (1993), 'Specificity of substrate and inhibitor probes for human cytochromes P450 1A1 and 1A2', *Journal of Pharmacology and Experimental Therapeutics*, 265 (1): 401-407.

- Testa, B and Abraham, DJ (2003), 'Principles of drug metabolism', In *Burger's Medicinal Chemistry and Drug Discovery, 7 edition*, eds DJ Abraham, Chapter 10: 431-498, John Wiley & Sons Inc., Weinheim.
- Tornio, A, Filppula, A, Kailari, O, Neuvonen, M, Nyrönen, T, Tapaninen, T, Neuvonen, P, Niemi, M and Backman, J (2014), 'Glucuronidation converts clopidogrel to a strong time-dependent inhibitor of CYP2C8: A phase II metabolite as a perpetrator of drug–drug interactions', *Clinical Pharmacology and Therapeutics*, 96 (4): 498-507.
- Tornio, A, Neuvonen, PJ, Niemi, M and Backman, JT (2017), 'Role of gemfibrozil as an inhibitor of CYP2C8 and membrane transporters', *Expert Opinion on Drug Metabolism and Toxicology*, 13 (1): 83-95.
- Total, RA and Rettie, AE (2005), 'Cytochrome P450 2C8: substrates, inhibitors, pharmacogenetics, and clinical relevance', *Clinical Pharmacology and Therapeutics*, 77 (5): 341-352.
- Tukey, RH and Strassburg, CP (2000), 'Human UDP-glucuronosyltransferases: Metabolism, expression, and disease', *Annual Review of Pharmacology and Toxicology*, 40 (1): 581-616.
- Uchaipichat, V, Mackenzie, PI, Elliot, DJ and Miners, JO (2006a), 'Selectivity of substrate (trifluoperazine) and inhibitor (amitriptyline, androsterone, canrenoic acid, hecogenin, phenylbutazone, quinidine, quinine, and sulfapyrazone) “probes” for human UDP-glucuronosyltransferases', *Drug Metabolism and Disposition*, 34 (3): 449-456.
- Uchaipichat, V, Mackenzie, PI, Guo, X-H, Gardner-Stephen, D, Galetin, A, Houston, JB and Miners, JO (2004), 'Human UDP-glucuronosyltransferases: Isoform selectivity and kinetics of 4-methylumbelliferone and 1-naphthol glucuronidation, effects of organic solvents, and inhibition by diclofenac and probenecid', *Drug Metabolism and Disposition*, 32 (4): 413-423.
- Uchaipichat, V, Winner, LK, Mackenzie, PI, Elliot, DJ, Williams, JA and Miners, JO (2006b), 'Quantitative prediction of *in vivo* inhibitory interactions involving glucuronidated drugs from *in vitro* data: The effect of fluconazole on zidovudine glucuronidation', *British Journal of Clinical Pharmacology*, 61 (4): 427-439.
- Udomuksorn, W, Elliot, DJ, Lewis, BC, Mackenzie, PI, Yoovathaworn, K and Miners, JO (2007), 'Influence of mutations associated with Gilbert and Crigler–Najjar type II syndromes on the glucuronidation kinetics of bilirubin and other UDP-glucuronosyltransferase 1A substrates', *Pharmacogenetics and Genomics*, 17 (12): 1017-1029.
- Venkatakrishnan, K, Von Moltke, LL and Greenblatt, DJ (1998), 'Relative quantities of catalytically active CYP 2C9 and 2C19 in human liver microsomes: Application of the relative activity factor approach', *Journal of Pharmaceutical Sciences*, 87 (7): 845-853.

- Virtanen, R, Scheinin, M and Iisalo, E (1980), 'Single dose pharmacokinetics of doxepin in healthy volunteers', *Acta Pharmacologica et Toxicologica*, 47 (5): 371-376.
- Walia, G, Smith, AD, Riches, Z, Collier, AC and Coughtrie, MWH (2017), 'The effects of UDP-sugars, UDP and Mg²⁺ on uridine diphosphate glucuronosyltransferase activity in human liver microsomes', *Xenobiotica*, 1-9.
- Walsky, RL, Bauman, JN, Bourcier, K, Giddens, G, Lapham, K, Negahban, A, Ryder, TF, Obach, RS, Hyland, R and Goosen, TC (2012), 'Optimized assays for human UDP-glucuronosyltransferase (UGT) activities: Altered alamethicin concentration and utility to screen for UGT inhibitors', *Drug Metabolism and Disposition*, 40 (5): 1051-1065.
- Walters, WP, Green, J, Weiss, JR and Murcko, MA (2011), 'What do medicinal chemists actually make? A 50-year retrospective', *Journal of Medicinal Chemistry*, 54 (19): 6405-6416.
- Wang, J, Evans, AM, Knights, KM and Miners, JO (2011), 'Differential disposition of intra-renal generated and preformed glucuronides: Studies with 4-methylumbelliferone and 4-methylumbelliferyl glucuronide in the filtering and nonfiltering isolated perfused rat kidney', *Journal of Pharmacy and Pharmacology*, 63 (4): 507-514.
- Wattanachai, N, Polasek, TM, Heath, TM, Uchaipichat, V, Tassaneeyakul, W, Tassaneeyakul, W and Miners, JO (2011), 'In vitro–in vivo extrapolation of CYP2C8-catalyzed paclitaxel 6 α -hydroxylation: Effects of albumin on in vitro kinetic parameters and assessment of interindividual variability in predicted clearance', *European Journal of Clinical Pharmacology*, 67 (8): 815-824.
- Wattanachai, N, Tassaneeyakul, W, Rowland, A, Elliot, DJ, Bowalgaha, K, Knights, KM and Miners, JO (2012), 'Effect of albumin on human liver microsomal and recombinant CYP1A2 activities: Impact on in vitro–in vivo extrapolation of drug clearance', *Drug Metabolism and Disposition*, 40 (5): 982-989.
- Wester, MR, Yano, JK, Schoch, GA, Yang, C, Griffin, KJ, Stout, CD and Johnson, EF (2004), 'The structure of human cytochrome P450 2C9 complexed with flurbiprofen at 2.0-Å resolution', *Journal of Biological Chemistry*, 279 (34): 35630-35637.
- WHO (2011), 'Use of glycated haemoglobin (HbA1c) in the diagnosis of diabetes mellitus: Abbreviated report of a WHO consultation'.
- Wienkers, LC and Heath, TG (2005), 'Predicting in vivo drug interactions from in vitro drug discovery data', *Nature Reviews Drug Discovery*, 4 (10): 825-833.
- Williams, JA, Hyland, R, Jones, BC, Smith, DA, Hurst, S, Goosen, TC, Peterkin, V, Koup, JR and Ball, SE (2004a), 'Drug-drug interactions for UDP-glucuronosyltransferase substrates: A pharmacokinetic explanation for typically observed low exposure (AUC_i/AUC) ratios', *Drug Metabolism and Disposition*, 32 (11): 1201-1208.

- Williams, PA, Cosme, J, Matak Vinković, D, Ward, A, Angove, HC, Day, PJ, Vonrhein, C, Tickle, IJ and Jhoti, H (2004b), 'Crystal structures of human cytochrome P450 3A4 bound to metyrapone and progesterone', *Science*, 305 (5684): 683-686.
- Williams, PA, Cosme, J, Sridhar, V, Johnson, EF and McRee, DE (2000), 'Mammalian microsomal cytochrome P450 monooxygenase: Structural adaptations for membrane binding and functional diversity', *Molecular Cell*, 5 (1): 121-131.
- Xiong, Y, Bernardi, D, Bratton, S, Ward, MD, Battaglia, E, Finel, M, Drake, RR and Radominska-Pandya, A (2006), 'Phenylalanine 90 and 93 are localized within the phenol binding site of human UDP-glucuronosyltransferase 1A10 as determined by photoaffinity labeling, mass spectrometry, and site-directed mutagenesis', *Biochemistry*, 45 (7): 2322-2332.
- Yamashiro, W, Maeda, K, Hirouchi, M, Adachi, Y, Hu, Z and Sugiyama, Y (2006), 'Involvement of transporters in the hepatic uptake and biliary excretion of valsartan, a selective antagonist of the angiotensin II AT1-receptor, in humans', *Drug Metabolism and Disposition*, 34 (7): 1247-1254.
- Yano, JK, Hsu, MH, Griffin, KJ, Stout, CD and Johnson, EF (2005), 'Structures of human microsomal cytochrome P450 2A6 complexed with coumarin and methoxsalen', *Nature Structural and Molecular Biology*, 12 (9): 822-823.
- Yano, JK, Wester, MR, Schoch, GA, Griffin, KJ, Stout, CD and Johnson, EF (2004), 'The structure of human microsomal cytochrome P450 3A4 determined by X-ray crystallography to 2.05-Å resolution', *Journal of Biological Chemistry*, 279 (37): 38091-38094.
- Yasukochi, Y and Masters, B (1976), 'Some properties of a detergent-solubilized NADPH-cytochrome c (cytochrome P-450) reductase purified by biospecific affinity chromatography', *Journal of Biological Chemistry*, 251 (17): 5337-5344.
- Yoshida, K, Maeda, K and Sugiyama, Y (2013), 'Hepatic and intestinal drug transporters: Prediction of pharmacokinetic effects caused by drug-drug interactions and genetic polymorphisms', *Annual Review of Pharmacology and Toxicology*, 53 (1): 581-612.
- Yu, A and Haining, RL (2001), 'Comparative contribution to dextromethorphan metabolism by cytochrome P450 isoforms *in vitro*: Can dextromethorphan be used as a dual probe for both CYP2D6 and CYP3A activities?', *Drug Metabolism and Disposition*, 29 (11): 1514-1520.
- Zangar, RC, Davydov, DR and Verma, S (2004), 'Mechanisms that regulate production of reactive oxygen species by cytochrome P450', *Toxicology and applied pharmacology*, 199 (3): 316-331.
- Zanger, UM and Schwab, M (2013), 'Cytochrome P450 enzymes in drug metabolism: Regulation of gene expression, enzyme activities, and impact of genetic variation', *Pharmacology and Therapeutics*, 138 (1): 103-141.

- Zhang, D, Chando, TJ, Everett, DW, Patten, CJ, Dehal, SS and Griffith Humphreys, W (2005), 'In vitro inhibition of udp glucuronosyltransferases by atazanavir and other HIV protease inhibitors and the relationship of this property to in vivo bilirubin glucuronidation', *Drug Metabolism and Disposition*, 33 (11): 1729-1739.
- Zhang, H, Coville, PF, Walker, RJ, Miners, JO, Birkett, DJ and Wanwimolruk, S (1997), 'Evidence for involvement of human CYP3A in the 3-hydroxylation of quinine', *British Journal of Clinical Pharmacology*, 43 (3): 245-252.
- Zhang, L, Zhang, Y and Huang, SM (2009), 'Scientific and regulatory perspectives on metabolizing enzyme-transporter interplay and its role in drug interactions: Challenges in predicting drug interactions', *Molecular Pharmaceutics*, 6 (6): 1766-1774.
- Zheng, L, Baumann, U and Reymond, J-L (2004), 'An efficient one-step site-directed and site-saturation mutagenesis protocol', *Nucleic Acids Research*, 32 (14): e115-e115.
- Zhou, D, Guo, J, Linnenbach, AJ, Booth-Genthe, CL and Grimm, SW (2010), 'Role of human UGT2B10 in N-glucuronidation of tricyclic antidepressants, amitriptyline, imipramine, clomipramine, and trimipramine', *Drug Metabolism and Disposition*, 38 (5): 863-870.
- Zhou, J and Miners, JO (2014), 'Enzyme kinetics of uridine diphosphate glucuronosyltransferases (UGTs)', In *Enzyme Kinetics in Drug Metabolism: Fundamentals and Applications*, eds S Nagar, UA Argikar and DJ Tweedie, Chapter 11: 203-228, Humana Press, New Jersey.
- Zhou, J, Tracy, TS and Rimmel, RP (2010), 'Glucuronidation of dihydrotestosterone and trans-androsterone by recombinant UDP-glucuronosyltransferase (UGT) 1A4: Evidence for multiple UGT1A4 aglycone binding sites', *Drug Metabolism and Disposition*, 38 (3): 431-440.
- Zhou, J, Tracy, TS and Rimmel, RP (2011), 'Correlation between bilirubin glucuronidation and estradiol-3-glucuronidation in the presence of model UDP-glucuronosyltransferase 1A1 substrates/inhibitors', *Drug Metabolism and Disposition*, 39 (2): 322-329.
- Zhou, Z-W and Zhou, S-F (2009), 'Application of mechanism-based CYP inhibition for predicting drug-drug interactions', *Expert Opinion on Drug Metabolism and Toxicology*, 5 (6): 579-605.
- Zientek, MA and Youdim, K (2015), 'Reaction phenotyping: Advances in the experimental strategies used to characterize the contribution of drug-metabolizing enzymes', *Drug Metabolism and Disposition*, 43 (1): 163-181.
- Zinman, B, Wanner, C, Lachin, JM, Fitchett, D, Bluhmki, E, Hantel, S, Mattheus, M, Devins, T, Johansen, OE and Woerle, HJ (2015), 'Empagliflozin, cardiovascular outcomes, and mortality in type 2 diabetes', *New England Journal of Medicine*, 373 (22): 2117-2128.